Study of Cu_2ZnSnS_4 (CZTS) Thin Films for Solar Cell Application

This thesis is submitted as a partial fulfillment of the Ph. D. programme in Physics

Indu Bala Vashistha

(ID No. 2011RPH7112)

Department of Physics

MALAVIYA NATIONAL INSTITUTE OF TECHNOLOGY JAIPUR

April, 2017

Dedicated to one word

"The Hope"

Supervisor's Certificate

This is to certify that the thesis entitled "**Study of Cu$_2$ZnSnS$_4$ (CZTS) Thin Films for Solar Cell Application**" describes the original research work carried out by **Ms. Indu Bala Vashistha** (ID No. 2011RPH7112) for the award of the degree of Doctor of Philosophy (Physics) in Malaviya National Institute of Technology Jaipur (India). This work was done by her during the period December 2011 to December 2016 under my supervision.

(Dr. S. K. Sharma)

Professor and Head

Department of Physics

MNIT Jaipur (India)

Acknowledgements

Abstract

Chapter 1 contains the introductory facts which motivated us to work in the field of Cu_2ZnSnS_4 (CZTS) based solar cell. Basic concepts related to solar cells and suitable materials have been discussed. Objectives derived from the motivation also have been presented.

Chapter 2 gives detailed literature survey for achieving framework for carrying out the work reported in the thesis. A brief introduction of prominent groups working in the field of CZTS photovoltaic material at national and international level has been presented.

Chapter 3 deals with the description of copper-zinc-tin-sulphide CZTS films synthesis methods and their properties. A detailed description of various characterization tools and techniques used in the thesis has been presented in this chapter.

Chapter 4 elaborates on the controlling and optimization of synthesis parameters for deposition of CZTS thin film by CBD method and surface modification effect of post deposition treatment i.e. thermal treatment. CZTS thin film as an absorber layer has been synthesized by low cost Chemical Bath Deposition (CBD) method by optimizing deposition parameters. Annealed films at various temperature show increase in crystalline nature, grain size and decrement in energy band gap value and resistance.

Chapter 5 explains the effect of chemical precursors on CZTS thin films. Two types of chemical precursors have been used for deposition i.e. chloride based precursors and sulphate based precursors as source for copper, zinc, tin and sulpher CZTS thin film have been synthesized by chloride based precursors with moderate Zn concentration and after annealing shows good crystallinity with interlocked cubic grains and optimal energy band gap.

Chapter 6 elaborates on the fabrication of heterojunction using CZTS as absorber layer and ZnS as buffer layer. ZnS and doped Al-ZnS buffer layer has been prepared with different concentrations. Investigations carried out for structural, morphological and optical properties of ZnS and doped Al-ZnS buffer layer showed improved performance for doped Al-ZnS buffer layer. Heterojunction glass-ITO/ZnS/CZTS/Ag devices have been characterized for solar cell performance.

Chapter 7 deals with the summary of conclusion of the present study mentioned in all chapters. It is also presented future aspects of this study.

Contents

Appendices

List of Tables

List of Figures

List of Abbreviations

Cu_2ZnSnS_4	:	Copper Zinc Tin Sulfide (CZTS)
ZnS	:	Zinc Sulfide
ITO	:	Indium Tin Oxide
TPD	:	Ternary Phase Diagram
TFPV	:	Thin Film Photovoltaic
Al	:	Aluminum
Ag	:	Silver
PVD	:	Physical Vapor Deposition
CVD	:	Chemical Vapor Deposition
EBE	:	Electron Beam Evaporation
MBE	:	Molecular Beam Evaporation
EDTA	:	Ethylenediaminetetraacetic Acid
TEA	:	Triethanolamine
DI	:	De-ionized
EM	:	Electromagnetic
XRD	:	X-ray diffraction
AFM	:	Atomic Force Microscopy
SEM	:	Scanning Electron Microscopy
EDAX	:	Energy Dispersive X-ray Analysis
UV-VIS	:	Ultra Violate Visible
SMU	:	Source Measurement System
I-V	:	Current Voltage
FWHM	:	Full width at half maximum
UV-VIS	:	Ultra Violet-Visible
E_g	:	Energy Band Gap

hυ	:	Energy of Photon
J_{SC}	:	Short circuit current density
V_{OC}	:	Open circuit voltage
FF	:	Fill factor
η	:	Efficiency

CHAPTER 1

INTRODUCTION AND MOTIVATION

1.1   Energy consumption scenarios

Electricity, heat and light are the common forms of used energy in daily life. Recent scenario of world energy consumption indicates its dependency on the fossil fuel, i.e. coal, oil and natural gas are main source of energy supply [1]. In India fossil fuels also gives major part of primary energy consumption.

The present energy expenditure in the world is startling due to the rapid deficiency of these conventional non-renewable energy resources because they are not instantly replaceable. Once they are removed from their source and used by us they could not be immediately replaced as these deposits took millions of years to form. Assuming that there would be no increase in consumption over the years, it is quite apparent that we are heading towards an energy crisis. BP's "Statistical Review of World Energy" published the details of reservoirs of coal, natural gas and crude oil in the world and they are 892 billion tons, 186 trillion cubic meters, and 1688 billion barrels respectively [2]. These reserves will last for few decades. In the context of India according to BP statistical review report fossil fuel reserves are in critical status as shown in Table 1.1.

Table 1.1: Fossil fuel reservoirs status of India

Source	Reserves	Longevity
Coal	10 5820 MT	70 years
Oil	1200 MT	~ 10 years
Gas	1.5 TCM	~ 20 years

Further, the energy demands of India continue to rise due to the dynamic economic growth and modernization and there is a widening gap between the demand and supply of fossil fuel [3].

1.2   Problems and solutions related to renewable energy resources

Conventional resources of energy are non-renewable and they are not only in decreasing state, they are also responsible for environmental pollution. One problem is that the 7 billion tons of CO_2 is released per year by burning of fossil fuels, which results in global warming and greenhouse effect type of environmental issues [4]. Uranium, which is used for nuclear energy, does not cause CO_2 emission but the disposal of the radioactive nuclear waste is problematic. So, nuclear energy has always been subject of intensive public discussion due to the security and health risks of nuclear power stations and the problems with radioactive waste. All these sources are limited and at the same time the world energy demand is still increasing. Thus, the requirement of some inexpensive and largely available energy source has become an essential way to meet the energy crises. To overcome the problems associated with conventional sources of energy, nowadays the development of non-conventional renewable sources of energy producing technologies, i.e. technologies related to sources that are unlimited are gaining increased interest of researchers. Solar, biomass, wind, geothermal and hydropower are outstanding sources among non-conventional resources.

Solar energy is the most promising, cleanest and highly approachable resource within the renewable energy resources. Solar energy not only has high input to fulfill our energy demand but also its output could last 10 billion years [5]. Thermal and photovoltaics are two ways to utilize solar energy and for fulfillment of future large amount of electricity. Photovoltaic is a good alternative which represents the production of electricity directly from sunlight. Sunlight is available around the world and it supplies huge amount of energy through photovoltaics which could be used for meeting the total global electricity demand [6-7].

A solar cell is a device that produces electricity using the photovoltaic effect. Solar cells have advantages which make them suitable alternate sources for meeting energy demands and those are listed below:

- Solar cell is an autonomous source of energy which can be used in any dimension, from solar power plants in the Giga Watt (GW) range up to the small one in a calculator.

- This technology has long lifetime as it has no moving part.

- Installation and utilization of solar cells are easy with long operating lifetime. These factors remove the need of continuous maintenance.

- Centralized and non-centralized electricity supply is possible by photovoltaic system due to the modular nature of these systems.

Today, many government organizations as well as industries recognized the benefit of using solar power [7]. So, investments in this research area are increasing which will lead to increment in the progress of solar cell technology. Progress in this field will reduce the cost further and will make it competitive with conventional electricity in the near future. Solar energy will occupy more and more portions of the whole energy demand.

1.3   Solar radiation

The radiative surface of the sun, or photosphere, has an average temperature of around 5,800 Kelvin [8]. The Sun's solar radiation spectrum is impending of a black body of 5800 K and it consists of electromagnetic (EM) radiation across most of the electromagnetic range as shown in Figure 1.1. The electromagnetic radiation originating from the surface of sun consists of X-rays, ultraviolet, visible band, infrared, and radio waves. Sun spectrum retains most of EM radiation energy in the visible band and moderate amount of energy in UV region and IR bands. Radio, microwave, X-ray and gamma ray bands hold small amounts of energy.

The spectrum of nearly all solar electromagnetic radiation striking the Earth's atmosphere spans a range of 250 nm to 2500 mm. Solar irradiation could be measured in outer space or on the Earth's surface. Solar irradiation on earth's surface occurs after atmospheric absorption, diffusion and scattering. The solar constant is the power per unit area produced by the Sun in the form of electromagnetic radiation that is incident on a plane perpendicular to the rays, at a distance of one astronomical unit from the Sun. It also can be considered as flux density and roughly is equal to 1362 W/m² [9]. The energy emitted by the sun passes through space until it is intercepted by planets, other celestial objects, or interstellar gas and dust. The Air Mass (AM) is

the path length which light takes through the atmosphere, and is useful to quantify the reduction in the power of light when it is absorbed by the atmosphere. The Air Mass is defined as:

$$AM = \frac{L}{L_0} = \frac{1}{Cos\,Z} \tag{1.1}$$

Where L is path length through the atmosphere, L_0 is the zenith path length (i.e. normal to the Earth's surface) at sea level and Z is the zenith angle (relative to the normal to the Earth's surface) in degrees. The standard spectrum outside the Earth's atmosphere is called AM0, because the light does not overcome the atmosphere barrier. This spectrum is typically used to predict the expected performance of cells in space. When the sun is directly perpendicular to Earth surface, AM is 1. The standard spectrum at the Earth's surface is called AM1.5G, (the G stands for *global*): the AM1.5G spectrum (Z = 48.2°) has been normalized to give 1 kW/m2. This spectrum is the normalized flux used to measure the performance of cells in laboratories. These AM spectra are used as the standard testing condition for solar panels depending on where the solar panel will be used. For example, AM0 (which implies that there is no atmosphere) would be used for solar panels in space and AM1.5 is generally used for terrestrial solar panels.
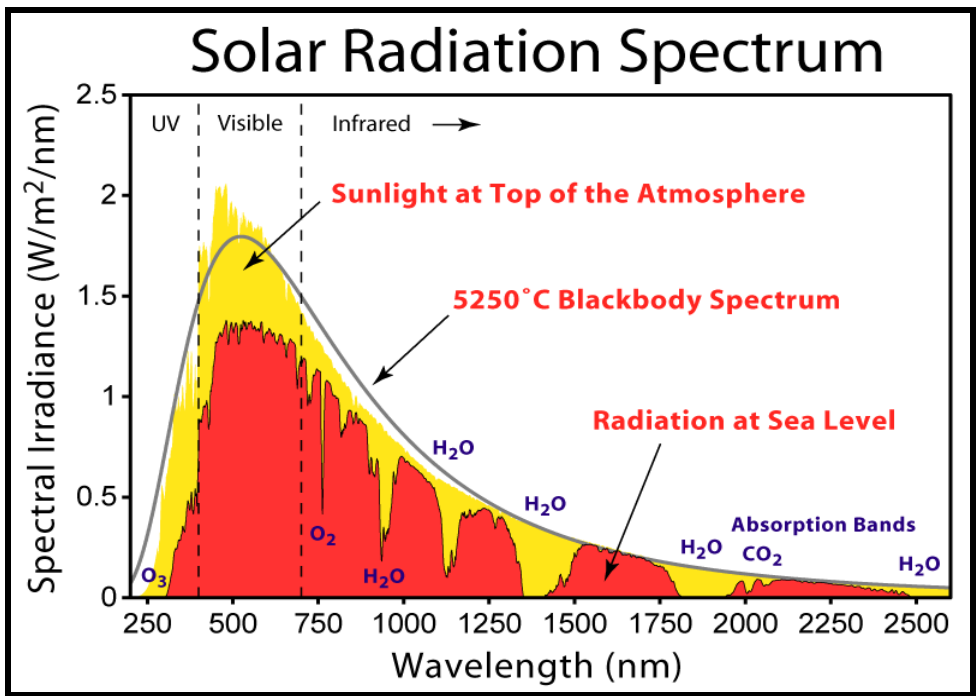
Figure 1.1: Spectral irradiance of the sun for various wavelengths [10].

1.4   **Photovoltaic effect**

In this phenomenon, separation of electron from the covalent bonds of zero-biased p-n junction in equilibrium occurs by the absorption of photons. These electrons will generate voltage by diffusing through the junction, until they recombine with a hole. Thus these photo generated electrons supply power to load through a circuit. So, photovoltaic effect is generating electrical power from solar radiation. As this effect is dependent on the absorption of photons, so it is required that for the separation of electron the incident photon energy must be equal or greater than the band gap of material.

In this effect, a pair of electron and hole is generated when a photon of *hυ* energy is absorbed having energy higher than the band gap of the semiconductor. This electron-hole pair should be separated by built-in electric field to avoid recombination and this field is provided by a p-n junction which is the main part of a photovoltaic device.

A photon contacting a semiconductor could be either reflected from the surface of the semiconductor, absorbed or transmitted throughout the semiconductor. If energy of the photon and the band gap of the semiconductor is E_{ph} & E_g respectively, then it is possible to determine if a photon is going to be absorbed or transmitted:

$E_{ph} < E_g$: Energy of photons is less than the band gap, photons are transmitted

$E_{ph} = E_g$: Energy of photons is equal to the band gap, photons are absorbed and can generate an electron hole pair.

$E_{ph} > E_g$: Photons with energy higher than the band gap are also absorbed.

In photovoltaic (PV) devices, reflected or transmitted photons are considered as a loss as they do not generate power. So, basically photovoltaic energy conversion consists following steps:

1.   Absorption process which transit material from ground state to an excited state.

2.   The conversion of the excited state into a charge carrier electron-hole,

3.   A transport mechanism results in the movement of negative-charge carriers to cathode and the positive-charge carriers to move to anode. These photogenerated negative-charge carriers reaching at the cathode produce

electrons. These electrons travel through an external path in the electrical circuit and lose their energy to an external load and finally they come back to the anode of the cell.

4.   At the anode, returning electrons combine with an arriving positive-charge, thereby returning the absorber to the ground state.

French physicists Edmond Becquerel first observed the photovoltaic effect in 1839. After that, first selenium-based solar cell (1883) was produced by an American engineer called Charles Fritts. The efficiency of Fritts's cell was less than 1% and due to the cost of gold contacts, it was not justified as a practical power source. For PV field, beginning of silicon technology was in 1954. Bell Labs discovered that a silicon p-n junction could convert 6% of the incoming sunlight into electrical energy. Further in 1960, efficiency for silicon solar cells was increased to 14%, and in the following five decades, the global PV production has reached over 368 GW [11]. Over other energy technologies, direct conversion of solar energy into electricity by a photovoltaic technology delivers various technological advantages. It is one of the most inviting forthcoming technologies, as these systems are easy to install, require low maintenance and environmentally harmless in their operation. Most commonly used electroluminescence device that converts the sun's energy into electrical by using the photovoltaic effect is solar cell. Generally, solar cells are p-n junctions, and due to their "built-in" electric field at the junction they can generate current and voltage. So, solar cell is basically a semiconducting device capable of developing very low voltages and current density depending on the material used and sunlight conditions.

1.5   Working principle of solar cell

1.5.1   Concept of energy band gap

In an atom every electron has its own discrete energy level governed by Pauli Exclusion Principle. In case of crystal due to the large number of atoms, electrons interact with each other and energies of these electrons may change. So, the identical energies in the isolated atom spread out and form quasi continuous energy band. Energy band related to different energy levels are separated by band gaps or energy gaps. The electrons in a crystal occupy lowest energy level first and higher energy levels fills afterwards. The level occupied by last electron is called Fermi energy or

Fermi level. Although there are many bands but only the surrounding bands of Fermi level are important. At zero temperature, highest band where electrons are present is called valence band. The next band above the valence band is called conduction band [12].

On the basis of energy band gap E_g, material can be characterized as insulator [E_g > 6 eV], conductor [E_g = 0] or semiconductor [E_g = 0.6 -5 eV]. Thai is if the energy gap between conduction band and valence band is large, then this indicates to an insulator. When these band overlap with each other, it is called conductor. A semiconductor has band gap in the range 0.6-5 eV and is intrinsic when it's all four bonds are completely filled. Silicon is a tetravalent element, so every atom has four bindings. In intrinsic silicon crystal, at room temperature number of electrons is less in the conduction band. Charge carrier density could be increased by doping of III and V group elements in intrinsic semiconductor. In the lattice of silicon, a pentavalent atom e.g. phosphor or arsenic replace a silicon atom, then one electron is not able to construct a covalent bond. This electron is very weakly bonded, so small amount of energy is sufficient to discard this electron from its atom. This type of doping is adduced as n-type doping as this electron (negative charge) work as a charge carrier and doping atoms are called donors.
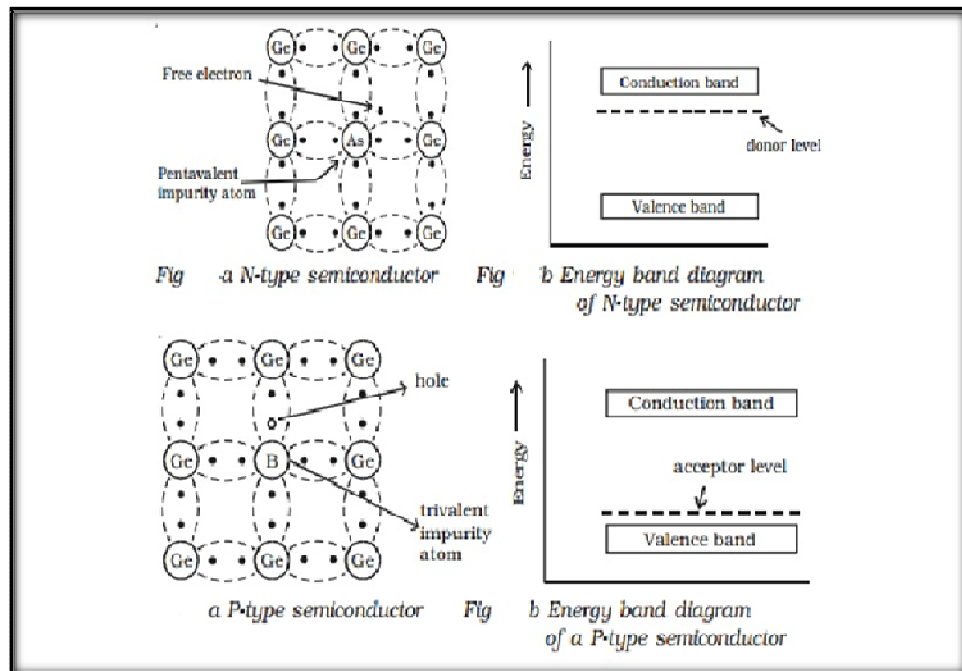
Figure 1.2: Crystal structure and energy band diagram of p and n type semiconductors [13].

On the other hand, if a silicon atom is substituted by trivalent element, one electron is shorter to form four bonds and vacancy is called *hole*. Doped atom is called *acceptor*, because it can acquire one more electron. This type of doping, with quasi free positive charges (holes) is called p-type doping.

1.5.2 Concept of p-n junction

In a p-n junction, p-type semiconductor and n-type semiconductor have high concentration of holes and electrons respectively. In case of homo-junction or heterojunction a p-n junction is formed when n-type and p-type semiconductors are put in contact with each other in such a way that allows flow of charge carriers. Once the two semiconductors are in contact, near the junction interface electrons from the n- region diffuse in the p-region and holes diffuse from p-region to n- region due to the concentration gradients and leave behind positive and negative ions respectively [14]. This phenomenon is called *"diffusion"*. Diffusion leads to creation of *space charge region* or *depletion region* at equilibrium nearby the p–n interface, as it is depleted of free carriers. The consequence of the formation of the space charge region is that positive and negative ions create an electric field which fights the diffusion for both electrons and holes and leads to drift of electrons and holes until the diffusions are canceled out. This phenomenon is called *"drift"*. So, in equilibrium condition there are two currents in the p-n junction. One is *diffusion current* or *forward current* and another is *drift current* or *reverse current*. In case of equilibrium, these two currents are identical to each other. An energy state diagram of p-n junction under equilibrium condition is shown in Figure 1.3.

When voltage is enforced to p-n junction, current can flow as there is no equilibrium anymore due to the modifications to the built-in potential barrier and to the width of the depletion region as there is an external electrical field added with existing one. There are two situations possible depending on how that voltage is applied: if the positive potential is connected to the p side (forward bias) then potential barrier and width both will decrease, on the other hand if negative terminal is at the p- side (reverse bias) their values will increase [14]. A p-n junction under non-equilibrium condition is shown as Figure 1.4.
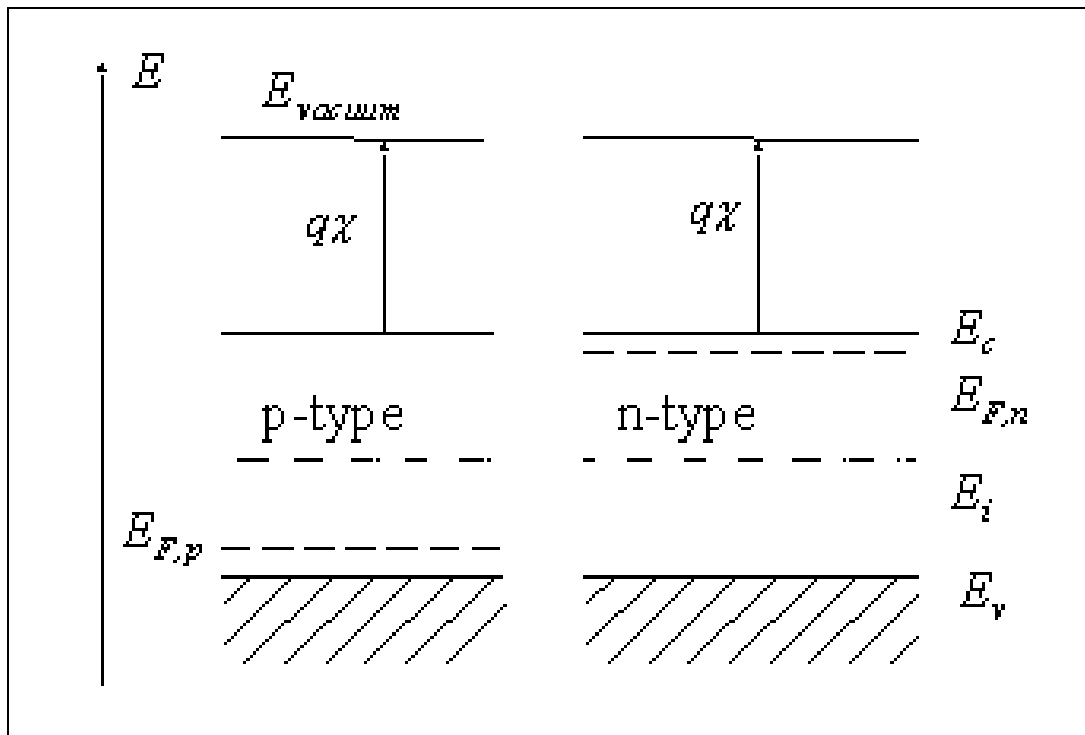
Figure 1.3: Energy state diagram of a p-n junction under equilibrium condition [13].
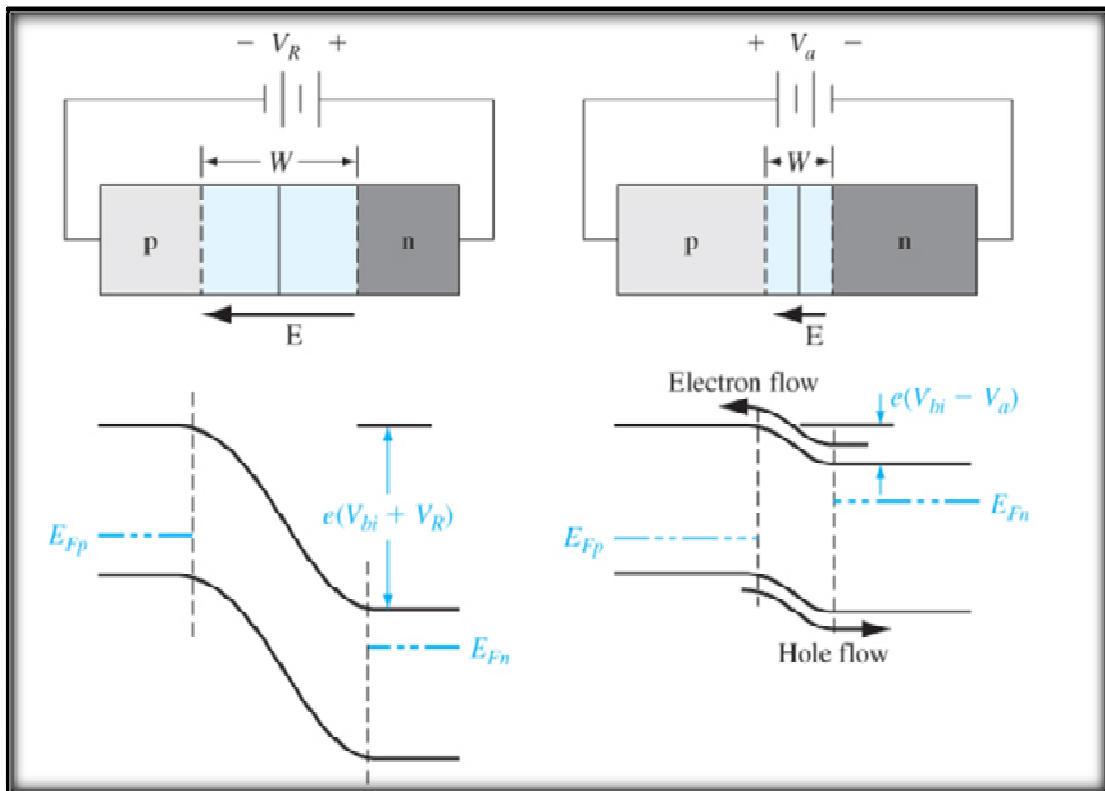
Figure 1.4: p-n junction under non-equilibrium condition [13].

1.5.3   **p-n** *junction as solar cell*

A solar cell is a p-n junction and when a p-n junction reaches a steady state condition or equilibrium, it is charge neutral but has a built-in electric field. This built in electric field is the key for obtaining usable electricity from solar radiation which is incident on the junction.

When a p-n junction is exposed to photons of light, light give appropriate energy to excite an electron from the valence band to the conduction band. Thus by absorption of a photon an electron-hole pair is created. At the p-n junction the built-in electric field works in such a way that this pair is separated by the down flow of electron across the potential gradient while the hole flows up it and create a current under steady state illumination. To extract usable electrical power from the junction a load is placed between these two charge carriers [15]. It is important to note that only photons with energy above the band gap of the absorbing material will excite electron-hole pairs and any photons with energy below the band gap will not be utilized by the solar cell.

A practical solar cell is more complicated than simple p-n junction and the equivalent circuit of solar cell is shown in Figure 1.5.
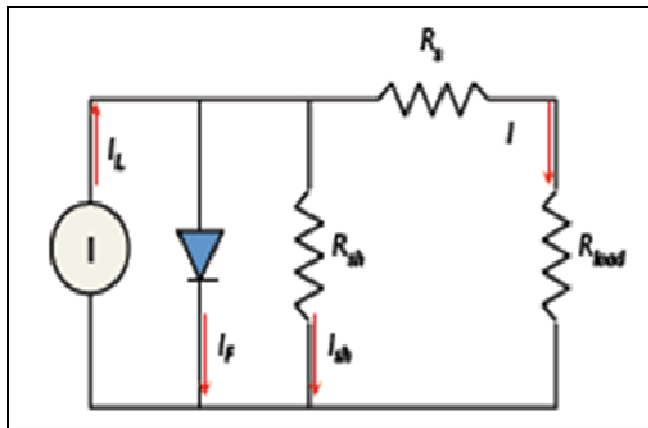
Figure 1.5: The equivalent circuit of solar cells.

This circuit consists of:
1.   A diode which represents the p-n junction (or heterojunction).
2.   A current source which represents the current generated due to incident light.
3.   A shunt resistor (R_{sh}) represents shunting paths in the solar cell for current to leak through.

4.   A series resistor (R_s), which represents resistance in the electrodes and contacts to the cell.

5.   A load resistor (R_{load}) which is used to dissipate the power from the solar cell.

We can then develop an equation for the current flowing through the load resistor, using this circuit by subtracting out the current flowing through the diode and the shunt resistor from the current generated by the light. This is given as equation 1.1:

$$I = I_L - I_D - I_{sh} \tag{1.2}$$

Where, I is the current drawing through the load resistor. I_L is the current caused due to incident light. I_D is the current flowing through the diode and I_{sh} is the current flowing through the shunt resistor.

1.5.4 I-V Characteristics under illumination

Current voltage measurements (I-V) characteristics are the primary way to characterize and evaluate the performance of a solar cell. A typical I-V characteristic of a solar cell under dark and illumination is shown in Figure 1.6.
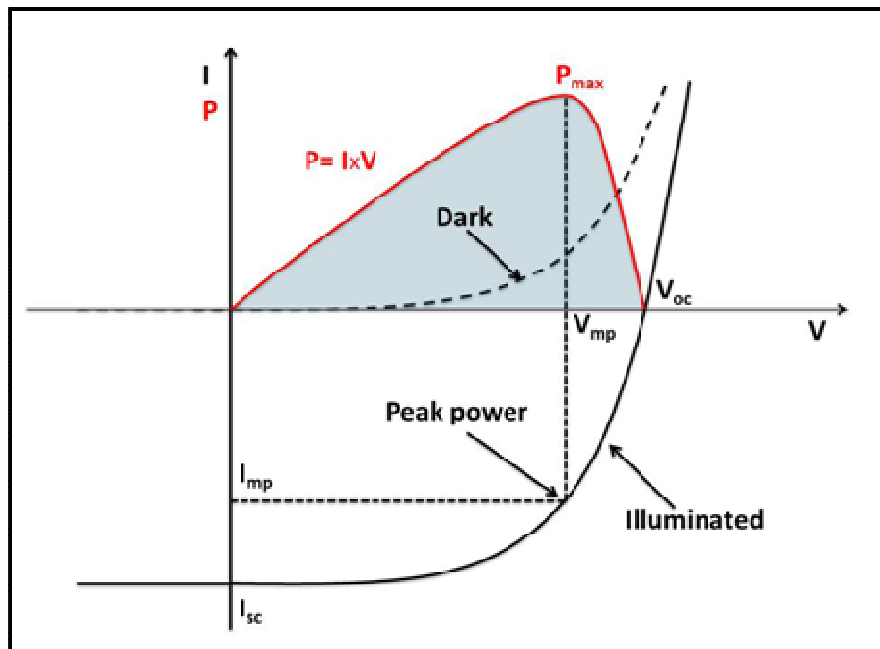
Figure 1.6: I-V curve of a solar cell under dark and illumination condition.

When a solar cell is illuminated, a photogenerated current (I_L) is generated due to creation of additional electron-hole pairs. By analyzing the I-V characteristics

curve, it could be concluded that I_L has the effect of shifting down the curve into the fourth quadrant [16]. For an ideal solar cell under illumination condition, the measured current is the sum of the photocurrent (I_L) with the junction's dark current, so the output current becomes:

$$I = I_0 \left(e^{\frac{qV}{kT}} - 1 \right) - I_L \tag{1.3}$$

1.5.5 Electrical parameters of a solar cell

For calculation of the performance of a solar cell one has to consider its I-V characteristics. By analyzing the referred curve, we can determine some important solar cell parameters like short circuit current (I_{SC}), open circuit voltage (V_{OC}), fill factor (FF), maximum power point (P_{max}) and most important of all efficiency (η).

Short-circuit current

Short-circuit current (I_{SC}) defined as the current through the solar cell when the terminals are in short circuit. So, I_{SC} is the maximum current solar cell is capable of producing when voltage across the solar cell is zero. It is one of the figures of merit of a solar cell. The light intensity, optical properties of the cell, thickness of the p-n junction and the collection probability are the typical factors influencing I_{SC} [17]. On the other hand, it is related to the developed photocurrent and as minority carrier drifts increases with temperature, so it is positively changed by a temperature increase.

Open-circuit voltage

Open-circuit voltage (V_{OC}) is the voltage at the output when no load is connected. So, V_{OC} is the maximum voltage the solar cell can produce at zero current. Voc variations depend on the amount of recombination in the solar cell as V_{OC} depends on I_0 and variations of I_0 depend on recombination inside the solar cell.

Maximum voltage and maximum current

Maximum voltage (V_m) and maximum current (I_m) are two parameters, whose values give the maximum power point P_m. The maximum power point is value along the curve where the solar cell produces the most power.

Fill factor

The fill factor (FF) is an important figure of merit in case of solar cell. The fill factor is a measure of the "squareness" of the curve and is defined as the ratio between the square drawn by the maximum power point ($P_m = V_m \times I_m$), and the square given by the product $V_{OC} \times I_{SC}$ as shown in equation:

$$FF = \frac{P_m}{V_{OC} \times I_{SC}} \qquad (1.4)$$

An ideal solar cell has a value of FF as closer as possible to unity. FF increases along with V_m and I_m as they approach towards respectively V_{OC} and I_{SC}. In that case, it is mandatory to decrease the losses due to parasitic resistances inside the solar cell. As the temperature increase, fill factor can be expected to diminish since the V_{OC} decreases with temperature.

Power conversion efficiency

Efficiency is a measure of conversion of the power of sunlight into usable electrical power by a solar cell. It also allows comparing solar cells with each other since it is independent of any convoluting factors. It is represented as the ratio between the generated electrical power (P_m) and the solar energy (P_{IN}) to which the cell is exposed.

$$\eta = \frac{P_m}{P_{IN}} = \frac{V_{OC} \times I_{SC} \times FF}{P_{IN}} \qquad (1.5)$$

Power Conversion Efficiency depends on several parameters such as the intensity of the incident sunlight, the type of solar spectrum, the working temperature of the solar cell. Typical measurement setup for terrestrial solar cells is at a temperature of 25°C with an AM1.5G.

1.5.6 Losses in solar cells

Efficiency or output of a solar cell is reduced by several losses, these could be described below.

1.   **Electrical losses**

In the equation for an ideal solar cell, series (R_S) and shunt resistances (R_{SH}) are not taken into account but they are present in real solar cells. The effects of these parasitic resistances are lead to decrement in the FF of the cells.

Series Resistance

Series Resistance (R_S) variation mainly arises due to the internal resistance of the materials or the resistance of the bulk of the semiconductor material i.e. front and backs contacts, and the resistance at the interface of the different layers [17]. High values of R_S may reduce the I_{SC}, but does not affect V_{OC}.
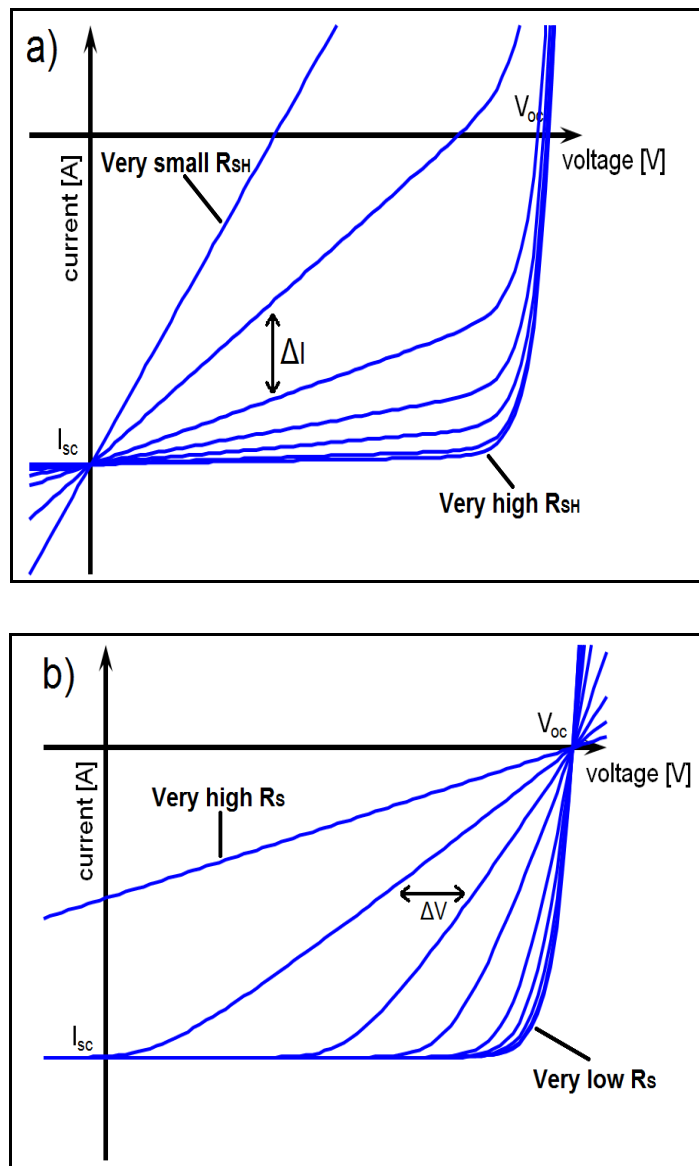
Figure 1.7: Impact of a) R_{SH} and b) R_S on photovoltaic characteristics under illumination.

Shunt resistance

Shunt resistance (R_{SH}) is generated from short circuits beyond the p-n-junction and provide alternative paths for current to flow. Variations in R_{SH} could be due to a non-perfect interface between the doped regions and the metal contacts and various types of defects (crystal defects, impurities and precipitates). Decrement in the value of FF arises due to this parallel resistance and decrease the efficiency of a cell. Loss in the value of V_{OC} is found for very low R_{SH} value.

Value of FF is decreased by both resistances as shown in Figure 1.7 [18]. Contrary to Series Resistance R_S, R_{SH} must be as high as possible in order to prevent lost in V_{OC} [19].

2.   Optical losses

Apart from electrical losses there are other types of losses, which affect the efficiency of solar cell. These losses are related to inability of photons to produce electron-hole-pairs in the cell. Due to these losses, charge carriers produced cannot contribute and reduce the current I_{SC}. These losses could be summarized as below.

*   *Reflection*: A black material does not reflect light, but as solar cell is not completely black, some light will always be reflected. The glass coating on modules also reflects light as well.

*   *Shading*: Metal grid on top of solar cell as a contact and other upper layer coatings like TCO shade the operating area of the cell between 5 and 15% [20]. Further frames and interconnect zones in a module lead to more area losses.

*   *Transmission*: Photons with long wavelengths are transmitted directly without producing electron-hole-pairs.

3.   Recombination

In the solar cell, imperfections, defects and impurity atoms work as localized recombination sources. Recombination sources are the points where electron-hole recombine and emit a photon. This effect reduces I_{SC} and also has an impact on the voltage V_{OC}, as lower the recombination is higher the voltage V_{OC}.

4.   Thermalization

Photons that have energy greater than the band gap of material not only produce charge carrier, but also give extra energy as by-product. This process heats up the device and reduces the efficiency.

Thermalization and transmission present an optimization problem. Value of band gap should be as much as possible for diminished thermalization. On the contrary, low band gap would be desirable for collection of more photons. Therefore, the optimum band gap for good theoretical efficiency is around 1.4-1.5 eV [20].

1.6   Types of PV technology

There are several different approaches to making of solar cells and dozens of variations of solar cells, but the two most common types are silicon based solar cells and use of thin film technology in their making.

1.6.1   Crystalline silicon

Silicon based solar cells are first generation solar cell, so they are the oldest, but it is still most common material used for solar cells. Silicon solar cells are further categorized as monocrystalline silicon solar cell and polycrystalline silicon solar cell.

Monocrystalline silicon solar cell

Monocrystalline silicon also called single-crystalline silicon, have the highest efficiency as they are made out of the highest-grade silicon and a record-breaking efficiency (21.5%) has been reported [21]. When compared to thin-film solar panels, monocrystalline solar panels give up to four times more electricity. At low-light conditions, performance of monocrystalline solar panels is better than other solar panels. Compared to any other types these panels give better power outputs because they require the least amount of space. Life time of monocrystalline solar panels is the longest with 25-year warranty.

But monocrystalline solar panels have some disadvantage such as: they are the most expensive and if the solar panel is partially under influence of shade or dirt, the entire circuit can break down. Monocrystalline silicon solar panels are produced by Czochralski process. Monocrystalline solar panels tend to be more efficient also in certain weather conditions.

Polycrystalline silicon solar cell

The solar panels based on polycrystalline silicon, which also is known as polysilicon (p-Si) and multi-crystalline silicon (mc-Si) do not use the Czochralski process. The process is simple and less expensive as well as waste silicon amount is less compared to monocrystalline. Due to the lower silicon purity, polycrystalline solar panels are not quite as efficient as monocrystalline solar panels and result in lower efficiency.

1.6.2 Thin film solar cells

This is second generation solar technology which was developed due to scarcity and cost of material used for silicon solar cells. Thin film solar cell also known as thin film photovoltaic (TFPV) technology are manufactured by deposition of thin layer/layers of photovoltaic material onto a substrate such as glass, plastic or metal. Crystalline silicon solar cell uses wafers of up to 200 µm while in TFPV technology film thickness are of few nanometers (nm) to tens of micrometers (µm), This fact induces flexibility and low weight in solar cell [22]. TFPV cells also have following features, which make them interesting option for solar cells.

i. Several sophisticated and simple techniques (physical, chemical and hybrid techniques) are available for deposition of thin-films and their mass production is easy.

ii. It minimizes the quantity of required material by utilization of materials that have high absorption coefficient which allow absorbing the majority of the solar spectrum using only few microns of materials. This makes them cheaper to manufacture than crystalline-based solar cells.

iii. In a thin film solar cell desired properties like band gap, composition, lattice constants and other optoelectronic properties can be obtained by different types of electronic junctions i.e. single and tandem junctions.

iv. Surfaces and interfaces modification can be done by post treatment for achievement of desired optical characteristics and other properties.

v. Different shapes, sizes, areas and substrates are available and flexibility is also achievable.

vi. Thin-film processes are generally eco-friendly and green and sometimes energy requirement for deposition and installation process are simpler then that required for silicon based solar cell [23].

vii. High temperatures and shading have less impact on solar panel performance.

Thin-film technology is cheaper but efficiency is lower than conventional Silicon technology. However, research in this field has significantly improved efficiency over the years. Recently, thin film technology has achieved significant growth. Approximately 8% of the global PV market was acquired by thin film technology in 2013 [24].

The thin film solar cells can be assorted by these different types on the basis of photovoltaic material:

- Amorphous silicon (a-Si)
- Chalcogenide-based solar cells

  ➢ Cadmium telluride (CdTe)

  ➢ Copper indium gallium selenide (CIGS)

1.6.2.1 Amorphous silicon (a-Si) solar sells

Amorphous silicon is a noncrystalline semiconductor in which the lattice structure of crystalline silicon is exterminated, and this changes the absorbance characteristics of the material. This is an abundant, non-toxic material and requires a low processing temperature and little silicon material is required. Amorphous silicon absorbs a very broad range of the light spectrum due to its band gap of 1.7 eV. Its basic electronic structure is the p-i-n junction which consists of very thin p-type and n-type layers and a thicker intrinsic layer where the majority of the light is absorbed. The p-type layer should be placed at the top where the light intensity is stronger, so that the majority of the charge carriers crossing the junction are electrons.

Manufacturing technique for amorphous silicon is called stacking. Silicon used in amorphous silicon solar cells is only 1% of the silicon required in crystalline silicon solar cells [25-26]. Amorphous silicon cells suffer from low efficiencies and there is a significant drop of about 10% to 30% in efficiency during the first six months of operation and this is further degraded (by about 20% of the initial value) when the cell is placed in sunlight for a long period of time [27]. On the other hand, creating multilayer stacks increases the complexity of the production process and as a result, this significantly makes them more expensive.

1.6.2.2 Chalcogenide-based solar cells

In this thin film solar cell category, $Cu(In,Ga)Se_2$ (CIGS), CdTe and $Cu_2ZnSn(S,Se)_4$ (CZTSSe) are the main candidates with potentially reduced manufacturing cost of solar energy. Compound semiconductor based solar cells are currently being commercialized using this technology: cadmium telluride (CdTe) and copper indium gallium selenide (CIGS).

Cadmium telluride (CdTe) solar cell

Cadmium telluride (CdTe) solar cells are based on the use of a thin semiconductor layer of cadmium telluride, developed to absorb and convert sunlight into electricity. Typical CdTe solar cells are manufactured in the superstrate configuration i.e. starting from a transparent glass and followed by the successive deposition of TCO, CdS buffer (n-type layer), CdTe absorber (p-type), back contact [28]. Cadmium telluride PV has the smallest carbon footprint, lowest water use and shortest energy payback time of all solar technologies with lower costs than conventional crystalline silicon solar cells [29-32]. The efficiency of solar panels based on cadmium telluride is found to be 17.3% [33]. CdTe has band gap of 1.45 eV and high absorption coefficient [34-36]. In case of CdTe Solar Cell toxicity of cadmium is an environmental concern [37-38]. Another limiting factor is use of telluride which is anionic form of rare material tellurium [39].

Copper indium gallium selenide (CIGS) solar cell

A copper indium gallium selenide (CIGS) solar cell is a thin-film solar cell for converting sunlight into electric power by using a thin layer of copper, indium, gallium and selenide on glass or plastic substrate having electrodes on the front and back to collect current. CIGS has a high absorption coefficient and strongly absorbs sunlight, thus thinner film is sufficient than of other semiconductor materials. Traditional methods of manufacturing involve vacuum processes including co-evaporation and sputtering. A CIGS is one of three mainstream thin-film PV technologies. The other two are cadmium telluride and amorphous silicon. CIGS layers are thin enough to be flexible, allowing them to be deposited on flexible substrates. The compound semiconductors CIGS based thin film solar cell has reached at the stage of fulfillment of commercialization requirements with efficiencies of 20.3% [40].

CdTe and CIGS solar cells are the commercially available in the market, but there are some significant disadvantages of these technologies. Tellurium which is used in anionic form as a telluride in CdTe based PV technology is by far the least abundant material in the earth's crust (10^{-3} ppm) and has one of the highest costs. In case of CIGS, Indium and Gallium are reasonably abundant (0.9ppm and 30ppm respectively) but there are the two most expensive elements [41]. Elements In, Ga, Se, Te used in thin film solar cells are produced primarily as by-products of other metals in mining operations such as copper and zinc, thus limiting manufacturing and commercialization of these solar cells due to production constraints [42]. Mass production of CdTe solar cells raises concerns due to the use of toxic element Cd and has been restricted by the European Union and China [43].

So, thin film photovoltaics face two difficult challenges: (i) to compete with silicon based PV in terms of power conversion efficiency and manufacturing costs and (ii) to contain only earth-abundant and non-toxic materials without severe degradation in the long term.

Copper zinc tin sulphide (Cu_2ZnSnS_4) solar cell

Nowadays, many researchers are trying to develop an earth-abundant and non-toxic material for solar cell technology. Cu_2ZnSnS_4 (CZTS) appears to be a very attractive and highly potential material for overcome those limitations [44-46]. CZTS is applied as a chalcogenide absorber in solar cells, as it is constituted from low-cost and non-toxic earth-abundant raw materials, and shows high-efficiency potential for the near future [47].

1.7   Objective of the present work

CZTS was derived by substituting the rare group III elements two 'In' or one 'In' and one 'Ga' atoms in the crystal structure of CIGS by one 'Zn' and one 'Sn' atom. Direct band gap and processing techniques are common between CZTS and CIGS. According to Shockley-Queisser limit CZTS solar cells are expected to have theoretical conversion efficiency of 32.2% [48]. In laboratory cells, recent material improvements have increased efficiency above 10% for CZTS [49]. So, more work is required for making them commercially viable. Although this is less efficient than the other technologies, but by utilizing less expensive materials and large scale

processing it could prove to be a cost effective solution in future technologies. Main objectives as envisaged for this study are as follows:

➢ To grow/synthesize the nanostructured CZTS thin films on glass or ITO substrates by using chemical bath deposition (CBD) method.

➢ To study the physical properties (surface morphological, optical and electrical properties.) of as-deposited and modified CZTS thin films. The surface modification of as-deposited thin film to be done through annealing.

➢ To characterize the as–deposited and annealed CZTS thin films for structural information by XRD, for surface morphology by SEM and AFM for band gap by spectrophotometer.

➢ To use CZTS thin films as absorber layer and synthesize ZnS/CZTS thin film heterojunction on ITO-coated glass substrate..

➢ To study I-V characteristics of glass-ITO/CZTS/ZnS/Ag under dark and illumination condition.

➢ To assess the feasibility for device making in terms of efficiency of CZTS material as solar cell in nanostructure form.

CHAPTER 2

LITERATURE REVIEW

2.1 Introduction

There has been considerable interest in the synthesis of Cu_2ZnSnS_4 (CZTS) quaternary compound semiconductor materials because of their technological and fundamental importance. The surface/interface and electrical properties of CZTS thin film based solar cells depend on its chemical and physical characteristics, which are strongly dependent on preparation methods, grain size and post annealing treatments.

2.2 International status

The research in thin film solar cells world over has been dominated by light absorber materials based on CdTe and $Cu(In,Ga)Se_2$ (CIGS) in the last several decades. The concerns of environment impact of cadmium and the limited availability of indium in those materials have driven the research at international level towards developing new substitute light absorbers made from earth abundant, environment benign materials. Recently, Cu_2ZnSnS_4 (CZTS) semiconductor material has emerged as one of the most promising candidates for this aim and has attracted considerable worldwide interest in these recently.

It is worthwhile to mention here that it was Ito and Nakazawa who gave the recognition of the photovoltaic effect of CZTS material in 1988 [50]. They fabricated a hetro-junction of CZTS and cadmium tin oxide thin films on stainless steel substrates. The CZTS thin film used in the study was grown by argon ion beam sputtering from pressed targets of CZTS and the device gave an open circuit voltage of 165 mV. They obtained the band gap of CZTS to be 1.45 eV, an optimum value for the photo-absorber layer of a single junction solar cell. Further, best energy

conversion efficiency produced by the cells was 2.3% as reported by Friedlmeier et al. in 1997 [51]. However, significant progress in this relatively new research area has been achieved in the last five years. The research highlights of research group in other countries involved in research on solar cell application of CZTS material are briefly mentioned below.

Katagiri's group is actively involved in the research field of CZTS thin film for solar cell applications [52-59]. In 1997, they published the first device characteristics of a CZTS thin film solar cell having the structure ZnO:Al/CdS/CZTS/ Mo/SLG. They found the open circuit voltage of ~400 mV and an efficiency of 0.66% [54]. This research group reported synthesis of CZTS solar cell with 2.63% power conversion efficiency in [55]. The efficiency of the solar cells was increased to 5.45% by optimization of parameters in sulfurization process in 2003 [56], and then to 6.7% in 2008 [57]. This group also reported two review papers in 2005 and in 2009, respectively regarding the CZTS-based thin film solar cells [58-59].

J.J. Scragg et al. reported [60-63] synthesis of CZTS thin film solar cell by electrodeposition method. Through modification of the stacking order they achieved energy conversion efficiency of 3.2% [62]. They also compared the effect of annealing in different gaseous atmospheres and found that H_2S containing atmosphere is better compared to the sulphur containing environment for enhanced crystallinity of the films [63].

K. Moriya et al. reported conventional electrodeposition approach for the fabrication of CZTS films and they reported that the pH value of the precursor solution had little influence on the composition of the film [64]. They also fabricated CZTS light absorber layer for thin film solar cells by vacuum-based pulsed laser deposition technique and obtained an efficiency of 1.74% [65-66].

K. Tanaka et al. employed spin-coating of a sol-gel precursor solution to synthesize CZTS thin films [67]. Efficiency of 1.01% was shown by CZTS solar cells which were fabricated by the non-vacuum methods [68]. Films made from the precursor solution with copper poor films (Cu/(Zn+Sn)) were found having large grains and larger band gap energy compared to the copper-rich films. The solar cell exhibited an efficiency of 2.03% [69]. S.Y. Chen et al. used DFT-based first principal

calculation for achieving thermodynamic stability and studied the defect mechanism of CZTS material [70-71].

In addition to the above predominant groups, there are some recent reports also in the literature on research work on CZTS materials for solar cell applications which are briefly mentioned below.

F. Y. Liu et al. reported CZTS films with a high light absorption coefficient (>105 cm−1) and further characterization showed that the carrier concentration of the films was in the order of 10^{18} cm^{-3} [72]. Similar approach was also explored by Momose et al. for the fabrication of CZTS thin films and found an efficiency of 3.7% of CZTS thin film solar cell [73].

Todorov et al. prepared a CZTS precursor which was based on hydrazine-based particle-solution slurry consisting of Cu, Zn, Sn, and S elements. The CZTS films or partly selenized CZTS (CZTSSe) thin films were obtained by annealing the precursor films in sulphur or sulfoselenide containing atmosphere at 540◦C. The films showed large grains and uniform composition. The best cell efficiency was 9.66% which was obtained with the CZTSSe based solar cells [49].

Kameyama et al. studied the effect of the reaction temperature in the hot-injection process on the formation of CZTS nanocrystals. They found that a single-phase CZTS was formed at temperature over 240◦C [74]. In contrast, CZTS nanocrystals which were annealed in Se vapour at 500°C for 15 min. showed an enhanced grain growth. The thin film solar cells using the CZTSSe light absorber showed an energy conversion efficiency of 7.2%, and the cell did not show significant degradation in a one-month light soaking test [75-76]. X. T. Lu et al. synthesized CZTS nanocrystals with wurtzite phase and found a new hexagonal structure which indicated energy band gap 1.4 eV [77]. Thomas Rath et al. reported a fast and simple method for the preparation of stoichiometric CZTS and CZTSe nanoparticles. The prepared nanoparticles exhibit diameters between 7 and 35 nm [78].

Fischereder et al. proposed a pyridine-based solution to prepare the CZTS thin films, which is again a toxic solvent [79]. Ki et al. synthesized CZTS films by using dimethyl sulfoxide (DMSO)-based and methanol-based solutions of Cu, Zn, Sn salts

and thiourea [47]. However, thiourea tended to form organic by-products that were present at relatively high annealing temperature of 380^{0}C [80]. Sun et al. devised an alcohol based homogenous solution, which is non-toxic and is expected to reduce the carbon content. They used a simple technique of multiple dip coating to grow the films [81]. To study the effect of alkali atoms, Tong et al. doped the CZTS thin films with potassium [82]. They prepared the CZTS thin films using spin coating of a precursor solution from metal acetate and thiourea in the solvent of methanol and ethanoldiamine. Compared to the undoped films, doping of 1% potassium improved the efficiency from 2.94% to 3.34%. Park et al. developed a non-toxic solvent based method for fabrication of CZTS thin films without producing a carbon interlayer [83]. Nguyen et al. prepared CZTS thin films by spin coating of a precursor solution formed from metal chloride and Thiourea in water and ethanol followed by sulfurization using a two-zone tube furnace [84].

Cao et al. prepared CZTS films from a single step CBD deposition of precursor film followed by sulfurization. Firstly, $CuSO_4.5H_2O$, $ZnCl_2.2H_2O$, $SnCl_2$ and deionized water were mixed and stirred for 5-8 min. to get clear and homogenous solutions, followed by adding C_2H_5NS, Na_2EDTA and H_2NCONH_2 into the above solutions. Finally, the pH value of the solutions was adjusted by adding diluted HCl or NaOH However; they got an efficiency of only 0.30% [85].

Liu et al. fabricated ZnO/CdS/CZTS p-n heterostructure NR arrays by the CBD process. The precursor solution for CZTS was prepared by dissolving analytically pure $Cu(CH_3COO)_2.H_2O$, $ZnCl_2$, $SnCl_2.H_2O$ and thiourea into dimethyl sulfoxide while stirring at room temperature until a clear solution was formed. Then, the substrate with ZnO/CdS core/sheath arrays was dipped into the above precursor solution for a few minutes and followed by annealing in N_2 atmosphere at 420^{0}C for 20 minutes [86].

Li et al. reported that CZTS thin film can be successfully prepared by sulpherization of the stacked precursor layers which were grown by the CBD process. The deposition sequence of the precursor layers was in the order of ZnS/Cu/SnS on Mo-coated glass substrates. The efficiency of the best performance CZTS based thin film solar cells was 2.2% [87].

2.3   National status

There are many groups working in the field of CZTS photovoltaic material for solar cell applications at national level.

B. S. Pawar et. al investigated the effect of annealing in different atmospheres. The results showed that energy band gap red shifted between 1.50 and 1.55 eV at various annealing condition which perfectly matches the solar energy spectrum [88]. They also considered the impact of the complexing agent tri-sodium on the crystallinity of the films [89].

A V Moholkar et. al synthesized and characterized Cu_2ZnSnS_4 thin films solar cells grown by PLD. The energy band gap is about 1.54 eV, which suggests its application as an absorber layer [90] .They also investigated the influence of pulse repetition for as-deposited and annealed thin films. The performance of solar cell based on CZTS absorber layer was tested and the efficiency is about 2% [91].

Sawanta S. Mali et al synthesized the non-toxic Cu_2ZnSnS_4 (CZTS) thin films by successive ionic layer adsorption and reaction (SILAR) [92]. They reported an efficiency of 0.396%. Later they reported an increased efficiency of 1.85% from the CZTS films grown by the same process. [93].

Y. B. Kishore Kumar et. al prepared and characterized spray-deposited Cu_2ZnSnS_4 thin films and results showed that better crystallinity could be obtained for substrate temperatures in the range 643–683K. [94]. They also studied the effect of starting-solution pH on the growth of Cu_2ZnSnS_4 thin films deposited by spray pyrolysis and reported that the good crystallinity of CZTS material was obtained with the precursor solution having pH = 4.5 [95].

V. G. Rajeshmon et. al fabricated Cu_2ZnSnS_4 thin film solar cell using CZTS as absorber layer and In_2S_3 as buffer layer and the cell exhibited an open circuit voltage of 430 mV, a short circuit current density of 8.02 mA/cm2, a fill factor of 45% and a conversion efficiency of 1.5% [96]. Recently, N. M. Shinde et al. reported a novel chemical route method for the deposition of CZTS thin films. They prepared CZTS thin films by the CBD process using a single precursor solution prepared from $CuCl$, $ZnCl_2$, $SnCl_4$ and $Na_2S_2O_3$. This method is anticipated to have the advantages

of being low cost and capable of producing large-area films. The effect of post-annealing treatment and the photovoltaic activity of the CZTS film are tested in polyiodide electrolyte [97]. They also used the SILAR technique to prepare the films from the cationic precursor solutions of CuCl, ZnSO$_4$ and SnCl$_4$ and anionic precursor solution of thioacetamide [98].

Maheswari and Kumar synthesized the CZTS thin films by the CBD process from solutions of metal chlorides and Thiourea in ethylene glycol. They studied the influence of annealing temperature and observed a phase transformation from tetragonal to orthorhombic kesterite structure [99]. Subramaniam et al. used metal nitrates and tiourea in methanol to prepare CZTS thin films on ITO coated glass substrates by the CBD process. They used monoethanolamine (MEA) as a stabilizer to prevent the formation of precipitates. They report an efficiency of 1.34% [100].

In the above paragraphs an attempt was made to present some of the major highlights of research work being done on CZTS based solar cells. In fact, CZTS has become an important material for solar research application and more publications on various aspects of this material are likely to be reported from various research groups worldwide.

CHAPTER 3

MATERIALS AND METHODS

3.1   Cu₂ZnSnS₄ (CZTS)

Quaternary Cu_2ZnSnS_4 (CZTS) thin films display an interesting set of wide range of properties such as p-type conductivity, a suitable direct energy band gap of 1.4–1.6 eV, while ideal value is 1.4 eV [101] and large absorption coefficient over 10^4 cm^{-1} for absorption of light in few micrometer [50]. Detailed description of these properties and crystal structure of CZTS is described below.

3.1.1   Electrical and optical properties

Study of point defects and other defect complexes in compound semiconductor CZTS in the field of formation and transition energy levels predict p-type conductivity. In the structure of CZTS, 'Zn' atom having lower formation energy and deeper accepter level are replaced by 'Cu' atoms which have higher formation energy of donor defects, thus CZTS exhibits p-type conductivity [71]. Resistivity values of CZTS thin films reported in various studies vary from 10^{-3} to 10^1 Ω cm [45, 102-104]. Hall effect measurements depict the hole mobility values change from 1 to 10 cm^2 V^{-1} s^{-1} [105-107]. Energy band gap value calculated by HSE06 calculations at experimental lattice constants is 1.5 eV by chen et al. [108], although, energy band gap value varies from 1.4 eV to 1.55eV according to many reports [109-111]. Theoretically determined dielectric constant value of CZTS is about 6.8 and 6.92 [112-113] and absorption coefficient is greater than10^4 cm^{-1} [114].

3.1.2 *CZTS crystal structure*

The crystal structure of CZTS is mainly of two types: kesterite and stannite. Kesterite structure belongs to the space group I4 (tetragonal) [115]. These structures have very similar lattice parameters and value of theoretical lattice constants are approximately a= 5.46 Å and c= 10.92 Å [116]. CZTS also crystallizes with the stannite structure as has been reported some structural modifications. This structure is of space group I42m, tetragonal system [117]. The difference between these structures is the different arrangements of 'Cu' and 'Zn' atoms, which arise due to difference of the alternation of cation layers. Kesterite structure has alternation between CuSn and CuZn, while in stannite it is between Cu_2 and ZnSn [117]. The kesterite structure was designated as more substantial state of CZTS as compared to stannite type [118-119]. Kesterite structured CZTS thin films have been claimed to have high performance as an absorber layer [120]. The detailed lattice data of a CZTS crystal was reported by Schäfer and Nitsche in 1974 (Table 3.1).

Table 3.1 Lattice data of the kesterite CZTS single crystal

2θ(degrees)	d (Å)	(hkl)	I/I_0 (%)
16.33	5.42	002	1
18.20	4.86	101	6
23.10	3.84	110	2
28.53	3.12	112	100
29.67	3.00	103	2
32.98	2.71	200	9
37.02	2.42	202	1
37.96	2.36	211	3
40.75	2.21	114	1
44.99	2.01	105	2
47.33	1.91	220	90
56.17	1.63	312	25
56.85	1.61	303	3
58.96	1.56	224	10
64.17	1.45	314	1
69.22	1.35	008	2
76.44	1.24	332	10

This depicts that corresponding lattice planes are (112), (220), (312), (224) and (332) with preferred orientation along (112) plane for CZTS material [121-124]. Peaks corresponding to (101), (110), (200), (211), (303), (224) and (332) planes were also reported [125-130].

3.1.3 The ternary phase diagram (TPD)

CZTS compound constitutes in the form of Cu_2S-ZnS-SnS_2. Phase analysis study initially for this Cu_2S-ZnS-SnS_2 system was done by Olekseyuk et al. [131].

(a)

(b)

(c)
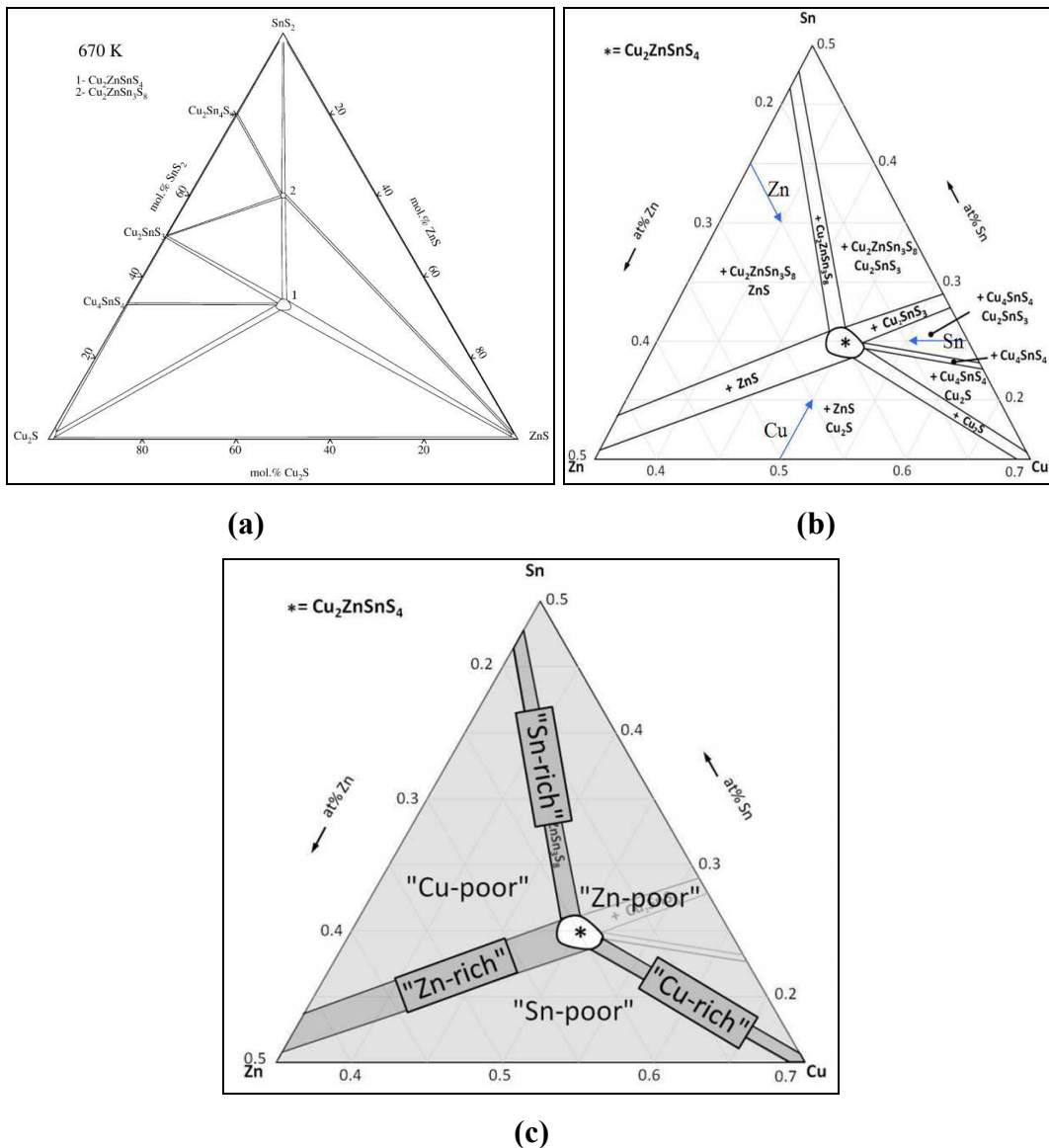
Figure 3.1: (a) Ternary phase diagram of CZTS by Olekseyuk et al. (b) Ternary phase diagram according to Scragg (c) TPD with different regions of composition.

Further detailed development was done by Scragg [132] which is represented by ternary phase diagram (TPD) as shown by Figure 3.1(b). This TPD shows an

isothermal section of the accepted phase diagram for this system containing eleven fields and valid at 400°C in equilibrium. Ten fields have the presence of Cu_2ZnSnS_4 (CZTS) and secondary phases. Single phase CZTS exist only in narrow range, which is represented by 'asterisk' at the middle of the diagram. Apart from this middle region, all other regions accommodate additional secondary phases also (i.e. ZnS, Cu2S and SnS_2 etc.) due to the narrow solubility limit of CZTS. In the TPD, five two-phase fields and five three-phase fields hold one secondary phase and two secondary phases, respectively in addition to CZTS. Six regions could be defined as shown in Figure 3.1(c) and described in Table 3.2.

Table 3.2: Different secondary phases in ternary phase diagram of CZTS.

Cu-poor	$Cu_2ZnSn_3S_8$ + ZnS
Sn-rich	$Cu_2ZnSn_3S_8$
Zn-poor	Cu_2SnS_3 + $Cu_2ZnSn_3S_8$ + Cu_1SnS_3+ Cu_2S+ Cu_4SnS_4
Cu-rich	Cu_2S
Sn-poor	Cu_2S, ZnS
Zn-rich	ZnS

These secondary phases are influenced by the stoichiometry and affect the morphology of the film. They have high influence on the properties of the cell. Some important secondary phases are discussed here. In case of Zn-rich films, secondary phase ZnS remain unreacted on the surface and can influence the additional processing steps for construction of solar cell and cause more series resistance to the cell. Cu_2S present in CZTS act as metals [133-134] and conducting phase causes recombination and trapping of electrons and holes [135].

3.2   Thin film deposition methods

For the deposition of a proper thin film, any deposition method must satisfy certain requirements:

•   Throughout the sample the deposition must be uniform.

•   A very good control of thickness is necessary.

•   Adhesion of the material should be good, and it should not peel off from the substrate.

- During the deposition process, dust & other foreign particles should not be present on the wafer.

- In case of deposition of alloys, uniform composition is required.
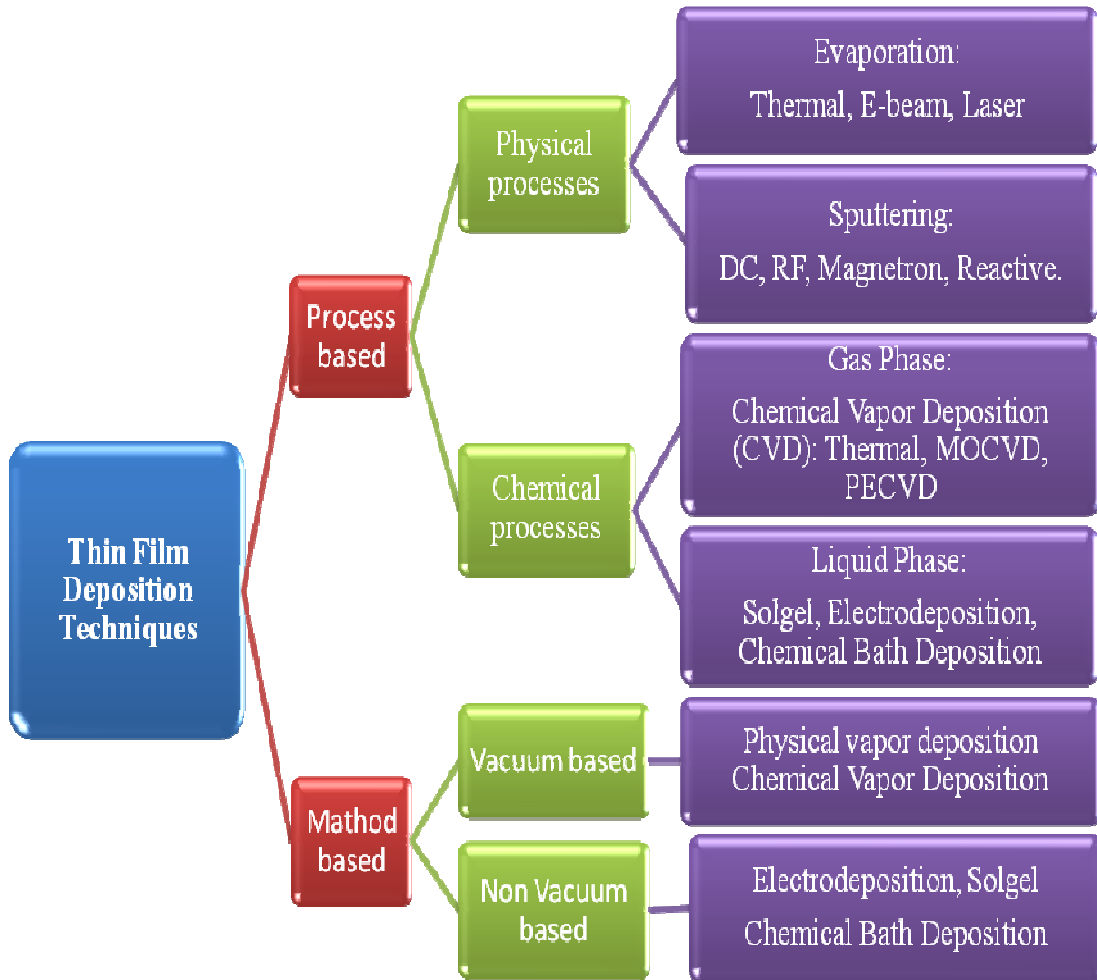
Figure 3.2: Deposition techniques for thin film deposition

3.2.1 Vacuum based method

3.2.1.1 Physical vapor deposition (PVD)

In this technique, physical process such as heating, sublimation or sputtering is used to convert material to be deposited into vapor form which is further deposited on the substrate as a thin film. So, basically PVD is fundamentally a vaporization coating technique, involving transfer of material on an atomic level and no chemical reaction is involved [136]. Deposition process under PVD technique takes place under vacuum or very carefully controlled atmosphere. The thickness of the deposit can vary from typically in the range of few nanometers to several micrometers. PVD

processes consist of three fundamental steps, these three fundamental steps are utilize in different PVD technologies but differ in the methods used to generate and deposit material. Following steps are involved in PVD method:

- Evaporation: In this step high energy source such as high temperature, electrons or ions beam eject atoms from the target or solid source of material to be deposited and vaporize them.

- Transportation: In controlled atmosphere i.e. vacuum or partial vacuum, vaporized atoms moved from the material source to the surface to be deposited.

- Deposition: This is the final step of process in which coating occurs on the substrate surface by condensation of the evaporant. This condensation may takes place by some simultaneous reactions or directly by the target material alone depending on the type of thin film to be deposited during deposition process.

Types of PVD technique

1.   Evaporation

Evaporation is the elementary physical deposition method for deposition of thin films. This process contains a material source and the substrate that are placed in the vacuum chamber. There are different approaches for heat transmission to the material source for vaporization: Thermal induction heating, electric resistance heating, and electron beam heating. For this reason this method further can be divided into these sub categories:

- Thermally Induced Evaporation: In this method heat is supplied to the source material directly or indirectly up to the point of sublimation or evaporation to create a plume of vapor to controllably transfer atoms, which move in straightaway paths. When the atoms, molecules, and clusters reach at the substrate, they coagulate from the vapor phase to solid film. When analyzing this method, evaporation rates and vapor pressure are key points for consideration. Other than pressure and temperature, the placement of the heater, source and substrate are important factors [137].

- Electron Beam Evaporation: In this process high energy focused electron beam, supplied from a heated filament is used to deliver energy to evaporate

the source material at a small area. Higher temperatures can be reached in this process as there are no boats, wires [16].

2. *Molecular beam epitaxy (MBE)*

This technique is applied for deposition of extremely pure semiconductor materials. In this process, the vacuum is in the extremely high range (10^{-9} to 10^{-11} Torr). This Ultrahigh vacuum ensures absence of impurity or contamination. Evaporation of materials is conducted using a special thermal evaporation effusion cells known as Knudsen cells, then deposition of this evaporated flux takes place onto the substrate by colliding with substrate and deposit epitaxial film [138-139]. The main features of MBE are: a low growth temperature, a slow growth rate, a simple growth mechanism, a variety of in situ analysis capabilities. The main disadvantage of MBE is that it is a very slow process and unsuitable for implementation in industry.

3. *Sputtering*

Sputter deposition is based on the theory that in this method physical interaction of ions to the source create vapor phase and thus involves an elastic transfer of momentum, which can be utilized to deposit a thin film onto the substrate. Energetic ions are accelerated towards a target by utilizing electric fields which acts as one electrode and they dislodge target atoms and other ions. The ejected atoms get deposited on the substrate, and a thin film of the target material is produced [140-141]. The substrate can be heated by employing dc or rf power depending upon the nature of the deposition and electrical conductivity of the target. There are various types of sputtering techniques that can be used to synthesis thin films.

DC sputtering

In this method, glow discharge due to an applied electric field in a gas is used as a source of ions for sputtering. When a certain minimum voltage is reached, the gas breaks down to conduct electricity and this ionized gas is called plasma. By a large electric field, acceleration of plasma ions occurs to the target. Atoms (or molecules) are ejected from the surface of the target into the plasma, when the ions impact the target and they are carried away and then deposited on the substrate. This type of sputtering is called "DC sputtering".

RF sputtering

For the deposition of insulating films, rf power is the only option to sputter deposit thin films. In the sputtering process, electrical charge of the plasma ions is neutralized by striking on the target. But in the case of insulator, a positive charge occurred results in repulsion of bombarding ions that break off the process. The polarity must be inverted to continue the process. To overcome this problem an alternate electric field is used to create plasma for periodic reversal of polarity automatically. DC power can be used only for conducting targets where rf power can be used for both conducting and insulating targets.

Reactive sputtering

In electrically conducting sputtering process limitation of type of materials that can be deposited can be solved by adding a reactive gas e.g. nitrogen, oxygen etc. to the discharge. The reactive gas goes in to a chemical reaction with the sputtered atoms to form a compound on the substrate.

If the sputtering rate is faster than the chemical reaction rate, then the deposition will take place by the combination of physical and chemical reaction on the substrate.

4. Pulsed laser ablation

In this process, a pulsed laser beam is focused onto the surface of a target and the interaction of the laser beam with the target surface at an oblique angle takes place. This focusing action produces a laser spot of high enough energy which creates conical powerful plasma-like bright plume of evaporant caused by ablation of the material. The axis of the vapor plume normal to the target's surface follows a cosine distribution rule and target material subsequently deposits onto the substrate [142-143]. In laser ablation process, presence of process variables are less as compared to other physical and chemical vapor processes. This is an important aspect of deposition method as it makes the process relatively easy to control. The important parameters of this method are substrate target distance, laser power density and ambient oxygen pressure. It was shown that high oxygen partial pressure results in films grown by 3-D island growth mode while low partial pressure of oxygen and high growth temperatures are crucial for epexital growth mode to occur.

3.2.1.2 Chemical vapor deposition CVD

Chemical vapor deposition (CVD) involves reaction between material compound and gases. In this process, a heat source converts precursor compounds into vapour phase and vapors introduced into the heated reaction chamber where a source of gas is present. So, volatile compound chemically react with gases present to produce a nonvolatile solid that deposits atomistically on substrate by gas phase and surface chemical reactions [144-145]. The main kinds of chemical reaction are: pyrolysis, oxidation, reduction and disproportionation. The residual gases and volatile products are exhausted away from the system. Various types of CVD methods are mentioned as under.

- MOCVD (metalorganic CVD)

- PECVD (plasma- enhanced CVD)

- Modified CVD processes such as low-pressure CVD (LPCVD), laser-enhanced CVD and aerosol-assisted CVD (AACVD).

The CVD process is good because of its versatility of depositing different films from the same precursors. Depositing films over large area substrates is another advantage. However complexity of process is present because of many process parameters to be controlled. Some other problems with CVD are toxicity of compound and some gases are highly corrosive also, good safety measures requirement, control of final composition, accurate phase diagrams and expensive high purity chemicals, which limit the application of the process on a wide scale. If the temperature and pressure are not controlled well, the reaction will occur in air itself [145].

3.2.2 Non- vacuum based method

3.2.2.1 Electrochemical

The process of electrodeposition involves an applied external electric field to reduce charged growth species (cations) of a desired material from a solution and coat that material as a thin film onto a conductive substrate surface. This is a film growth process that results in the deposition of metals, alloys, semiconductors and conductive polymers coatings on conductive substrates, starting from metal ion precursors in a suitable solvent and occurring via a charge transfer process [146-147]. There are a number of advantages of this process as electrodeposition offers reliability and

environmental advantage over vacuum based methods. It also can accommodate the whole range of vastly different length scales found on a large 200 mm or 300 mm diameter wafer. It also provides relatively low temperature (room temperature) operating conditions. Disadvantages of this method are:

- Requirement of repetition and over again as it works on molecular level and

- Coating is extremely thin, it may end up being much more time consuming and expensive.

- Electroplating may not be uniform and this may result in a substandard appearance of the plated material.

- Coating may often be brittle and easy to crack which can let in impurities and lead to the overall destruction of the electroplated layer.

3.2.2.2 Sol-gel method

Sol-gel is a chemical solution based process used to make materials in the form of thin films, fibers, or powders. A sol is a colloidal i.e. a dispersion phase of the solid particles (~ 0.1-1 μm) in a liquid where only Van der Waals forces and surface charges are present and Brownian motions suspend the solid particles of ions in a solvent. A gel is a semi-rigid mass state where both liquid and solid are dispersed in each other and forms when the solvent from the sol begins to evaporate and the particles or ions left behind, which presents a solid network containing liquid components.

Generally, the sol-gel coating process usually consists of 4 steps [148-150].

(1)   To form a sol, desired colloidal particles once dispersed in a liquid.

(2)   The deposition of sol solution by spraying, dipping or spinning produces the coatings on the substrates.

(3)   Through the removal of the stabilizing components particles in sol are polymerized and produce a gel in a state of a continuous network.

(4)   The remaining organic or inorganic components pyrolyze by heat treatments and form an amorphous or crystalline coating.

Disadvantages of Sol-Gel process:

- Compared to mineral based metal ion sources in the case of metal alkoxides, raw materials for this process is expensive.

- Products of sol gel process would contain high carbon content when organic reagents are used in preparative steps which would inhiblt densification during sintering.

- Continuous monitoring of the process is needed as several steps are involved,

3.2.2.3 Chemical bath deposition

(CBD) is a method to deposit thin films and nanomaterials which can be employed for large-area or continuous deposition. This process involves deposition of thin film from a solution containing required liquid precursor (reacting solution) in desired stoichiometry by a chemical change [151-153]. Initially each precursor needs to be dissolved in separate solvents which are then mixed together later in stoichiometric quantities of precursors of desired substances to form homogeneous solution. It can be carried out at room temperature or higher temperature depending on the characteristics of precursors in the respective solvents. Once the solution is made, pH is adjusted by adding appropriate solutions. Finally, previously cleaned substrates immersed vertically in the as-prepared solution inside a beaker and left for the required dip times at the appropriate deposition temperature.

CBD process consists of (i) generation of supersaturation, (ii) nucleation, and (iii) subsequent growth, which involved three step: (i) creation of atomic/molecular/ionic species, (ii) transport of these species through a medium, and (iii) condensation of the species [154]. In chemical bath deposition (CBD) process, a metal complex interacts with a chalcogenide source to form a thin film. The ionic product must exceed the solubility product then ion-by-ion condensation takes place for formation of thin films on substrates. Controlled precipitation of the desired compound from a solution of its constituents is the basic principle involved in the synthesis of thin films by the chemical bath method. From chemical aspects, steps of the process are as follows

1. Equilibrium between the complexing agent and water
2. Hydrolysis of the chalcogenide source
3. Formation/dissolution of ionic metal-ligand complexes

Reaction mechanism governed by above mentioned steps, involves two steps: nucleation and particle growth. In nucleation, at the surface of the substrate arriving

atoms and molecules (called ad atoms) lose thermal energy and the surface absorbs that energy. As nuclei continue to form, the film grows into a continuous sheet covering the substrate. Once a few monolayers of evaporant have condensed on the substrate, the film continues to grow in thickness as if the entire substrate were made of the material being deposited [152].

Fundamentals of nucleation and crystal growth

This step is crucial as it controls the crystallinity and microstructure of the film. There are three basic modes of nucleation: (i) island or Volmer–Weber, (ii) layer or Frank–van der Merwe, and (iii) island–layer or Stranski–Krastonov nucleation. In the solution a new phase appears when concentration of a solute in the solvent exceeds its equilibrium solubility. A solution possesses a high Gibbs free energy with solute exceeding the solubility or supersaturation and then the overall energy of the system would be reduced by segregating solute from the solution [155-158]. This reduction in Gibbs free energy is the motivation for both nucleation and growth.

After the initial nucleation, the concentration of the growth species decreases and when it corresponds to the critical energy, the concentration decreases below this specific concentration, no more nuclei would form. After the formation of stable nuclei, increment in size occurs until the concentration of growth species has attained the equilibrium concentration or solubility.

Effect of preparative parameters

The growth of thin films strongly depends on growth conditions, such as duration of deposition, composition and temperature of the solution. The effect of deposition conditions on preparative parameters are discussed below:

(a)   pH of the bath: pH of the bath indicates the concentration of OH- ion in the solution. The rate of deposition and reaction rate depends on the formation of solid phase of a solute exceeding the solubility (supersaturation) condition. The formation of MO^-/MOH^- would be slower if supersaturation is lower. If the pH of the solution is higher, concentration of M ion will be lesser resulting in slow reaction rate. At an appropriate pH, the concentration of M ion increases and ionic product of M and O^-/OH^- becomes more than the solubility of MO^-/MOH^- and a film will be deposit [159].

(b) Complexing agent: The complexing agent in chemical bath mitigates precipitation by controlling the release of the metallic ions. The complexant (complexing agent or ligand) is selected according to its property of bonding toward the metal. This works as the reaction rate determination factor by giving control over the rate of reaction and hence rate of solid formation .Consequently, leading to produce different morphologies with various thickness of the film.

(c) Temperature: Temperature is the main deciding factor for dissociation of precursor chemicals (MX) into cation and the anion of the compound. Higher concentrations of M and X ions result in higher rates of deposition which is greater at the higher temperatures. Thickness of the thin film depends upon optimization of temperature incorporated with pH values. Supersaturation is high even at low temperature at low pH values, and increases further with increasing temperature. Low supersaturation occurs at high pH values and most of the product is formed on the substrate surface and higher thickness is obtained at higher temperature.

The major advantage of CBD is that

- It requires in its simplest form only solution containers and substrate mounting devices.

- Chemical bath deposition yields stable, adherent, uniform and hard films with good reproducibility by a relatively simple process.

- It provides deposition at lower temperatures with respect to physical vapor deposition methods.

- Substrate shape and area is not a constraint in CBD method, it can be used for large area deposition.

- It does not require vacuum facilities, which in turns make it cost effective method.

- There is no sophisticated equipment requirement so handling of deposition setup is easy.

It uses simple chemicals unlike pallets or targets used in physical vapor deposition method.

3.3   Surface modification

Surface modification is the result of applying combination of physics and chemistry process, after deposition or synthesis on the surface of a material. It is used to modify materials to enhance surface properties by causing physical, chemical characteristics different from the properties of original surface of a material. The act of modification can be done for altering a wide range of characteristics of the surface by different methods according to requirement [160-161].

Annealing is one of the easily approachable post treatment techniques which can be used for surface/interface modification. In material science, annealing is a heat process which involves heating a material to a specific temperature in the furnace and to maintain this suitable temperature for appropriate time and ambient and then cooling is done at slow rate. This process alters the properties of a material to make it more applicable. Annealing is used to modify subjected material in order to exhibit different effects. This can be applied in order to activate dopants, create defects, change in substrate-film or film-film interface, increase density of deposited films, change states of grown films, change in the position of dopants from one film into another film or to enhance properties. Annealing is performed by using furnaces especially built to heat semiconductor samples. This processing could be done in different atmosphere at different temperatures for different annealing times.

During annealing, in a solid material heat provides appropriate energy needed to break bonds and thus increase the rate of diffusion of atoms or atom migration in the crystal lattice. The migration of atoms cause the redistribution and removal of the dislocations in materials which further progresses towards its equilibrium state and the number of dislocations decreases. In the process of annealing with increase in temperature, annealing process proceeds in three stages: recovery, recrystallization, and grain growth.

- Recovery: This is the first stage of annealing which take place at the lower temperature. It results removal of dislocations and internal stresses which arise due to this primarily linear defects. In this stage grain size and shape of material do not transform [162].

- Recrystallization: During this stage new defects-free grains are nucleated and developed. This nucleation process continues until the original grains have

41

been entirely consumed and replacement of deformation formed by internal stresses takes place [162]. So, the grain structure in the final product develops due to the recrystallization.

- Grain growth: After the completion of recrystallization, if annealing is allowed to continue, then third stage of grain growth occurs. This stage could be controlled by cooling rate.

3.4 Characterization technique

3.4.1 X-ray diffraction

Researchers use X-ray diffraction (XRD) to probe crystalline structure at the atomic level and use XRD as a most important non-destructive tool in the field of research to analyze all kinds of matter ranging from crystals powders and fluids used in solid state chemistry and materials science. XRD is an indispensible method for structural materials characterization of unknown crystalline materials and the determination of their structure by the use of the Debye-Scherrer method in fields such as metallurgy, mineralogy, forensic science, archeology and the biological and pharmaceutical sciences.

The sample consist minuscule grains of crystalline material where crystalline domains are randomly oriented in the sample to be studied. When the two dimensional diffraction pattern is recorded, it shows scattering peaks corresponding to the various 'd' spacing in the crystal lattice. In the diffraction pattern diffracted intensity is shown as function of the scattering angle 2θ. The intensities and the positions of the peaks are used for identifying the structure or phase of the sample. Identification is done by comparison of the diffractogram to known standards or to international databases X-Ray Diffraction and Crystal Structure (XRD). After material identification, X-ray crystallography may be used to determine its structure, i.e. atoms packing in the crystalline state, inter atomic distance etc.

In a diffraction experiment, a wave is aimed to a material specimen and intensity and direction of outgoing diffracted waves are recorded by a moving detector. These outgoing diffracted waves interfere constructively and comprise the diffraction pattern. This diffraction pattern is a spectrum of real space periodicities in a sample and atomic periodicities with long repeat distances cause diffraction at small angles, while short repeat distances results in diffraction at high angles. Crystals with

precise periodicities have sharp and clear diffraction peaks, while crystals with defects are not as accurately periodic and their diffraction peaks are broad, distorted and weak. Order of the wavelength of incident waves must be equal to the spacing between atoms. X-rays are electromagnetic radiation of wavelength about 1 Å (10^{-10} m), which is about the same size as an atom.

When an incident X-ray beam contacts with planes of atoms in the specimen, there are the possibilities of the beam being transmitted, absorbed, refracted and scattered and diffracted. Diffraction of X-rays occurs differently by different materials, depending on type and arrangement of atoms. An electron of an atom will oscillate with the same frequency as the field in an alternating electromagnetic field of X-ray. We will have destructive interference in almost all directions, however the atoms in a crystal are arranged in a regular pattern, and we will have constructive interference in a very few directions. Now, when an X-ray beam is diffracted, by applying Bragg's Law we can measure the distances between the planes of the atoms that constitute the sample. Bragg's Law is: $n\lambda = 2d \sin\theta$, where the integer n is the order of the diffracted beam, λ is the wavelength of the incident X-ray beam, d is the distance between adjacent planes of atoms and θ is the angle of incidence of the X-ray beam. Since we know λ and we can measure θ, we can calculate the d-spacings. The set of d-spacings generated in a typical X-ray pattern provides a unique characteristic of the sample. This condition is described by the Bragg law as shown in Figure 3.3. The Figure 3.4 and Figure 3.5 represents the schematic of X-ray detection and diffractometer PANalytical X'pert PRO PW-3040 model operated at 40 kV voltage and 40 mA current is used at Material Research Centre, MNIT, Jaipur.

The most usually employed instrument to generate X-rays is X-ray tubes, which generate X-rays by bombarding a metal target with high energy electrons such as 10-100 KeV, to knock out core electrons. Thus, an electron in an outer shell fills the hole in the inner shell and emits an X-ray photon. Two common targets are molybdenum (Mo) and copper (Cu), which have strong K_α radiation having X-ray emissions wavelength of 0.7107 and 1.5418 Å respectively. In powder diffractometer a photon detector replaces the photographic film (or some annular detector) used in cameras. Early designs were non-focusing systems that utilized X-ray tube spot foci and required relatively long data collection times, giving rather poor resolution.

Actually the majority of commercially available powder diffractometer use the Bragg-Brentano para-focusing arrangement.
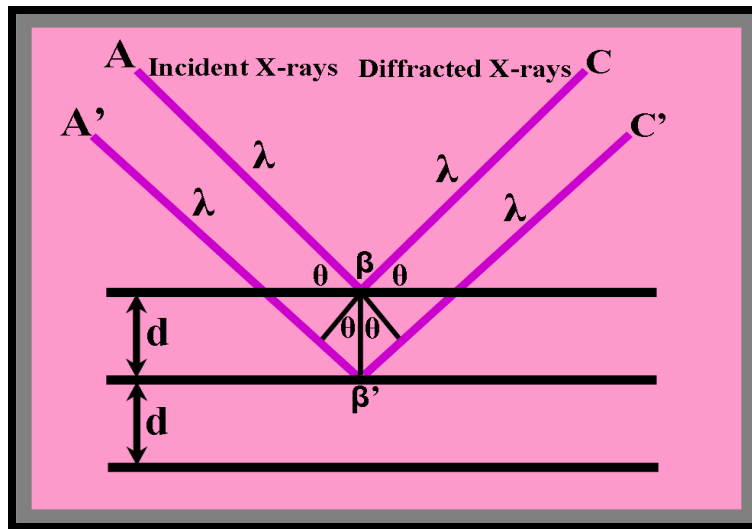
Figure 3.3: Interaction of X-rays with crystalline matter
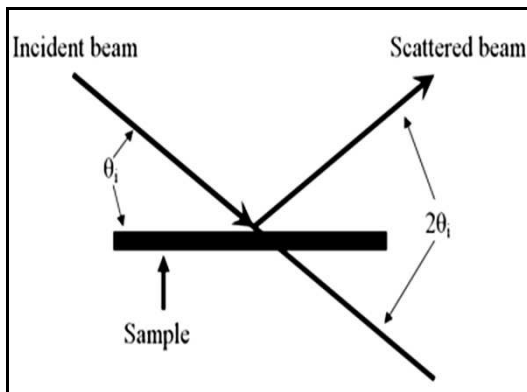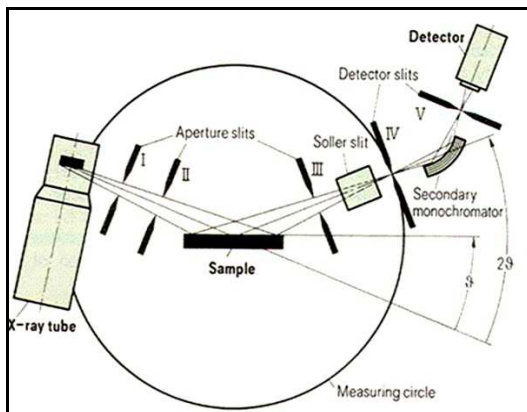
Figure 3.4: Schematic of X-ray detection

Figure 3.5: X-ray diffractometer unit

Applications

- X-ray diffraction provides structural information, Interatomic distances and bond angles.

- We can determine the size and the shape of the unit cell for any compound by using X-ray diffraction.

- Amorphous materials are readily recognized by absence of sharp diffraction peaks.

- Other applications of XRD analysis include determination of phase transitions in a given substance, measurement of crystallite size particularly in nano materials, analysis of stress and crystal structure analysis by Reitveld refinement.

- It is used in the determination of size of particles of crystals by Scherrer equation. This formula relates the size of crystallites, in a solid to the broadening of a peak in a diffraction pattern. The Scherrer equation can be written as [163].

$$D = \frac{0.9\lambda}{\beta Cos\theta}$$

- Where λ is X-ray wavelength, β is the full width at half maximum (FWHM) in radians), and θ is the Bragg angle.

3.4.2 *Scanning electron microscope*

The scanning electron microscope (SEM) is an electron microscope that uses a focused beam of high-energy electrons. The electrons interact with atoms in the sample to generate various signals that reveal information about the sample including external morphology, surface topography and chemical composition, and crystalline structure and orientation of materials making up the sample. The electron beam is generally scanned in a raster scan pattern, and the beam's position is combined with the detected signal to produce an image. When the wavelength became the limiting factor in light microscopes the electron microscope was developed, because electrons have much shorter wavelengths ($\lambda \sim$ 6 to 0.03 nm for E$\sim$ 0.2 to 40 keV), enabling better resolution. Essential components of all SEMs include the following:

- Electron Source ("Gun")
- Electron Lenses
- Sample Stage

- Detectors for all signals of interest
- Display / Data output devices

In a SEM, an electron beam is emitted from an electron gun fitted with tungsten filament cathode. The electron beam typically has an energy ranging from 0.2 keV to 40 keV, is focused by condenser lenses to a spot about 0.4 nm to 5 nm in diameter. The beam passes in the final lens, which deflect the beam in the 'x' and 'y' direction so that it scans in a raster fashion over a rectangular area of the sample surface. Energetic electrons in an SEM carry significant amounts of kinetic energy, and when the incident electrons are decelerated in the solid sample this energy is dissipated as a variety of signals are produced by electron-sample interactions. These signals include secondary electrons (that produce SEM images), backscattered electrons (BSE), diffracted backscattered electrons (EBSD), photons (characteristic X-rays) and visible light (cathodoluminescence–CL). SEM can produce very high-resolution images of a sample surface thus revealing details less than 1 nm in size. BSE images can provide information about the distribution of different elements in the sample. EBSD are used to determine crystal structures and orientations of minerals, photons are used to identify the composition and measure the abundance of elements in the sample.

Each of signals can be detected by specialized detectors and electronic amplifiers are used to amplify these signals, which are displayed as variations in brightness on a computer as a distribution map of the intensity of the signal being emitted from the scanned area of the specimen and are saved as digital images [164].

Applications

- The SEM is used to generate high-resolution images of objects.
- To show spatial variations in chemical compositions.
- Acquiring elemental maps or spot chemical analyses using EDS,
- Discrimination of phases in multiphase samples based on backscattered electron images.
- Precise measurement of very small features and objects down to 50 nm in size is also accomplished using the SEM.

- SEMs equipped with diffracted backscattered electron detectors (EBSD) can be used to examine microfabric and crystallographic orientation in many materials.

A typical schematic representation of SEM setup is shown in Figure 3.6.
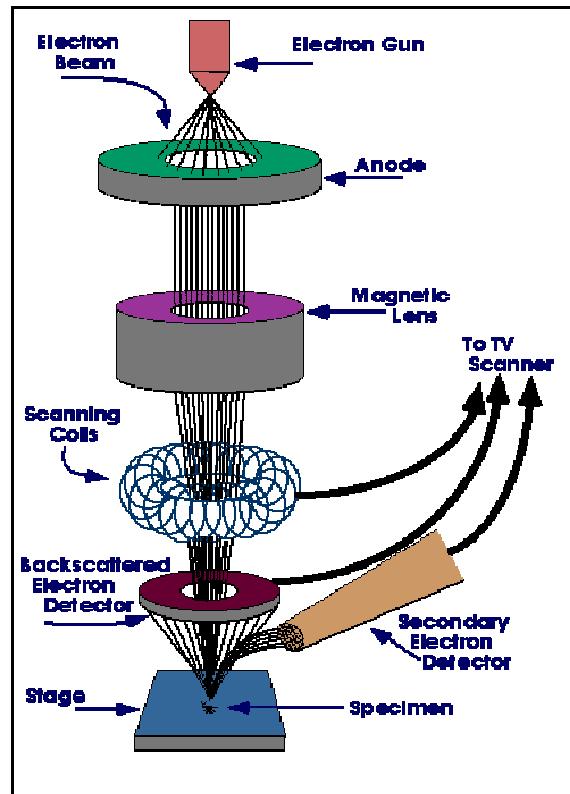
Figure 3.6 (a): Schematic Representation of Scanning Electron Microscope (SEM)

Figure 3.6 (b): Typical SEM Instrument

3.4.3 *Atomic force microscopy*

AFM is a specific type of microscopy that gives surface topographic features and give a 3D profile by scanning the surface using a very sharp probe and checking forces between probe and surface to image and measure properties of surfaces [165]. A representative view of the function of schematic representation of the function of AFM is shown in Figure 3.7 and Atomic Force Microscope (AFM) set up is shown in Figure 3.8.
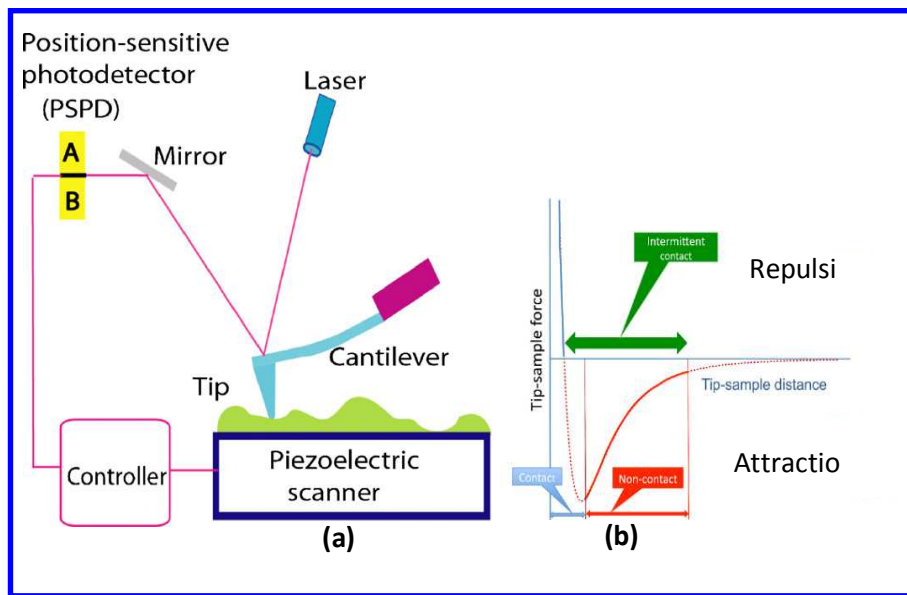
Figure 3.7: Schematic representation of Atomic Force Microscope (AFM)

Figure 3.8: AFM instrument set up

The probe is supported on a flexible cantilever and the AFM tip gently touches the surface and records the small force between the probe and the surface. The amount of force between the probe and surface depends on their intermediate distance and spring constant. This force can be described using Hooke`s law:

$$F = -k.x \quad (1)$$

Where F = Force; k = Spring constant; x = Cantilever deflection.

Cantilever bends if its spring constant is less than surface and beam bounce method is used to measure the deflection of the probe. In this method a semiconductor diode laser is bounced off the back of the cantilever onto a position sensitive photodiode detector and this detector measures the bending of cantilever. The measured cantilever deflections are used to generate a map of the surface topography.

In AFM there are three primary imaging modes:
(i)   Contact AFM
(ii)   Intermittent contact (tapping mode AFM)
(iii)   Non-contact AFM

Contact mode AFM: Cantilever bends if its spring constant is less than surface and force on the tip is repulsive. An image of the surface is obtained by maintaining a constant cantilever deflection (using the feedback loops) and the force between the probe and the sample remains constant.

The intermittent mode: This is also called tapping mode and imaging in this mode is similar to contact mode but in this mode the cantilever makes intermittent contact with the surface and oscillated at its resonant frequency (hundreds of kHz). During scanning, the probes lightly tap on the sample and makes contact at the bottom of its swing. An image of the surface is obtained by maintaining constant oscillation amplitude and a constant tip-sample interaction.

Non-contacting mode: In this mode the probe does not touch the sample but oscillates above it during scanning. A feedback loop is used for measurement of surface topography by monitoring changes in the amplitude due to the attractive forces between the probe and the sample.

The choice of use of mode of AFM relies on the attribute of surface under study and on the hardness of the sample. Contact mode is most useful for hard surfaces. Intermittent mode is good for imaging soft biological specimen and for samples with poor surface adhesion. Non-contact mode is another useful mode for imaging soft surfaces, but its sensitivity to external vibrations and the inherent water layer on samples in ambient conditions often causes problems.

3.4.4 Optical characterization

Investigation of the optical properties of semi conducting thin films is essential for their proper application in semiconductor electronics. The fundamental optical properties which have been investigated are reflectance, transmittance and absorption of light at various wavelength and angles of the beam. The optical properties of a thin film are generally different from that of the bulk. The differences are contributed to the microstructure of the films. Here thin films are ideally suited for the study of optical absorption etc. The optical properties of a semi conducting thin films are governed by the interaction between the atoms and electric field of the electromagnetic wave.

Study of the interaction of electromagnetic waves and matter is termed as molecular spectroscopy. Ultraviolet and Visible Spectroscopy are carried out by electromagnetic radiations with wavelength ranging from 190 nm to 800 nm [ultraviolet (UV, 190-400 nm) and visible (VIS, 400-800 nm)]. It is also often called as electronic spectroscopy, because the absorption of ultraviolet or visible radiation by a molecule leads transition among electronic energy levels of the molecule. So, it studies the changes in electronic energy levels [166-167]. The absorption spectrum of a molecule should show few very sharp lines. Ultraviolet and visible spectrum of most molecules consists of a few humps rather than sharp lines and it show the molecule is absorbing radiation over a band of wavelengths.

UV – Vis spectrophotometer

A spectrophotometer is an instrument that measures the amount of optical absorption, transmission and reflection as a function of wavelength. The typical UV-Vis spectrophotometer consists of a light source, a monochromater and a detector. The light source is usually a deuterium lamp which can emit electromagnetic radiation in the ultraviolet region of the spectrum. A second light source is a tungsten

lamp that can be used for wavelength in visible region. The monochromater is used to spread the beam of light into its certain wavelengths. A system of slit focuses the desired wavelength on the sample. The light that passes through the sample will reach the detector. The detector is will then records the intensity of the transmitted light. A schematic diagram of UV-Vis Spectrophotometer is shown in Figure 3.9 and an UV-Vis Spectrophotometer set up (HITACHI U-2900 model) is shown in Figure 3.10.
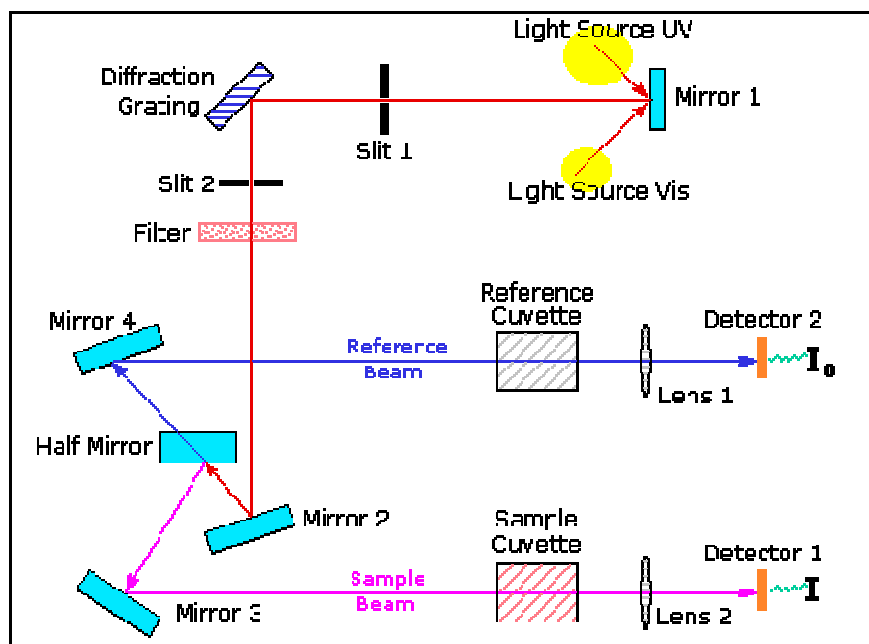
Figure 3.9: Schematic diagram of UV-Vis Spectrophotometer

Figure 3.10: UV-Vis Spectrophotometer set up

51

3.4.5 Current voltage (I-V) characteristics

For the I-V characteristics of the absorber layer CZTS/ITO-glass, corresponds to the measurement of the current produced due to the application of varying electric field (voltage) both in forward and reverse direction, Lab equipped Keithley, model SMU-2400 computer interface set up unit was used at our Lab, MNIT Jaipur as shown in Figure 3.11.
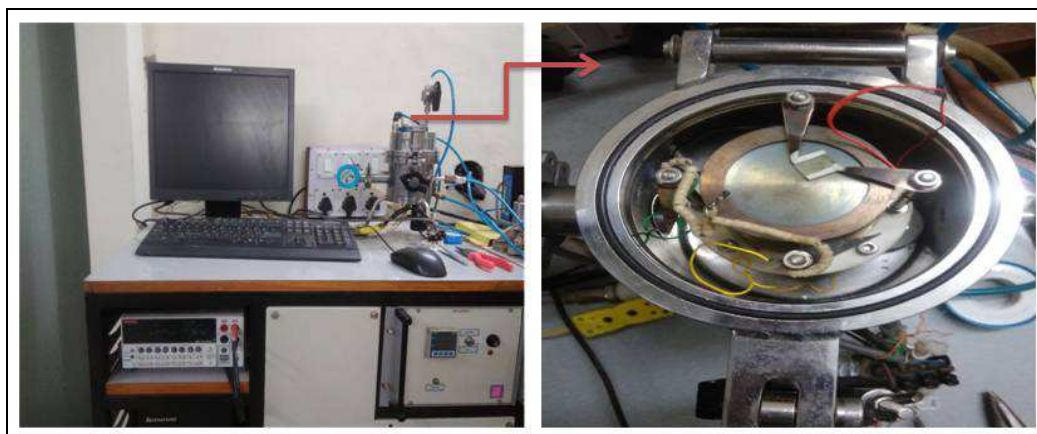
Figure 3.11: I-V characteristics set up (Keithley electrometer-2400 SMU)

Finally, the devices glass-ITO/ZnS/CZTS/Ag and glass-ITO/Al-ZnS/CZTS/Ag were characterized in terms of current-voltage (I-V) measurements by solar simulator in dark and under illumination 100 mW/cm^2 source of light at Thin Film and Nano Technology Lab, Department of Physics, Dr. Babasaheb Ambedkar Marathwada University, Aurangabad as shown in Figure 3.12. I-V measurement consists of monitoring the change in current to that applied voltage under ambient condition such as dark and illumination.

The most useful aspect of this technique is its application to the qualitative diagnosis of single and heterojunction material. Depending on the nature of the response and the plot the material characteristics can be defined like if the observed output exhibits nonlinear nature of the graph and upon illumination condition the same response is observed but shift in the output current then the material would be called as photosensor. If under illumination condition the current is drastically moving towards the IV quadrant of the I-V plot then the material can be called as photovoltaic material.

Figure 3.12: Sun simulator set up

I-V response can be used to:

i.   Study the nature of the material whether photosensor or photovoltaic.

ii.   Estimate process of charge transportations in the material.

The simplest technique that uses the photo response under dark and illumination conditions to calculate the energy conversion efficiency of the material. The conversion efficiency is the measure of total energy falling on the material and the energy converted to electrical form.

CHAPTER 4

SYNTHESIS AND CHARACTERIZATION OF CZTS THIN FILM

4.1   Introduction

Worldwide energy requirement and its dependency on fossil fuels are creating issues related to environmental impact such as CO_2 emission and scarcity of their reservoir. Non conventional resources of energy are considered as the solution of this problem from last decades. Solar energy is one of the most promising alternatives among all nonrenewable energy resources. Compound semiconductors thin film solar cells are of great interest in the field of solar energy. Researchers have achieved the optimal commercialization requirements for $Cu(In,Ga)Se_2$ (CIGS), CdTe based thin film solar cell with efficiencies of 20.3% [40], 17.3% [33], respectively. However, there is a need to find alternative materials with high abundance and low cost due to limited supply and high price of elements such as In and Ga, and toxicity of elements such as Cd.

Cu_2ZnSnS_4 (CZTS) is an interesting alternative of Chalcopyrite CIGS and CdTe based solar cells as it is analogous with chalcopyrite solar cells. Quaternary semiconductor CZTS of I-II-IV-VI group have required set of properties with p-type conductivity , direct band gap of ~1.5 eV and absorption coefficient of ~10^4 cm^{-1} [50]. All elements of CZTS are non-expensive, abundant in earth and non-toxic environment friendly [168].

Several methods were explored by different research groups for synthesis of CZTS thin films. The commonly methods have been used to grow this p-type

absorber layer are DC and RF magnetron sputtering [169], co-evaporation [170], pulsed laser deposition [171], thermal and electron-beam evaporation [172], screen printing [173], chemical vapor deposition [174], spray pyrolysis [95], sol-gel spin-coated deposition [175], electrodeposition [176-177]. However, several successful attempts have been reported by above mentioned vacuum based methods earlier, but there are some issues related to these techniques, these do not fulfill basic theme related to CZTS based solar cell technology, which is cost effectiveness leading to easy commercialization process. Above mentioned methods are mostly vacuum based, they are expensive, require sophisticated expensive equipments, thus resulting in high production cost. Apart from cost constraints, limited area deposition is also an issue of vacuum based techniques. Another disadvantage is high temperature deposition condition which reduces the simplicity of deposition process. All factors indicate expensive nature and sophisticate handling of these methods. So, the main focus of researchers in this field is developing a simple method which can turn into commercially adaptable method.

As compared to the other deposition methods, Chemical Bath Deposition (CBD) method is interesting one because it is simple, reproducible, non-hazardous, cost effective and well suited for producing large-area thin films at low temperatures. So, the central theme of this work is optimizing and controlling of synthesis parameters because after going through the literature, there are very few reports on the synthesis of CZTS thin film using CBD method. These films have been characterized by different characterization tools for as grown and modified CZTS thin film. Further, post treatment thermal annealing has been used as it can control the morphology and structural properties of polycrystalline thin film [178-179]. Considering this aspect the annealing effect on the solar cell performance of CZTS thin films has also been investigated in this work.

4.2   CZTS thin film deposition

4.2.1   Experimental details

4.2.1.1 Materials and substrate cleaning

All the chemicals used for preparation of chemical bath were analytical reagent grade (AR) provided by Sigma Aldrich with 99.9% purity. Copper Chloride dehydrate ($CuCl_2.H_2O$), Zinc Chloride ($ZnCl_2$), Tin Chloride pentahydrate ($SnCl_4.5$

H$_2$O) and Thiourea (NH$_2$CSNH$_2$) were used as precursor chemicals for Cu^{2+},Zn^{2+},Sn^{2+} and S^{2-} ions. Ethylenediaminetetraacetic acid (EDTA) was used as complexing agent for controlling the reaction mechanism. Thin films were deposited on glass substrate. Before the deposition, substrates were cleaned by detergent and distilled water then ultrasonically cleaned by acetone, methanol and de-ionized (DI) water and dried in air.

4.2.1.2 Synthesis of CZTS thin film

Chemical concentrations were taken as 0.1 M CuCl$_2$, 0.05ZnCl$_2$, 0.05 SnCl$_4$, 0.5 NH$_2$CSNH$_2$ in equal volume ratio and EDTA was taken as complexing agent. Initially chemicals were dissolved separately in distilled water by magnetic stirring. After preparing all the solutions they were mixed and pH was measured. Final pH (~10) was controlled by adding ammonia. Cleaned SLG substrate was immersed in the solution and solution was heated up to 60°C. Schematic diagram for the deposition is shown in Figure 4.1. In chemical bath when reaction started metal complex was formed and white solution became yellow after some minutes and after formation of precursor metal sulfides, brown blackish color solution has formed. Precipitation started to form in the bath after 1 hr and deposition of CZTS film started on the substrates. The substrate with CZTS film was removed after 7 hr, rinsed in DI water to remove the ions from film, dried in air and preserved in desiccator.
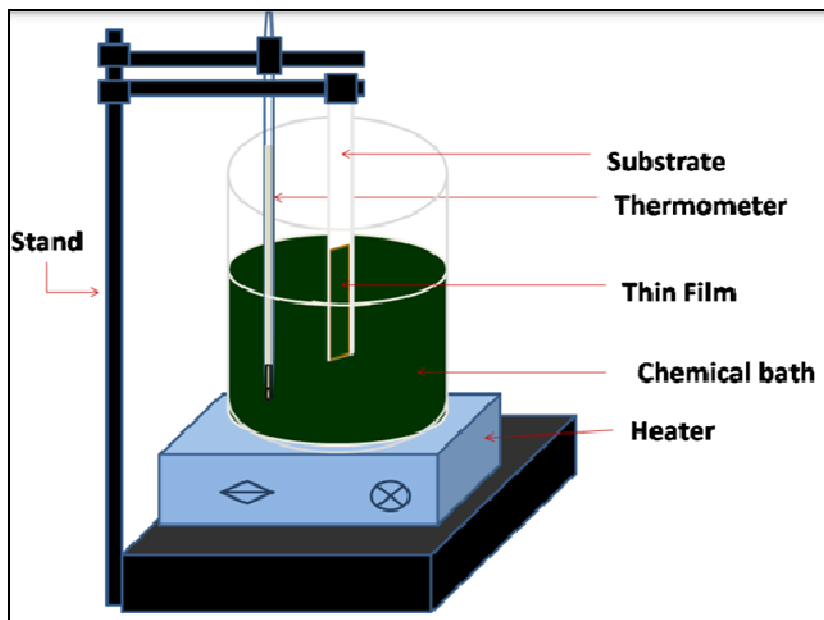
Figure 4.1: Schematic diagram of chemical bath deposition method for deposition of CZTS thin film

The steps involved in CBD method were represented by the flow chart for thin film deposition as given below:
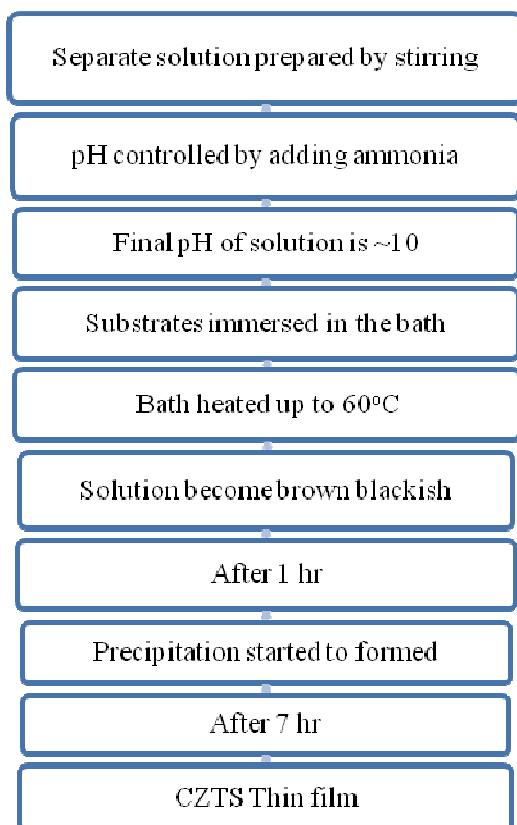
Separate solution prepared by stirring

↓

pH controlled by adding ammonia

↓

Final pH of solution is ~10

↓

Substrates immersed in the bath

↓

Bath heated up to 60°C

↓

Solution become brown blackish

↓

After 1 hr

↓

Precipitation started to formed

↓

After 7 hr

↓

CZTS Thin film

The surface/interface of the thin film can be modified by providing the post deposition treatments like thermal annealing. As- deposited CZTS thin films were annealed in air at 150°C for 2 hr in tubular furnace.

4.2.1.3 Reaction mechanism of CZTS thin film

Deposition of thin film takes place by reaction of metal cations and sulfur anion which were occurred from metal and sulfur sources respectively. This deposition process completed through some steps as under.

(1)   Dissociation of Sulfur ions takes place by the hydrolysis of thiourea with hydroxide ion produced from ammonia. Soluble ammonia produces ammonia ion and hydroxide ions solution in equilibrium with ammonia and water.

$$NH_4OH \rightleftharpoons NH_4^+ + OH^- \rightleftharpoons NH_3 + H_2O \qquad (4.1)$$

$$(NH_2)_2 + OH^- \rightleftharpoons SH^- + CH_2N_2 + H_2O \qquad (4.2)$$

$$SH^- + OH^- \rightleftharpoons S^{-2} + H_2O \qquad (4.3)$$
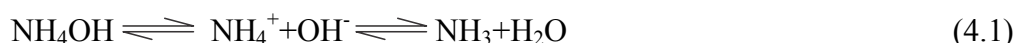
(2)   Formation of metal complex occurs by reaction of metal source with ammonia. Ammonia molecule reacts with the metal ion to produce a complex ion. Less concentration of ammonia in solution gives metal hydroxide but in case of high concentration of ammonia, complex ions formed govern by below reactions.
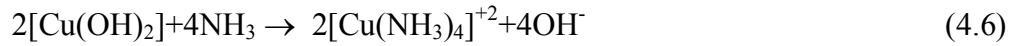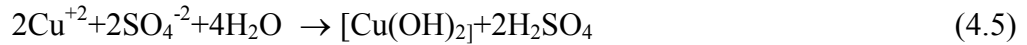
$$2CuSO_4 \rightarrow 2Cu^{+2}+2SO_4^{-2} \tag{4.4}$$

$$2Cu^{+2}+2SO_4^{-2}+4H_2O \rightarrow [Cu(OH)_{2]}+2H_2SO_4 \tag{4.5}$$

$$2[Cu(OH)_2]+4NH_3 \rightarrow 2[Cu(NH_3)_4]^{+2}+4OH^- \tag{4.6}$$

Similarly $ZnSO_4$ and $SnSO_4$ give Zn and Sn complex ion in reaction

$$2ZnSO_4+4H_2O+4NH_3 \rightarrow [Zn(NH_3)_4]^{+2}+4OH^-+2H_2SO_4 \tag{4.7}$$

$$2SnSO_4+4H_2O+4NH_3 \rightarrow 2[Sn(NH_3)_4]^{+2}+4OH^-_{]}+2H_2SO_4 \tag{4.8}$$

In above reaction formation of complex ion controlled by complexing or chelating agent EDTA as it control the release of metal ion in solution which further results in formation of metal complex ion.

(3)   In final step replacement of complex ion by sulfur ion takes place as under expressed reaction

$$2[Cu(NH_3)_4]^{+2}+[Zn(NH_3)_4]^{+2}+[Sn(NH_3)_4]^{+2}+4S^{-2} \rightarrow Cu_2ZnSnS_4+12NH_3 \tag{4.9}$$
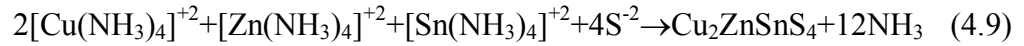
When the ionic product exceeds the solubility product of final compound Cu_2ZnSnS_4, then it precipitate out as colloid in the solution and as a film on the substrate.

4.2.1.4 Characterization

The structural properties of as deposited and annealed CZTS thin film were studied by X-ray diffraction (XRD) by using PANalytical X'Pert Pro X-ray Diffraction Unit with copper (Cu) target, which have strong K_α radiation having X-ray emissions wavelength of 1.5418 Å in range of 20-60°. Average crystal sizes were determined according to broadening of peaks using Scherrer relationship (equation 10). The surface morphological study was carried out using scanning electron microscope (SEM) JEOL JSM model 6360 and Atomic Force Microscope (AFM). I-

V characteristic studied using Lab equipped Keithley, model SMU-2400 computer interface set up unit.

4.2.2 Results and discussion

4.2.2.1 Structural analysis

X-ray diffraction (XRD) technique was used for performing structural analysis of as-deposited, annealed thin films on glass substrate. Figure 4.2 shows the XRD pattern of as-deposited and annealed CZTS film. Figure 4.2(a) shows no diffraction peaks indicating amorphous nature of as deposited film. Figure 4.2(b) shows XRD pattern of annealed film at 150^{0}C for 2 hrs and exhibit sharp peaks at different angles 23.1^{0}, 28.5^{0}, 32.6^{0} and 47.8^{0} and by comparing calculated 'd' values from experimental data with 'd' values from standard kestarite structured CZTS crystal (JCPDS card 26-0575), corresponding phases are determined as (110) , (112), (200) and (220).

This analysis confirmed the synthesis of kesterite structured CZTS thin film with tetragonal structure. This result is in agreement with previously reported results [98,180]. Intensity of peak corresponding to (112) phase is observed to be much greater than other peaks, reveling preferred orientation along this phase for annealed film. The size of particle in the film can be calculated from the Scherrer's formulas as given in equation 4.10.

$$D = \frac{0.9\lambda}{\beta Cos\theta} \tag{4.10}$$

Where λ is X-ray wavelength, β is the full width at half maximum (FWHM) in radians, and θ is the Bragg angle. Crystallite size of the CZTS thin film was calculated corresponding to diffraction peaks as summarized in Table 4.1.

Table 4.1: Parameters of XRD spectra for Cu_2ZnSnS_4 films

2 Theta (degree)	d(Å)	Intensity	hkl	FWHM	Particle Size (nm)
23.1	3.84	2	110	0.477	17.75
28.59	3.11	100	112	0.403	21.41
32.68	2.73	9	200	1.199	7.20
58.73	1.57	10	224	0.492	19.36
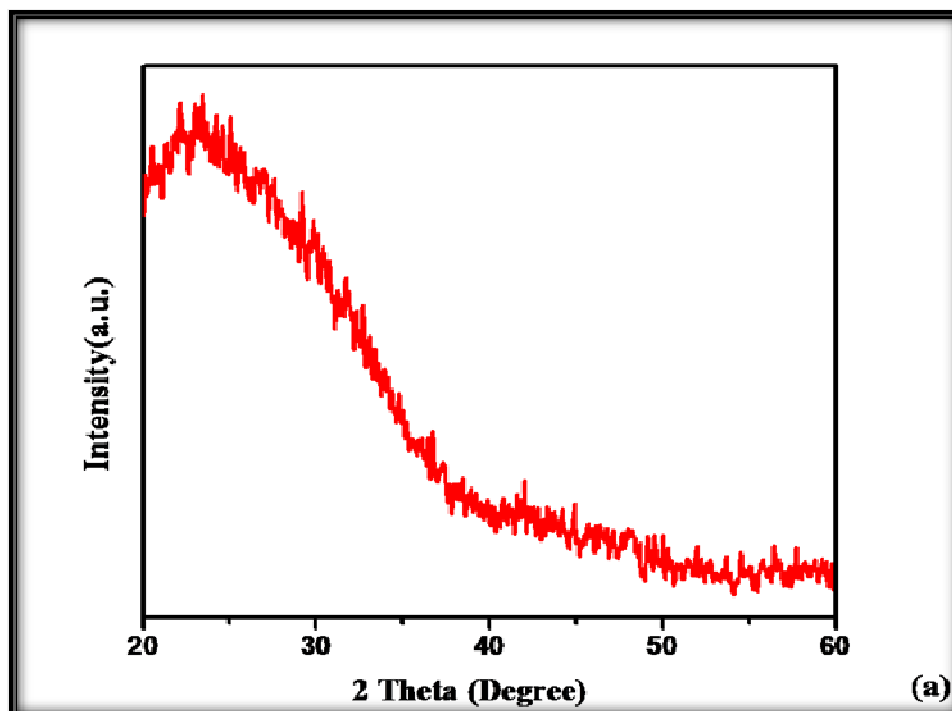
Figure 4.2(a): XRD spectra of as-deposited CZTS thin film
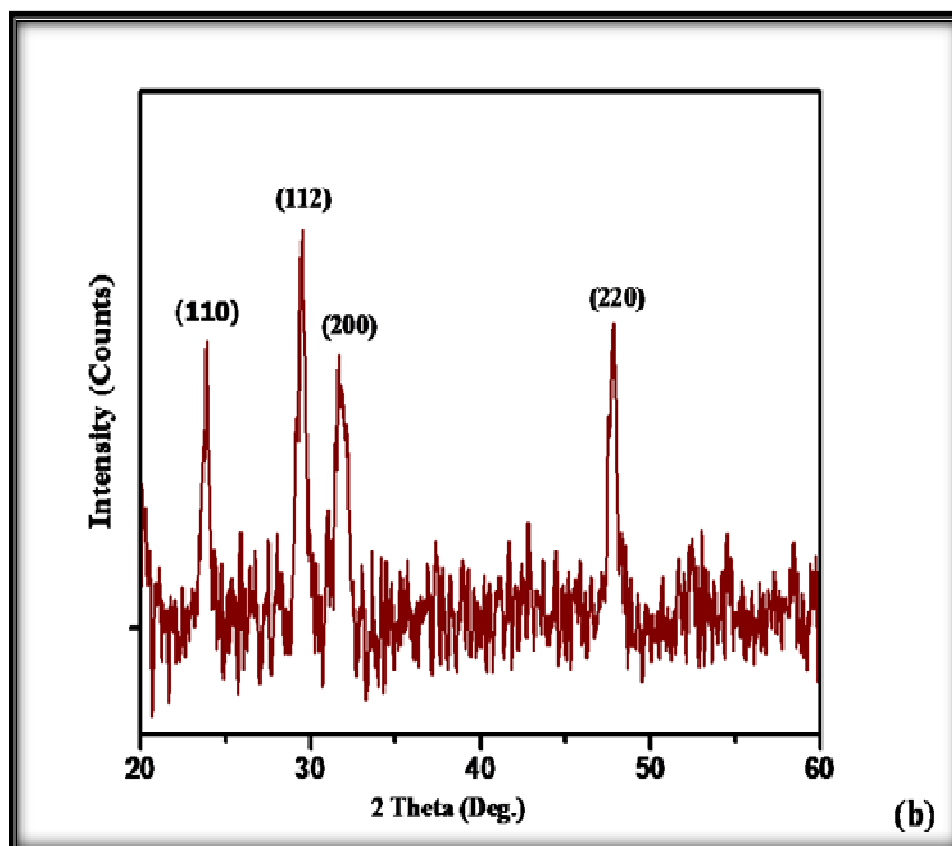
Figure 4.2(b): XRD spectra of annealed CZTS thin films at 150°C in air for 2 hrs.

4.2.2.2 Surface morphological analysis

Surface morphological analysis was done by Scanning Electron Microscope (SEM) and Atomic Force Microscope (AFM). Figure 4.3 shows SEM image of the as-deposited and annealed CZTS thin film. Figure 4.3(a) shows surface image of the as-deposited thin film grown by CBD method. The image shows that the surface morphology of the film is smooth, highly uniform and the film is compact in nature with smaller densely packed grains. Figure 4.3(b) shows surface image of film after annealing and indicates that surface modification occur after post temperature treatment which increased crystallinity and grain size of CZTS thin film. The interlocked crystal grains are clearly visible in SEM image for sample. These grains are useful for solar cell application because it reduce localized recombination sources [181]. Such type of results has been reported by other authors with different deposition techniques [92,182].
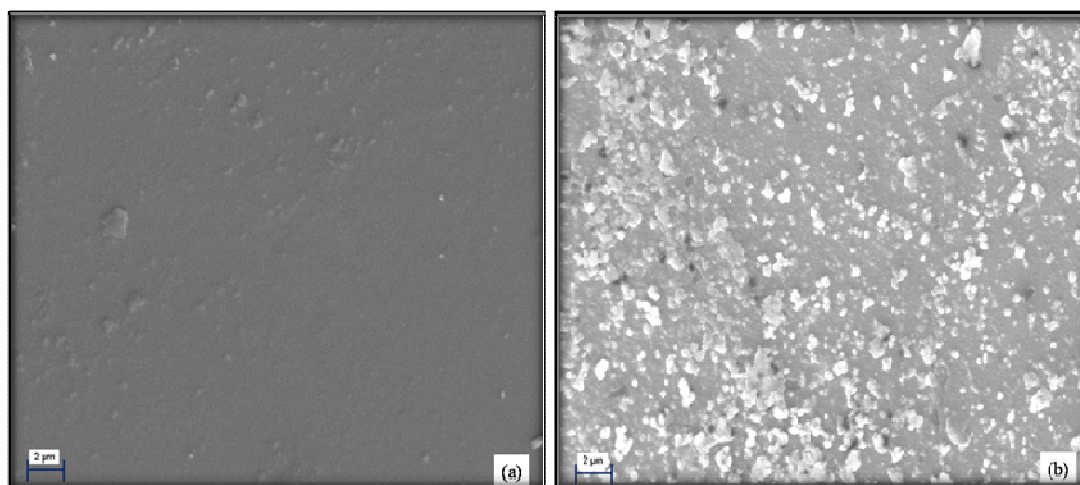
Figure 4.3: The SEM images of (a) as deposited and (b) annealed CZTS thin film at 150° C in air for 2 hrs.

Figure 4.4 shows AFM image of CZTS thin films. Figure 4.4(a) and (b) show 2D and 3D AFM images of as-deposited and annealed CZTS thin films, respectively. 2D AFM image for as-deposited film indicates the homogeneous background of amorphous phase. It was observed that some particles existed on the surface of CZTS thin films from 3D AFM image. This may be because during deposition process nucleation sites were developed. On annealing, grain growth started and spherical grains were found to get merged in each other.
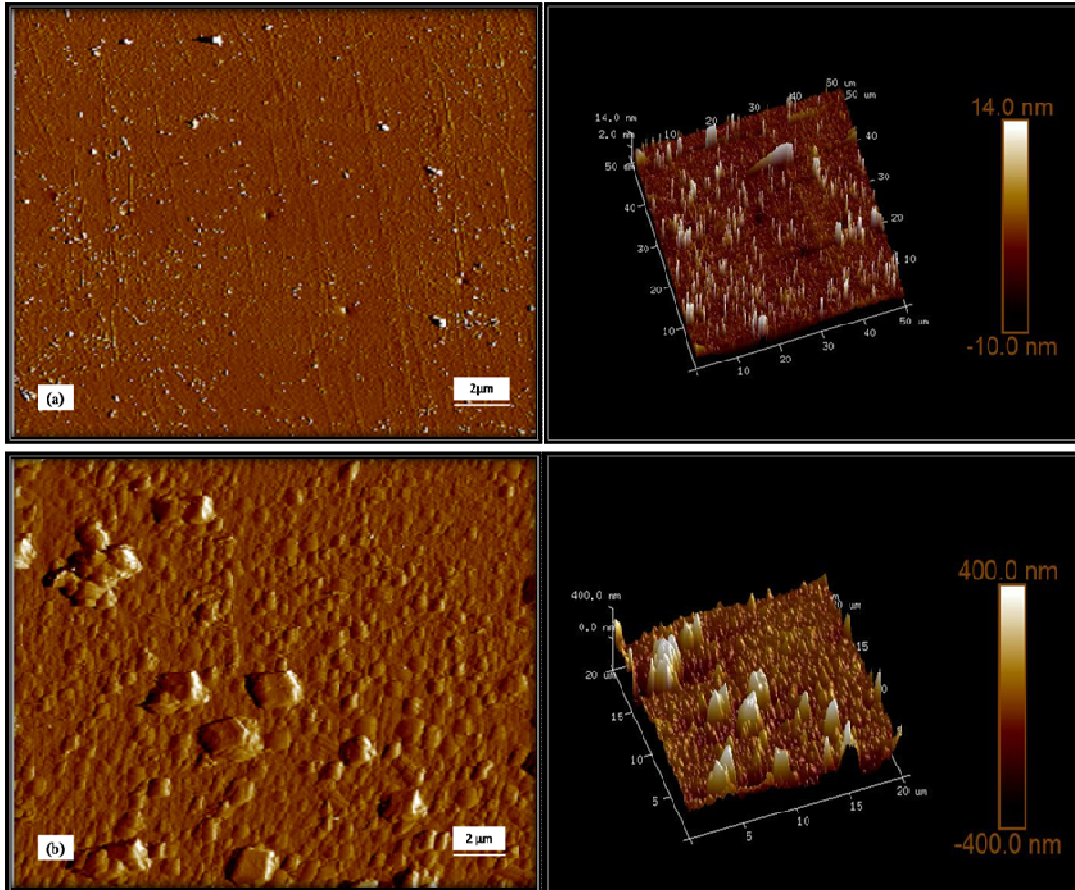
Figure 4.4: The 2D and 3D AFM images of (a) as deposited and (b) annealed CZTS thin film at 150° C in air for 2 hrs.

From Figure 4.4(a) the average surface roughness and root mean squared roughness of the film are found to be around 1.31 and 4.10 nm respectively. The average particle size from 3D AFM images is observed to be 4 μm ± 1 μm from Figure 4.4(b). Surface roughness and root mean squared roughness of the film are found to be around 171 and 205 nm, respectively. The film roughness increases with increased grain size. This result agrees with that reported by Hossain et al. [183]. This observation indicates polycrystalline nature of CZTS thin film due to annealing.

4.2.2.3 I-V characteristics

For detecting the photosensitivity of CZTS absorber layer the Schottky diode was constructed by metal contact on top of CZTS samples and I-V measurement was obtained under the illumination intensity of 60 mW /cm^2. Figure 4.5 shows I-V characteristic of thin film using Lab equipped Keithley 2400 computer interface set up unit. Figure 4.5(a) shows the current–voltage (I-V) characteristics curve for as

deposited CZTS absorber layer and Figure 4.5(b) shows the I-V characteristics of annealed film at 150°C in air for 2 hrs

.
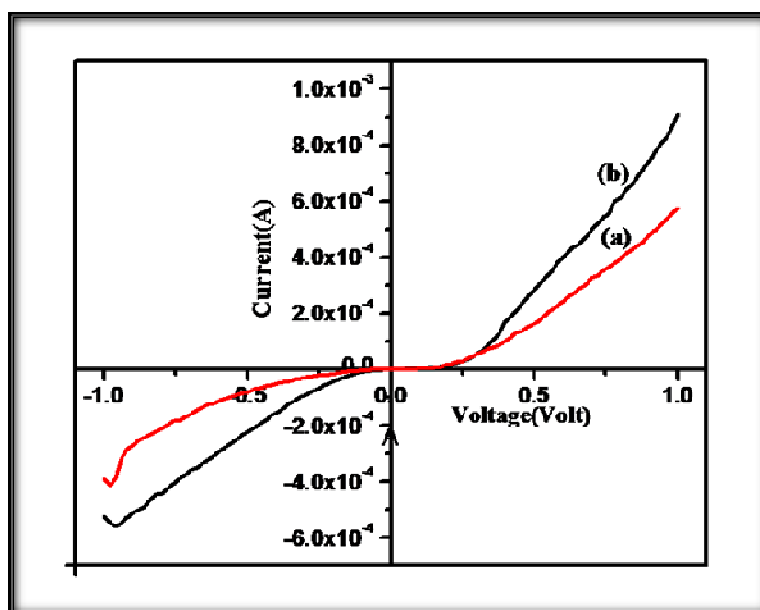
Figure 4.5: I-V characterstics of (a) as-deposited CZTS films (b) annealed CZTS films at 150° C in air for 2 hrs.

It is observed from this figure that as deposited film shows ohmic behavior while after annealing treatment schottky like diode behavior is shown by absorber layer. It is seen that after annealing treatment , the resistance for absorber layer decreases indicating that recombination is less, thus results in lower value of characteristic resistance (R_{ch}) (4.45 KΩ for as deposited and 1.11 KΩ for annealed thin film). It is concluded that after annealing temperature current also increases, which is accordance with previously drawn results by H.J. Hovel (184).

4.3   Effect of annealing

Chemical Bath Deposition method is simple and economical method and earlier optimization of parameter for chemical bath deposition in order to achieve the goal of deposition by low cost method has been mentioned. Now, efficiency of solar cell is next step in CZTS based PV technology. Efficiency of a solar cell is surface, interface and composition dependent phenomenon. The surface/ interface can be modified by providing the post deposition treatments such as the post annealing treatment at different temperatures. Efficiency of thin film solar cell increases as grain size increases and this morphology and grain size of the absorber layer can be

controlled by thermal annealing. It has been observed that the annealing treatment to the CZTS thin films is not only helpful for modifying the interface but it can also increase the open circuit voltage (V_{OC}) value of the junction, thereby improving the conversion efficiency of the solar cell. Optimization of annealing temperature is required because due to heat treatment at high temperature, films became Sulpher-deficient and Sn volatiles, thus defects generates which could affect the properties of absorber layer. Considering these aspects it is proposed to study the annealing effect on the solar cell performance of CZTS nanostructured thin films.

So, as-deposited CZTS thin films were annealed in air for 2 hr in tubular furnace and annealing temperature was varied by $50^{o}C$ started from $100^{o}C$ to $250^{o}C$. Partial evaporation of films takes place at temperature, which is more than this temperature. Annealed films were cooled naturally as abrupt quenching of temperature could result in cracks or defects generation. Further as deposited and annealed thin films were labeled as S_1, S_2, S_3 and S_4.

4.3.1 Results and discussion

4.3.1.1 Structural analysis

The structural analysis of as-deposited and annealed CZTS thin films was performed using X-ray diffraction (XRD) technique. Figure 4.6 shows the XRD pattern of as-deposited CZTS films. It is seen that and as there is no clear diffraction peaks and indicates amorphous nature of these films.

Figure 4.7 shows the XRD patterns of annealed CZTS thin films which indicate occurrence of crystallinity as diffraction peaks appeared at different angle after annealing. CZTS thin films annealed at $50^{0}C$ show diffraction peaks at 28.5^{0}, 32.6^{0} and 47.8^{0} and by comparing the calculated 'd' values with experimental 'd' values from JCPDS card 26-0575, corresponding planes are (112) (200) (220). XRD pattern of annealed film at $150^{0}C$ shows another peak at 23.1^{o} for (110) plane. As annealing temperature increases, intensity of diffraction peaks also increases which can be seen by XRD pattern of CZTS film at $250^{0}C$. Thus XRD patterns of annealed CZTS thin films confirm the formation of kesterite structure CZTS with tetragonal structure on the other hand degree of preferred orientation for annealed films is (112). These results are in good agreement with reported data (98,180).
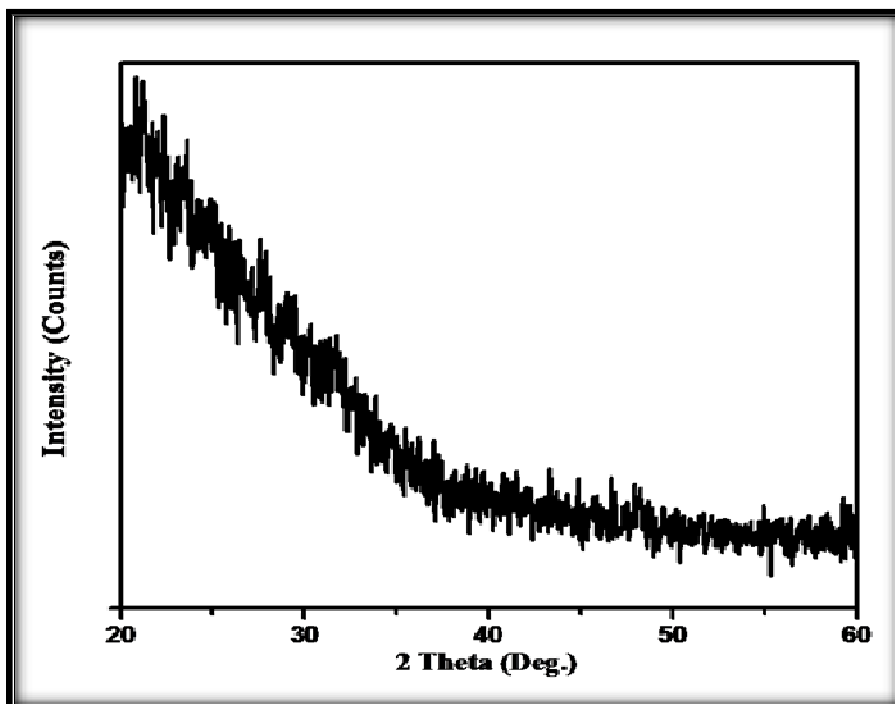
Figure 4.6: XRD patterns of as deposited CZTS thin film.
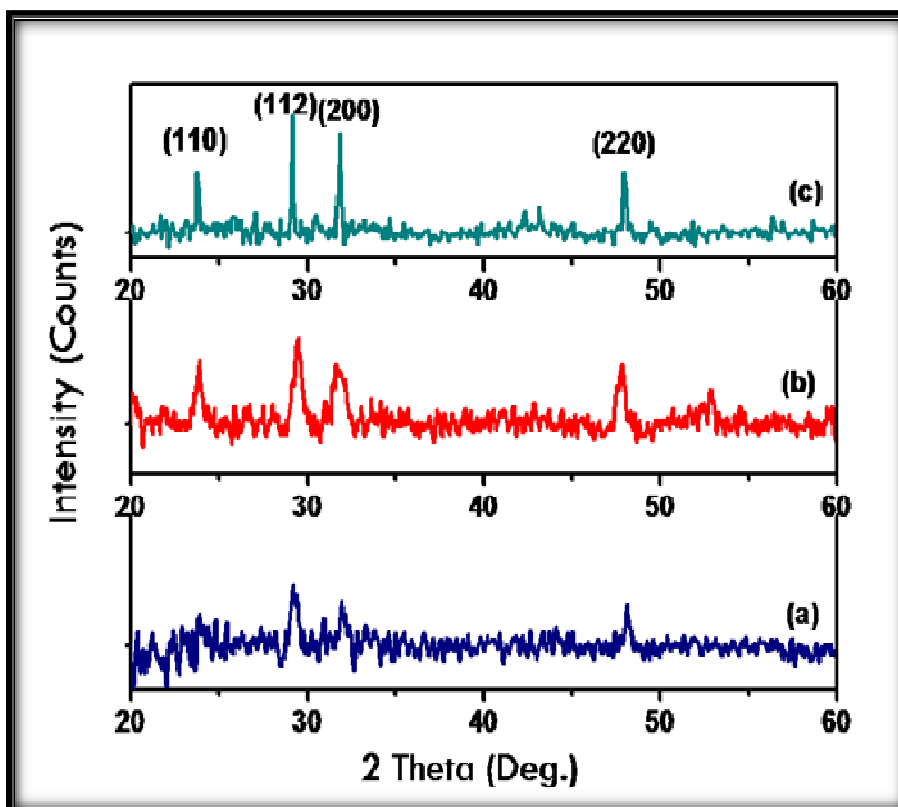
Figure 4.7: XRD patterns of (a) annealed CZTS thin film at 50^0C, (b) at 150^0C and (c) at 250° C in air for 2 hrs.

Particle size in the film was calculated from the Scherrer's formula. The particle size for (112) plan for as-deposited and annealed CZTS films have been summarized in Table 4.2. and also shows the variation of the grain size for (112) plane with the annealing temperature. With the increase of the annealing temperature from 50^0C to 250^0C, the grain size becomes larger. Figure 4.8 shows the dependence of full width at half maximum (FWHM) of the 112 peak on the annealing temperature. The FWHM decreased with the increase of the annealing temperature. This indicates that the grain sizes in CZTS thin films increase with increasing the annealing temperature. The effects of grain size are very important for fabrication of solar cells.

Table 4.2: The FWHM values and grain sizes of (112) orientation of the CZTS thin films obtained at different annealing temperatures.

Sample	S1	S2	S3	S4
Annealing Temperature	As deposited	50^0C	150^0C	250^0C
FWHM	-	0.51	0.40	0.15
Grain Size (mm)	-	16.79	21.41	57.1
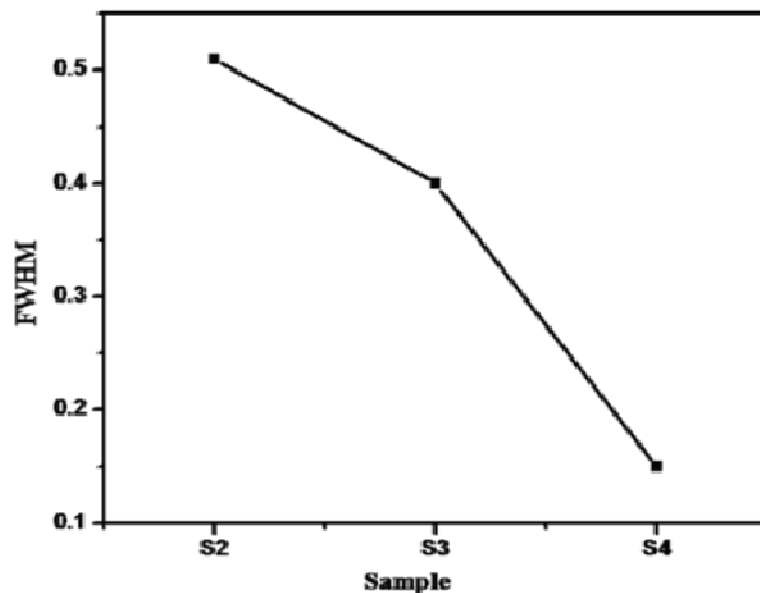
Figure 4.8: The FWHM values of sample S2 (annealed CZTS thin film at 50^0C), S3 (annealed at 150^0C) S4 (annealed at 250° C).

4.3.1.2 Surface morphological analysis

The surface morphology of CZTS films were studied by SEM images. Figure 4.9(a) shows SEM surface image of as-deposited CZTS film and indicates smooth, compact and dense morphology in nature and very small agglomerated particles with flat film surface. Figure 4.9(b, c & d) show the surface images of annealed films at 50°C, 150°C and 250°C, respectively. At lower annealing temperature (50°C) large agglomerated flakes grains were found and smooth surface started to become rough. As annealing temperature increases, (at 150°C and 250°C) the flaky grains size further increased and roughness of the film surface was enhanced with less grain boundaries. Similar results were reported by H. Park et.al [182] and S.S. Mali et.al. [92]. These large grain size is useful for solar cell application because decrement in grain boundaries reduce localized recombination sources (a surface or a grain boundary) within a diffusion length of the junction, which results high short circuit current [183].
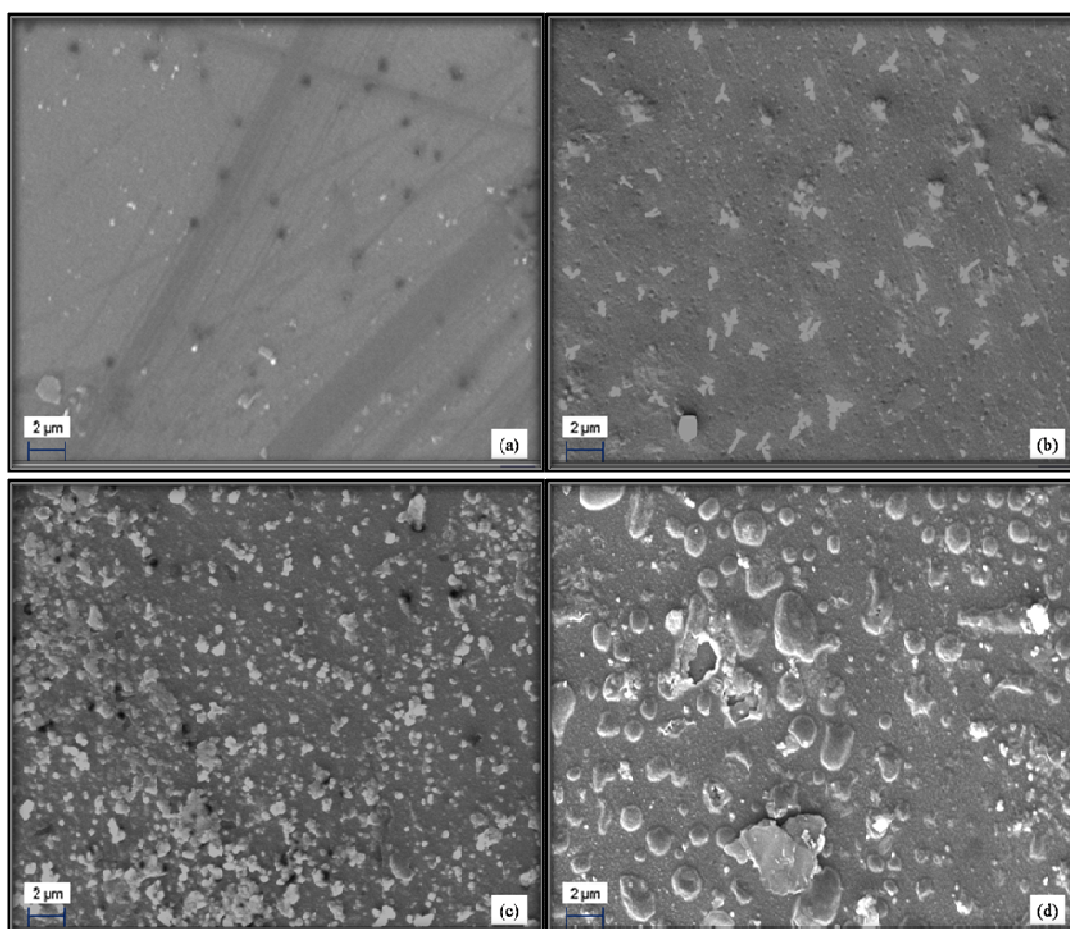
Figure 4.9: SEM images of (a) as deposited and (b) annealed CZTS thin film at 50° C (c) at 150°C (d) at 250°C in air for 2 hrs

The elemental compositions in thin film were measured by energy dispersive X-ray analysis (EDAX) spectrum. Figure 4.10 show the EDAX spectrum of CZTS thin film annealed at 250^0C and it shows the presence of the copper (Cu), zinc (Zn) tin (Sn) and sulpher (S) in the annealed film. We also observed the element oxygen (O) and silicon (Si) in the spectrum, due to the glass substrate (SiO_2). The EDAX measurement indicate copper rich films that may have the probable reason of more amount of Cu present in chemical Precursor used for the synthesis.
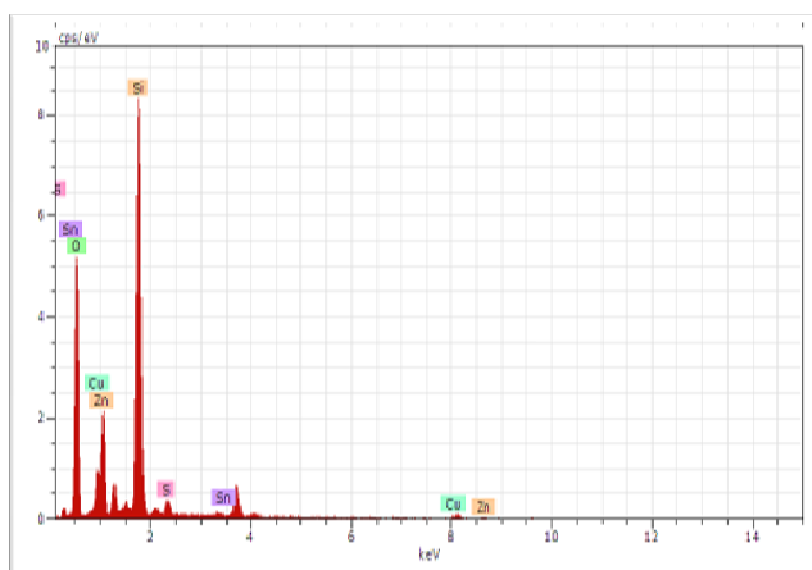
Figure 4.10: EDAX spectra of annealed CZTS thin film at 250° C.

Table 4.3: Elemental composition analysis of annealed CZTS film.

Elements	AN	Series	unn. C (Wt %)	norm. C (Wt %)	Atom. C (at %)
O	8	K-series	36.28	52.23	69.28
Si	14	K-series	24.80	35.71	26.98
Cu	29	K-series	3.53	5.08	1.69
Sn	50	L-series	3.23	4.65	0.83
S	16	K-series	0.95	1.36	0.90
Zn	30	K-series	0.67	0.97	0.37
Total			69.45	100.00	100.00

4.3.1.3 Optical absorption study

The electronic transition in the material can be monitored by studying the energy band transition within the material by using the optical absorption

spectroscopy. The optical absorption of CZTS films was studied in the wavelength range 280 nm to 800 nm. Figure 4.11 represents the optical absorbance spectra of as-deposited CZTS films which show that CZTS film have high absorbance in visible region (380-750 nm), suggesting its applicability for an absorber layer. Optical absorption was found to increase with increasing annealing temperature.

Further optical data were analyzed by using Tauc relation [165] from which the absorption coefficient α, for semiconductor material is given by

$$\alpha = \frac{A\left(h\nu - E_g\right)^n}{h\nu} \qquad (4.11)$$

Where α is absorption coefficient, A is a constant, hν is incident photon energy, E_g is energy band gap i.e. separation between bottom of conduction band and top of the valance band, n is constant which depends on the nature of transition i.e. n=1/2 for allowed direct transition, n=2 for allowed indirect transition. Plot of $(\alpha h\nu)^2$ (by taking n=1/2) vs hυ is a straight line which show it is a direct band gap material. This type of transition was reported already by previous researchers for CZTS thin films [5, 19]. Extrapolation of Tauc plot to zero absorption coefficient (α=0) give energy band gap values.

Figure 4.12 shows that energy band gap decreases with increase in annealing temperature and results for as-deposited and annealed CZTS films were summarized in Table 4.4. The red shift in band gap was found due to increase of grain size and calculated energy band gap values are nearly equal to theoretical values of optimized band gap of solar energy spectrum [185-187].

Table 4.4: Energy Band Gap values for as-deposited and annealed CZTS thin film.

Sr. No.	Sample	Band Gap (ev)
1	As deposited CZTS	1.8
2	Annealed CZTS at 50°C	1.7
3	Annealed CZTS at 150°C	1.6
4	Annealed CZTS at 250°C	1.4
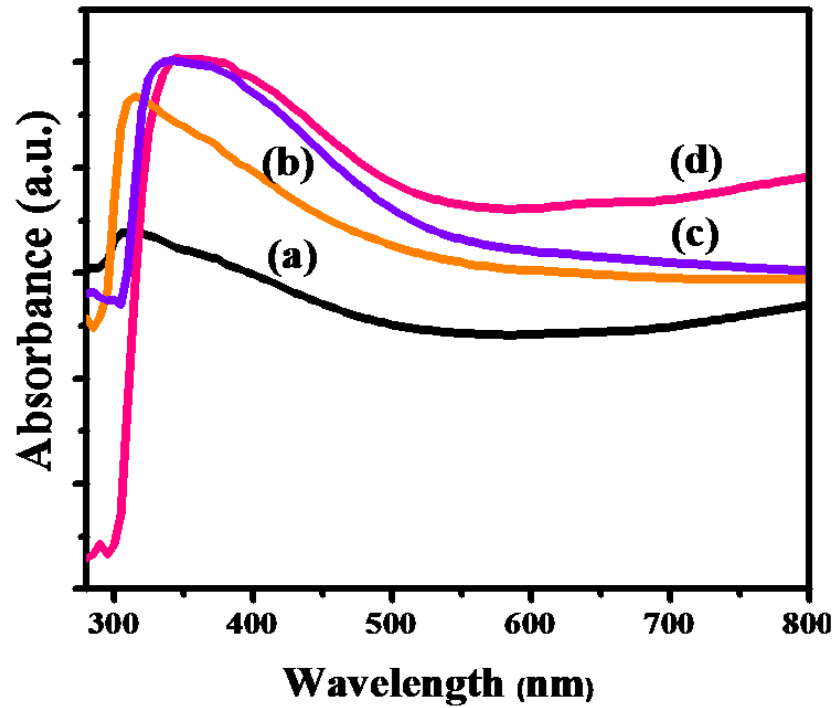
Figure 4.11: Variation of absorption (a.u.) with wavelength (nm) of (a) as deposited and (b) annealed CZTS thin film at 50° C (c) annealed CZTS thin film at 150°C (d) annealed CZTS thin film at 250°C in air for 2 hrs.
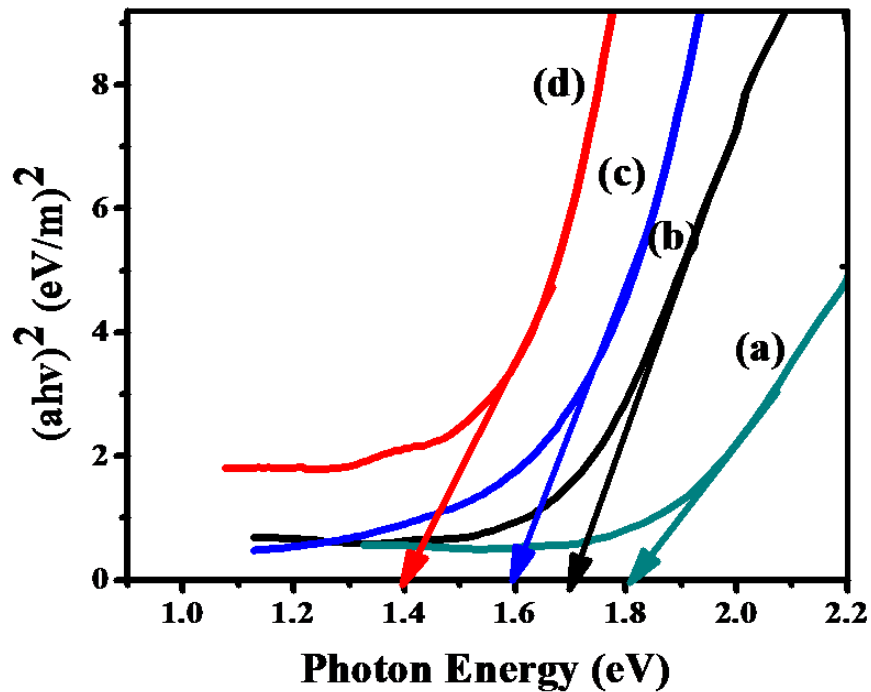
Figure 4.12: The plots of $(\alpha h\upsilon)^{2}$ vs hυ of (a) as deposited (b) annealed CZTS thin film at 50° C (c) annealed CZTS thin film at 150°C (d) annealed CZTS thin film at 250°C in air for 2 hrs.

4.3.1.4 I-V Characteristics

For detecting the photosensitivity of CZTS absorber layer the Schottky diode was constructed by metal contact on top of CZTS samples. Figure 4.13 shows the I-V characteristics curve for as-deposited CZTS absorber layer and Figure 4.14 shows the I-V characteristics of film annealed at 50°C, 150°C, 250°C. It was observed that as deposited film show ohmic behavior while after annealing treatment Schottkey like diode behavior is shown by absorber layer.
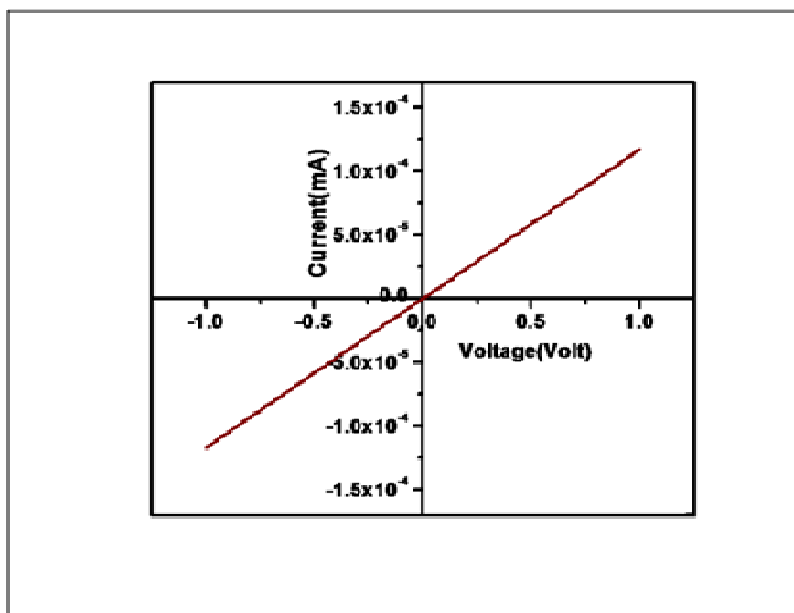
Figure 4.13: I–V characteristics of as-deposited CZTS films
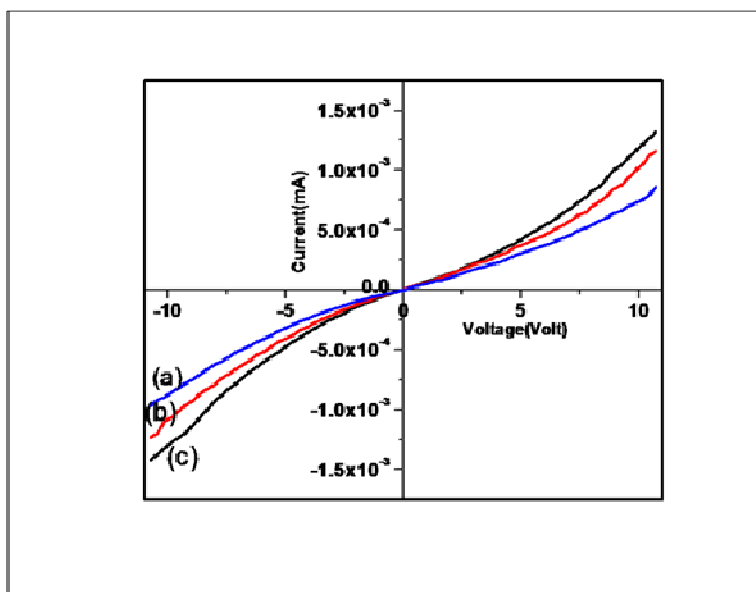
Figure 4.14: I–V characteristics of (a) annealed CZTS thin film at 50° C (b) annealed CZTS thin film at 150°C (c) annealed CZTS thin film at 250°C in air for 2 hrs.

As annealing temperature increases short circuit current (I_{sc}) increase (Table 4.5) which shows that recombination is decreasing as annealing temperature is increasing. This gives an important parameter for increasing the efficiency of absorber layer. It is seen that at higher annealing temperature resistance for absorber layer decreases indicating less characteristic resistance (R_{ch}) (Table 4.5). It is concluded that as annealing temperature increases band gap decreases and short circuit current increases, which is accordance with previously drawn results by H.J. Hovel [184].

Table 4.5: Electrical parameters values for as-deposited and annealed CZTS thin films.

Sr. No.	Sample	Resistance (R_{ch})	Resistivity (R_s)	Conductivity
1	Annealed CZTS at 50°C	9.0×10^3	0.36×10^5	2.77×10^{-5}
2	Annealed CZTS at 150°C	8.13×10^3	0.32×10^5	3.12×10^{-5}
3	Annealed CZTS at 250°C	6.99×10^3	0.27×10^5	3.70×10^{-5}

4.4   Conclusion

CZTS thin film absorber layer was synthesized by low cost Chemical Bath Deposition (CBD) method after optimizing deposition parameters. Conclusively, deposition temperature of 60^{0}C and deposition time of 7 hrs is optimum for synthesis of CZTS thin film. The formation of kesterite structured CZTS phase with tetragonal structure for annealed film at 150^{0}C was confirmed. Surface morphology of CZTS film shows increase in grain size with annealing temperature. A schottky diode like behavior was observed after annealing and enhancement in conductivity suggested application of CZTS thin films as photo active absorber layer.

Further, effect of annealing was studied as initial work depicts the importance of annealing in alteration of characteristics properties of CZTS thin film. We were successfully done the annealing at various temperatures starting from 50^{0}C to 250^{0}C with variation of 100^{0}C. Structural studies indicated amorphous nature of as-deposited CZTS films which were converted to polycrystalline CZTS films after annealing. As annealing temperature increases, intensity of diffraction peaks also increases and FWHM decreases. This indicates that the grain sizes in CZTS thin films

increase with increasing the annealing temperature. Surface morphological study also showed increase in grain size with increasing annealing temperature and roughness of the film surface was enhanced with less grain boundaries. Optical properties have been studied using optical absorption spectroscopy. Optical absorption was found to increase with increasing annealing temperature and energy band gap decreases with increase in annealing temperature. The optical absorption study indicates the direct transition with a direct energy band gap 1.4 eV.

CHAPTER 5

EFFECT OF SYNTHESIS PARAMETERS ON CZTS THIN FILM

5.1   Introduction

In terms of commercialization of thin film solar cells, chalcopyrite solar cells have reached up to commercial level, but these solar cells has some limiting factors. Therefore, working and exploring in the field of new material Copper-Zinc-Tin-Sulphide (CZTS) is concern of researchers working in photovoltaics field. However, as mentioned in an earlier chapter several successful attempts have been reported by various mentioned vacuum based methods, but there are some issues related to these techniques. Vacuum based technique requires sophisticated, expensive equipments, which results in high production cost as well as limited area deposition is also an shortcoming of vacuum based techniques. Another disadvantage is high temperature deposition condition which reduces the simplicity of deposition process. So, researchers in this field are trying to develop a simple method which can be used commercially.

Chemical Bath Deposition method is simple and economical method. The optimization of parameter for chemical bath deposition (CBD) method has been given in earlier chapter, although effect of precursors and concentration plays a vital role in the film deposition. So, the central theme of this work is optimizing and controlling the deposition parameter of CBD method for different chemical precursors as well its impact on different properties. The effects of synthesis parameters on CZTS thin film absorber layer are described in this chapter.

5.2   Effect of chemical precursor

5.2.1. Experimental detail

Synthesis of CZTS thin film

Cu_2ZnSnS_4 (CZTS) thin films were deposited on glass substrate which was cleaned earlier by detergent, acetone and DI Water ultrasonically. Two types of chemical precursors were used for deposition i.e. chloride based precursors ($CuSO_4.5H_2O$, $ZnSO_4.7H_2O$, $SnSO_4$, NH_2CSNH_2) and sulphate based precursors ($CuCl_2.H_2O$, $ZnCl_2$, $SnCl_4.5\ H_2O$, NH_2CSNH_2) for the source of copper, zinc, tin and sulpher respectively and EDTA was used as complexing agent. Details of these precursors and their concentrations were mentioned in Table 5.1.

Table 5.1: Chemical concentration of different chemical precursors for CZTS thin film deposition.

Copper	Zinc Precursor	Tin Precursor	Sulpher Precursor	Complexing Agent
(i) Sulphate Based Presursors				
Copper Sulfate pentahydrate ($CuSO_4.5H_2O$)	Zinc Sulfate heptahydrate ($ZnSO_4.7H_2O$)	Stannous Sulfate ($SnSO_4$)	Thiourea (NH_2CSNH_2)	Ethylenediamin etetraacetic acid (EDTA)
0.1 M	0.05 M	0.05 M	0.5 M	0.075 M
(ii) Chloride Based Presursors				
Copper Chloride dehydrate ($CuCl_2.H_2O$)	Zinc Chloride ($ZnCl_2$)	Tin Chloride pentahydrate ($SnCl_4.5\ H_2O$)	Thiourea (NH_2CSNH_2)	Ethylenediamin etetraacetic acid (EDTA)
0.1 M	0.05 M	0.05 M	0.5 M	0.075 M

Initially separate solution was prepared and after mixing by magnetic stirrer pH was controlled by adding ammonia and final pH of solution was ~10. After controlling the pH, previously cleaned substrates were immersed in the bath and then bath was heated up to 60^oC. During reaction white solution became yellow after 5-7 minutes and presence of precursor metal sulfide give reaction a brown blackish color. Precipitation started to form in the bath after 1 hrs and deposition of CZTS film

started on the substrates and after 7 hrs substrate with CZTS film was removed, rinsed in DI water, dried in air and preserved in desiccators. The details of experimental set up were described in chapter 4. Further, as-deposited CZTS thin films were annealed in air at 250°C for 2 hrs in a tubular furnace.

5.2.2   Characterization

The structural properties of as-deposited and annealed CZTS thin film were studied by X-ray diffraction (XRD) by using PANalytical X'Pert Pro X-ray Diffraction Unit with copper (Cu), which have strong Kα radiation having X-ray emissions wavelength of 1.5418 Å in 2θ range of 20-60°. The surface morphological study was carried out using scanning electron microscope (SEM) JEOL JSM model 6360 and Atomic Force Microscope (AFM). UV- characteristic studied using LAMBDA 950 UV/Vis/NIR Spectrophotometer. Electrical measurements were taken using custom built unit in the laboratory equipped with Keithely, model SMU-2400 and interface with a personal computer rements.

5.2.3   Results and discussion
5.2.3.1 Structural analysis

Figure 5.1 shows the XRD pattern of annealed chloride based and sulfate based CZTS film. XRD pattern of annealed sulfate based CZTS thin film [Figure 5.1(a)] exhibit sharp peaks at different angles and by comparing calculated 'd' values with experimental 'd' values corresponding phases can be determined, those are (110), (112), (200) and (220). XRD pattern of annealed CZTS thin films at 250°C in air for 2 hrs in Figure 5.1(b) depicts phases (112), (200), (220), (103) and (224). This confirms the synthesis of CZTS kestarite tetragonal crystal structure. This result is in agreement with previously reported results [98,180]. Hence we were verified the formation of kesterite structured CZTS phase to tetragonal structure at 250^{0}C with better crystalline nature for chloride based precursors.

5.2.3.2 Surface morphological analysis

Surface morphological analysis of modified CZTS thin films of different precursors was done by Scanning Electron Microscope (SEM) and Atomic Force Microscope (AFM). Figure 5.2(a) shows morphology of sulfate based thin film annealed at 250^{0}C for 2 hrs; it shows the agglomerated grains with rough surface. Figure 5.2(b) shows surface morphology of chloride based annealed film at 250^{0}C for

76

2 hrs and depicts the growth of dense background of fine grains with well covered interlinked cubic crystal on the surface.
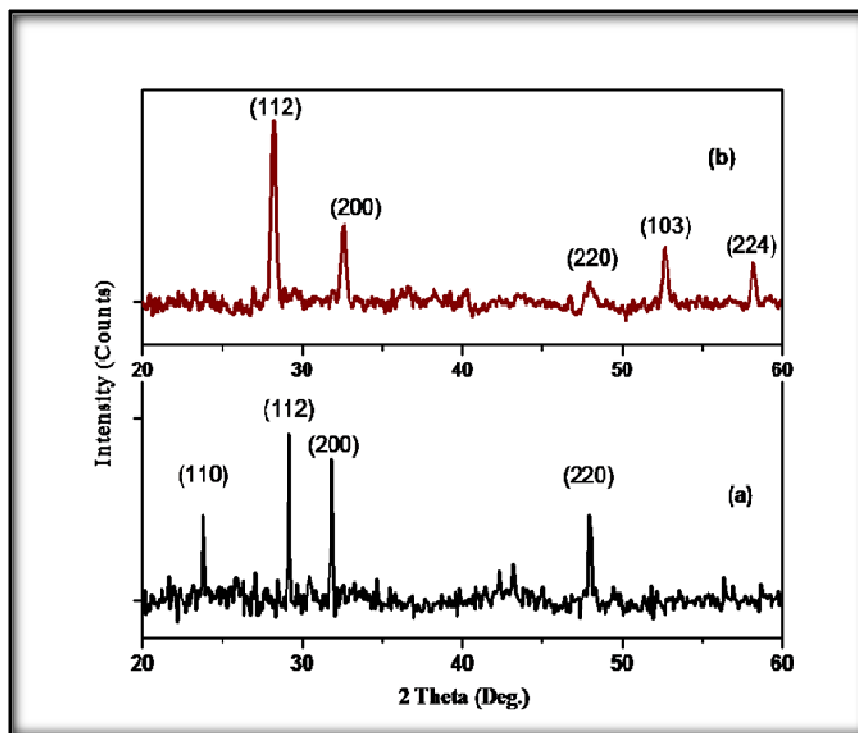
Figure 5.1: XRD patterns of sulfate based (a) annealed CZTS thin films at 250°C in air for 2 hr and (b) chloride based annealed CZTS thin films at 250°C in air for 2 hrs.
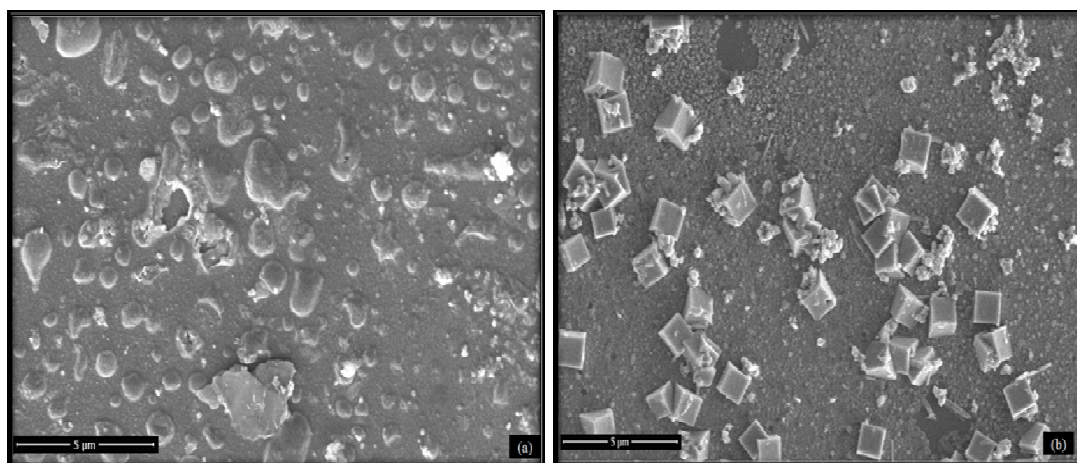
Figure 5.2: SEM image of sulfate based (a) annealed CZTS thin films at 250°C in air for 2 hrs and (b) chloride based annealed CZTS thin films at 250°C in air for 2 hrs.

Figure 5.3(a,b) shows 2D and 3D AFM micrographs of annealed sulfate based and chloride based CZTS thin films, respectively. Figure 5.3(a) show AFM micrographs of the sulfate based film, which indicate rough and compact morphology in nature with some agglomerated particles that existed on the surface. Figure 5.3(b)

depicts the surface morphology of the chloride based films. It indicates that for chloride based annealed film after annealing morphology was found to improve and film were homogenous background with densely packed distinct grains. These homogenous grains are useful for solar cell application because it reduce localized recombination sources [183].
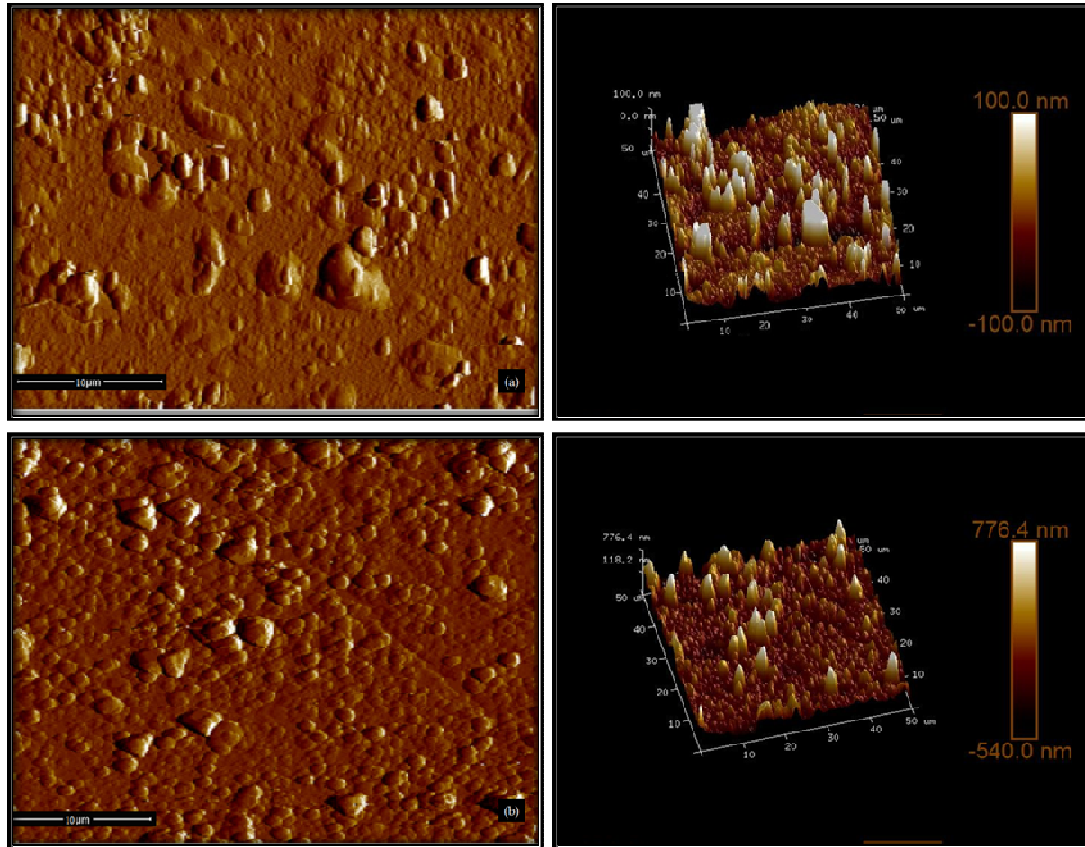
Figure 5.3: 2D &3D AFM image of (a) sulfate based annealed film at 250°C in air for 2 hrs and (b) chloride based annealed film at 250°C in air for 2 hrs.

AFM variables for sulfate based and chloride based annealed films are represented in Table 5.2.

Table 5.2: Variation of surface roughness for sulfate based and chloride based annealed films

Variables	Sulfate based annealed film	Chloride based annealed film
Average surface roughness	39.6 nm	26.4 nm
Root mean square roughness	69.5 nm	45.4 nm

5.2.3.3 Optical absorption Study

In order to study absorption spectra and energy band gap of as-deposited and annealed chloride based CZTS thin film, the optical absorption was studied in the wavelength range 300-800 nm. Figure 5.4 suggested that films have high absorbance in visible region.
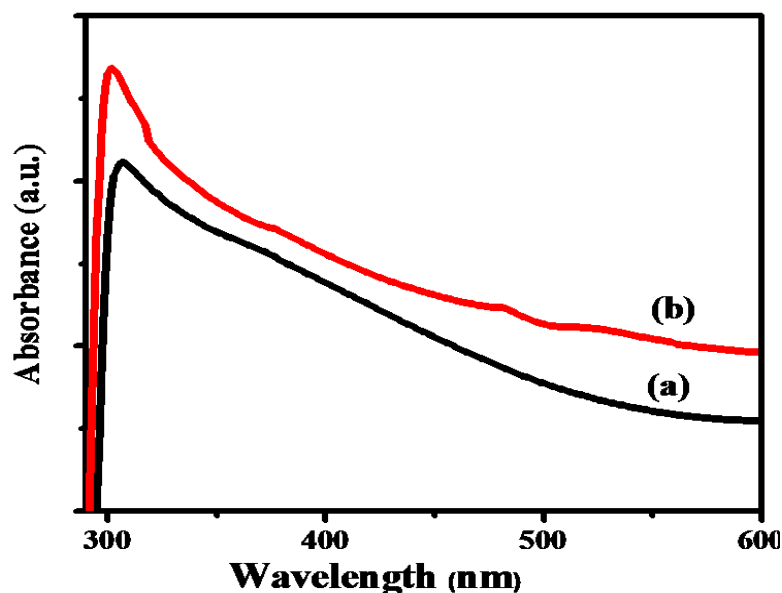
Figure 5.4: Variation of absorption (a.u.) with wavelength (nm) of chloride based (a) as deposited and (b) annealed film at $250^o\,C$ in air for 2 hrs
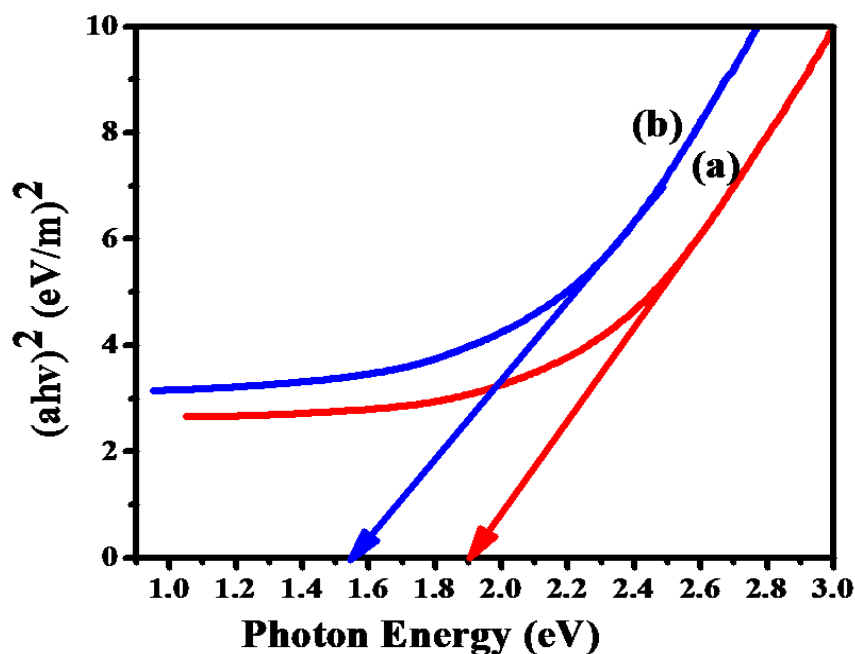
Figure 5.5: The plots of $(\alpha h\upsilon)^2$ vs $h\upsilon$ of chloride based (a) as deposited and (b) annealed film at $250^o\,C$ in air for 2 hrs.

Further, energy band gaps of film were analyzed by using Tauc relation [165] as mentioned earlier. Plot of $(\alpha h\upsilon)2$ (by taking n=1/2) vs hυ is a straight line which show it is a direct band gap material. Energy band gap values determined by extrapolation of Tauc plot to zero absorption coefficient (α=0). Figure 5.5 shows that band gap energy decrease from 1.9 eV to 1.54eV with increase in annealing temp.

5.3   Effect of precursor concentration

From above it is observed that properties of CZTS thin films depend upon choice of chemical precursors. Now, the effect of precursor concentration could be an important point. Chemical concentration of precursors may affect the efficiency due to the possible lattice mismatch and vacancies. The effect of chemical precursor concentration on the properties of CZTS thin film deposited by various other methods was discussed by researchers. It was found that Cu-poor films shows improved efficiency as Cu vacancy work as acceptors in CZTS by chen et. al [170]. Other studies show that in case of Cu-rich and Sn-poor films, Cu_2S or Cu_4SnS_4 can form inclusions or pin-holes in the film. Cu_2S present in CZTS act as metals [133-134] and conducting phase causes recombination and trapping of electrons and holes due to the lower band gap of this phase (Eg =1.21) [135]. A Cu poor film can enhance the p-type behavior and the best combination is copper-poor/zinc-rich due to compensating phenomena [70].

Although, above mentioned results show that Cu- poor and Zn- rich CZTS thin films are good for efficient absorber layer, but in case of films deposited by CBD method, there is no work reported in the literature to the best of our knowledge So, controlling the concentration of chemical precursors and found the appropriate composition is the focus of this work. In this study, we investigate the influence of chemical concentration of precursors on synthesis and properties of CZTS thin film by CBD method.

5.3.1 Experimental detail
Synthesis of CZTS thin film:

Glass substrates were cleaned by detergent then ultrasonically cleaned by acetone, methanol and de-ionized (DI) water and dried in air. Chemical bath was prepared by analytical reagent grade (AR) chemicals provided by Sigma Aldrich with 99.9% purity. Copper chloride dehydrate ($CuCl_2.H_2O$), zinc chloride ($ZnCl_2$), tin

chloride pentahydrate ($SnCl_4.5\ H_2O$) and thiourea (NH_2CSNH_2) were used as precursor chemicals for $Cu^{2+}, Zn^{2+}, Sn^{2+}$ and S^{2-} ions and EDTA was taken as complexing agent. Chemical concentrations of $CuCl_2$, $ZnCl_2$, $SnCl_4$, NH_2CSNH_2 and EDTA were taken in equal volume ratio and described in Table 5.3.

Table 5.3: Chemical concentrations of precursors.

Sample No.	Chemicals (In moles)					Ratios				
	$CuCl_2$	$ZnCl_2$	$SnCl_4$	NH_2CSNH_2	EDTA	C/(Z+T+S)	Z/(C+T+S)	S/(C+Z+T)	(C+T)/Z	(Z+T)/C
S_A	0.2	0.05	0.05	0.5	0.075	0.33	0.07	0.60	5.00	0.50
S_B	0.1	0.05	0.05	0.5	0.075	0.17	0.08	0.40	3.00	1.00
S_C	0.1	0.2	0.05	0.5	0.075	0.13	0.31	0.70	0.75	2.50
S_D	0.1	0.4	0.05	0.5	0.075	0.11	0.62	1.10	0.38	4.50

Details of deposition method and parameters has been reported in an earlier chapter [chapter 4], while steps of CZTS thin film deposition are following:

Separate solution prepared by stirring

pH controlled by adding ammonia

Final pH of solution is ~10

Substrates immersed in the bath

Bath heated up to 60°C

After 5-7 min.

Solution become brown blackish

After 1 hr

Precipitation started to formed

After 7 hr

CZTS Thin film

81
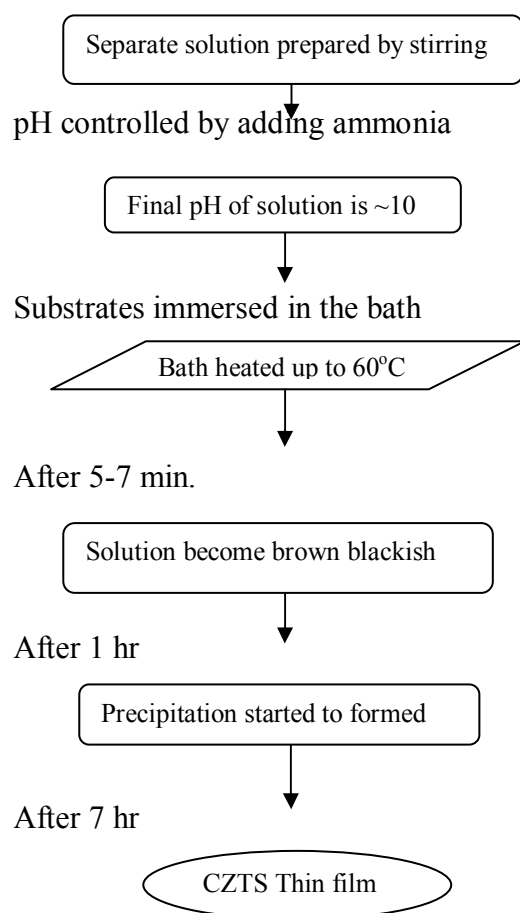
Samples prepared for different concentrations were collected, dried in air, labeled as S_A, S_B, S_C and S_D and preserved in dessicator. Further, according to our previously drawn results for post annealing treatment, samples were annealed at 250° C in air for 2 hrs for surface modification.

5.3.2   Characterization

The structural property of CZTS thin film was studied by X-ray diffraction (XRD) by using PANalytical X'Pert Pro X-ray diffraction unit. Average crystallite sizes were determined according to broadening of peaks using Scherrer relationship. The surface morphological study was carried out using scanning electron microscope (SEM) and Atomic Force Microscope (AFM). The optical absorption spectra were recorded using UV–vis spectrophotometer. I-V characteristic studied using custom built set up Keithely, model SMU-2400 computer interface with a pc.

5.3.3   Results and discussion

5.3.3.1 Structural analysis

X-ray diffraction (XRD) technique was used for performing the structural analysis of samples S_A, S_B, S_C and S_D (Figure 5.6). From XRD patterns for the annealed CZTS films, crystalline nature was observed for the annealed films of different concentrations. Figure 5.6(a) shows the XRD pattern of sample S_A and there are peaks appearing at 28.4^o, 33° and 59°, by comparing the calculated 'd' values with experimental 'd' values (from JCPDS card 26-0575) corresponding (112), (200) and (224) planes are found. Figure 5.6(b) shows the XRD pattern of sample S_B which indicate diffraction patterns of peaks at 28.4^o, 33°, 47.3^o and 59° were attributable to the planes (112), (200), (220) and (224). Figure 5.6(c) indicates XRD pattern of CZTS film (sample S_C) and depicts that plans are (112), (200), (220), and (224). XRD pattern of sample S_D shows the planes (112), (200) and (220) . These diffracting plans for annealed films are characteristic of tetragonal type kesterite structure of Cu_2ZnSnS_4 [117]. An extra peak at 52° is also present in all samples, which is attributed to (103) plan of wurtzite structured CZTS film. The phenomenon of more than one strong peak is attributed to the polycrystallinity of a deposited CZTS thin film. No secondary phase is observed, suggesting that the CZTS films were close to stoichiometric.

The diffraction patterns indicated CZTS thin film preferred orientation along (112) plane. Change in intensity of (112) peak is observed for the films for different concentrations. The intensity of the (112) diffraction line increased with increasing the Zn concentration, but the sample S_C gives a relatively more intense and sharper diffraction peaks than the other concentrations, which suggested that the sample S_C has good crystallinity. The grain size of the CZTS thin film was calculated using Scherer's equation. The grain size for (112) plan for as-deposited and annealed CZTS films were summarized in Table 5.4.
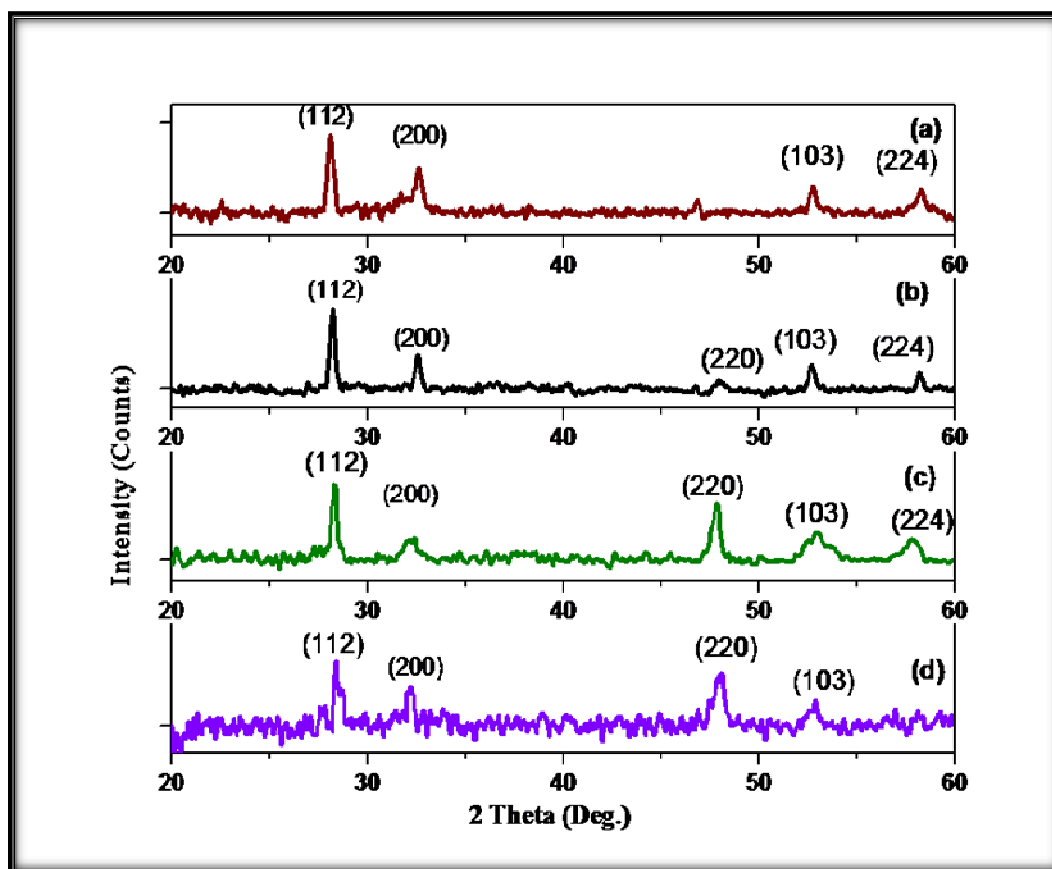
Figure 5.6: XRD patterns of (a) sample S_A (b) sample S_B (c) sample S_C (d) sample S_D annealed CZTS thin films at 250^oC in air for 2 hrs.

Table 5.4: The FWHM values and grain sizes of (112) orientation of the CZTS thin films obtained at different concentrations.

Sample	S_A	S_B	S_C	S_D
FWHM	1.522	0.799	0.48	.902
Particle Size (nm)	5.62	10.72	17.84	12.81

5.3.3.2 Surface morphological analysis

The surface morphology of CZTS films were studied by SEM images. Figure 5.7 (a) shows SEM surface image of sample S_A and indicates the growth of fine grains in the background with few cubic crystals on the surface. These fine grains keep growing after increasing Zn concentration and chicken mesh like structure prominently started to appear with few agglomerated cubic crystal on surface. Figure 5.7 (b) indicate that as Zn concentration increases, growth of grains on surface as well as in background also increase. Figure 5.7(c) shows morphology of sample S_C, it shows the growth of well covered interlinked cubic crystal with dense background. Figure 5.7(d) shows the XRD pattern of sample S_D at higher Zn concentration, cubic crystal started to form agglomerated and uneven distribution on the surface occur.

Analysis of SEM images implies that as the Zn concentration increases, grain growth occurs and there is compact grain growth for sample S_C. Further concentration increment leads to disordered distribution with lower crystallization. Figure 5.7(e & f) shows SEM image of CZTS film for sample S_C at higher magnification and reveals two distinct grain structure i.e. cubic and rice shape grains with definite boundaries. Average grain size is $1.25+0.1$ μm and 0.01 μm for cubic and rice shape grains, respectively. Cubic grains are highly interlocked and consist of smooth surface at corners and densely arranged rice shape grains. It is well known that dense films with interlocked grains are high performance photovoltaics devices.

This analysis shows that high Zn concentration could improve the crystallinity and increase the grain size of thin films and may result in high grain growth but after certain concentration. Crystal structure tends to come under influence of disorder and uneven agglomeration and some voids and cracks could be seen at high magnification. It gives a very important parameter in respect of concentration effect of precursors on CZTS thin films.

Atomic Force Microscope (AFM) was utilized to study the evolution of the morphological state of CZTS thin films as a function of concentration. Figure 5.8 shows 2D and 3D AFM micrographs of CZTS thin films at different concentration. Figure 5.8(a) depicts that AFM image of CZTS thin film (sample S_A) and shows that some agglomerated particles exist on the surface of CZTS thin films. This may be

because the nucleation process started during synthesis and growth of grains takes place at this concentration.
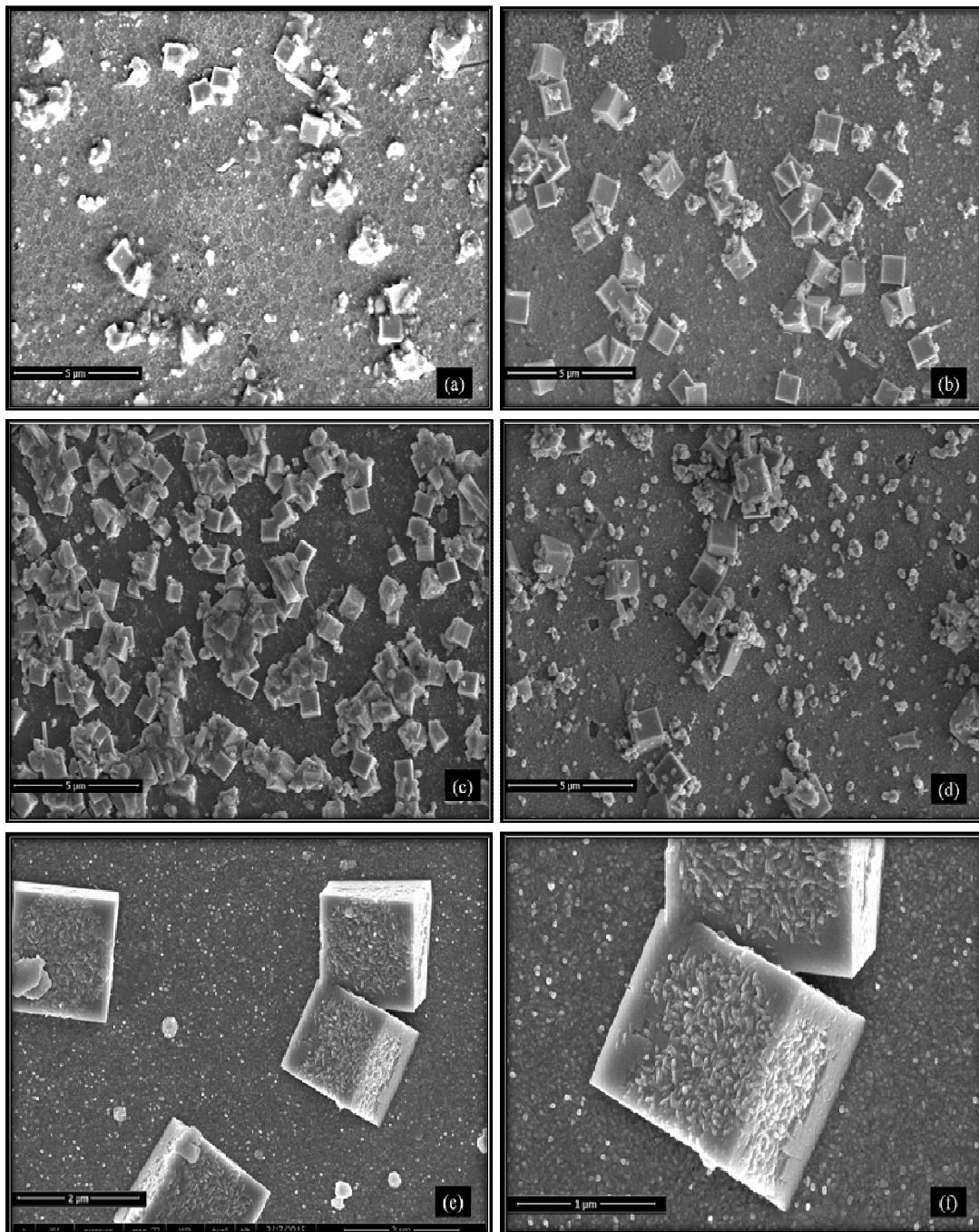
Figure 5.7: SEM images of (a) sample S_A (b) sample S_B (c) sample S_C (d) sample S_D annealed CZTS thin films at 250°C in air for 2 hr (e) & (f) sample S_C at higher magnification
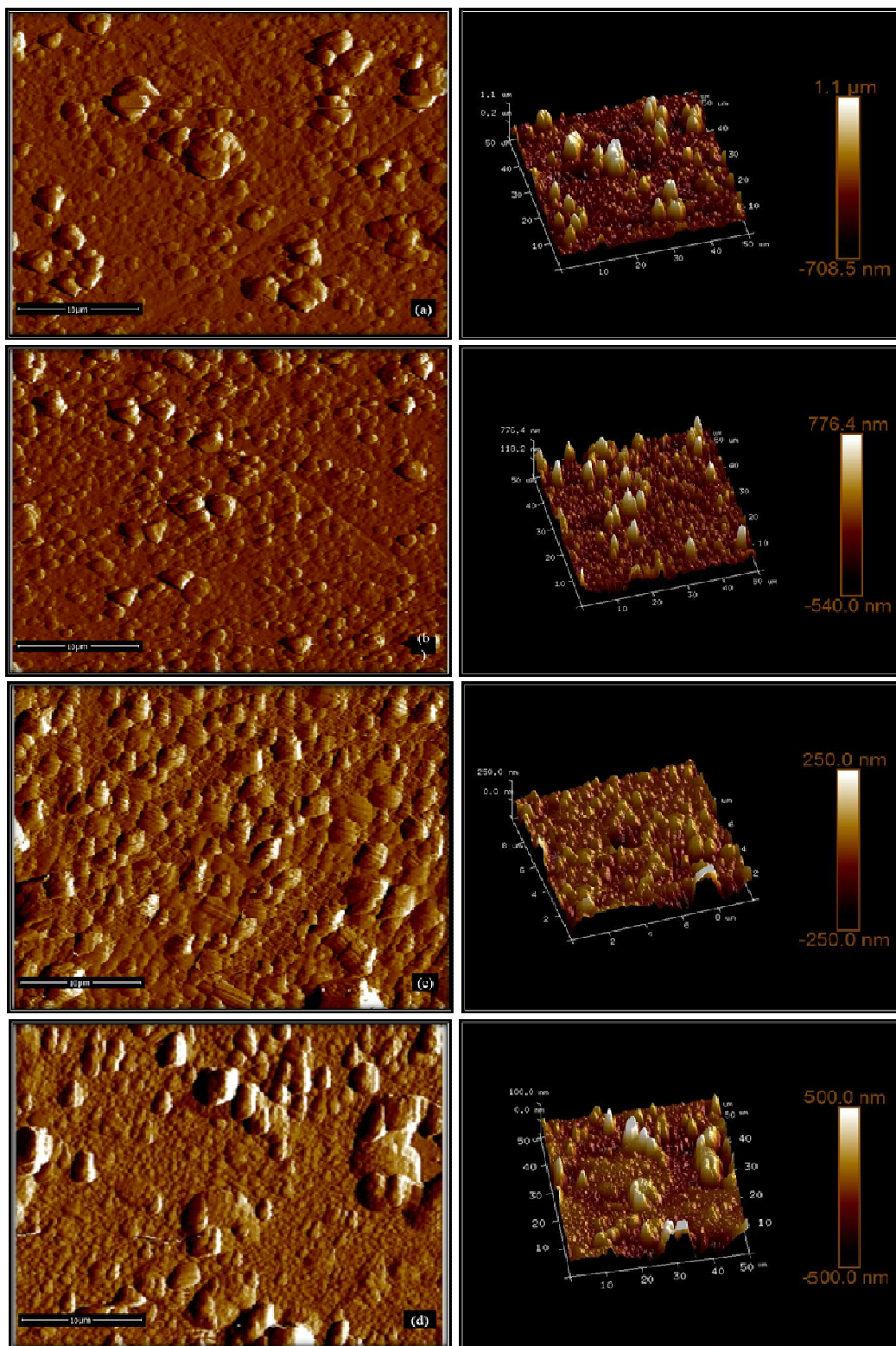
Figure 5.8: 2D & 3D AFM image of (a) sample S_A (b) sample S_B (c) sample S_C (d) sample S_D annealed CZTS thin films at 250°C in air for 2 hrs.

Figure 5.8(b) indicates that as concentration increases, the morphology is found to improve and distinct grains are seen. Figure 5.8(c) for sample S_C shows the presence of homogenous grains throughout the film. Figure 5.8(d) shows that modification takes place and at some places grain joint together in clusters for sample S_D. It can be clearly discerned that an important structural property that was affected by precursor concentration is the grain size. Figure 5.8(c) also exhibited highest crystallinity, highest grain size, which again prove best results for sample S_C.

Table 5.5: Variation of surface roughness for all samples.

Image Rq	Image Ra	Image Rmax	Film Thickness	grain size
69.8 nm	45.6 nm	772 nm	1316	2.5 to 3.07 μm
205 nm	171 nm	1520 nm	1233	2.85 to 3.22 μm
223 nm	153 nm	2118 nm	1808	3.4 to 3.6 μm
39.8 nm	26.5 nm	395 nm	200	2 to 4 μm

AFM variables for all samples are shown in Table 5.5. Higher roughness values of annealed films are attributed to larger grain size and due to better nucleation process during annealing process.

5.3.3.3 Optical absorption study

The variation of the optical absorption with wavelength is analyzed to find out the nature of optical transition involved and the optical band gap in the wavelength range 300-800 nm. Figure 5.9 shows variation of absorbance (a.u.) of as deposited and annealed CZTS films with wavelength (nm). These spectra revealed that CZTS thin films shows high absorbance of light in the visible region. Figure 5.9 shows that as the concentration increase, the absorbance of the samples increases. Absorption for sample S_C was maximum and shifts to higher wavelength side because the secondary phases can absorb light with lesser wavelength and it decreased with the increase of the concentration. So, as the concentration increase, absorption spectra shift to lower to higher wavelength (red shift).
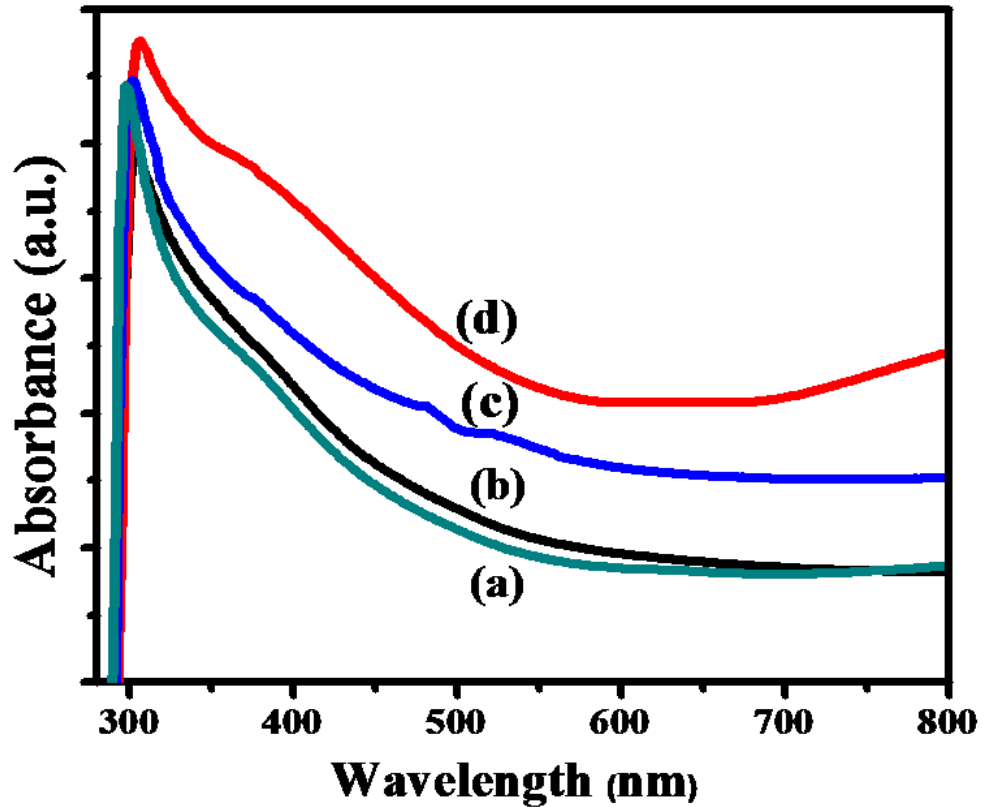
Figure 5.9: The variation of the optical absorption with wavelength (a) sample S_A (b) sample S_B (c) sample S_C (d) sample S_D annealed CZTS thin films at 250^oC in air for 2 hrs.

Figure 5.10 shows the variation of $(\alpha h\nu)^2$ vs hν, which is a straight line in the domain of higher energies, indicating a direct optical transition. The optical band gap energy (E_g) of the CZTS thin films was obtained by extrapolating the linear absorption edge part of the curve to the intersection with energy axis to zero absorption coefficients (a = 0). It can be seen that the optical band gap energies of the CZTS thin films using different precursor concentration were 1.7eV, 1.55eV,1.45eV and 1.4eV, respectively.

The energy band gap (E_g) of the CZTS thin films becomes smaller with the increase of the precursor concentration. The band gap of the film is close to the optimum band gap required for a solar cell with high conversion efficiency, indicating that CZTS is a promising material for thin film solar cell application.
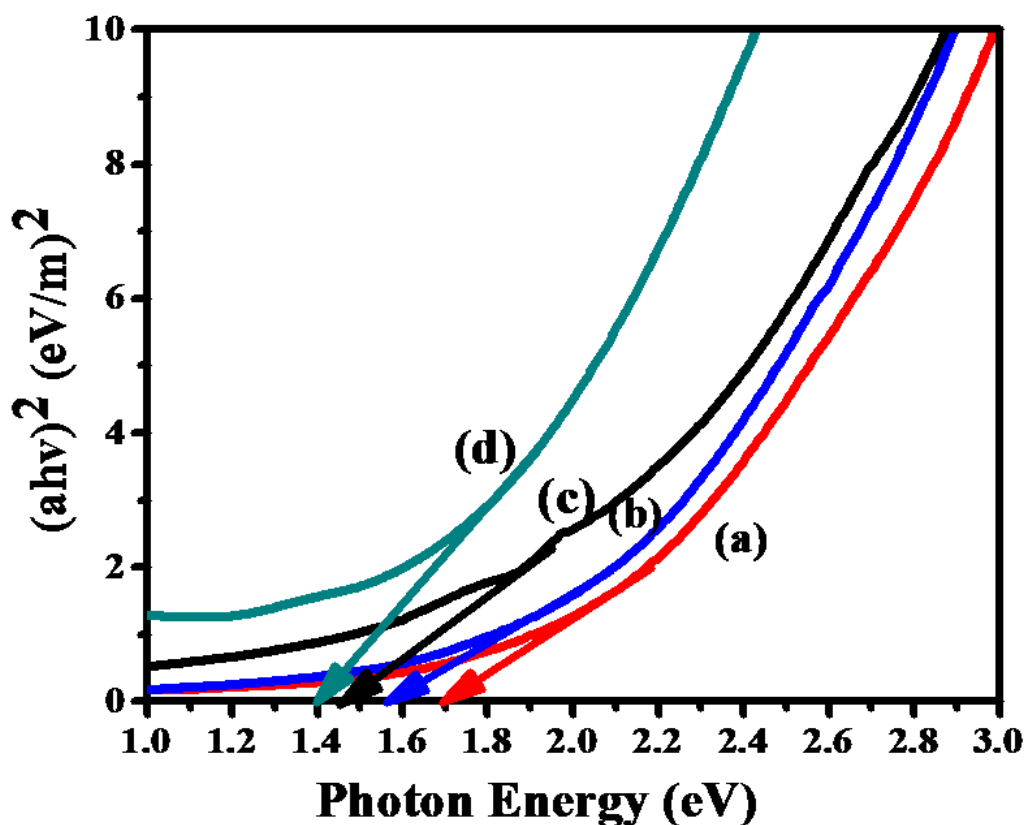
Figure 5.10: The plots of $(\alpha h\upsilon)^2$ vs hυ of (a) sample S_A (b) sample S_B (c) sample S_C (d) sample S_D annealed CZTS thin films at 250^oC in air for 2 hrs.

5.4   Conclusion

CZTS thin film as absorber layer was synthesized by low cost CBD technique after optimizing deposition parameters. Conclusively, previously optimized parameters, 60^0C temperature and deposition time of 7 hrs were used for synthesis of CZTS thin film for chloride based precursors and sulphate based precursors. The formation of kesterite structured CZTS phase with tetragonal structure at 250^0C was observed with better crystalline nature for chloride based precursors. Surface morphology of CZTS film shows increase in grain size with annealing and larger grains for chloride based precursors. The band gap of annealed CZTS films was calculated to be 1.54eV which is in the range of optimal band gap as found by absorption spectroscopy.

Further, CZTS thin film absorber layer was synthesized for various chemical precursor concentrations. The XRD patterns indicated characteristics of tetragonal type kesterite structure of CZTS thin film and preferred orientation is along (112)

plane. The intensity of the (112) diffraction line increased with increasing Zn concentration, but the sample S_C gives a relatively more intense and sharper diffraction peaks than the other concentrations, indicating that the sample S_C has good crystallinity. Surface morphology analysis shows that as Zn concentration increase the grain size of thin films, but after certain concentration uneven grains started to appear. The optical absorption study indicates the direct transition and energy bandgap (E_g) of the CZTS thin films becomes smaller with the increase of the precursor concentration. Therefore, chemical concentration has some effects on the crystallinity, phase, and optical properties of the CZTS thin film, and films have moderate Zn concentration shows relatively good properties.

CHAPTER 6

FORMATION OF ZnS/CZTS THIN FILM HETEROJUNCTION

6.1   Introduction

Thin film technologies hold considerable promise for a substantial reduction of the manufacturing costs of solar cells due to the reduction of material costs and the deposition on large area substrates. Moreover, thin film solar cells are stable, lightweight, flexible, and durable [188-191]. There are various materials used to fabricate solar cells. Each material has its own advantages and disadvantages.

Heterojunction solar cells have the potential to achieve the goals of higher efficiency, reliability and low cost, necessary for the large scale applications [192]. The advantages of hetero-junction solar cells over conventional p-n junction solar cells include: enhanced short wavelength spectral response because most photons are absorbed inside the depletion region of the second semiconductor, thus surface recombination of high-energy photon generated electron hole pairs is greatly decreased; they have lower series resistance because the first semiconductor can be heavily doped without causing the lifetime of minority carriers short; high radiation tolerance [193]. The solar cells consist of a number of films which are deposited onto a rigid or flexible substrate. The first film p-type film absorbs most of the light and generates the photocurrent (absorber). The heterojunction is formed by depositing a very thin n-type buffer layer and a p-type absorber layer.

6.2   The role of the buffer layer

In a heterojunction solar cell buffer layer play a vital role by constructing a junction with absorber layer and generating inbuilt electric field essential for

separation of photo-charge carriers [194-195]. Another function of buffer layer is admitting solar spectrum in the appropriate region to the absorber layer with maximum amount [196]. Wide energy band gap and low electrical resistivity are key issues for a good buffer layer, so that it can provide maximum amount of photons to the junction and absorber layer with minimum recombination losses. So, large energy band gap, lattice mismatch and appropriate doping density are the requirements of materials used for buffer layer.

In most of the reports of CZTS based solar cells, CdS was used as the buffer layer. CdS is established commercially chosen buffer layer as it fulfills all the requirements [197-198]. But toxicity of CdS is a major problem which leads to the environment health and safety impact issues [199-200]. So, the development of Cd free device is an area of research investigations. In research laboratories, work is being carried out on thin films like ZnS, ZnSe, In_2Se_3 for replacement of Cd based buffer layer [201-202]. Among these materials zinc sulphide is considered the most promising III-VI semiconductor material for optoelectronic, photovoltaic and photo-electrochemical solar cell applications due to its stability, wider band gap (3.54 eV) and photo conducting behavior which fulfill the requirement of maximum solar energy availability for absorber layer.

In this chapter, ZnS/CZTS thin films heterojunction was formed by depositing n-type ZnS buffer layers on glass substrate or ITO-coated glass and p-type CZTS absorber on ZnS/ITO-coated glass substrate. The structural, morphological and optical investigations of ZnS thin films as buffer layer were done by x-ray diffraction (XRD), atomic force microscopy (AFM) and optical absorbance respectively. The electrical properties of the fabricated glass/ITO/ZnS/CZTS/Ag heterojunction solar cells were investigated.

6.3   ZnS thin film as buffer layer

ZnS thin film can be deposited by different techniques [203-206]. Chemical bath deposition (CBD) is one of the attractive methods due to its advantages like simplicity, low deposition temperature, low cost and large area depositions [207-209]. Properties of thin films depend not only on the deposition method but also on the modification method. Post annealing treatment is easily approachable method which can be used for surface modification. In case of annealing, temperature is most

important parameter for treatment as at lower temperatures effects on the properties could be negligible. On the other hand at higher temperature defects generation and partial evaporation can take place. So, optimization of temperatures parameter for most suitable result is a work of concern. The purpose of this work is to establish a relation between annealing temperature and properties of ZnS thin film, and thus to find out most appropriate temperature for annealing to fulfill our objective of using ZnS thin film as a buffer layer.

Further, for enhancing the conductivity of buffer layer (ZnS), doping of elements such as Al, Cu, and Ni was done, in order to improve the performance of the solar cell [210-211]. So, the central theme of this work is optimizing and controlling the synthesis parameters for pure and doped ZnS thin films and to carry out a comparative study of the effect of doping on the properties of the deposited films. Further, thermal annealing on previously optimized temperature was used to control the morphology and structural properties of polycrystalline thin film. Considering this aspect we studied the annealing effect on the pure and doped ZnS thin films. Different characterizations were done by different characterization tools on as deposited and annealed pure and doped ZnS thin film specimens.

6.3.1 Experimental detail
Synthesis ZnS thin film

Chemical bath for synthesis was prepared by chemicals provided by Sigma Aldrich with 99.9% purity of analytical reagent grade (AR). Zinc Sulphate ($ZnSO_4$) and Thiourea (NH_2CSNH_2) was used as precursor chemicals for Zn^{2+} and S^{2-} ions. Chemical concentrations were taken as 0.1 M $ZnSO_4$ and 0.1 M NH_2CSNH_2 in equal volume ratio and hydrazine hydrate and Triethanolamine (TEA) were taken as complexing agent. Thin films were deposited on glass substrate. Before the deposition, substrates were cleaned by detergent and distilled water then ultrasonically cleaned by Acetone, Methanol and De-ionized (DI) water and then dried in air.

Initially solution was prepared by dissolving chemicals in distilled water by magnetic stirring separately. After preparing all the solutions they were mixed and final pH (~12) was controlled by adding sodium hydroxide solution. Cleaned glass and ITO coated glass substrate was immersed in the solution and solution was heated

up to 80$^{\text{o}}$C. After 10 min. precipitation started to form in the bath and deposition of ZnS film started on the substrates. After 2 hr ZnS film was deposited on substrate. Deposited films were removed, rinsed in DI water to remove the ions from film, dried in air and preserved in desiccator.

6.3.2   Surface modification

The surface of thin films can be modified by providing the post deposition treatments like thermal annealing. Annealing is heat processes in the furnaces which involve heating a material to a specific temperature and maintain it at a suitable temperature for appropriate time and then do slow cooling. This process alters the physical and sometimes chemical properties of a material. So, as-deposited ZnS thin films were annealed in air for 2 hrs in tubular furnace at 100 $^{\text{o}}$C to 400$^{\text{o}}$C. These ZnS thin films were characterized by different characterization techniques.

6.3.3   Result and discussion

6.3.3.1 Structural analysis

The structural analysis study was done by X-ray diffraction (XRD) technique. Figure 6.1 depicts the XRD pattern of as deposited and annealed ZnS thin films. Figure 6.1 reveals the amorphous nature of as deposited film due to the lack of diffraction peaks. Figure 6.2 (a to d) represented the XRD pattern of annealed ZnS thin films which show diffraction peaks at diffraction angles and indicate to crystallite nature. ZnS thin film annealed at 100^{0}C shows diffraction peak at 28.5^{0} and by comparing with JCPDS card (05-0566), sphalerite crystal structure with (111) plane is confirmed as Figure 6.2(a). XRD pattern of ZnS thin film annealed at 200^{0}C unveil the presence of more diffraction peaks at 47.5^{0} and 56.3^{0}, thus conveying the presence of plane (111), (220) and (311) as Figure 6.2(b). Crystal structure of ZnS thin film annealed at 300^{0}C is demonstrated by Figure 6.2(c), which show another extra peak at 33.1^{0} corresponding (200) plane. As the annealing temperature increases up to 400^{0}C, less intense diffraction peaks of plane (111) and (311) also occur as Figure 6.2(d). It also observed that the intensity of diffraction peaks increase with increasing annealing temperature and best results was at 300^{0}C and showing preferred degree of orientation along (111) plane as Figure 6.2(c). These results are in good agreement with reported data [212-213].
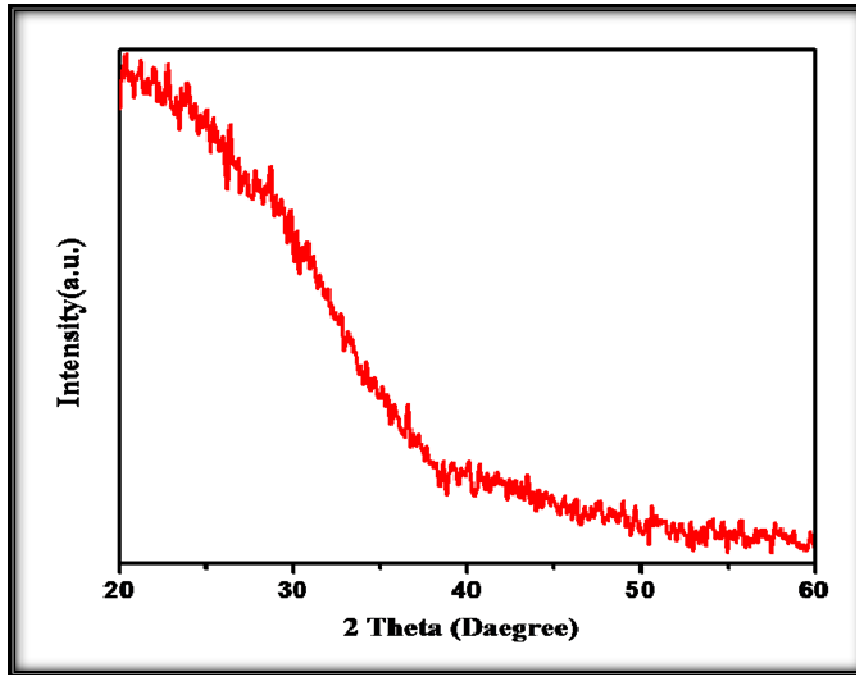
Figure 6.1: XRD patterns of as deposited ZnS thin film.
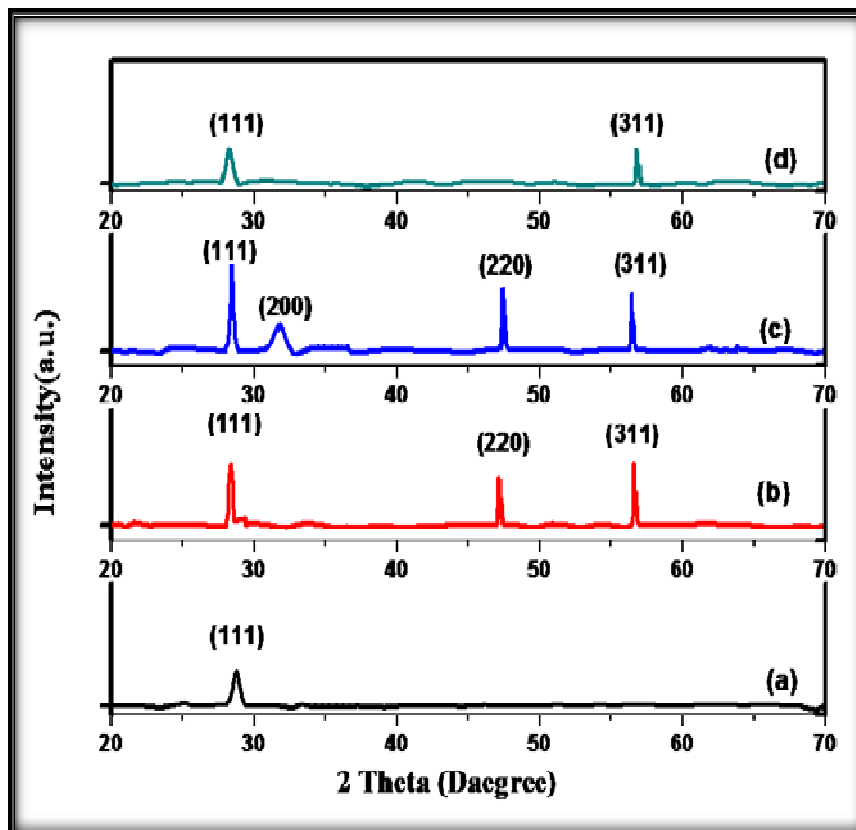
Figure 6.2: XRD patterns of (a) annealed ZnS at 100° C (b) at 200° (c) at 300° C and (d) at 400° C in air for 2 hrs.

6.3.3.2 Surface morphological analysis

The surface morphological analysis was done by Atomic Force Microscopy (AFM). Figure 6.3 shows the 2D and 3D AFM images of as deposited and annealed ZnS thin film.
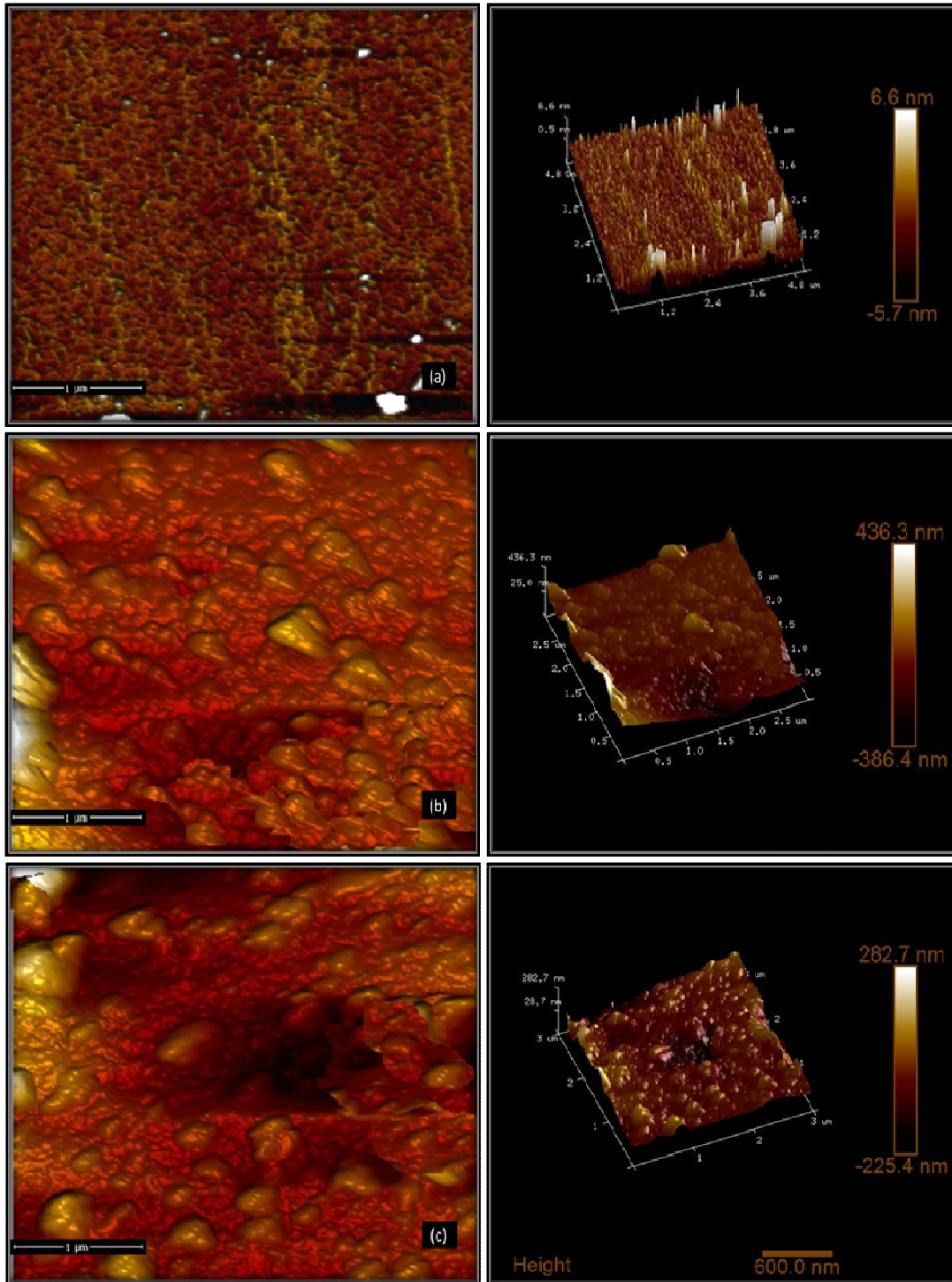
Figure 6.3: The 2D and 3D AFM images of (a) as deposited ZnS thin film (b) annealed ZnS thin film at 100°C (c) annealed ZnS thin film at 200°C in air for 2 hrs.
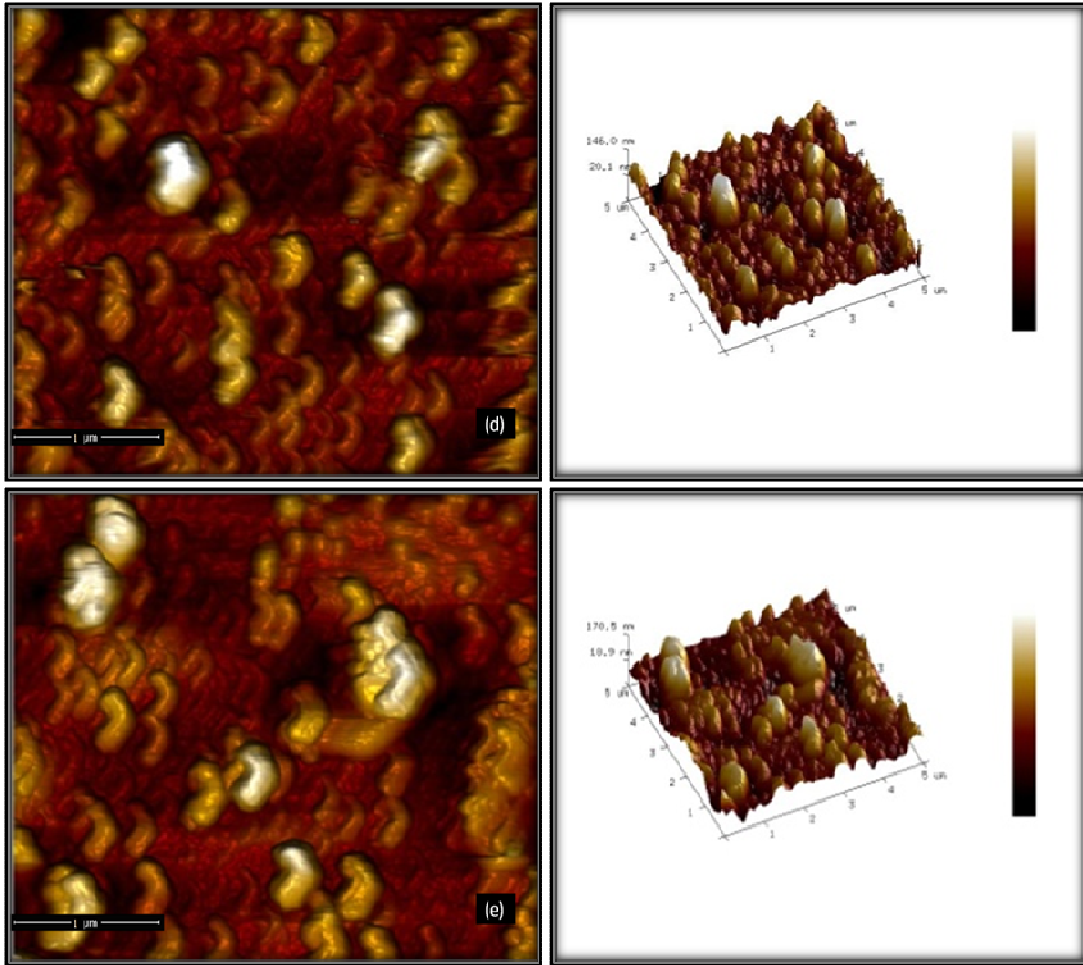
Figure 6.3: The 2D and 3D AFM images of (d) annealed ZnS thin film at 300° C (e) annealed ZnS thin film at 400° C in air for 2 hrs.

AFM image of as-deposited film leads to unvarying surface morphology of ZnS thin film [Figure 6.3(a)]. ZnS thin film started to show grain growth after annealing at 100^{0}C [Figure 6.3(b)] which turns film morphology to uneven grains of varying size from 0.25 μm±0.01 μm to 0.35±0.01 μm at surface. Same pattern was followed in the case of ZnS thin film annealed at 200^{0}C [Figure 6.3(c)] with slight variation in grain size. Figure 6.3(d) represents the morphology picture of film annealed at 300^{0}C and reveals that the surface is well covered by hemisphere shape grains of size 0.4±0.01 μm to 0.5±0.01 μm with equal distribution. Figure 6.3(e) indicates that grain shape and size almost remain same for film annealed at 400^{0}C, but on the other hand agglomeration of grains started to take place. It is thus concluded that annealing at 300^{0}C gives an evenly well covered consistent surface with higher grain size. The average surface roughness and root mean squared roughness of the annealed films is shown in Table 6.1.

Table 6.1: Surface Morphological parameters for annealed ZnS thin films

Sample	Average surface roughness	Root mean squared roughness
Annealed ZnS thin film at 100° C	92.1 nm	58.5 nm
Annealed ZnS thin film at 200° C	90.3 nm	41.4 nm
Annealed ZnS thin film at 300° C	41.6 nm	32.3 nm
Annealed ZnS thin film at 400° C	33.8 nm	25.7 nm
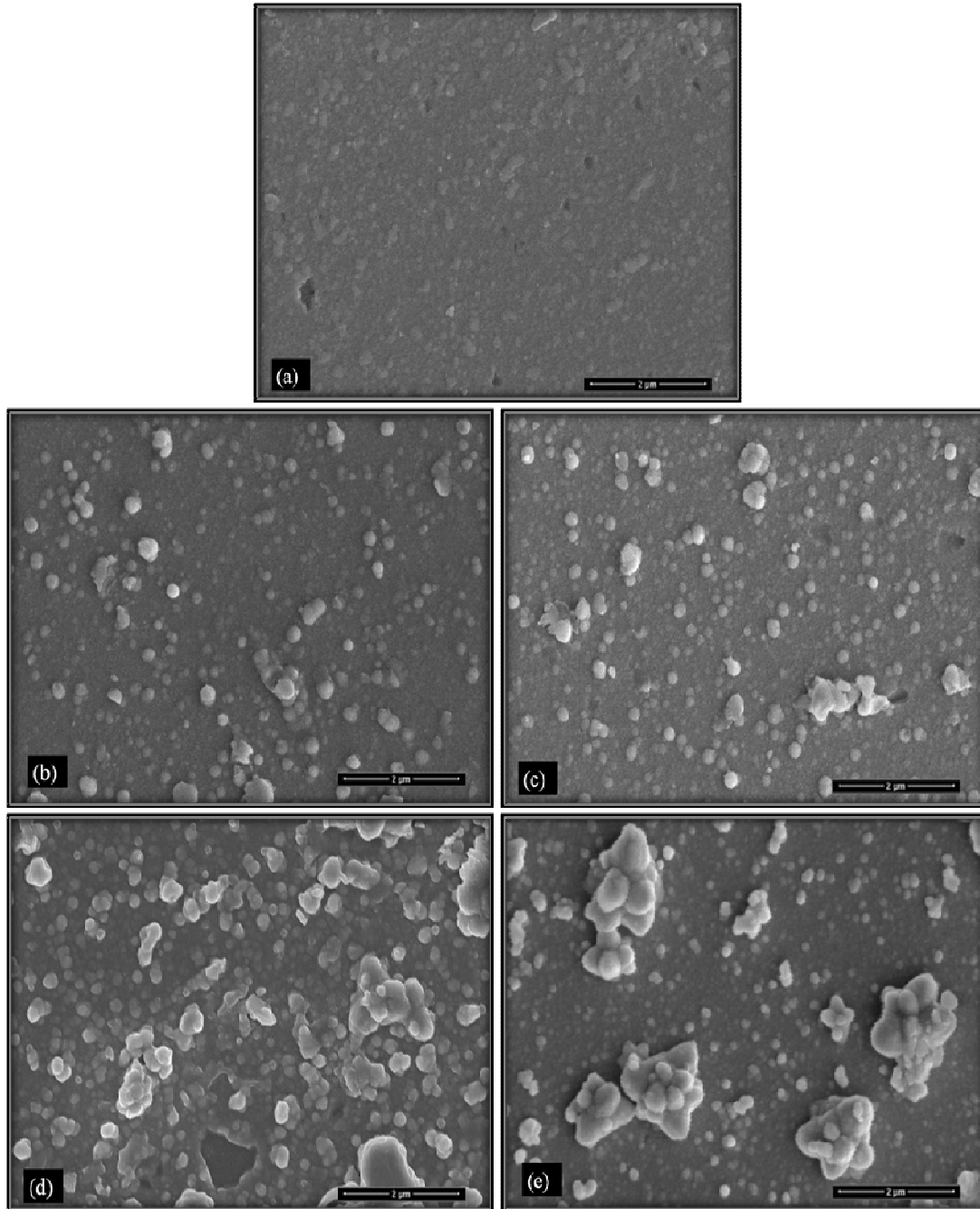
Figure 6.4: SEM images of (a) as deposited ZnS thin film (b) annealed ZnS at 100° C and (c) at 200° (d) at 300° C (e) at 400° C in air for 2 hrs.

SEM analysis was also done for confirmation of annealing effect on surface morphology. Figure 6.4(a) shows SEM surface image of as-deposited ZnS film and Figure 6.4(b, c, d & e) show the surface images of films annealed at 100°C, 200°C, 300°C and 400°C respectively. As-deposited film show smooth surface while for annealed film grain growth increased with increased annealing temperature from 100^{0}C to 300^{0}C and above 300^{0}C agglomeration started to occur. This analysis reveals that high temperature annealing could improve the crystallinity and increase the grain size of thin films but after certain temperature crystal structure tends to come under influence of uneven agglomeration. This gives a very important parameter in respect of the effect of annealing temperature on ZnS thin films. SEM surface images support the previously drawn conclusions by AFM images.

6.3.3.3 Optical absorption study

Optical properties of as deposited and treated ZnS thin film were studied by absorption spectra. Figure 6.5 displays the optical absorbance spectra of ZnS thin film, which demonstrates that variation of absorbance (a. u.) with respect to wavelength (λ) had high absorbance in ultraviolet region. Optical absorption was found to increase with increasing annealing temperature and absorbance was reached highest value of intensity at 300^{0}C.

Optical data were analyzed by using Tauc relation [165]. Plot of $(\alpha h\upsilon)^2$ (by taking n=1/2) vs hυ is a straight line which show it is a direct band gap material. Extrapolation of Tauc plot to zero absorption coefficient (α=0) give energy band gap values. Figure 6.6 shows that band gap energy increases with increase in annealing temperature and results for as-deposited and annealed ZnS films were summarized in Table 6.2. Energy band gap of ZnS film annealed at 300^{0}C is 3.54 eV which is optimal band gap for buffer layer [214].

Table 6.2: Energy band gap values for ZnS thin films

Sr. No.	Sample	Band Gap (eV)
1.	As deposited ZnS Thin film	3.47
2.	Annealed ZnS thin film at 100° C	3.49
3.	Annealed ZnS thin film at 200° C	3.50
4.	Annealed ZnS thin film at 300° C	3.54
5.	Annealed ZnS thin film at 400° C	3.4
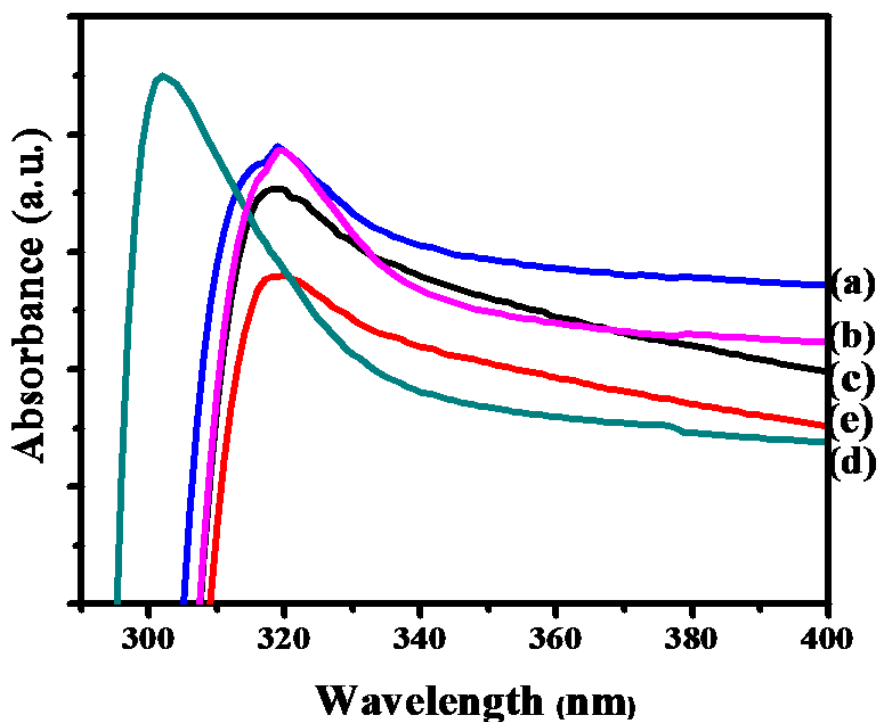
Figure 6.5: Variation of absorption (a.u.) with wavelength (nm) of images of (a) as deposited ZnS thin film (b) annealed ZnS at 100° C and (c) at 200° (d) at 300° C (e) at 400° C in air for 2 hrs.

Figure 6.6: The plots of $(\alpha h\upsilon)^2$ vs $h\upsilon$ of (a) as deposited ZnS thin film(b) annealed ZnS at 100° C and (c) at 200° (d) at 300° C (e) at 400° C in air for 2 hrs.

6.4 Doped Al-ZnS thin film as buffer layer

6.4.1 Experimental detail

Synthesis of doped Al-ZnS buffer layer

All the chemicals used for preparation of chemical bath were analytical reagent grade (AR) provided by Sigma Aldrich with 99.9% purity. Zinc Sulfate heptahydrate ($ZnSO_4.7H_2O$) and Thiourea (NH_2CSNH_2) were used as precursor chemicals for Zn^{2+} and S^{2-} ions for pure ZnS thin film and aluminum sulfate 16-hydrate ($Al_2(SO_4)_3.16H_2O$) was used for doping ion Al^{+2}. Hydrazine hydrate and TEA were used as complexing agent for controlling the reaction mechanism. For deposition of doped Al-ZnS thin film 0.1 M $ZnSO_4$, 0.01 M $Al_2(SO_4)_3$ and 0.1 NH_2CSNH_2 were taken in equal volume ratio. Thin films were deposited on glass and ITO substrate. Before the deposition, substrates were cleaned by detergent and distilled water and also ultrasonically cleaned by acetone, methanol and de-ionized (DI) water and dried in air. Details of deposition method and parameters were reported in our earlier work, while steps of deposition are shown below:

Deposited films were removed, rinsed in DI water to remove the ions from film, dried in air and preserved in desiccator. The surface of the thin film can be modified by providing the post deposition treatments like thermal annealing. So, as deposited and doped ZnS thin films were annealed in air at 300^0C for 2 hrs in a tubular furnace.
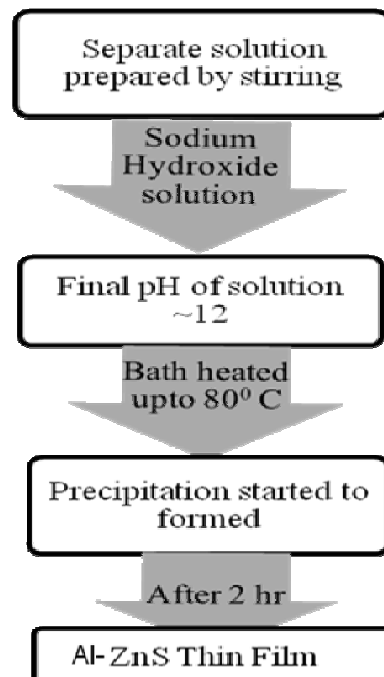
6.4.2   Result and discussion

6.4.2.1 Structural analysis

X-ray diffraction (XRD) technique was used for performing structural analysis of as-deposited, annealed thin films on glass substrate. Figure 6.7(a) shows the XRD patterns of as-deposited Al-ZnS exhibit sharp peaks at diffraction angles 28.55°, 33.20°. After comparing the calculated 'd' values with experimental 'd' values, it corresponds to standard sphalerite structured ZnS crystal (JCPDS card 05-0566), with phases (111), (200). Figure 6.7(b) shows XRD pattern of annealed Al-ZnS film at 300^{0}C for 2 hrs. which gives sharp peaks at angles 28.55°, 33.20°, 47.48° and 56.50° and by comparing with standard sphalerite structure corresponding phases are determined as (111), (200), (220) and (311). This analysis confirms the synthesis of sphalerite cubic structured Al-ZnS thin film. This result is in agreement with previously reported results [212-213]. Intensity of peak corresponding to (111) phase is observed to be much greater than other peaks, revealing preferred orientation along this phase for annealed film.

Particle size in the doped film was calculated from the Scherrer's formula

$$D = \frac{0.9\lambda}{\beta Cos\theta} \tag{6.1}$$

Where λ is X-ray wavelength, β is the full width at half maximum (FWHM) in radians, and θ is the Bragg angle. FWHM of diffraction peaks and grain size and other parameters for doped film are shown in Table 6.3.

Table 6.3: Parameters of XRD spectra for doped Al-ZnS thin films

2 Theta (degree)	d(Å)	Intensity	hkl	FWHM	Grain Size (nm)
28.55	3.36	100	111	0.322	26.53
33.60	2.69	10	200	0.324	26.73
47.48	1.91	51	220	0.227	39.95
56.50	1.62	30	311	0.197	47.83
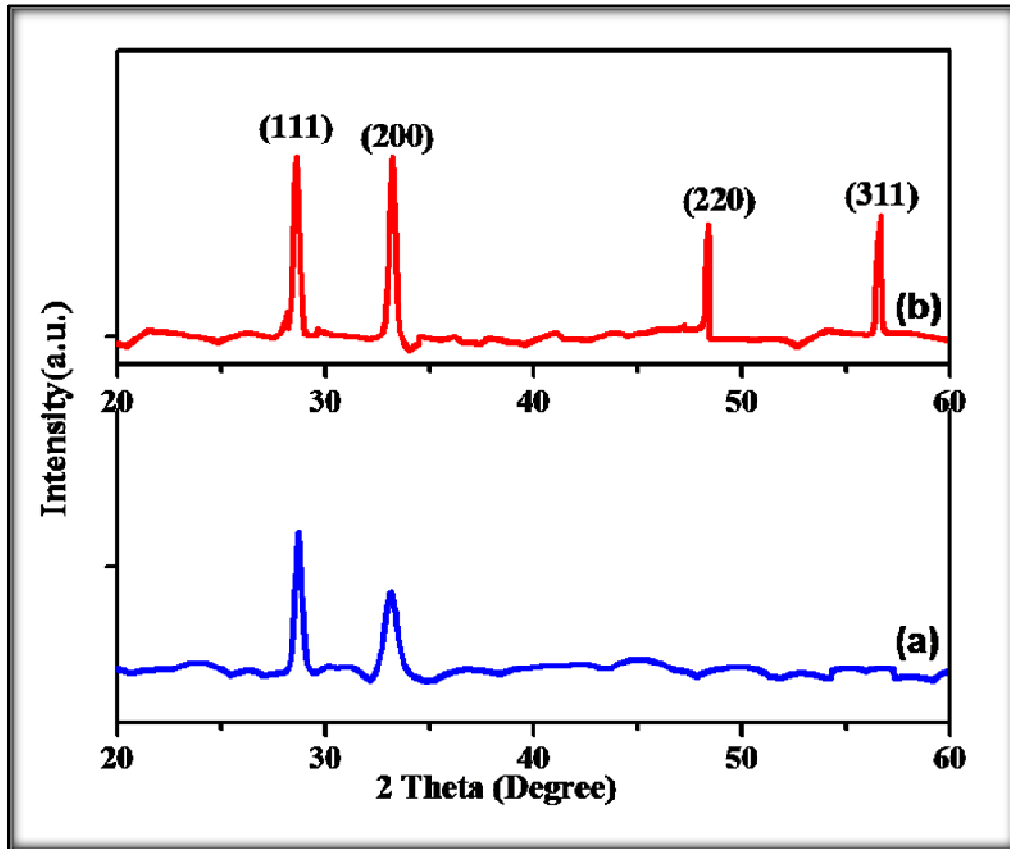
Figure 6.7: XRD patterns of (a) as-deposited Al-ZnS and (b) annealed Al-ZnS thin film at 300° C in air for 2 hrs.

6.4.2.2 Surface morphological analysis

Surface morphological analysis was done by Atomic Force Microscope (AFM). Figure 6.8 shows 2D AFM image of as-deposited Al-ZnS and annealed Al-ZnS thin films. Figure 6.8 (a) shows that AFM image of as-deposited Al-ZnS films indicate a homogenous background with smaller densely packed grains. It was observed that some particles exist on the surface of film which may be present because during deposition process nucleation sites were developed. Figure 6.8(b) shows the AFM images after annealing and observed that the grain growth started and on surface of Al-ZnS film. This indicates surface modification occurs after post temperature treatment which increases crystallinity and grain size of thin film.

Average surface roughness of as-deposited Al-ZnS and annealed Al-ZnS thin films at 300° C were found 12.7nm and 33.7nm and root mean square roughness values are 8.74nm and 17.5nm, respectively.
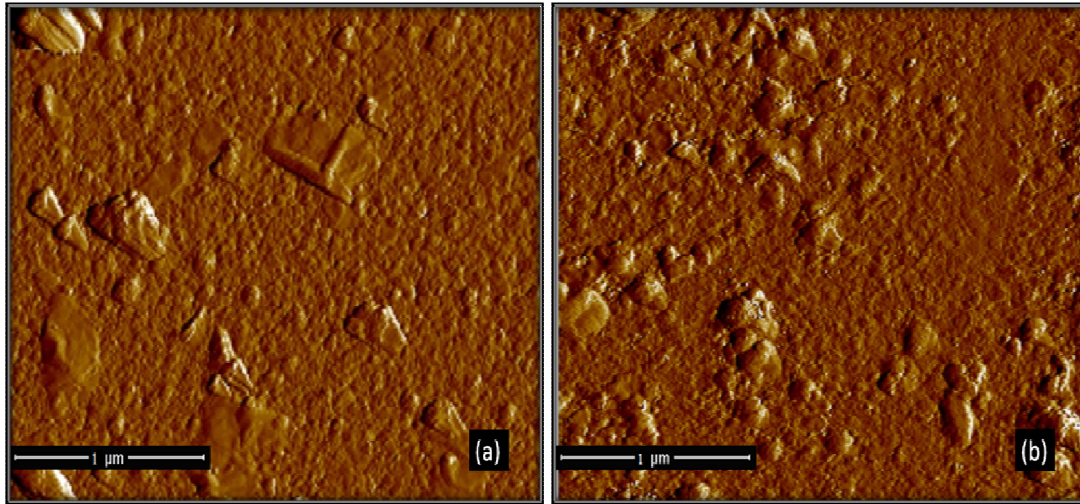
Figure 6.8: AFM images of (a) as-deposited Al-ZnS (b) annealed Al-ZnS thin film at 300° C in air for 2 hrs.

6.4.2.3 Optical absorption study

In order to study absorption spectra and energy band gap of ZnS thin film the optical absorption was studied in the wavelength range 800 nm to 300 nm. In Figure 6.9 variation of absorbance (a. u.) with respect to wavelength (λ) shows that ZnS films have high absorbance in ultraviolet region.

Further optical data were analyzed by using Tauc relation. Plot of $(\alpha h\upsilon)^2$ vs hυ is a straight line which indicates a direct band gap material. Extrapolation of Tauc plot to zero absorption coefficient (α=0) give energy band gap values as in Figure 6.10. Energy band gap for as-deposited Al-ZnS thin film was found 3.7eV as shown in Figure 6.10(a) and after annealing energy band gap was 3.5eV as shown in Figure 6.10 (b) . These energy band gap values are in optimum range for buffer layer [215].
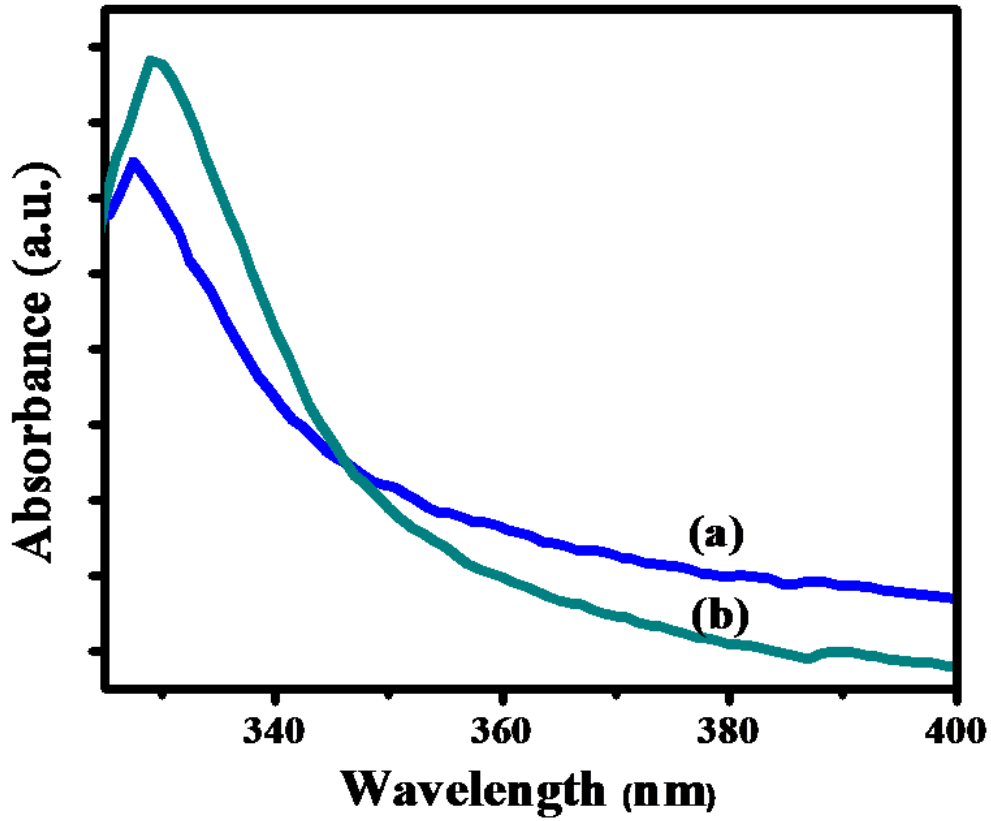
Figure 6.9: Variation of absorption (a.u.) with wavelength (nm) of (a) as-deposited Al-ZnS (b) annealed Al-ZnS thin film at 300° C in air for 2 hrs.
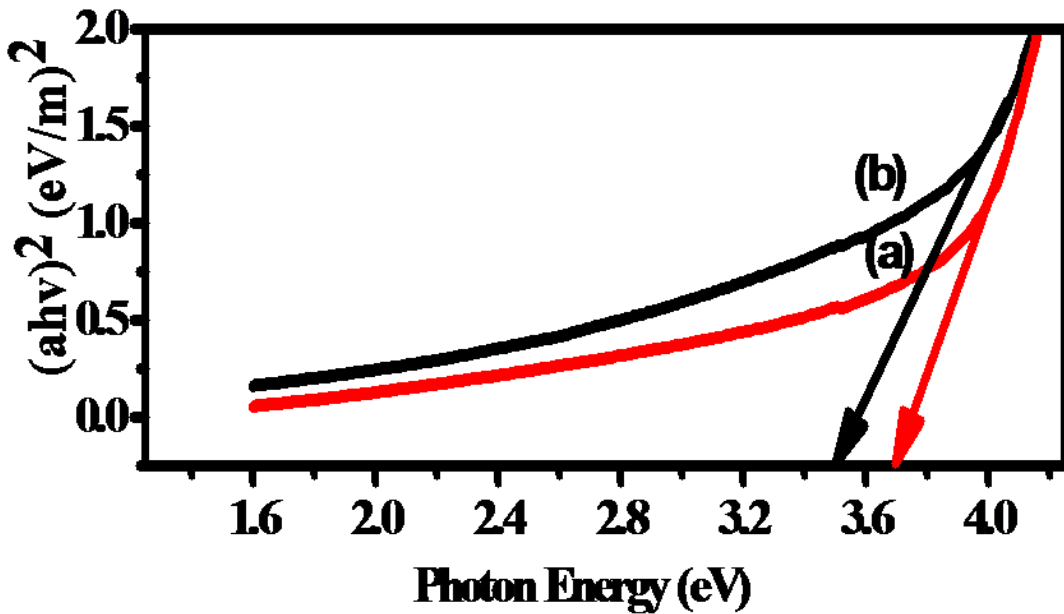
Figure 6.10: The plots of $(\alpha h\upsilon)^2$ vs $h\upsilon$ of (a) as-deposited ZnS and (b) as-deposited Al-ZnS (c) annealed doped Al-ZnS thin film at 300° C in air for 2 hrs.

6.5   Formation of ZnS/CZTS thin film heterojunction

The p-CZTS thin films were deposited on onto the pre-deposited ZnS thin film on ITO-coated glass substrates by solution growth method at optimized parameters. The resultant ZnS/CZTS thin films heterojunction was formed by ion exchange between buffer layer ZnS and absorber layer of CZTS showing homogenous interface and good stability [216]. Detailed set up for the CZTS thin film growth has been explained in chapter IV and V. The device was completed by the deposition of top electrode using silver (Ag) paste on CZTS absorber layer and the structure of glass-ITO/ZnS/CZTS/Ag heterojunction device configuration as shown in Figure 6.11.
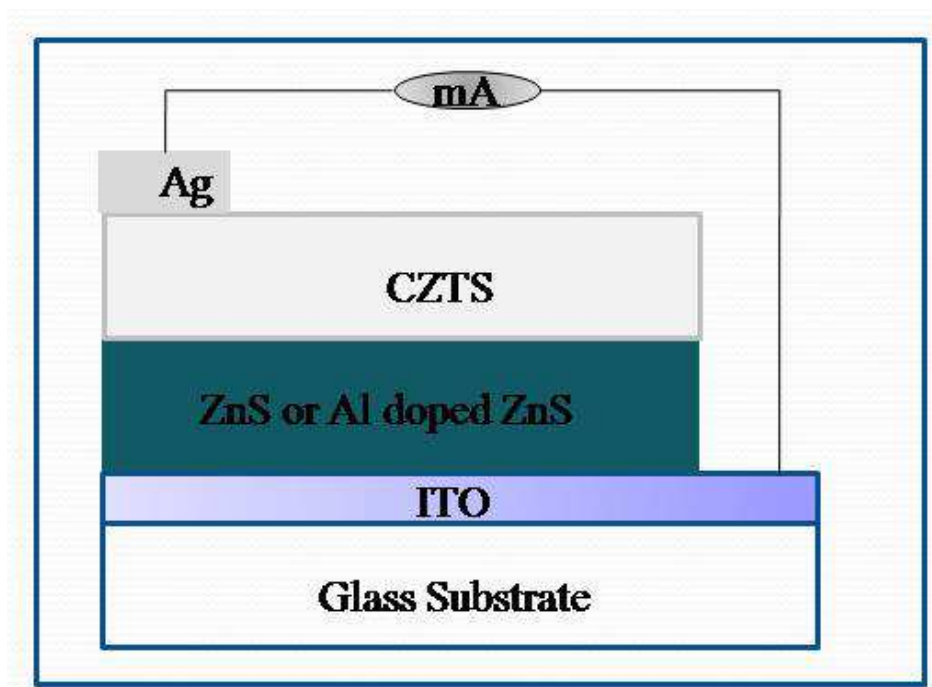
Figure 6.11 Back-wall heterojunction (ZnS/CZTS) on ITO-coated glass

A cross-sectional view of ZnS/CZTS heterojunction obtained by scanning electron microscopy (SEM) is shown in Figure 6.12, which indicates the proper formation of ZnS/CZTS junction.

106
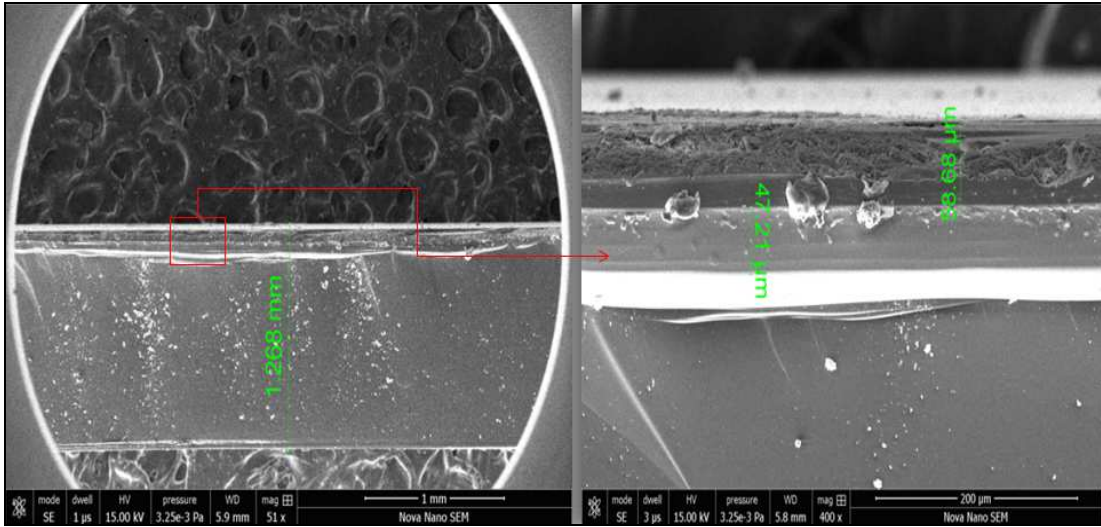
Figure 6.12: SEM images (a) & (b) cross section images of ZnS/CZTS Junction

6.6 Characterization of ZnS/CZTS heterojunction device

The junction characteristic was analyzed in terms of current-voltage (I-V) measurements in dark and under illumination using 100 mW/cm^2 source of light. The cell parameters V_{OC}, I_{SC}, Fill Factor (F.F.) and the conversion efficiency have also been calculated using following formulae [34];

$$\eta \ (\%) \quad = \quad \frac{P_{max}}{P_{in}} \times 100 \qquad\qquad (6.1)$$

Where, P_{max}: maximum output power observed in the thin film, and P_{in}: the input power applied on the film surface. The conversion efficiency of nanostructured CZTS based solar cell are being improved with various physical and chemical methods but these have some limitations due to low photo-generation voltage, which naturally restricts the open circuit voltage (Voc) value and corresponding short circuit current (Isc) of the device resulting in lower conversion efficiency of the device [217]. Ultimately these values (Voc and Isc) are surface, interface and composition dependent hence the improvement in these values can be made by modifying the surface or interface properties of the materials or otherwise there is one more way for increasing the photo generation voltage in nanostructured heterojunction device, that is, by enhancement of conductivity of buffer layer. Alluminium (Al) metal is a very good candidate for improving the properties of n-ZnS buffer layer. So the desired surface and homogenous interface in the heterojunction solar cell can be obtained using doped Al-ZnS buffer layer. There would be increase in the relative electron-

hole density in the resultant The net effect of this may be an increase in V_{OC} and corresponding I_{SC} values and hence also in the light conversion efficiency of the material [218]. Such nanostructured ZnS/CZTS heterojunction was investigated for light conversion efficiency and other optoelectronic properties.
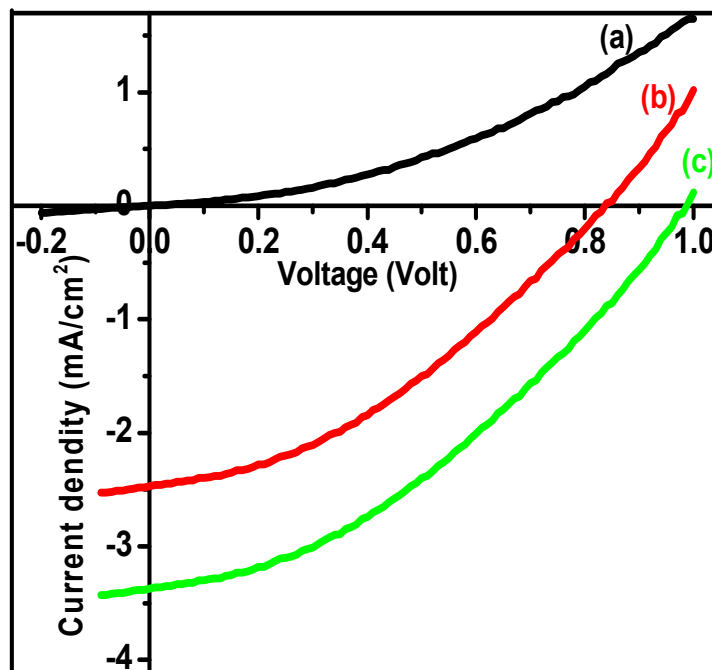
Figure 6.13: I-V characteristics of (a) pure ZnS/CZTS under dark and (b) pure ZnS/CZTS & (c) Al doped ZnS/CZTS heterojunction under illumination to 100 mW/cm^2 source of light.

The solar energy conversion efficiency calculated from these I-V curves for nanostructured heterojunction ZnS/CZTS and 10% doped Al-ZnS/CZTS under illumination to 100 mW/cm^2 source of light have been found to be 0.75% and 1.08%, respectively. The observed variations in these values can be related to doping of Al metal in buffer layer dependent electron-hole pair generation and separations in thin film solar cell and these were summarized in Table 6.4.

Table 6.4: Solar cell parameters for pure ZnS/CZTS and doped Al-ZnS/CZTS heterojunction under illumination of 100 mW/cm^2 source of light

Sr. No.	Samples	V_{OC} (V)	I_{SC} (mA)	V_{max} (V)	I_{max} (mA)	FF (%)	η (%)
1.	Pure ZnS/CZTS	0.84	2.46	0.38	1.88	34.57	0.75
2.	Doped Al-ZnS/CZTS	0.98	3.36	0.40	2.67	32.31	1.08

After comparing these efficiencies with other research reports these values are in the range of good efficiencies. Cao et al. reported 0.3% efficiency by CBD method [85]. Subramaniam reported 1.34% efficiency by using monoethanolamine (MEA) as a stabilizer [87]. An increased efficiency (2.2%) was presented by J. Li et al., but they used annealing in N_2 atmosphere [100].

6.7 Conclusion

ZnS buffer were successfully synthesized by low cost Chemical Bath Deposition (CBD) method. Post annealing treatment was performed. Structural studies indicated amorphous nature of as-deposited ZnS films, which was converted to polycrystalline after annealing. Surface morphology of ZnS film shows increase in grain size with annealing and even grains occur for film annealed at 300^0C. When the annealing temperature is 300^0C, ZnS film depicts sphalerite structured thin film and preferred degree of orientation is (111) plane. ZnS annealed film at 300^0C shows grains of size 0.4 ± 0.01 μm to 0.5 ± 0.01 μm with equal distribution. For this film not only the grain size becomes larger, but also the energy band gap 3.54eV value is in the range of optimal band gap. So, ZnS buffer layer deposited by CBD method exhibit good properties which are favorable for making a heterojunction solar cell.

Further, study on the effect of doping of Al in ZnS thin film was carried out. Al-ZnS thin films were synthesized by low cost Chemical Bath Deposition (CBD) method. As deposited and annealed thin films of Al-ZnS were characterized by different characterization tools. Conclusively, structural analysis confirms the synthesis of sphalerite cubic structured ZnS thin films. Surface image of as-deposited and annealed film indicates increased crystallinity and grain size for doped thin film. Optical study shows that band gap energy decrease from 3.7eV to 3.5eV after annealing for Al-ZnS thin film.

Heterojunction device of ZnS/CZTS thin films on ITO glass substrate was fabricated by chemical bath deposition method. A cross-sectional view of ZnS/CZTS heterojunction indicates the proper formation of ZnS/CZTS junction. The junction was characterized by I-V measurements in dark and under illumination. Effect of doped Al-ZnS buffer layer was studied and observable shift in the I-V characteristics was noticed under illumination to 100 mW/cm^2 source of light. The cell parameters under illumination were calculated and the highest conversion efficiency of device was achieved as 0.75% for pure ZnS buffer layer and 1.08% for doped Al-ZnS buffer layer in this thesis work.

CHAPTER 7

CONCLUSIONS AND FUTURE ASPECTS

7.1   Introduction

Commercially available thin film modules suffer from low efficiency in case of a-Si, shortage of raw material like 'Te' in the case of CdTe, and 'In' in the case of CIGS technology, or materials toxicity like Cd in CdTe technology. In this respect, Cu_2ZnSnS_4 (CZTS) seems to be a very attractive and highly potential material as absorber in thin film solar cells. Further, it is made from non-toxic, earth-abundant and low-cost raw materials, and shows high-efficiency potential for the near future.

In the research work carried out and reported here, the deposition parameters for deposition of CZTS using chemical bath deposition method were optimized and a heterojunction thin film solar cell using CZTS as absorber layer and ZnS as buffer layer was formed. Through various modifications of absorber and buffer layers, performance of the device was enhanced and finally ZnS/CZTS and doped Al-ZnS/CZTS heterojunctions for solar cell application were developed. Physical investigation of prepared thin films was carried out by different characterization techniques such as, structural by X-ray diffraction (XRD), elemental composition by energy dispersive X-ray analysis (EDAX), surface morphology by scanning electron microscope (SEM), atomic force microscopy (AFM), electronic transitions and energy band gap determinations using optical absorbance spectroscopy and I-V characteristics to evaluate performance of photovoltaic devices.

7.2   Conclusions

i.   CZTS films were synthesized by low cost Chemical Bath Deposition (CBD) technique at optimized deposition parameters, 60^0C temperature and deposition time of 7 hrs.

- After annealing at 150^0C, kesterite structured CZTS phase with tetragonal structure was formed [Figure 4.2(b)].

- Particle size corresponding to (112) plane of film was found to be about 21.41nm from XRD analysis [Table 4.1].

ii.   Further, effect of annealing was studied for surface modification in altering the properties of CZTS thin film. Annealing was carried out at various temperatures starting from 50^0C to 250^0C with variation of 100^0C in air for 2 hrs.

- Structural studies indicated amorphous nature of as-deposited CZTS films which are converted to polycrystalline CZTS films after annealing. The XRD patterns of annealed CZTS thin films confirmed the formation of kesterite structure CZTS film with preferred orientation (112) plane [Figure 4.6 and Figure 4.7].

- The particle size corresponding to (112) plane was calculated in the range of (16.79±2nm to 57.1±2nm) and it was observed that the particle sizes in CZTS thin films increase with increase in annealing temperature [Table 4.2].

- Surface morphological study by SEM also showed increase in grain size with increasing annealing temperature and roughness of the film surface was enhanced with less grain boundaries. This large grain size was very useful for solar cell application because decrement in grain boundaries reduce localized recombination sources within a diffusion length of the junction [Figure 4.9].

- Optical properties were studied using optical absorption spectroscopy and a band gap 1.4 eV for CZTS film annealed at 250^0C was found [Table 4.4].

- I–V characteristics show diode like behavior for CZTS films after annealing and enhancement in conductivity suggested application of

CZTS thin films as photo active absorber layer [Figure 4.13 and Figure 4.14].

iii. Further, the effect of various chemical precursors on the properties of CZTS absorber layer was studied [Table 5.1] . The previously optimized parameters were used for synthesis of CZTS films for chloride based precursors and sulphate based precursors. These as-deposited films were later annealed in air at 250°C for 2 hrs.

- The formation of kesterite structured CZTS phase with tetragonal structure at 250^0C was observed with better crystalline nature for chloride based precursors [Figure 5.1(b)].

- Surface morphology of CZTS film shows larger grains for chloride based precursors [Figure 5.2(b)].

- The band gap of annealed CZTS films was calculated to be 1.54eV [Figure 5.5].

iv. Further, the effect of synthesis parameters with various chemical precursor concentrations on the properties of CZTS absorber layer was studied [Table 5.3]. CZTS films for chloride based precursors were deposited and annealed in air at 250°C for 2 hrs.

- The formation of kesterite structured CZTS phase with tetragonal structure was observed with preferred orientation along (112) plane [Figure 5.6].

- The intensity of the (112) diffraction line increased with increasing Zn concentration, but the sample S_C (having the ratio $Z/(C+T+S) = 0.31$) gives a relatively more intense and sharper diffraction peaks than the other concentrations, indicating that the sample S_C has good crystallinity [Figure 5.6].

- Surface morphology analysis showed that as Zn concentration increases ($Z/(C+T+S) = 0.07$ to 0.62), the grain size of thin films also increases, but after certain concentration uneven grains start to appear [Figure 5.7 and Figure 5.8].

- The optical absorption study indicates that it is a direct transition and energy band gap (E_g) of the CZTS thin films becomes smaller (1.7 eV to 1.4 eV) with the increase of the precursor concentration (Z/(C+T+S) = 0.07 to 0.31) [Figure 5.10].

- Therefore, chemical concentration has effects on the crystallinity, phase, and optical properties of the CZTS thin film, and films with moderate Zn concentration (Z/(C+T+S) = 0.31) shows relatively good properties.

v. In this work the focus was also on formation of heterojunction device for solar cell application. For this study ZnS buffer layer on glass and ITO-coated substrates by low cost chemical bath deposition (CBD) method were synthesized. The properties of the ZnS buffer layer were modified by annealing treatment.

- Structural analysis indicated amorphous nature of as-deposited ZnS films which were converted to polycrystalline after annealing at 300^0C and ZnS film depicts sphalerite structured thin film and preferred degree of orientation is (111) plane [Figure 6.1 and Figure 6.2].

- Surface morphology of ZnS film showed increase in grain size with annealing and even grains were noticed for film annealed at 300^0C. When the annealing temperature is 300^0C and grains of size 0.4±0.01 μm to 0.5±0.01 μm with equal distribution [Figure 6.3 and Figure 6.4].

- For this film the energy band gap was determined as 3.54eV [Table 6.2].

- So, ZnS buffer layer deposited by CBD method exhibit good properties for use in heterojunction solar cell.

vi. The conductivity of buffer layer (ZnS) was enhanced by doping of Al with the object of improving the performance of the solar cell. Hence a detailed study on the effect of Al doping in ZnS thin film was carried out. As-deposited and annealed Al-ZnS films were characterized by different characterization tools.

- Structural analysis confirmed sphalerite cubic structured ZnS thin films [Figure 6.7].

113

- Surface image of as-deposited and annealed Al-ZnS films indicate increased crystallinity and grain size [Figure 6.8].

- From optical study energy band gap was found as 3.7eV for as-deposited and 3.5eV for annealed Al-ZnS thin film [Figure 6.9 and Figure 6.10].

vii. Finally, ZnS/CZTS and doped Al-ZnS/CZTS heterojunction on ITO glass substrate were formed by ion exchange between buffer layer ZnS and absorber layer of CZTS.

- Silver (Ag) is the most used top contact in CZTS based solar cells. The device was completed by the deposition of top electrode using silver (Ag) paste on CZTS absorber layer and this formed a glass-ITO/ZnS/CZTS/Ag heterojunction device configuration [Figure 6.11].

- A cross-sectional view of heterojunction indicates the proper formation of ZnS/CZTS junction [Figure 6.12].

- This heterojunction devices were characterized by I-V measurements in dark and under illumination A cross-sectional view of heterojunction indicates the proper formation of ZnS/CZTS junction [Figure 6.13].

- Similarly a heterojunction device configuration with doped Al-ZnS buffer layer was formed and a red shift in the I-V characteristics under illumination to 100 mW/cm^2 source of light was observed.

- The cell parameters under illumination were calculated and the highest conversion efficiency of device achieved was 0.75% for glass-ITO/ZnS/CZTS/Ag and 1.08% for doped glass-ITO/Al-ZnS/CZTS/Ag in this thesis work [Table 6.4].

So, the results obtained in the present work are new and add to the volume of database in this research field. Optimization of parameters for low cost CBD method is one of them, as it overcomes the problem of cost effectiveness aspect in the PV industry. Optimization of deposition parameters for depositing a good quality stable film by an easy approach is one of novel features of our work. Further, enhancement in appropriate properties as is evident from measurement of optical and electrical properties by using optimized precursors and their concentration give a ground for

further work in this research area. Improvements in properties were done not only in the case of CZTS absorber layer but also buffer layer conductivity was found to increase by appropriate doping.

7.3   Future scope of the present work

CZTS is a complex material. Recently, various research groups have identified several high impact research topics that could accelerate the development of CZTS technology in order to take it to the level of other thin film technologies like CIGS and CdTe.

- The research work mentioned in this thesis adds an important contribution for the development of CZTS films for solar cell application with enhanced efficiency. Further improvement in conductivity of buffer layer and conversion efficiency of solar cell is desirable topic for further research.

- Study the effect of various other dopants in the absorber CZTS films, such as nano particles like Ag and polymer like PANI may be considered for future work.

- Comparison of surface modification effect by annealing in air with various other atmospheres or in vacuum will be very useful.

- Study the effect of other surface modification techniques like ion beam irradiation may give useful data on change in their properties with irradiation.

- Another aspect could be the replacement of ZnS buffer layer, with some other wide band gap n-type semiconductor, and the optimization of deposition conditions for new buffer layer

In the end, a major point needed to be studied is the possibility to really implement bandgap gradient in kesterite solar cells. Simulations demonstrated that this approach should increase CZTS solar cell efficiency without playing on the material quality.

REFERENCES

[1] Statistical Review of World Energy BP "Consumption by fuel, 1965–2008". (2009).

[2] BP Statistical Review of world energy (2016).

[3] Eric yep, "India's Widening Energy Deficit" The Wall Street Journal, (2011).

[4] J.T. Kiehl, K. E. Trenberth,, "Earth's Annual Global Mean Energy Budget" , Bulletin of the American Meteorological Society,78, (1997) pp.197–208.

[5] D. Goldsmith, T. Owen, "The search for life in the universe" University Science Books (2001), pp.96.

[6] T. Suntola, Proceedings of the PV CON '95, (1995).

[7] L.D. Partain, "Solar Cells and Their Applications" John Wiley & Sons, (1995).

[8] NASA Solar System Exploration, "Sun: Facts & Figures" (2011).

[9] G. Kopp, J.L. Lean, "A new, lower value of total solar irradiance: Evidence and climate significance" Geophysical Research Letters, 38, (2011), pp 1-7.

[10] P. Würfel, u. Würfel, "Physics of Solar Cells." Wiley-VCH, (2009).

[11] International Energy Agency "Snapshot of Global PV 1992-2014" Photovoltaic Power Systems Programme, (2015).

[12] H. Ibach, H. Lüth, "Solid state physics - Introduction to the basics", Springer, (2002).

[13] B. Van Zeghbroeck, "Principles of semiconductor devices", (2011).

[14] N. Sobolev, " Lectures of Sensors and Semiconductors", (2009).

[15] D. Carlson, C. Wronski, "Topics in Applied Physics: Amorphous Semiconductors: Amorphous silicon solar cells", Springer Berlin / Heidelberg (1985).

[16] S. M. Sze, K. Kwok, "Physics of Semiconductor Devices", John Wiley & Sons, (2007).

[17]   A. Luque, S. Hegedus, "Handbook of Photovoltaic Science and Engineering" (2011).

[18]   U. Zimmermann, "Solar Cell technology", lecture script PhD course, (2007).

[19]   D. Neamen, "Semiconductor Physics and Devices", McGray-Hill, (2003).

[20]   Green, A. Martin, "Solar cells" The University of New South Wales, (1998).

[21]   A. Wang ,J. Zhao, S. R. Wenham, M. A. Green "21.5% Efficient thin silicon solar cell" Progress in PHOTOVOLTAICS, Vol. 4, (1996), pp.55–58,

[22]   Lewis Fraas and Larry Partain. "Solar cells and their applications", John Wiley & Sons, (2010).

[23]   F. Kessler, D. Rudmann. Solar Energy, Vol. 77, (2004) pp.685.

[24]   Fraunhofer ISE. "Photovoltaics Report", (2014).

[25]   A. Shah, J. Meier, A. Buechel, U. Kroll, J. Steinhauser, F. Meillaud, H. Schade, D. Dominé, "Towards very low-cost mass production of thin-film silicon photovoltaic (PV) solar modules on glass", Thin Solid Films 502 (1-2), (2006), pp.292-299.

[26]   M. A. Kreiger et al., "Life Cycle Analysis of Silane Recycling in Amorphous Silicon-Based Solar Photovoltaic Manufacturing", Resources, Conservation & Recycling, 70, (2013), pp.44-49.

[27]   Amit Sahay, V. K. Sethi, Tiwari, "A comparative study of attributes of thin film and crystalline photovoltaic cells", International Journal of Mechanical, Civil, Automobile and Production Engineering, 3, (2013), pp.267.

[28]   J. J. Scragg, P. J. Dale, D. Colombara, L. M. Peter, "Thermodynamic aspects of the synthesis of thin-film materials for solar cells", ChemPhysChem, 13, (2012), pp.3035-3046.

[29]   K. Zweibel, J. Mason, V. Fthenakis, "A Solar Grand Plan", Scientific American, 298, (2008), pp. 64-73.

[30]   Peng et al. "Review on life cycle assessment of energy payback and greenhouse gas emission of solar photovoltaic systems", Renewable and Sustainable Energy Reviews. 19, (2013), pp.255–274.

[31]   V. Fthenakis and H. C. Kim. "Life-cycle uses of water in U.S. electricity generation", Renewable and Sustainable Energy Reviews. 14, (2010), pp. 2039–2048.

[32]   De Wild-Scholten, Mariska, "Energy payback time and carbon footprint of commercial photovoltaic systems", Solar Energy Materials & Solar Cells, 119, (2013), pp.296–305.

[33]   First Solar, Press Release, July 26, (2011).

[34]   L. Grenet, S. Bernardi, D. Kohen, C. Lepoittevin, S. Noel, N. Karst, A. Brioude, S. Perraud, H. Mariette, "$Cu_2ZnSn(S_{1-x}Se_x)_4$ based solar cell produced by selenization of vacuum deposited precursors" Solar Energy Materials and Solar Cells, 101, (2012), pp. 11-14.

[35]   D. A. Jenny and R. H. Bube "Semiconducting CdTe" Phys. Rev., 96, (1954), pp.1190–1191.

[36]   R. H. Bube "Photoconductivity of the Sulfide, Selenide, and Telluride of Zinc or Cadmium". Proceedings of the IRE., 43, (1955), pp. 1836–1850.

[37]   M. Fthenakis, M. Vasilis. "Life cycle impact analysis of cadmium in CdTe PV production", Renewable and Sustainable Energy Reviews, 8, (2004), pp.303–334.

[38]   H. Jürgen, "Toxic Substances In Photovoltaic Modules" The 21st International Photovoltaic Science and Engineering Conference, (2011) pp. 2.

[39]   National Renewable Energy Laboratory, "Supply Constraints Analysis".

[40]   P. Jackson, D. Hariskos, E. Lotter, S. Paetel, R. Wuerz, R. Menner, W. ischmann, M. Powalla, "New world record efficiency for Cu (In, Ga) Se2 thin film solar cells beyond 20%" Progress in Photovoltaics: Research and Application, 19, (2011), pp.894–897.

[41]   L. M. Peter, "Towards sustainable photovoltaics: the search for new materials," Philosophical Transactions of the Royal Society A: Mathematical, Physical and Engineering Sciences, 369, (2011), pp.1840–1856.

[42]   V. Fthenakis, Renewable and Sustainable Energy Reviews, 13, (2009), pp.2746-2750.

[43]   P. Sinha, C.J. Kriegner, W.A. Schew, S.W. Kaczmar, M. Traister, D.J. Wilson, Energy Policy, 36, (2008), pp. 381-387.

[44]   L. A. Wahab, M. B. El-Den, A. A. Farrag, S. A. Fayek , K. H. Marzouk, J. Phys. Chem. Solids, 70, (2009), pp. 604.

[45]   J. Zhang, L. Shao, Y. Fu, E. Xie., Rare metals, 25, (2006), pp. 315.

[46] C.Wadia, A.P. Alivisatos, D.M. Kammen "Materials availability expands the opportunity for large-scale photovoltaics deployment" Environmental Science & Technology, 43, (2009), pp.2072–2077.

[47] W. Ki, H. W. Hillhouse, Adv. Energy Mater, 1, (2011), pp.732–735.

[48] W. Shockley and H. J. Queisser "Detailed Balance Limit of Efficiency of p-n Junction Solar Cells" J. Appl. Phys., 32, (1961), pp.510.

[49] K. Todorov, K. B. Reuter, and D. B. Mitzi, "High-efficiency solar cell with earth-abundant liquid-processed absorber" Advanced Materials, 22, (2010), pp. E156–E15.

[50] K. Ito, T. Nakazawa "Electrical and optical properties of stannite-type quaternary semiconductor thin films" Jpn. J. Appl. Phys., 27, (1988), pp.2094–2097.

[51] T. M. Friedlmeier, N. Wieser, T. Walter, H. Dittrich, and H. W. Schock, "Heterojuncitons based on Cu_2ZnSnS_4 and $Cu_2ZnSnSe_4$ thin films" in Proceedings of the 14th European Conference of Photovoltaic Science and Engineering and Exhibition, Bedford, UK, (1997), pp.1242 .

[52] H. Katagiri, M. Nishimura, T. Onozawa et al., "Rare-metal free thin film solar cell" in Proceedings of the Power Conversion Conference, pp. 1003–1006, Nagaoka, Japan, August (1997).

[53] H. Katagiri, N. Ishigaki, T. Ishida, and K. Saito, "Characterization of Cu_2ZnSnS_4 thin films prepared by vapor phase sulfurization" Japanese Journal of Applied Physics, 40, (2001) pp.500–504.

[54] H. Katagiri, N. Sasaguchi, S. Hando, S. Hoshino, J. Ohashi, T. Yokota, Sol. Energy Mater. Sol. Cells, 49, (1997), pp.407.

[55] H. Katagiri, K. Saitoh, T. Washio, H. Shinohar a, T. Kuruma-dani, and S. Miyajima, "Development of thin film solar cell based on Cu_2ZnSnS_4 thin films" Solar Energy Materials and Solar Cells, 65, (2001) pp. 141–148,.

[56] H. Katagiri, K. Jimbo, K. Moriya, and K. Tsuchida, "Solar cell without environmental pollution by using CZTS thin film" in Proceedings of the 3rd World Conference on Photovoltaic Energy Conversion, Osaka, Japan, May (2003), pp. 2874–2879.

[57] H. Katagiri, K. Jimbo, S. Yamada et al., "Enhanced conversion effeciencies of Cu_2ZnSnS_4 based thin film solar cells by using preferential etching technique" Applied Physics Express, 1, (2008), pp. 041201 .

[58]   H. Katagiri, "Cu$_2$ZnSnS$_4$ thin film solar cells" Thin Solid Films, 480, (2005), pp. 426–432.

[59]   H. Katagiri, K. Jimbo, W.S. Maw, K. Oishi, M. Yamazaki, H. Araki, A. Takeuchi, "Development of CZTS-based thin film solar cells" Thin Solid Films. 517, (2009), pp. 2455–2460.

[60]   J.J. Scragg, P.J. Dale, and L.M. Peter, "Towards sustainable materials for solar energy conversion: preparation and photoelectrochemical characterization of Cu$_2$ZnSnS$_4$" Electrochemistry Communications, 10, (2008), pp.639–642.

[61]   J. J. Scragg, P. J. Dale, and L. M. Peter, "Synthesis and characterization of Cu$_2$ZnSnS$_4$ absorber layers by an electrodeposition annealing route" Thin Solid Films, 517, (2009), pp.2481–2484.

[62]   J.J. Scragg, D.M. Berg, and P. J. Dale "A 3.2% efficient Kesterite device from electrodeposited stacked elemental layers" Journal of Electroanalytical Chemistry, 646, (2010), pp. 52–59.

[63]   J.J. Scragg, P.J. Dale, L.M. Peter, G. Zoppi, I.Forbes "New routes to sustainable photovoltaics: evaluation of Cu$_2$ZnSnS$_4$ as an alternative absorber material" Physica Status Solidi (b), 245, (2008), pp.1772–1778.

[64]   K. Moriya, K. Tanaka, and H. Uchiki, "Characterization of Cu$_2$ZnSnS$_4$ thin films prepared by photo-chemical deposition" Japanese Journal of Applied Physics, 44, (2005), pp. 715–717.

[65]   K. Moriya, K. Tanaka, and H. Uchiki, "Fabrication of Cu$_2$ZnSnS$_4$ thin-film solar cell prepared by pulsed laser deposition" Japanese Journal of Applied Physics, 46, (2007), pp.5780–5781.

[66]   K. Moriya, K. Tanaka, and H. Uchiki, "Cu$_2$ZnSnS$_4$ thin films annealed in H$_2$S atmosphere for solar cell absorber prepared by pulsed laser deposition" Japanese Journal of Applied Physics, 47, (2008) pp.602–604.

[67]   K. Tanaka, N. Moritake, and H. Uchiki, "Preparation of Cu$_2$ZnSnS$_4$ thin films by sulfurizing sol-gel deposited precursors" Solar Energy Materials and Solar Cells, 91, (2007), pp.199–1201.

[68]   K. Tanaka, M . O onuki, N. Moritake, and H. Uchiki, "Cu$_2$ZnSnS$_4$ thin film solar cells prepared by non-vacuum processing" Solar Energy Materials and Solar Cells,93, (2009) pp.583–587.

[69] K. Tanaka, Y. Fukui, N. Moritake, and H. Uchiki, "Chemical composition dependence of morphological and optical properties of Cu_2ZnSnS_4 thin films deposited by sol-gel sulfurization and Cu_2ZnSnS_4 thin film solar cell efficiency" Solar Energy Materials and Solar Cells , 95, (2011) pp. 838–842.

[70] S.Y. Chen, X.G. Gong, A. Walsh , and S.H. Wei, "Defect physics of the kesterite thin-film solar cell absorber Cu_2ZnSnS_4" Applied Physics Letters , 96, (2010), Article ID021902.

[71] S.Y. Chen, J. H. Yang, X.G. Gong, A. Walsh, and S. H. Wei, "Intrinsic point defects and complexes in the quaternary kesterite semiconductor Cu_2ZnSnS_4" Physical Review B, 81, (2010), Article ID 245204.

[72] F. Y. Liu, K. Zhang, Y. Q. Lai, J. Li, Z. A. Zhang, and Y. X. Liu, "Growth and characterization of Cu_2ZnSnS_4 thin films by dc reactive magnetron sputtering for photovoltaic applications" Electrochemical and Solid-State Letters, 13, (2010), pp. H379–H381.

[73] N. Momose, M. T. Htay, T. Yudasaka et al., "Cu_2ZnSnS_4 thin film solar cells utilizing sulfurization of metallic precursor prepared by simultaneous sputtering of metal targets" Japanese Journal of Applied Physics, 50, Article ID 01BG09, (2011) 4 pages.

[74] T. Kameyama, T. Osaki, K. I. Okazaki et al., "Preparation and photoelectrochemical properties of densely immobilized Cu_2ZnSnS_4 nanoparticle films" Journal of Materials Chemistry, 20, (2010), pp.5319–5324.

[75] P. C. Dai, X. N. Shen, Z. J. Lin, Z. Y. Feng, H. Xu, and J. H. Zhan, "Band-gap tunable $(Cu_2Sn)_{x/3}Zn_{1-x}S$ nanoparticles for solar cells" Chemical Communications, 46, (2010), pp.5749–5751.

[76] Q. J. Guo, G. M. Ford, W. C. Yang et al., "Fabrication of 7.2% efficient CZTSSe solar cells using CZTS nanocrystals" Journal of the American Chemical Society, 132, (2010), pp.17384– 17386.

[77]   X. T. Lu, Z. B. Zhuang, Q. Peng, and Y. D. Li, "Wurtzite Cu_2ZnSnS_4 nanocrystals: a novel quaternary semiconductor" Chemical Communications, vol. 47, no. 11, (2011), pp.3141–3143.

[78]   Thomas Rath , Wernfried Haas , Andreas Pein , RobertSaf , EugenMaier , BirgitKunert , Ferdinand Hofer , Roland Resel , Gregor Trimmel "Synthesis and characterization of copper zinc tin chalcogenide nanoparticles: Influence

of reactants on the chemical composition" Solar Energy Materials & Solar Cells vol.101 (2012) pp.87–94

[79]   A. Fischereder, T. Rath, W. Haas, H. Amenitsch, J. Albring, D. Meischler, S. Larissegger, G. Trimmel, Chem. Mater., 22,(2010), pp.3399.

[80]   M. Krunks, V. Mikli, O. Bijakina, H. Rebane, A. Mere, T. Varema, E. Mellikov, Thin Solid Films, 361, (2000), pp.61.

[81]   Y. Sun, Y. Zhang, H. Wang, M. Xie, K. Zong, H. Zheng, Y. Shu, W. Lau, J. Mater. Chem. A, 1, (2013), pp.680.

[82]   Z. Tong, C. Yan, Z. Su, F. Zeng, J. Yang, Y. Li, L. Jiang, Y. Lai, F. Liu, Appl. Phys. Lett., 105, (2014), pp.223903.

[83]   S. N. Park, S. J. Sung, D. H. Son, D. H. Kim, M. Gansukh, H. Cheong, J. K. Kang, RSC Adv., 4, (2014), pp.9118.

[84]   V. T. Nguyen, D. Nam, M. Gansukh, S. Park, S. J. Sung, T. H. Tran , H. Cheong, Solar Energy Materials and Solar Cells, 136, (2015), pp.113.

[85]   M. Cao, L. Li , B. L. Zhang, J. Huang, L. J. Wang, Y. Shen, Y. Sun, J. C. Jiang, G. J. Hu, Solar Energy Mater. Solar cells, 117, (2013), pp.1139.

[86]   X. Liu., C. /Wang, J. Xu, X. Liu, R. Zou, L. Ouyang, X. Xu, X. Chen , H. Xing, CrystEngComm, 15, (2013), pp.1139.

[87]   J. Li, G. Chen, C. Xue, X. Jin, W. Liu, C. Zhu, Solar Energy Mater. Solar Cells, 137, (2015), pp.131.

[88]   B. S. Pawar, S. M. Pawar, K .V. Gurav S. W. Shin, S. S. Kolekar and J.H. Kim "Effect of Annealing Atmosphere on the Properties of Electrochemically Deposited Cu_2ZnSnS_4 (CZTS) Thin Films" International Scholarly Research Network ISRN Renewable Energy Volume 2011, Article ID 934575, (2011).

[89]   B.S. Pawar, S.M. Pawar, S.W. Shin, D.S. Choi, C.J. Park, S.S. Kolekar, J.H. Kim "Effect of complexing agent on the properties of electrochemically deposited Cu_2ZnSnS_4 (CZTS) thin films" Applied Surface Science, 257, (2010), pp.1786–1791.

[90]   A V Moholkar, S S Shinde, A R Babar, Kyu-Ung Sim, Ye-bin Kwon "Development of CZTS thin films solar cells by pulsed laser deposition: Influence of pulse repetition rate" Solar Energy, 85, (2011), pp.1354-1363. .

[91]   A.V. Moholkar , S.S. Shinde, A.R. Babar, Kyu-Ung Sim, Hyun Kee Lee, K.Y. Rajpure, P.S. Patil, C.H. Bhosale, J.H. Kim "Synthesis and characterization of

Cu$_2$ZnSnS$_4$ thin films grown by PLD: Solar cells" Journal of Alloys and Compounds, 509, (2011), pp.7439–7446.

[92] Sawanta S. Mali, Pravin S. Shinde, Chirayath A. Betty, Popatrao N. Bhosale, Young Woo Oh, Pramod S. Patil "Synthesis and characterization ofCu$_2$ZnSnS$_4$ thin films by SILAR method" Journal of Physics and Chemistry of Solids, 73, (2012), pp.735–740.

[93] S. S. Mali, B. M. Patil, C. A. Betty, P. N. Bhosle, Y. W. Oh, Y. R. Ma, P. S. Patil, Electrochim. Acta 66, (2012), pp.216.

[94] Y. B. Kishore Kumar, G. Suresh Babu, P. Uday Bhaskar, V. Sundara Raja "Preparation and characterization of spray-deposited Cu2ZnSnS4 thin films" Sol. Energy Mater. Sol. Cells, 93, (2009), pp.1230.

[95] Y. B. K. Kumar, G. S. Babu, P. U. Bhaskar, and V. S. Raja "Effect of starting-solution pH on the growth of Cu$_2$ZnSnS$_4$ thin films deposited by spray pyrolysis" Physica Status Solidi A , 206, (2009), pp.1525–1530.

[96] V. G. Rajeshmon, C. Sudha Kartha, and K. P. Vijayakumar "Spray Pyrolysed Cu$_2$ZnSnS$_4$ Solar Cell Using Cadmium Free Buffer Layer" Solid State Physics, proceedings of the 55th DAE Solid State Physics symposium (2010).

[97] N. M. Shinde, C. D. Lokhande, J. H. Kim, J. H. Moon "Low cost and large area novel chemical synthesis of Cu$_2$ZnSnS$_4$ (CZTS) thin Films" Journal of Photochemistry and Photobiology A:Chemistry doi:10.1016/j.jphotochem .2012.02.006

[98] N. M. Shinde, D. P. Dubal, D. S. Dhawale, C. D. Lokhande, J. H. Kim, J. H. Moon, Mater. Res. Bull., 47, (2012), 302.

[99] B Uma Maheswari , V. Senthil Kumar, J. Modern Optics, 61, (2014), 1225.

[100] E. P. Subramaniam, G. Rajesh, N. Muthukumarasamy, M. Thambiduari, V. Asokan, D. Velauthapillai, Ind. J. Pure & Appl. Phys, 52, (2014), 620.

[101] Kemell Marianna, Ritala Mikko, Leskelä Markku, Thin Film Deposition Methods for CuInSe2 Solar Cells, Critical Reviews in Solid State Materials Sciences, 30, (2005), pp.1-31.

[102] Y. B. Kishore Kumar, P. uday Bhaskar, G. Suresh babu and V. Sundara raja., Phys. Status Solidi A , 207, (2010), pp.149.

[103] N. Nakayama and K. Ito., Appl. Surf. Sci., 92, (1996), pp.171.

[104] T. Tanaka, T. Nagatomo, D. kawasaki, M. Nishio, Q. Guo, A. Wakahara, A. Yoshida and H. Ogawa., J. Phys. Chem. Solids, 66, (2005), pp. 1978.

[105] F. Liu, Y. Li, K. Zhang, B. Wang, C. Yan, Y. Lai, Z. Zhang, J. Li and Y. Liu., Sol. Energy Mater. Sol. Cells, 94, (2010), pp. 2431.

[106] C. P. Chan, H. Lam and C. Surya., Sol. Energy Mater. Sol. Cells, 94, (2010), pp. 207.

[107] W. Xinkun, L. Wei, C. Shuying, L. Yunfeng and J. Hongjie., J. Semicond., 33, (2012), pp. 022002.

[108] S. Chen, X. G. Gong, A. Walsh and S. Wei. 2009, Appl. Phys. Lett., 94, (2009), p p. 041903.

[109] J. Seol, S. Lee, J. Lee, H. Nam and K. Kim., Sol. Energy mater. Sol. Cells, 75, (2003), pp.155.

[110] K. Moriya, J. Watabe, K. Tanaka and H. Uchiki., Phys. status solidi (c), 3, (2006), pp. 2848.

[111] T. Prabhakar and J. Nagaraju. s.l. : Proceedings of the IEEE 35th Photovoltaic Specialist Conference,Hawaii, USA, (2010), pp.1964.

[112] H. Zhao and C. Persson., Thin Solid Films, 519, (2011), pp. 7508.

[113] S. Levcenko, G. Gurieva, M. Guc and A. Nateprov., Moldavian Journal of the Physical Sciences , 8, (2009), pp.173.

[114] Y. Cui, S. Zuo, J. Jiang, S. Yuan and J. Chu., Sol. Energy Mater. Sol. Cells, 95, (2011), pp. 2136.

[115] G. Babu, Y. Kumar, P. Bhaskar, V. Raja, Effect of post-deposition annealing on the growth of Cu_2ZnSnS_4 thin films for a solar cell absorber layer, Semiconductor Science and Technology, 23, (2008).

[116] S. R. HallSzymanski, J.T. ; Stewart, J.M.: Kesterite, "$Cu_2(Zn,Fe)SnS_4$, and stannite, $Cu_2(Fe,Zn)SnS_4$, structurally similar but distinct minerals" Canadian Mineralogist, 16, (1978), pp.131–137.

[117] J. Paier, R. Asahi, A. Nagoya, G. Kresse, "Cu_2ZnSnS_4 as a potential photovoltaic material: A hybrid Hartree-Fock density functional theory study", Physical Review B, 79, (2009).

[118] S. Schorr., Thin Solid Films, 515, (2007), pp. 5985.

[119] T. Maeda, S. Nakamura, T. Wada, "Electronic Structure and Phase Stability of In-free Photovoltaic Semiconductors, Cu2ZnSnSe4 and Cu2ZnSnS4" Mater. Res. Soc. Symp. Proc., 1165, (2009).

[120] T. Washio, H. Nozaki, T. Fukano, T. Motohiro, K. Jimbo and H. katagiri., J. Appl. Phys., 110, (2011), pp. 074511.

[121] A. Wangperawong, J. S. King, S. M. Herron, B. P. Tran, K. Pangan- Okimoto and S. F. Bent., Thin Solid Films, 519, (2011), pp. 2488.

[122] X. Zhang, X. Shi, W. Ye, C. Ma and C. Wang., Appl. Phys. A, 94, (2009), pp.381.

[123] S. M. Pawar, B. S. Pawar, A. V. Moholkar, D. S. Choi, J. H. Yun, J. H. Moon, S. S. Kolekar and J. H. Kim., Electrochemica Acta, 55, (2010), pp. 4057.

[124] Y. Zhou, W. Zhou, Y. Du, M. Li and S. Wu., Mater. Lett., 65, (2011), pp. 1535.

[125]   M. Cao and Y. Shen., J. Crystal Growth, 318, (2011), pp. 1117.

[126] H. Araki, Y. Kubo, A. Mikaduki, K. Jimbo, W. Maw, H. Katagiri, M. Yamazaki, K. Oishi and A. Takeuchi., Sol. Energy Mater. Sol. Cells, 93, (2009) pp. 996.

[127] H. Katagiri, N. Ishigaki, T. Ishida and K. Saito., Jpn. J. Appl. Phys., 40, (2001), pp. 500.

[128] H. Araki, A. Mikaduki, Y. Kubo, T. Sato, K. Jimbo, W. Maw, H. Katagiri, M. Yamazaki, K. Oishi and A. Takeuchi., Thin Solid Films, 517, (2008), pp. 1457.

[129]   H. Araki, Y. Kubo, K. Jimbo, W. Maw, H. Katagiri, M. Yamazaki, K. Oishi and A. Takeuchi., Phys. Status Solidi (c), 6, (2009), pp. 1266.

[130]   P. A. Fernandes, P. M. P. Salome and A. F. da Cunha., J. Alloys Compd., 509, (2011), pp. 7600.

[131] I. D. Olekseyuk, I.V. Dudchak, L. V. Piskach, "Phase equilibria in the Cu2S-ZnS-SnS2 system" Journal of Alloys and Compounds, 368, (2004), pp.135–143.

[132] J. J. Scragg, "Studies of Cu_2ZnSnS_4 films prepared by sulphurisation of electrodeposited precursors", University of Bath, Diss, (2010).

[133] R. Wagner, H. D. Wiemhöfer, "Hall effect and conductivity in thin films of low temperature chalcocite Cu2S at 20°C as a function of stoichiometry", Journal of Physics and Chemistry of Solids, 44, (1983), pp.801–805.

[134] H. Nozaki, K. Shibata, N. Ohhashi, "Metallic hole conduction in CuS" Journal of Solid State Chemistry, 91 (1991), pp.306–311.

[135] G. Liu, T. Schulmeyer, J. Brötz, A. Klein, W. Jaegermann, Thin Solid Films, 431, (2003), pp.477-482.

[136] He, Zhenping; Kretzschmar, Ilona, "Template-Assisted Fabrication of Patchy Particles with Uniform Patches". Langmuir. 28, (2012), pp. 9915–9919.

[137] Jaeger, C. Richard, "Film Deposition Introduction to Microelectronic Fabrication" (2nd ed.). Upper Saddle River: Prentice Hall, (2002).

[138] Secondo Franchi, "Molecular Beam Epitaxy: From Research to Mass Production" Elsevier, (2013).

[139] A. Herman and Helmut Sitter, "Molecular Beam Epitaxy: Fundamentals and Current Status" Springer, (1996).

[140] R. Behrisch "Sputtering by Particle bombardment", Springer, Berlin, (1981).

[141] R. Behrisch and W. Eckstein "Sputtering by Particle bombardment: Experiments and Computer Calculations from Threshold to Mev Energies", Springer, Berlin, (2007).

[142] Pulsed Laser Deposition of Thin Films, edited by Douglas B. Chrisey and Graham K. Hubler, John Wiley & Sons, (1994).

[143] Lippmaa, M.; Nakagawa, N.; Kawasaki, M.; Ohashi, S.; Koinuma, H. (2000). "Growth mode mapping of SrTiO[sub 3] epitaxy". Applied Physics Letters., 76, (2000), pp. 2439.

[144] "Low Pressure Chemical Vapor Deposition – Technology and Equipment", Crystec Technology Trading GmbH, Germany.

[145] Plasma Enhanced Chemical Vapor Deposition – Technology and Equipment, Crystec Technology Trading GmbH, Germany.

[146] ASTM International. In B374-96 Standard Terminology Relating to Electroplating; ASTM International: West Conshohocken, PA, (2003).

[147] Kanani, N. Electroplating: Basic Principles, Processes and Practice; Elsevier Advanced Technology: Oxford, U.K., (2004).

[148] C. J. Brinker and G. W. Sherer, "Sol-Gel Science", Academic Press, San Diego, (1990).

[149] C. J. Brinker, A. J. Hurd, P. R. Schunk, C. S. Ashely, R. A. Cairncross, J. Samuel, K. S. Chen, C. Scotto and R. A. Schwartz, "Sol-Gel Derived Ceramic Films--Fundamentals and Applications", in: K. Stern (Ed.), Metallurgical and Ceramic Protective Coatings, Chapman & Hall, London, (1996), pp. 112-151.

[150] T. Troczynski and Q. Yang, "Process for Making Chemically Bonded Sol-Gel Ceramics". U.S. Pat. No. 6,284,682, May, (2001).

[151]   J. George, "Preparation of Thin Films", Marcel Dekker, Inc., New York. (1992).

[152]   T.P. Niesen, M.R. De Guire, Solid State Ionics, 151, (2002), pp.61.

[153]   C. D. Lokhande, Mater. Chem. Phys., 27, (1991), pp.1.

[154]   G. Hodes, "Chemical Solution Deposition of Semiconductor Films", Marcel Dekker Inc., New York. (2001).

[155]   K.L. Chopra, "Thin Film Phenomena" Mc Graw Hill Book Co., New York. (1996).

[156]   D.J. Pietrzyk and C.W. Frank, "Analytical Chemistry: an Introduction", Academic Press, New York, (1974).

[157]   D.A. Skoog and D.M. West, "Fundamentals of Analytical Chemistry", Holt, Rinehart & Winston, New York, (1980).

[158]   D.A. Skoog and D.M. West, "Analytical Chemistry: an Introduction", Holt, Rinehart & Winston, New York, (1979).

[159]   R.S. Mane and C.D. Lokhande, Mater. Chem. Phys., 65, (2000), pp.1.

[160]   R. V. Lapshin; A. P. Alekhin; A. G. Kirilenko; S. L. Odintsov; V. A. Krotkov (2010). "Vacuum ultraviolet smoothing of nanometer-scale asperities of poly(methyl methacrylate) surface". Journal of Surface Investigation. X-ray, Synchrotron and Neutron Techniques, 4, (2010), pp.1–11.

[161]   A. P. Alekhin; G. M. Boleiko; S. A. Gudkova; A. M. Markeev; A. A. Sigarev; V. F. Toknova; A. G. Kirilenko; R. V. Lapshin; E. N. Kozlov; D. V. Tetyukhin, "Synthesis of biocompatible surfaces by nanotechnology methods" . Nanotechnologies in Russia, 5, (2010), pp.696–708.

[162]   Verhoeven, J.D. Fundamentals of Physical Metallurgy, Wiley, New York, (1975), pp. 326.

[163]   B.D. Cullity, Elements of X-ray diffraction, 2nd edition, Addison- Wessley, California, USA, (1978).

[164]   A. Cottrell, Introduction to Metallurgy (Arnold, London), (1995), pp.173.

[165]   C.D. Lokhande, S.H. Pawar, Physica Status Solidi A, 111, (1989), pp.17.

[166]   S.M. Sze, Physics of Semiconductor Devices, 2nd ed. (John Wiley & Sons), (1981), pp.30.

[167]   Tauc J (ed.) Amorphous and Liquid Semiconductors, Plenum Press, New York (1974), pp.159.

[168] K. Jimbo, R. Kimur, T. Kamimur et al. "Cu_2ZnSnS_4 -type thin film solar cells using abundant materials," Thin Solid Films, vol. 515, no. 15, (2007), pp.5997–5999.

[169] H. Nukala, J. L. Johnson, A. Bhatia, E. A. Lund, W. M. Hlaing, M. M. Nowell, L. W. Rieth, M. A. Scarpulla , Mater. Res. Soc. Symp. Proc, 1268, (2010), pp.03-04.

[170] T. Tanaka , A. Yoshida , D. Saiki , K. Saito , Q. Guo , I. Nishio , T. Yamaguchi , Thin Solid Films , 518, (2010), pp. S29–S33.

[171] K. Sekiguchi, K. Tanaka, K. Moriya, H. Uchiki , phys. Stat. sol. (c), 3, (2006), pp.2618-2621.

[172] J. Madarasz , P. Bombicz , M. Okuya , S. Kaneko, Solid State Ionics, 142, (2001), pp. 439–446.

[173] Z. Zhoun, Y. Wang, D. Xu, Yafei Zhang, Solar Energy Materials & Solar Cells, 94, (2010), pp. 2042–2045.

[174] K. Ramasamy, M. A. Malik and Paul O'Brien, chem. commun 48, (2011), pp. 1170-117.

[175] M. Y. Yeh, C. C. Lee, D. S. Wuu, J Sol-Gel Sci Techno, 52, (2009), pp.65–68.

[176] C.P.Chan, H. Lam, K.Y. Wong, C. Surya, Mater. Res. Soc. Symp. Proc, 1123, (2009), pp. 05-06.

[177] S.C. Riha, S.J.Fredrick, J.B.Sambur,Y. Liu, A. L. Prieto, B. A. Parkinson, ACS Appl. Mater. Interfaces, 3, (2011), pp. 58–66.

[178] E. Moons, D. Gal, J. Beier, G. Hodes, D. Cahen, L. Kronik, L. Burstein, B. Mishori, Y. Shapira, D. Hariskos, H.W. Schock, "Effect of air annealing on the electronic properties of $CdS/Cu(In,Ga)Se_2$ solar cells", Sol. Energy Mater. Sol. Cells, 43, (1996), pp. 73-78.

[179] S. Ikeda, R. Kamai, S. Min Lee, T. Yagi, T. Harada, M. Matsumura, "A superstrate solar cell based on $In_2(Se,S)_3$ and $CuIn(Se,S)_2$ thin films fabricated by electrodeposition Combined with annealing" Sol. Energy Mater. Sol. Cells In Press, Corrected Proof.

[180] N. Muhunthan, Om Pal Singh, Son Singh, and V. N. Singh, International Journal of Photoenergy, Article ID 752012, (2013), 7 pages.

[181] Lakshman Singh, Manish Saxena & P K Bhatnagar, Indian J. Pure and Appl Phys, 42, (2004), pp.841.

[182] Hyungjin Park, Young Hwan Hwang, J Sol-Gel Sci Technol, DOI 10.1007/s10971-012-2703-0.

[183] M.I. Hossain et al. Chalcogenide Letters, 9, (2012), pp. 231 – 242.

[184] H.J. Hovel, Semiconductor and Semimetals; Solar cells, Academic Press, New York, Vol. 11, (1975), pp.38.

[185] T. Zdanowicz, T. Rodziewicz, and M. Zabkowska-Waclawek, Sol. Energy Mater. Sol. Cells, 87, (2005), pp.757–769.

[186] H. Katagiri, N. Ihigaki, T. Ishida, K. Saito, Jpn. J. Appl. Phys., 40, (2001), pp. 500.

[187] J. Seol, S. Lee, J. Lee, H. Nam, K. Kim, Sol. Energy Mater. Sol. Cells, 75, (2003), pp.155.

[188] U. Rau and M. Scmidt, Thin Solid Films, 387, (2001), pp.141.

[189] A. P. Alivisatos, Journal of Physical Chemistry, 100, (1996), pp.13226.

[190] Visweswaran Jayaraman, "Fabrication and Characterization of CIS/CdS and Cu_2S/CdS. Devices for Applications in Nano Structured Solar Cells" University of Kentucky, M.S. Thesis (2005).

[191] M. C. Sharma, B. Tirpathi, S. K., S. Srivastava and Y.K. Vijay, Materials Chemistry and Physics, 131, (2012), pp.600.

[192] K.L. Chopra, P.D. Paulson, V. Dutta, Prog. Photovoltaics Res. Appl., 12, (2004) pp.69-92.

[193] K. Mitchell, C. Eberspacher, J. Ermer and D. Pier, Conf. Record, 20th IEEE Photovoltaic Specialists Conference, Las Vegas, (1988), pp.1384.

[194] T. Kropp, L. Weinhardt, C. Heske, H.-W.Schock, Ch.-H. Fischer and M.C. Lux-Steiner Chem. Phys. Lett. 433, 71, pp.71.

[195] U. Gangopadhyay, K. Kim, D. Mangalaraj and J. Yi, "Low cost CBD ZnS antireflection coating on large area commercial mono-crystalline silicon solar cells" Appl. Surf. Sci. 230, (2004), pp.364-370.

[196] McCandless BE, Hegedus SS., "Influence of CdS Window Layers on Thin Film CdS/CdTe Solar Cell Performance" Proc. of the 22th IEEE Photovoltaic Specialists Conference, (1991), pp. 967–972.

[197] M. Powalla, B. Dimmler, R. Schaeffler, G. Voorwinden, U. Stein, H.-D. Mohring, F. Kessler, D. Hariskos, Proc. 19th European Photovoltaic Solar Energy Conference Paris, France, (2004).

[198] K.M. Hynes, J. Newham, "A comparison of window/buffer layer materials for CdTe thin film modules using environmental risk assessment" Proc. 16th European Photovoltaic Solar Energy Conference, (2000) pp.2297.

[199] Directive 2002/96/EC of the European parliament and of the council of 27 January 2003 on waste electrical and electronic equipment (WEEE), Official Journal of the European Union L37/24, (2003).

[200] De Wild MJ, Wamback K, Alsema EA, Ja¨ger-Waldau A. Conference Record, 20th European Photovoltaic Solar Energy Conference, Barcelona, 3143, (2005).

[201] S.H. Deulkara, C.H. Bhosalea and M. Sharonb., 'A comparative study of structural, compositional, thermal and optical properties of non stoichiometric (Zn,Fe)S chalcogenide pellets and thin films", J. Phys. Chem. Solids, 65, (2004), pp. 1879-1885.

[202] H. Pang, Y. Yuan, Y. Zhou, J. Lian, L. Cao, J. Zhang and X. Zhou, "ZnS/Ag/ZnS coating as transparent anode for organic light emitting diodes" J. Lumin. 122, (2007), pp.587-589.

[203] M. Yoneta, M. Ohishi, H. Saito, J. Cryst. Growth, 127, (1993), pp.314.

[204] A. Aboundi, M. Diblasio, D. Bouchara, Phys. Rev., B 50, (1994), pp.11677.

[205] D. Barreca, A. Gasparotto, C. Maragno, E. Tondello and C. Sada, "CVD of Nanophasic (Zn, Cd)S Thin Films: From Multi-Layers to Solid Solutions" Chem. Vapour Depos., 10, (2004), pp.229-236.

[206] M.A. Hernandez-Fenollosa, M.C. Lopez, V. Donderis, M. Gonzalez, B. Mari and J.R. Ramos-Barrado, Thin Solid Films, 516, (2008), pp.1622.

[207] B. Krishnan, A. Arato, E. Cardenas, T.K. Das Roy, G.A. Castillo, "On the structure, morphology, and optical properties of chemical bath deposited Sb2S3 thin films" Appl. Surf. Sci., 254, (2008), pp.3200-3206.

[208] P. Prathap, N. Revathi, Y.P. Subbaiah, K.T.Ramakrishna Reddy, R.W. Miles, "Preparation and characterization of transparent conducting ZnS:Al films", Solid State Sci., 11, (2009), pp.224-232.

[209] Q. Liu, M. Guobing, A. Jianping, Appl. Surf. Sci., 254, (2008), pp.5711

[210] J. H. Lee, W. C Song, K. J. Yang, Y. S. Yoo, Thin Solid Films, 416, (2002), pp.416.

[211] L. Qi, X Gu, M. Grujicic, W.G. Samuels, G.J. Exarhos, Appl. Phys. Lett., 83, (2003), pp.1136.

[212] J.M. Dona, J. Herrero, "Process and Film Characterization of Chemical-Bath-Deposited ZnS Thin Films", J. Electrochem. Soc., 141, (1994), pp.205-210.

[213] J. Vidal, O. Vigil, O. De Melo, N. Lopez, O. Zelaya-Angel, "Influence of NH_3 concentration and annealing in the properties of chemical bath deposited ZnS films" Mater. Chem. Phys., 61, (1999), pp.139-142.

[214] I.O. Oladeji, L. Chow, "A study of the effects of ammonium salts on chemical bath deposited zinc sulfide thin films" Thin Solid Films, 339, (1999), pp.148-153.

[215] T. Nakada, M. Mizutani, Y. Hagiwara, A. Kunioka, "Improved Jsc in CIGS thin film solar cells using a transparent conducting ZnO:B window layer," Sol. Energy Mater. Sol. Cells, 67, (2001), pp.67-271.

[216] R. Sharma, R.S. Mane, G. Cai, A. Ghule, D.H. Ham, S.K. Min, S.E. Lee, S.H. Han, "Room temperature synthesis of nanostructured mixed-ordered-vacancy compounds (OVCs) and chalcopyrite $CuInSe_2$ (CIS) thin films in alkaline chemical bath", J. Phys. D: Appl. Phys., 42, (2009), pp.055313.

[217] S. Yoon, T. Yoon, K.S. Lee, K. Yoon, J.M. Ha,S. Choe, "Nanoparticle-based approach for the formation of CIS solar cells", Solar Energy Materials & Solar Cells, 93, (2009), pp.783-788.

[218] W. Wang, E. Schiff,Q. Wang, "Amorphous silicon/polyanilne heterojunction solar cell:Fermi levels and open circuit voltages", Journal of Non-Cryastalline Solids, 354, (2008), pp.2862-2865.

Appendix A

BIO-DATA

Education and training

- SLET Qualified
- M. Phil (Energy), 2007-2008 (74%)
  University of Rajasthan, Jaipur, India
- M. Sc. (Physics), 2005-2007 (71.17%)
  University of Rajasthan, Jaipur, India

Professional Experience

- Women Scientist Fellow – August 2015 to Present
- Junior Research Fellow (JRF)/ Senior Research Fellow (SRF) - July 2013 to August 2015.
- Lecturer (Physics) - August 2011-December 2011
  S.S. Jain Subodh P.G. College, Jaipur, India
- Lecturer (Physics) -July 2010 - August 2011.
  Agrawal P.G. College, Jaipur, India

Fellowships & Awards

- Women scientist fellowship DST funded for August 2015-Present
- Junior/Senior research fellowship (JRF/SRF) MHRD funded - July 2013 to August 2015.
- First rank award in M. Sc. (Physics).

Research Summary

- Research Publications: 07
- Communicated: 03
- Conference Presentations: 15

Appendix B

Detailed List of Research Publications

Publications related to Ph. D. Thesis

1. **Indu B. Vashistha**, Mahesh C. Sharma, Ramphal Sharma and S.K. Sharma, "Post annealing treatment of ZnS Thin Film as a buffer layer" *Surface Engineering,* DOI : 10.1080/02670844.2016.1254978. (2016).

2. **Indu B. Vashistha,** Mahesh C. Sharma, Ramphal Sharma and S.K. Sharma, "Annealing Effect on Cu2ZnSnS4 Thin Films Deposited by Chemical Bath Method for Solar Cell Application" *Energy Environ. Focus,* 5, 174–180 (2016).

3. **Indu B. Vashistha**, Mahesh C. Sharma, Ramphal Sharma and S.K. Sharma "Chemical precursor impact on the properties of Cu2ZnSnS4 absorber Layer**"** *AIP Conference Proceedings*, 1724, 020041 (2016) .

4. **Indu B. Vashistha**, Mahesh C. Sharma, Ramphal Sharma and S.K. Sharma "Effect of dopent on the structural and optical properties of ZnS Thin Film as a buffer layer in solar cell application" , *AIP Conference Proceedings* 1675, 030020 (2015).

5. **Indu B. Vashistha**, Mahesh C. Sharma, Ramphal Sharma, and S. K. Sharma, "Synthesis and Characterization of Cu_2ZnSnS_4 Absorber Layer for Solar Cell Application" *Advanced Electrochemistry,* 2, 29-33, (2014).

Paper Communicated in Journals

1. **Indu B. Vashistha,** Mahesh C. Sharma, and S.K. Sharma, "Impact of thermal treatment parameter on the properties of Cu_2ZnSnS_4 solar absorber layer" *Advance materials letters* (Under review).

2. **Indu B. Vashistha,** Mahesh C. Sharma, Ramphal Sharma and S.K. Sharma," Effect of precursor concentration on the properties of Cu_2ZnSnS_4 thin film" *Material Characterization* (Communicated).

3. **Indu B. Vashistha,** Mahesh C. Sharma, Ramphal Sharma and S.K. Sharma," Formation of ZnS/CZTS heterojunction for solar cell application." *Solar Energy Materials* (Communicated).

Others Papers in International Journals

1. Mahesh C. Sharma, **Indu B. Vashistha**, R. Singhal, S. K. Sharma, Y. K. Vijay, and Ramphal Sharma "Effect of Thickness on Structural, Surface Morphological and Optical Properties of Thermally Evaporated CdS Widow Layer" *Advanced Electrochemistry*, Vol- 2, pp - (2014).

2. Mahesh C. Sharma, **Indu B. Vashistha** and Y.K. Vijay, "Preparation and Characterization of the Heterojunction of $CuInSe_2$/CdS Thin Films Prepared by Stacked Elemental Layer Technique" *American Institute of Physics (AIP) Conference proceeding*, 536 (2013) 485-486.

Papers presented in Conferences

1. **Indu B. Vashistha**, Mahesh C. Sharma, B.L. Chaudhary, Ramphal Sharma and S.K. Sharma "Synthesis and Characterization of Cu_2ZnSnS_4 (CZTS) Thin Film by Chemical Bath Deposition Method" "National Conference on Perspectives of Physics in Multi disciplinary Research" organized by Department of Physics, University of Rajasthan, Jaipur during 12-13 March 2014.

2. **Indu B. Vashistha**, Mahesh C. Sharma, Ramphal Sharma and S.K. Sharma. "Effect of annealing time on the properties of Cu_2ZnSnS_4 thin film grown by CBD" National workshop on Advanced Functional Materials organized by Department of Physics, MNIT, Jaipur on 5 September 2014.

3. **Indu B. Vashistha,** Mahesh C. Sharma, Ramphal Sharma and S.K. Sharma. "Study of optical and electrical properties of $Cu_2ZnS_nS_4$ (CZTS) particles for low

cost solar cell" International Conference "BICON-14" organized by Department of Science Biyani Girls College, Jaipur during 12-17 October 2014.

4. **Indu B. Vashistha**, Mahesh C. Sharma, Ramphal Sharma and S.K. Sharma "Synthesis and Characterization of Cu_2ZnSnS_4 Absorber Layer for Solar Cell Application" , NCME-14 organized by S.S. Jain Subodh College, Jaipur during 21-24 December 2014.

5. **Indu B. Vashistha**, Mahesh C. Sharma, Ramphal Sharma and S.K. Sharma "Effect of dopent on the structural and optical properties of ZnS Thin Film as a buffer layer in solar cell application", 4th National Conference on Advanced Materials and Radiation Physics (AMRP-2015) organized by SLIET Longowal, Punjab during 13-14 March 2015.

6. **Indu B. Vashistha**, Mahesh C. Sharma and S.K. Sharma, "Growth mechanism of different chemical precursor based chemical bath deposition method for Cu_2ZnSnS_4 thin film deposition", National Conference on Recent Advancement in Chemical Sciences (RAICS) organized by Department of Physics, MNIT, Jaipur during 21-23 August 2015.

7. **Indu B. Vashistha**, Mahesh C. Sharma, and S.K. Sharma, "Chemical precursor impact on the properties of Cu_2ZnSnS_4 absorber Layer" International Conference on Emerging Technologies: MICRO TO NANO 2015 (ETMN) organized by Manipal University, Jaipur during 24-25 Oct. 2015.

8. **Indu B. Vashistha**, Mahesh C. Sharma, and S.K. Sharma "Post annealing treatment of ZnS Thin Film as a buffer layer", Conference on Advanced Materials and Processing (CAMP-2015) organized by Department of Physics, MNIT, Jaipur during 2-4 Dec. 2015.

9. **Indu B. Vashistha**, Mahesh C. Sharma, and S.K. Sharma "Impact of thermal treatment parameter on the properties of Cu_2ZnSnS_4 solar absorber layer", International Conference on Materials Science & Technology (ICMTECH 2016) organized by Delhi University, Delhi during 1-4 March 2016.

10. Mahesh C. Sharma, **Indu B. Vashistha** and Y.K. Vijay, "Formation of Ordered Vacancy Compound CuIn2Se3 on the Surface CuInSe2 Thin Film by Swift Heavy Ion Irradiation of 120 MeV Sliver Ion" International Conference on Materials Science & Technology (ICMTECH 2016) organized by Delhi University, Delhi during 1-4 March 2016.

11. Mahesh C. Sharma, **Indu B. Vashistha**, R. Singhal, S. K. Sharma, Y. K. Vijay, and Ramphal Sharma "Effect of Thickness on Structural, Surface Morphological and Optical Properties of Thermally Evaporated CdS Widow Layer" National Conference on Material and their Energy Application (NCME2014) organized by Department of Physics, S.S. Jain Subodh College, Jaipur during 21-24 December 2014.

12. Mahesh C, Sharma, **Indu B. Vashistha** and Y.K. Vijay, "Deposition of CdS Thin Films by Vacuum Evaporation Method and their Characterization" National Conference on Perspectives of Physics in Multi-disciplinary Research (NCPJ 2014) organized by University of Rajasthan, Jaipur, during March 12-13, 2014.

13. Mahesh C. Sharma, **Indu B. Vashistha** and Y.K. Vijay, "Preparation and Characterization of the Heterojunction of $CuInSe_2$/CdS Thin Films Prepared by Stacked Elemental Layer Technique" International Conference on Recent Trends in Applied Physics & Material Science (RAM 2013) organized by Govt. College of Engineering and Technology, Bikaner, Rajasthan, during February 1-2, 2013.

14. Mahesh C. Sharma, **Indu B. Vashistha** and Y.K. Vijay, "Effect of Swift Heavy Ion Irradiation on the Physical Properties of $CuInSe_2$ Thin Films Prepared by Stack Elemental Layers Technique" International Conference on Swift Heavy Ions in Materials Engineering and Characterization (SHIMEC 2012) organized by IUAC, New Delhi, during October 9-12, 2012.

15. Mahesh C. Sharma, **Indu B. Vashistha** and Y.K. Vijay, "Growth and Characterization of CIS Thin Film Prepared by Stacked Elemental Layers Technique" National Conference on Current Trends on Material Research

(CTMR- 2012) organized by Department of physics, University of Rajasthan, Jaipur, during March 17-19, 2012.

Participation in schools/workshops

1. Advance training of XRD at Materials Research Center, MNIT, and Jaipur on April 21, 2014.

2. International Symposium on "Frontier Materials" at Materials Research Center, MNIT, Jaipur on October 12, 2014.

3. Workshop on "Promoting Techno-Entrepreneurship" under education quality improvement programme at Department of Metallurgical & Materials Engineering, MNIT, Jaipur on May 19, 2014.

4. Short term course on "Characterization Techniques of Materials" at Department of Physics, MNIT, Jaipur during June 17-21, 2013.

5. Short term course on "Frontier Materials" at Department of Physics, MNIT, Jaipur during August 12-17, 2013.

6. School on "Thin Films" at IUAC, Delhi during December 11-13, 2012.

Appendix C

Declaration

I herewith declare that I have produced this thesis without the prohibited assistance of third parties and without making use of aids other than those specified; notions taken overly directly or indirectly from other sources have been identified as such. This thesis has not previously been presented in identical or similar form to any other Indian or foreign examination board.

This thesis work was conducted from December, 2011 to December, 2016 under the supervision of Dr. S. K. Sharma at Department of Physics, Malaviya National Institute of Technology, Jaipur.

JAIPUR   **(Indu Bala Vashistha)**

Appendix D

Research Publications

Post annealing treatment of zinc sulphide thin film as a buffer layer for solar cell application

I. B. Vashistha, M. C. Sharma & S. K. Sharma

Published online: 25 Nov 2016.

Submit your article to this journal ⬈

View related articles ⬈

View Crossmark data ⬈

Post annealing treatment of zinc sulphide thin film as a buffer layer for solar cell application

I. B. Vashistha*[1], M. C. Sharma[2] and S. K. Sharma[1]

In the present study, buffer layer of zinc sulphide (ZnS) thin film for solar cell has been deposited by chemical bath deposition method and followed by annealing at different temperatures in order to control the surface morphology and grain size of the thin film. Effect of annealing is also analysed by structural, morphological and optical properties. The X-ray diffraction analyses revealed that ZnS thin film is polycrystalline in nature with cubic crystal structure. The atomic force micrographs images indicated change in grain size which further confirmed by scanning electron microscopy analysis. Optical measurement data give band gap of 3.5 eV which is optimal band gap for buffer layer for solar cell application.

Introduction

Solar cell technology is one of the well-established solutions of the energy demand. Researchers are focusing mainly on the materials suitable for the absorber layer for solar cell,[1,2] but in case of heterojunction solar cell working on buffer layer is also a field of concern.[3,4] In a heterojunction solar cell, buffer layer plays a vital role by constructing a junction with absorber layer and generating inbuilt electric field essential for separation of photo-charge carriers. Another function of buffer layer is admitting solar spectrum in the appropriate region with maximum amount.[5] Wide energy band gap and low electrical resistivity are key issues for a good buffer layer, so that it can provide maximum amount of photons to the junction and absorber layer with minimum recombination losses. So, large energy band gap, lattice mismatch and appropriate doping density are the requirements of materials used for buffer layer.

CdS is established commercially chosen buffer layer as it fulfils all the requirements.[6,7] But toxicity of CdS is a major problem which leads to the environment health and safety impact issues.[8,9] So, the development of Cd-free device is an area of concern. In laboratories, work is under process for thin film like ZnS, ZnSe, In_2Se_3 for replacement of Cd-based buffer layer.[10,11] In these materials, zinc sulphide (ZnS) achieved a good position for serve the purpose.[12] ZnS is an important wide direct band gap II–VI semiconductor material having band gap energy (Eg) of 3.5 eV or 350 nm. ZnS transmits more high-energy photons to the junction and enhance the blue region and provides better lattice matching with absorbers having energy band gaps in the range of 1.3–1.5 eV.

ZnS thin film can be deposited by different techniques.[13–16] Chemical bath deposition (CBD) is one of the attractive methods due to its advantages like simplicity, low deposition temperature, low cost and large area depositions. Properties of thin films depend not only on the deposition method but also on the modification technique. Post annealing treatment is easily approachable technique which can be used for surface/interface modification. In case of annealing, temperature is most important parameter for treatment as at lower temperature effects on the properties could be negligible on the other hand at higher temperature defects generation and partial evaporation can take place. So, optimisation of temperature parameter for most suitable result is a work of concern. The purpose of this work is establish a relation between annealing temperature and properties of ZnS thin film, thus find out most appropriate temperature for annealing to fulfil our purpose of serve ZnS thin film as a buffer layer.

Materials and methods

Synthesis of ZnS thin film

Chemical bath for synthesis have been prepared by chemicals provided by Sigma Aldrich with 99.9% purity of analytical reagent grade (AR). Zinc sulphate ($ZnSO_4$) and thiourea (NH_2CSNH_2) have been used as substrates and cleaned by detergent then ultrasonically cleaned by acetone, methanol and de-ionised (DI) water and dried in air. Chemical concentrations have been taken as 0.1 M $ZnSO_4$ and 0.1 M NH_2CSNH_2 in equal volume ratio and hydrazine hydrate and TEA have been taken as complexing agent. Details of deposition method and parameters are reported in our earlier work,[17] while steps of ZnS thin film deposition are following:

[1]Department of Physics, Malaviya National Institute of Technology, Jaipur 302017, India
[2]National Institute of Solar Energy, Gurgaon 122003, India

*Corresponding author, email indu_139@yahoo.com

1 *a* XRD patterns of as-deposited ZnS thin film. *b* XRD patterns of (a) annealed ZnS at 100°C (b) at 200°C (c) at 300°C and (d) at 400°C in air for 2 h
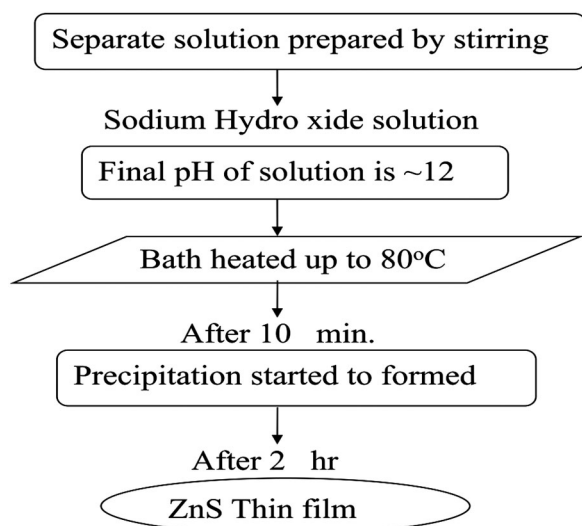
Surface modification

The surface/interface of the thin film can be modified by providing the post deposition treatments like thermal annealing. Annealing is a heat process in the furnace, which involves heating a material to a specific temperature and maintenance of this suitable temperature for appropriate time and then slow cooling. This process alters the physical and sometimes chemical properties of a material. In case of annealing there are two important parameters, i.e. temperature and time. In our study initially we start the process from 100°C with subsequent gap of 50°C. We find out that gap of 50°C does not give any drastic change in properties of ZnS films. So, we increase the gap and made it 100°C. Effect of annealing time is another parameter as lower time does not raise appropriate change in concern properties while as the time increase thin film started to peel off. So, we take the moderate time of 2 h. Thus, as-grown ZnS thin films has been annealed in air for 2 h in tubular furnace and annealing temperature *have been* varies with 100°C started from 100 to 400°C.

Characterisation

The structural properties of as-grown and annealed ZnS thin film have been studied by X-ray diffraction (XRD) pattern by using PANalytical X'Pert Pro X-ray Diffraction Unit with copper (Cu), which have strong K_α radiation having X-ray emissions wavelength of 1.5418 Å in range of 20–60°. The surface morphological studies have been carried out using scanning electron microscope (SEM) JEOL JSM model 6360 and atomic force microscope (AFM). The optical absorption spectra have been recorded using UV–vis spectrophotometer (HITACHI U-2900) within the wavelength range of 280–800 nm.

Results and discussion

Structural analysis

The structural analysis study has been done by XRD technique. Figure 1 depicts the XRD pattern of as-grown and annealed ZnS thin films. Figure 1*a* reveals the amorphous nature of as-deposited film due to the
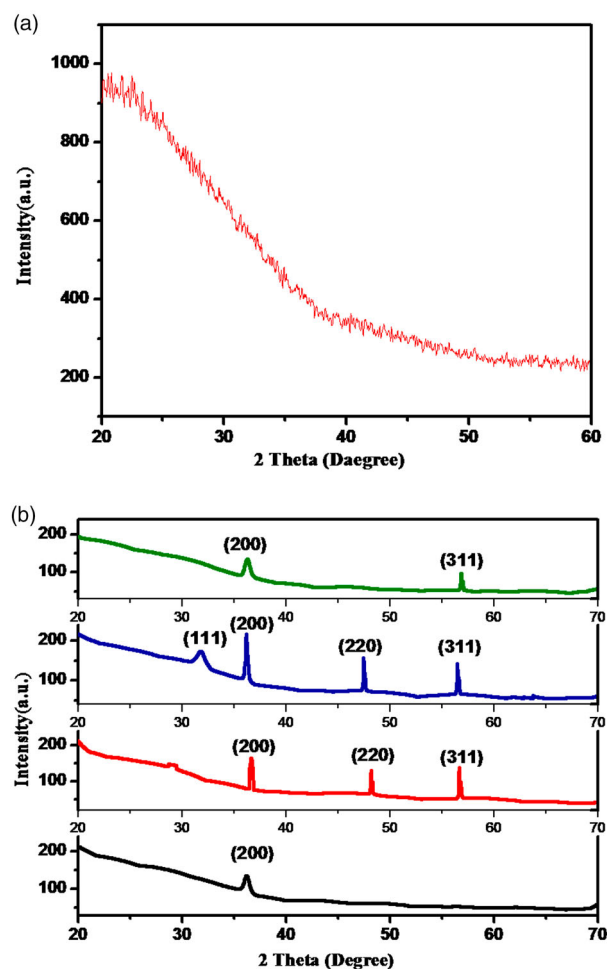
lack of diffraction peaks. Figure 1*b* displays the XRD pattern of annealed ZnS thin films which consists diffraction peaks at diffraction angles and indicate the crystal structure. ZnS thin film annealed at 100°C shows diffraction peak at 28.5 and by comparing with JCPDS card (05–0566), sphalerite crystal structure with (111) plane is confirmed [Fig. 1(*b*, a)]. XRD pattern of ZnS thin film annealed at 200°C unveil the presence of more diffraction peaks at 47.5 and 56.3, thus conveying the presence of plane (111), (220) and (311) [Fig. 1(*b*, b)]. Crystal structure of ZnS thin film annealed at 300°C demonstrated by Fig. 1(*b*, c) has another extra peak at 33.1 for corresponding (200) plane. As the annealing temperature increase up to 400°C, less intense diffraction peaks of plane (111) and (311) occur. Figure 1*b* reveals that the intensity of diffraction peaks increase with increased annealing temperature and give best results at 300°C, on the other hand preferred degree of orientation is (111) plane for sphalerite structured annealed thin film. These results are in good agreement with reported data.[18,19]

Surface morphological analysis

The surface morphological analysis have been displayed by 2D and 3D image of AFM of as-deposited and annealed ZnS thin film in Fig. 2. AFM image of as-
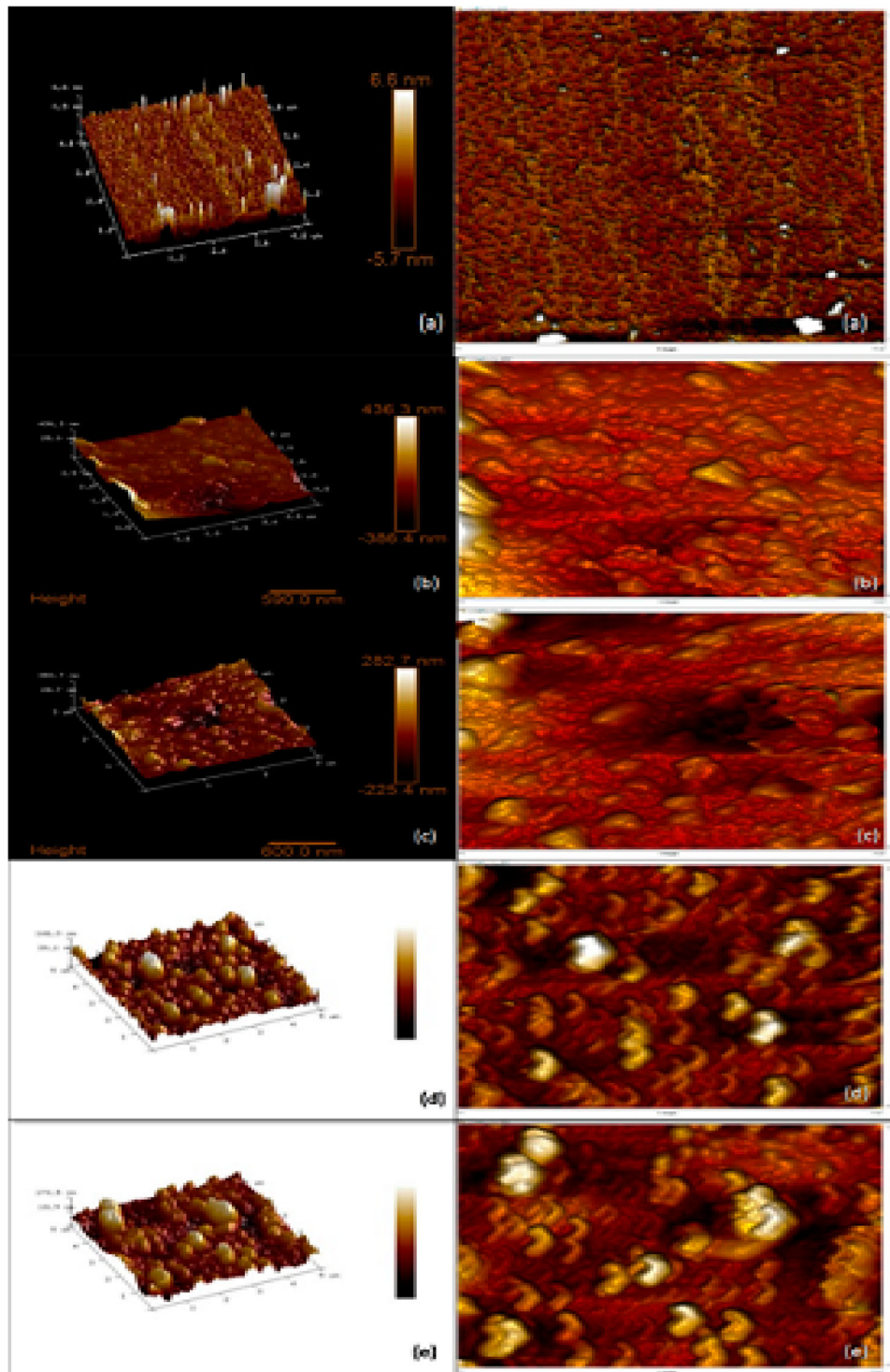
2 The 2D and 3D AFM images of *a* as-deposited ZnS thin film *b* annealed ZnS thin film at 100°C in air for 2 h *c* annealed ZnS thin film at 200°C in air for 2 h *d* annealed ZnS thin film at 300°C in air for 2 h *e* annealed ZnS thin film at 400°C in air for 2 h

deposited film leads to unvarying surface morphology of ZnS thin film [Fig. 4(a)]. ZnS thin film started to show grain growth after annealing at 100°C [Fig. 4(b)] which turns film morphology in uneven grain of varying size from 0.25 ± 0.01 μm to 0.35 ± 0.01 μm at surface. Same pattern followed by ZnS thin film annealed at 200°C [Fig. 4(c)] with slight variation in grain size. Figure 4(d) represents the morphology picture of film annealed at 300°C and reveal that the surface is well covered by hemi-sphere shape grains of size 0.4 ± 0.01 μm to 0.5 ± 0.01 μm

with equal distribution. Grain shape and size is almost remain same for film annealed at 400°C but on the other hand agglomeration of grains started to take place which leads us to conclusion that annealing at 300°C gives an evenly well covered consistent surface with higher grain size. This large grain size is useful for buffer layer application because decrement in grain boundaries reduce localised recombination sources.[20] The average surface roughness, root mean squared roughness and grain size of the annealed films is shown in Table 1.

**Table 1 Surface morphological parameters for annealed thin films**

Sample	Average surface roughness	Root mean squared roughness	Grain size
Annealed ZnS thin film at 100°C	92.1 nm	58.5 nm	0.25 ± 0.01 μm to 0.35 ± 0.01 μm
Annealed ZnS thin film at 200°C	90.3 nm	41.4 nm	0.3 ± 0.01 μm to 0.45 ± 0.01 μm
Annealed ZnS thin film at 300°C	41.6 nm	32.3 nm	0.4 ± 0.01 μm to 0.5 ± 0.01 μm
Annealed ZnS thin film at 400°C	33.8 nm	25.7 nm	0.4 ± 0.01 μm to 0.8 ± 0.01 μm

SEM analysis also has been done for confirmation of annealing impact on surface morphology. Figure 3*a* shows SEM surface image of as-grown ZnS film and Fig. 3*b–e* shows the surface images of annealed films at 100, 200, 300 and 400°C, respectively. Previously drawn conclusion by AFM images has been confirmed by SEM surface images. As-grown film shows smooth surface while for annealed film grain growth increased with increased annealing temperature from 100 to 300°C and above 300°C agglomeration started to occur. Nature of island formation is of chemical nucleation and growth process followed by further agglomeration.

This analysis exposes that high-temperature annealing could improve the crystallinity and increase the grain size of thin films but after certain temperature crystal structure tends to come under influence of uneven agglomeration. This gives a very important parameter in aspect of effect of annealing temperature on ZnS thin films. Similar result has been reported by Manjulavalli and Kannan.[21]

Optical absorption study

Optical properties of as-deposited and treated ZnS thin film have been studied by absorption spectra in the
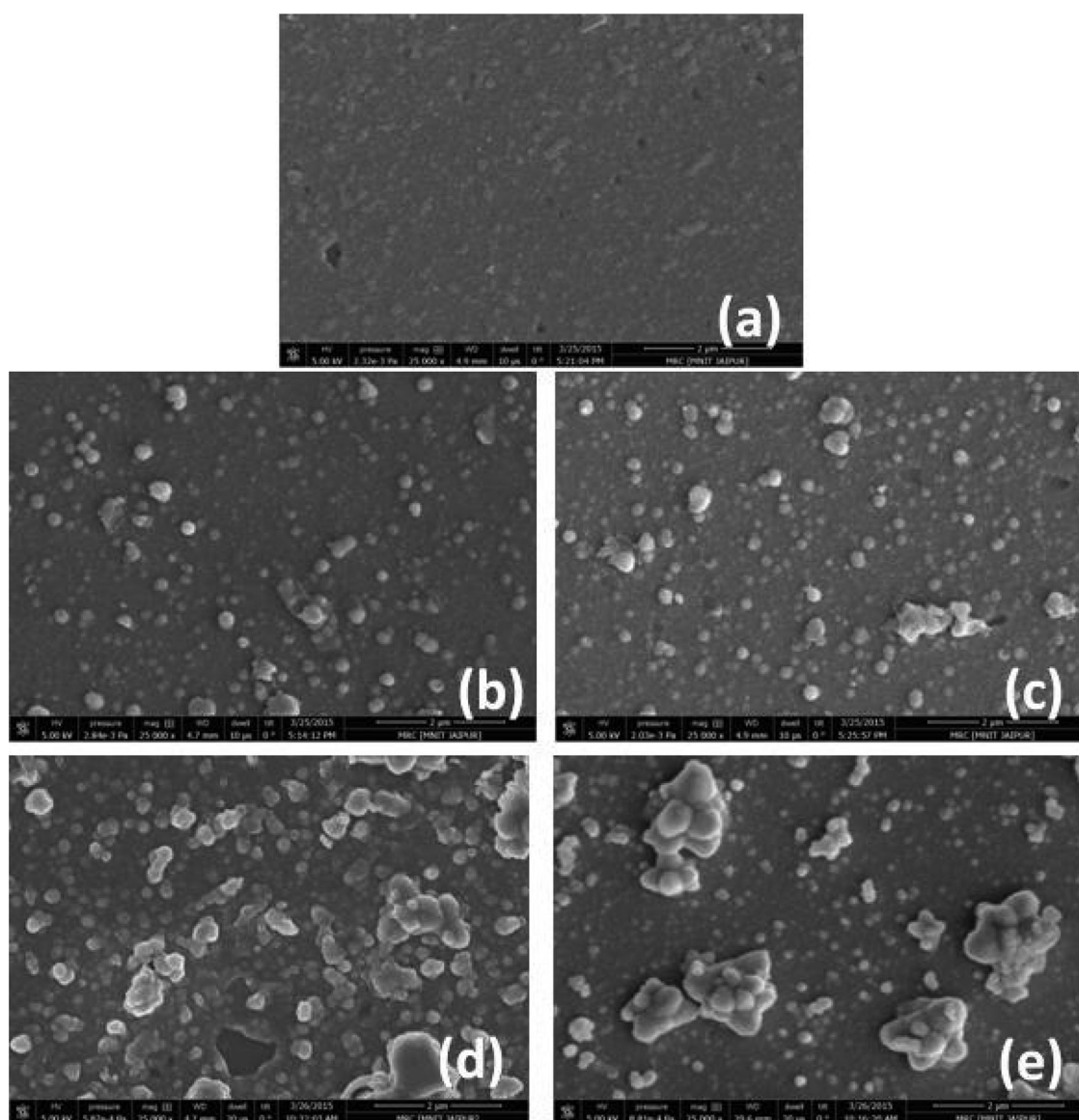
3 SEM images of *a* as-deposited ZnS thin film *b* annealed ZnS at 100°C and *c* at 200°C *d* at 300°C *e* at 400°C in air for 2 h
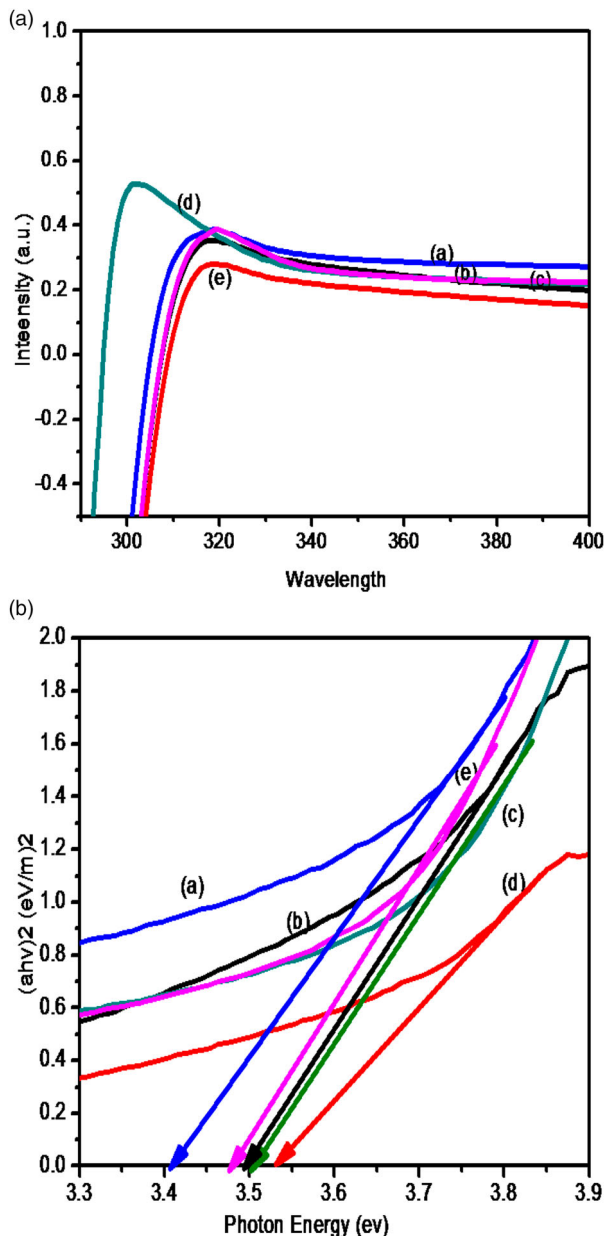
4 *a* Variation of absorption (a.u.) with wavelength (nm) of images of (a) as-deposited ZnS thin film (b) annealed ZnS at 100°C and (c) at 200°C (d) at 300°C (e) at 400°C in air for 2 h. *b* The plots of $(\alpha h\upsilon)^2$ vs. *h*υ of (a) as-deposited ZnS thin film (b) annealed ZnS at 100°C and (c) at 200°C (d) at 300°C (e) at 400°C in air for 2 h

wavelength range 280 to 800 nm. Figure 4*a* displays the optical absorbance spectra of ZnS thin film which demonstrate that variation of absorbance (a. u.) with respect to wavelength (λ) have high absorbance in ultraviolet region. Optical absorption has been found to be increased with

increasing annealing temperature and has highest intensity for 300°C. Further optical data has been analysed by using Tauc relation[22] from which the absorption coefficient α, for semiconductor material is given by

$$\alpha = \frac{A(h\upsilon - E_g)^n}{h\upsilon} \qquad (1)$$

where α is absorption coefficient, *A* is constant, *h*υ is incident photon energy, E_g is energy band gap, i.e. separation between bottom of conduction band and top of the valance band, *n* is constant which depends on the nature of transition, i.e. $n = 1/2$ for allowed direct transition, $n = 2$ for allowed indirect transition. Plot of $(\alpha h\upsilon)^2$ (by taking $n = 1/2$) vs. *h*υ is a straight line which shows it is a direct band gap material. Extrapolation of Tauc plot to zero absorption coefficient ($\alpha = 0$) gives energy band gap values. Figure 4*b* shows that band gap energy increases with increase in annealing temperature and results for as-grown and annealed ZnS films have been summarised in Table 2. Energy band gap of ZnS film annealed at 300°C is 3.5 eV which is optimal band gap for buffer layer. Energy band gap in this range is also shown by other researches.[23]

Conclusion

ZnS buffer layer by low-cost CBD technique has been synthesised. Post annealing treatment has been performed and characterised for different properties, structural studies indicated amorphous nature of as-deposited ZnS films which have been converted to polycrystalline after annealing. Surface morphology of ZnS film shows increase in grain size with annealing and even grains occur for film annealed at 300°C. The optical absorption study indicates transition with a direct energy band gap and dependence on annealing temperature. Therefore, annealing temperature has some effects on the crystallinity, surface and optical properties of the ZnS thin film. When the annealing temperature is 300°C, ZnS film depicts sphalerite structured thin film and preferred degree of orientation is (111) plane. ZnS annealed film at 300°C shows grains of size 0.4 ± 0.01 μm to 0.5 ± 0.01 μm with equal distribution. For this film not only the grain size becomes larger, but also the energy band gap 3.54 eV is in the range of optimal band gap. CBD method is cost effective and simple method other than physical deposition methods. So, ZnS buffer layer deposited by CBD method exhibits good properties those further could be used in heterojunction PV structure.

Acknowledgements

References

1. P. Jackson, D. Hariskos, E. Lotter, S. Paetel, R. Wuerz, R. Menner, W. Ischmann and M. Powalla: 'New world record efficiency for Cu (In,Ga)Se2 thin-film solar cells beyond 20%', *Prog. Photovoltaics Res. Appl.*, 2011, **19**, 894–897.

Table 2 Energy band gap for ZnS thin films

Sr. no.	Sample	Band gap (eV)
1	As-deposited ZnS thin film	3.47
2	Annealed ZnS thin film at 100°C	3.49
3	Annealed ZnS thin film at 200°C	3.50
4	Annealed ZnS thin film at 300°C	3.54
5	Annealed ZnS thin film at 400°C	3.4

2. First Solar, Press Release, available at http://investor.firstsolar.com/releasedetail.cfm, (accessed July 26, 2011).

3. T. Kropp, L. Weinhardt, C. Heske, H.-W. Schock, Ch.-H. Fischer and M. C. Lux-Steiner: 'The electronic structure of the [Zn(S,O)/ZnS]/CuInS2 heterointerface – impact of post-annealing', *Chem. Phys. Lett.*, 2006, **433**, 71–74.

4. U. Gangopadhyay, K. Kim, D. Mangalaraj and J. Yi: 'Low cost CBD ZnS antireflection coating on large area commercial mono-crystalline silicon solar cells', *Appl. Surf. Sci.*, 2004, **230**, 364–370.

5. B. E. McCandless and S. S. Hegedus: Proc. of the 22th IEEE Photovoltaic Specialists Conference, 1991, 967–972.

6. M. Powalla, B. Dimmler, R. Schaeffler, G. Voorwinden, U. Stein, H.-D. Mohring, F. Kessler and D. Hariskos: Proc. 19th European Photovoltaic Solar Energy Conference Paris, France, 2004.

7. K. M. Hynes and J. Newham: Proc. 16th European Photovoltaic Solar Energy Conference, 2000, 2297.

8. Directive 2002/96/EC of the European Parliament and of the Council of 27 January 2003 on Waste Electrical and Electronic Equipment (WEEE), *Official Journal of the European Union*, 2003.

9. M. J. DeWild, K. Wamback, E. A. Alsema and A. Jäger-Waldau: Conference Record, 20th European Photovoltaic Solar Energy Conference, Barcelona, 2005, 3143.

10. S. H. Deulkara, C. H. Bhosalea and M. Sharonb: 'A comparative study of structural, compositional, thermal and optical properties of non stoichiometric (Zn,Fe)S chalcogenide pellets and thin films', *J. Phys. Chem. Solids*, 2004, **65**, 1879–1885.

11. H. Pang, Y. Yuan, Y. Zhou, J. Lian, L. Cao, J. Zhang and X. Zhou: 'ZnS/Ag/ZnS coating as transparent anode for organic light emitting diodes', *J. Lumin.*, 2007, 122, 587–589.

12. X. D. Gao, X. M. Li and W. D. Yu: 'Morphology and optical properties of amorphous ZnS films deposited by ultrasonic-assisted successive ionic layer adsorption and reaction method', *Thin Solid Films*, 2004, **468**, 43–47.

13. M. Yoneta, M. Ohishi and H. Saito: 'Low temperature molecular beam epitaxial growth of ZnS/GaAs(001) by using elemental sulfur source', *J. Cryst. Growth*, 1993, **127**, 314–317.

14. J. S. Patil, S. S. Dhasade, J. V. Thombare and V. J. Fulari: *J. Shivaji Univ.(Sci. Technol.)*, 2014, **41**, (2).

15. D. Barreca, A. Gasparotto, C. Maragno, E. Tondello and C. Sada: 'CVD of nanophasic (Zn, Cd)S thin films: from multi-layers to solid solutions', *Chem. Vapour Depos.*, 2004, **10**, 229–236.

16. M. A. Hernandez-Fenollosa, M. C. Lopez, V. Donderis, M. Gonzalez, B. Mari and J. R. Ramos-Barrado: 'Role of precursors on morphology and optical properties of ZnS thin films prepared by chemical spray pyrolysis', *Thin Solid Films*, 2008, **516**, 1622–1625.

17. I. B. Vashistha, M. C. Sharma, R. Sharma and S. K. Sharma: AIP Conference Proceedings, 2015, 1675, 030020.

18. J. M. Dona and J. Herrero: 'Process and film characterization of chemical-bath-deposited ZnS thin films', *J. Electrochem. Soc.*, 1994, **141**, 205.

19. J. Vidal, O. Vigil, O. De Melo, N. Lopez and O. Zelaya-Angel: 'Influence of NH3 concentration and annealing in the properties of chemical bath deposited ZnS films', *Mater. Chem. Phys.*, 1999, **61**, 139–142.

20. L. Singh, M. Saxena and P. K. Bhatnagar: 'Short circuit current variation of CIGS solar cells with grain boundaries recombination velocity', *Indian J. Pure Appl. Phys.*, 2004, **42**, 841–844.

21. T. E. Manjulavalli and A. G. Kannan: 'Structural and optical properties of ZnS thin films prepared by chemical bath deposition method', *Int. J. Chem. Tech. Res.*, 2015, **8**, (11), 396–402.

22. J. Tauc: 'Amorphous and liquid semiconductor', 1974, New York, Plenum, 159.

23. R. Sahraei, A. Daneshfar, A. Goudarzi, S. Abbasi, M. H. Majles Ara and F. Rahimi: 'Optical properties of nanocrystalline ZnS:Mn thin films prepared by chemical bath deposition method', *J. Mater. Sci. Mater. Electron.*, 2013, **24**, (1), 260–266.

Energy and Environment Focus

MANUSCRIPT 16-196-R

"Annealing Effect on Cu2ZnSnS4 Thin Films Deposited by Chemical Bath Method for Solar Cell Application"

DECISION LETTER

 I am pleased to inform you that your manuscript has now been accepted for publication in Energy and Environment Focus (EEF) (www.aspbs.com/efocus).

In order to publish your manuscript, please send the following documents directly to efocus.asp@gmail.com as soon as possible (within one week from the date of acceptance):

1) Final accepted version of your manuscript in .doc file form, formatted according to the guidelines of EEF at http://www.aspbs.com/efocus/inst-auth_efocus.htm. Improvement of English grammar and usage is MANDATORY before the manuscript may be sent for proof compilation. Please seek the assistance of a native English-speaking colleague, or contact a professional editing service to assist you with this task before you submit the finalized accepted manuscript text.

2) a Graphical Table of Content (TOC) Abstract for your manuscript, which should include the following separate items:
- a representative color figure/artwork: this may not necessarily be a figure already included in the paper, and should essentially reflect the main content/significance of your work;
- max 8-10 lines of explanatory text: this should not include a caption of the TOC figure, but a very succinct summary of the paper content and its significance (please, do not use unexplained acronyms).

3) a signed copy (pdf file) of the Copyright Transfer Agreement for your manuscript, according to the guidelines and the .pdf form that can be download at: http://www.aspbs.com/efocus.htm

Thank you very much for submitting your work to Energy and Environment Focus (EEF).

I am looking forward to receiving your next interesting manuscript for publication in EEF.

With kind regards,

Ahmad Umar
Editor-in-Chief
Energy and Environment Focus (EEF)

P.S.: You may be interested in highlighting the subject of your research paper in the front Cover Page of a EEF issue. If so, you may email us your layout suggestions with a short narrative description of the cover content and significance.

Instructions for compiling the cover artwork:

- The area that is used by the EEF cover is approximately 6.615 inches wide by 4.75 inches high. If you are submitting a photograph, the best resolution would be at 300 dpi, which would be an image of 1985 pixels by 1422 pixels.

-If image is all-line art, then the dpi would best be at 600 dpi which
makes an image of 3970 X 2844 pixels. If your image is a vector image
then you only need to worry about the dimensions as a vector is
printer-independent.

- CMYK is the best color mode. Images provided in RGB may be then
converted to CMYK for the printer. In such cases, however, the printed
blues or greens may not look as bright as the original ones due to the
color conversion process.

- Do not use obscure fonts.

REVIEWER 1

Home | **Submit Manuscript** | **History-Status Report** | **Test Drive** | **Pricing** | **Contact**

Low Cost Deposition of Cu_2ZnSnS_4 Thin Films by Chemical Bath Deposition Method for Solar Cell Application

Indu B. Vashistha[1*], Mahesh C. Sharma[2], and S.K. Sharma[1]

[1]*Department of Physics, Malaviya National Institute of Technology, Jaipur, India*

[2]*National Institute of Solar Energy, Gurgaon, India*

* indu_139@yahoo.com

Abstract

I_2–II–IV–VI_4 compound semiconductors are important solar cell materials with optical and electrical properties that can be tuned for optimum device performance. Recently, studies have been an effort to investigate direct band gap Cu_2ZnSnS_4 material which could be used as a solar cell absorber material because of its low-cost and non-toxicity. In the present paper, CZTS absorber thin films have been successfully synthesized onto glass substrate by Chemical Bath Deposition method. These as-grown CZTS films have been further subjected to thermal annealing for controlling morphology and grain size of the absorber layer in solar cell. The as-grown and annealed films have been characterized by X-Ray diffraction (XRD), optical absorption, scanning electron microscope (SEM) for structural, optical and surface morphological properties, respectively. XRD analysis revealed that structure of CZTS film is polycrystalline in nature with tetragonal structure after annealing. The SEM exhibits grain growth as a function of annealing treatments corresponding for modifications in the grain size. The band gap of annealed CZTS films has found 1.51 eV which are calculated by absorption spectroscopy and band gap value is nearly equal to theoretical value of solar energy spectrum.

Keywords: **CZTS Thin Films, XRD, SEM and Energy Band Gap**

I.   INTRODUCTION

The present worldwide energy consumption rate is alarming due to rapid depletion of conventional energy resources. These sources of energy are non-renewable and limited in quantities, they can also be polluting to the environment. To solve these problems, new alternative energy sources development efforts have been made over the two last decades. Within the renewable energies resources, solar energy is the most promising source of clean energy we can use and it is necessary to develop the solar cells with high efficiency, low cost and less environmental damage. By using thin film solar cells, price of solar energy become low due to the small amounts of materials and low cost manufacturing thin film technology. Research on thin film solar cell technologies such as compound semiconductors are great interest in the field of solar energy. The compound semiconductors Cu(In,Ga)Se$_2$ (CIGS) and CdTe based thin film solar cell have reached at the stage of fulfillment of commercialization requirements with efficiencies of 20.3% [1], 17.3% [2] respectively. However, due to limited supply and high price of rare metals, such as indium and gallium, there is a need to find alternative materials with high abundance and low cost.

Recently, there has been an effort to investigate direct band gap Cu$_2$ZnSnS$_4$ (CZTS) and Cu$_2$ZnSnSe$_4$ (CZTSe) thin films for photovoltaic applications. The CZTS-based thin film solar cells are interesting materials from research point of view, since all elements Cu, Zn, Sn and S are abundant in the crust of the earth and are relatively cheap and non-toxic [3-4]. Also CZTS contains less toxic material S rather than Se which is desirable for environment friendly applications. Quaternary Cu$_2$ZnSnS$_4$ (CZTS) thin films display an interesting set of wide range of properties such as p-type conductivity, a suitable direct energy band gap of 1.4–1.5 eV, and large absorption coefficient over 10^4 cm^{-1}[5]. On the other hand, according to Shockley-Queisser limit CZTS solar cells are expected to have theoretical conversion efficiency of 32.2% [6]. In laboratory cells recent material improvements have increased efficiency above 10% for CZTS [7], but more work is required for making them commercially viable.

Several methods have been used to grow this p-type absorber layer such as DC and RF magnetron sputtering [8], co-evaporation [9], pulsed laser deposition [10], thermal and electron-beam evaporation [11-12], screen printing [13], chemical vapor deposition [14], spray pyrolysis [51], sol-gel spin-coated deposition [16], electrodeposition [17-18]. However, the physical techniques have some drawbacks such as costly, sophisticated instrumentation and toxic byproducts. On the other hand, As compared to the other deposition methods, Chemical Bath Deposition (CBD) method is attractive one because of its advantages such as simplicity, reproducibility, non-

hazardous, cost effectiveness and well suited for producing large-area thin films at low temperatures and after going through the literature, there are very few reports on the synthesis of CZTS thin film using CBD method.

In this research paper we report the synthesis of thin film of semiconductor compound CZTS by using Chemical Bath Deposition (CBD) method which is preferable for making low-cost solar cell. It has been reported that the efficiency of polycrystalline thin film solar cell has dependence on morphology and grain size of the absorber layer, which can be controlled by post treatments such as thermal annealing. Considering this aspect we study the annealing effect on CZTS thin films for solar cell performance. Therefore as-grown and annealed CZTS thin films characterized by different characterization tools.
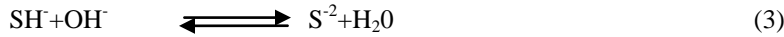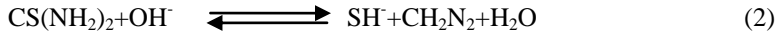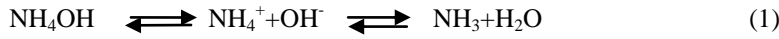
II. EXPERIMENTAL DETAILS

A. Sample preparation

Cu_2ZnSnS_4 (CZTS) thin films have been deposited on glass substrate by Chemical Bath Deposition (CBD) method. The glass substrate and ITO-coated substrates have been cleaned ultrasonically in detergent, acetone, methanol and De-ionized water and dried in oven. Chemical bath has prepared by using analytical reagent grade (AR) chemicals. $CuSO_4$, $ZnSO_4$, $SnSO_4$, NH_2CSNH_2 chemicals have been used for Cu^{2+}, Zn^{2+}, Sn^{2+} and S^{2-} ions sources and Ethylenediaminetetraacetic acid (EDTA) for complexing agent for controlling the reaction and precipitation formation in bath. Chemical solutions have been separately prepared of 0.1 M $CuSO_4$, 0.05 M $ZnSO_4$, 0.05 $SnSO_4$, 0.5 NH_2CSNH_2 in equal volume ratio and later mixing these solutions in biker. The pH of the resultant solution has controlled by adding ammonia and final pH ~10. After controlling the pH, previously cleaned substrates has immersed in the bath and then bath heated up to $60^{o}C$. The schematic diagram for chemical bath deposition method has been shown in Fig. 1.

During reaction white solution became yellow after 5-7 min. and presence of precursor metal sulfides gave a brown blackish color. After 1 hr precipitation started to form in the bath and deposition of CZTS film started on the substrates. By changing the deposition time films of different thickness have been obtained. After 5 hr substrate with CZTS film has removed, rinsed in DI water, dried in air and preserved in desiccator. The deposited CZTS thin films have been annealed at $50^{o}C$, $150^{o}C$, and $250^{o}C$ for 2 hr in air in tubular furnace. After annealing films have been allowed to cool naturally as abrupt quenching could result in cracks or defects generation.
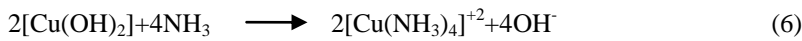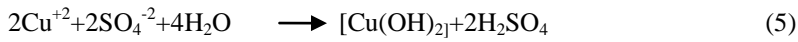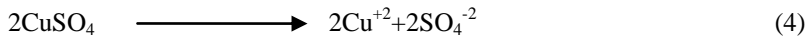
B. Growth mechanism of CZTS Film

For the formation of metal sulfide, metal cation and sulfur anions are required firstly. These cations and anion occurred from metal sources and sulfur source respectively through some intermediate reactions.
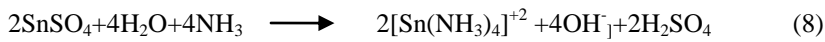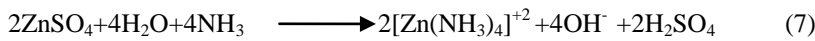
(1) Dissociation of Sulfur ions takes place by the hydrolysis of thiourea with hydroxide ion produced from ammonia. Soluble ammonia produces ammonia ion and hydroxide ions solution in equilibrium with ammonia and water.

$$NH_4OH \rightleftharpoons NH_4^+ + OH^- \rightleftharpoons NH_3 + H_2O \qquad (1)$$

$$CS(NH_2)_2 + OH^- \rightleftharpoons SH^- + CH_2N_2 + H_2O \qquad (2)$$

$$SH^- + OH^- \rightleftharpoons S^{-2} + H_2O \qquad (3)$$

(2) Formation of metal complex by reaction of metal source with ammonia. Ammonia molecule reacts with the metal ion to produce a complex ion. Less concentration of ammonia in solution give metal hydroxide but in case of high concentration of ammonia, complex ion formed govern by below reactions.

$$2CuSO_4 \longrightarrow 2Cu^{+2} + 2SO_4^{-2} \qquad (4)$$

$$2Cu^{+2} + 2SO_4^{-2} + 4H_2O \longrightarrow [Cu(OH)_{2]} + 2H_2SO_4 \qquad (5)$$

$$2[Cu(OH)_2] + 4NH_3 \longrightarrow 2[Cu(NH_3)_4]^{+2} + 4OH^- \qquad (6)$$

Similarly $ZnSO_4$ and $SnSO_4$ give Zn and Sn complex ion in reaction

$$2ZnSO_4 + 4H_2O + 4NH_3 \longrightarrow 2[Zn(NH_3)_4]^{+2} + 4OH^- + 2H_2SO_4 \qquad (7)$$

$$2SnSO_4 + 4H_2O + 4NH_3 \longrightarrow 2[Sn(NH_3)_4]^{+2} + 4OH^-_] + 2H_2SO_4 \qquad (8)$$

In above reaction formation of complex ion controlled by complexing or chelating agent EDTA as it control the release of metal ion in solution which further results in formation of metal complex ion.

(3) In final step replacement of complex ion by sulfur ion takes place as under expressed reaction

$$2[Cu(NH_3)_4]^{+2} + [Zn(NH_3)_4]^{+2} + [Sn(NH_3)_4]^{+2} + 4S^{-2} \longrightarrow Cu_2ZnSnS_4 + 12NH_3 \qquad (9)$$

When the ionic product exceeds the solubility product of final compound Cu_2ZnSnS_4 (CZTS) then it precipitate out as collide in the solution and as a film on the substrate.

C. Characterization Techniques

The structural properties of as grown and annealed CZTS thin film have been studied by X-ray diffraction (XRD) pattern by using PANalytical X'Pert Pro X-ray Diffraction Unit with copper (Cu), which have strong K_α radiation having X-ray emissions wavelength of 1.5418 Å in range of 20-60°. Average crystal sizes have been determined according to broadening of peaks using Scherrer relationship. The surface morphological study has been carried out using scanning electron microscope (JEOL JSM model 6360). The optical absorption spectra have been recorded using UV–vis Spectrophotometer (HITACHI U-2900) within the wavelength range of 280-800 nm. The current voltage (I-V) characteristics were studied using Lab equipped Keithley (model SMU-2400) computer interface set up unit.

III. RESULTS and DISCUSSION

A. Structural Analysis

The structural analysis of as-grown and annealed CZTS thin films have been performed using X-ray diffraction (XRD) technique. Figure 2(A) show the XRD pattern of as-grown CZTS films and as there is no clear diffraction peaks which indicate amorphous nature of these films. Figure 2(B) show the XRD pattern of annealed CZTS thin films which indicate occurrence of crystal structure as diffraction peaks appeared at different angle after annealing. CZTS thin films annealed at 50^0C shows diffraction peaks at 28.5,32.6 and 47.8 by comparing the calculated 'd' values with experimental 'd' values from JCPDS card 26-0575 corresponding planes are (112) (200) (220). XRD pattern of annealed film at 150^0C shows one another peak at 23.1° for (110) plane. As annealing temperature increase, intensity of diffraction peaks also increases which can be depict by XRD pattern of CZTS film at 250^0C. XRD pattern of annealed CZTS thin films confirms the formation of kesterite structured CZTS film with tetragonal structure on the other hand degree of preferred orientation for annealed films is (112).These results are in good agreement with reported data (19-20). Particle size in the film has been calculated from the Scherrer's formula:

$$D = \frac{0.9\lambda}{\beta Cos\ \theta} \qquad (10)$$

Where λ is X-ray wavelength, β is the full width at half maximum (FWHM) in radians, and θ is the Bragg angle. The grain size for (112) plan for as-grown and annealed CZTS films have been summarized in table 1.Table 1 shows the variation of the grain size for (112) plane with the annealing temperature. With the increase of the annealing temperature from 50^0C to 250^0C, the grain size becomes larger. Figure 3 shows the dependence of full width at half maximum (FWHM) of the 112 peak on the annealing temperature. The FWHM decreased with the increase of the annealing temperature. This indicates that the grain sizes in CZTS thin films increase with increasing the annealing temperature. The effects of grain size are very important for fabrication of solar cells.

B. Surface Morphological Analysis

The surface morphology of CZTS films have been studied by SEM images. Figure 4(A) shows SEM surface image of as-grown CZTS film and indicates smooth, compact and dense in nature and very small agglomerated particles with flat film surface. Figure 4(b, c & d) show the surface images of annealed films at 50^oC, 150^oC and 250^oC respectively. At lower annealing temperature (50^oC) large agglomerated flakes grains have been found and smooth surface started to become rough. As annealing temperature increases, (at 150^oC and 250^oC) the flaky grains size further increased and roughness of the film surface has been enhanced with less grain boundaries.Similar results have been reported by H. Park et.al [22] and S.S. Mali et.al. [23]. These large grain size is useful for solar cell application because decrement in grain boundaries reduce localized recombination sources (a surface or a grain boundary) within a diffusion length of the junction, results high short circuit current [24].

To study the elemental compositions of thin film, an energy dispersive X-ray analysis (EDAX) spectrum has been carried out. Figure 4(B) show the EDAX spectrum of CZTS thin film annealed at 250^0C and it shows the presence of the Copper (Cu), Zinc (Zn) Tin (Sn) and Sulpher(S) in the annealed film. We also observed the element Oxygen (O) and Silicon (Si) in the spectrum, due to the glass substrate (SiO_2). Table 2 shows Elemental compositions of thin film which indicate Copper rich films that may have the probable reason of more amount of Cu chemical Precursor used for the synthesis.

C Optical absorption Study

The electronic transition in the material can be monitored by studying the energy band transition within the material which can be possible by going through the optical absorption spectroscopy. The optical absorption of CZTS films

has been studied in the wavelength range 280 nm to 800 nm. Fig. 5(A), represents the optical absorbance spectra of as-grown CZTS films which shows that CZTS film have high absorbance in visible region (380-750 nm), suggesting its applicability for an absorber layer. Optical absorption has been found to be increased with increasing annealing temperature. Further optical data has been analyzed by using Tauc relation (25) from which the absorption coefficient α, for semiconductor material is given by

$$\alpha = \frac{A(h\upsilon - Eg)^n}{h\upsilon} \qquad (11)$$

Where α is absorption coefficient, A is constant, hv is incident photon energy, E_g is energy band gap i.e. separation between bottom of conduction band and top of the valance band, n is constant which depends on the nature of transition i.e. n=1/2 for allowed direct transition, n=2 for allowed indirect transition. Plot of $(\alpha h\upsilon)^2$ (by taking n=1/2) vs hv is a straight line which show it is a direct band gap material. This type of transition has been reported already by previous researchers for CZTS thin films [5, 19]. Extrapolation of Tauc plot to zero absorption coefficient (α=0) give energy band gap values. Fig. 5(B) shows that band gap energy decrease with increase in annealing temp and results for as-grown and annealed CZTS films have been summarized in table 3.

The red shift in band gap has been found due to increase of grain size and calculated energy band gap values are nearly equal to theoretical values of optimized band gap of solar energy spectrum [26-28].

D Electrical analysis

For detecting the photosensitivity of CZTS absorber layer the Schottky diode was constructed by metal contact on top of CZTS samples. Figure 6(A) shows the current –voltage characteristics curve for as deposited CZTS absorber layer and Figure 6(B) shows the I-V characteristics of annealed film at 50^OC (fig 5a) ,150^OC (fig 5b),250^OC (fig. 5c). It was observed that as deposited film show ohmic behavior while after annealing treatment schottkey like diode behavior is shown by absorber layer. As annealing temperature increases short circuit current (I_{sc}) increase (Table 4) which shows that recombination is decreasing as annealing temperature is increasing.

This gives an important parameter for increasing the efficiency of absorber layer. It is seen that at higher annealing temperature resistance for absorber layer decreases indicating less characteristic resistance (R_{ch}) (Table 4). It is concluded that as annealing temperature increases band gap decreases and short circuit current increases, which is accordance with previously drawn results by H.J. Hovel (44).

IV CONCLUSIONS

We have successfully synthesized Cu_2ZnSnS_4 (CZTS) nanostructured thin film by low cost Chemical Bath Deposition (CBD) method. From structural studies indicated amorphous nature of as-deposited CZTS films which are converted to polycrystalline CZTS films after annealing. Surface morphological study showed that increase in grain size with increasing annealing temperature. Optical properties are studied using optical absorption spectroscopy. The optical absorption study indicates the direct transition with a direct energy band gap 1.4 eV.

V ACKNOWLEDGMENT

Reference

[1]   P. Jackson, D. Hariskos, E. Lotter, S. Paetel, R. Wuerz, R. Menner, W. ischmann, M. Powalla, *Progress in Photovoltaics: Research and Application* vol.19, no.7, pp.894–897 2011.

[2]   First Solar, Press Release, http://investor.firstsolar.com/releasedetail.cfm July 26, 2011.

[3]   J.J. Scragg, P.J. Dale, L.M. Peter, G. Zoppi, I. Forbes *Physica Status Solidi* vol.245, pp.1772–1778, 2008.

[4]   C. Wadia, A.P. Alivisatos, D.M. Kammen *Environmental Science & Technology* vol.43, pp.2072–2077, 2009.

[5]   K. Ito, T. Nakazawa, *Jpn. J. Appl. Phys.* Vol. 27, pp. 2094–2097, 1988.

[6]   W. Shockley and H. J. Queisser , *J. Appl. Phys.* vol. 32, pp. 510,1961.

[7]   K. Todorov, K. B. Reuter, and D. B. Mitzi, *Advanced Materials*, vol. 22, no. 20, pp. E156–E15, 2010

[8]   H. Nukala, J. L. Johnson, A. Bhatia, E. A. Lund, W. M. Hlaing, M. M. Nowell, L. W. Rieth, M. A. Scarpulla , *Mater. Res. Soc. Symp. Proc*, 1268, pp.03-04, 2010

[9]   T. Tanaka , A. Yoshida , D. Saiki , K. Saito , Q. Guo , I. Nishio , T. Yamaguchi , *Thin Solid Films ,* 518, pp. S29–S33, 2010

[10]   K. Sekiguchi, K. Tanaka, K. Moriya, H. Uchiki , *phys. Stat. sol. (c)*, 3, pp.2618-2621,2006 .

[11]   Y.L. Zhou, W.H.Zhou, Y.F. Du, M. Li, S.X. Wu, *Materials Letters*, 65, pp. 1535–1537, 2011.

[12] J. Madarasz , P. Bombicz , M. Okuya , S. Kaneko, *Solid State Ionics* , 142, pp. 439–446, 2001.

[13] Z. Zhoun, Y. Wang, D. Xu, Yafei Zhang, *Solar Energy Materials & Solar Cells,* 94 2042–2045, (2010).

[14] K. Ramasamy, M. A. Malik and Paul O'Brien, *chem. commun* 48, pp. 1170-117, 2011Y. B. K. Kumar, G. S. Babu, P.U. Bhaskar, V. S. Raja, *Phys. Status Solidi* (A) 206 pp.1525–1530, 2009 .

[15] M. Y. Yeh, C. C. Lee, D. S. *Wuu , J Sol-Gel Sci Techno*, 52, pp.65–68, 2009.

[16] C.P.Chan, H. Lam, K.Y. Wong, C. Surya ,*Mater. Res. Soc. Symp. Proc ,* 1123, pp. 05-06, 2009.

[17] S.C.Riha,S.J.Fredrick, J.B.Sambur,Y. Liu, A. L. Prieto, B. A. Parkinson, *ACS Appl. Mater. Interfaces* , 3, pp. 58–66, 2011.

[18] N.M. Shinde, D.P. Dubal, D.S. Dhawale, C.D. Lokhande, J.H. Kim, J.H. Moon, *Materials Research Bulletin* 47, pp.302-307, 2012.

[19] N. Muhunthan, Om Pal Singh, Son Singh, and V. N. Singh*, International Journal of Photoenergy*, Article ID 752012, 7 pages, 2013.

[20] Xiaotang Lu, Zhongbin Zhuang, Qing Peng and Yadonh Li Chem, *Chem. Commun.*, Vol.47, pp. 3141-3143,2011.

[21] Hyungjin Park , Young Hwan Hwang*, J Sol-Gel Sci Technol* DOI 10.1007/s10971-012-2703-0.

[22] Mali, Sawanta S.Shinde, Pravin S.   Betty,   Chirayath   A.   Bhosale, Popatrao N.   Oh, Young Woo, Patil, Pramod S., *Journal of Physics and Chemistry of Solids*, Volume 73, Issue 6, pp. 735-740.

[23] Lakshman Singh, Manish Saxena & P K Bhatnagar, *Indian J. Pure and Appl Phys,* 42:841, 2004.

[24] Tauc J, *Amorphous and liquid semiconductor* (New York: Plenum), pp. 159, 1974.

[25] T. Zdanowicz, T. Rodziewicz, and M. Zabkowska-Waclawek, *Sol. Energy Mater. Sol. Cells* **87**, pp.757–769, 2005.

[26] H. Katagiri, N. Ihigaki, T. Ishida, K. Saito, *Jpn. J. Appl. Phys.* 40 1 pp. 500, 2001.

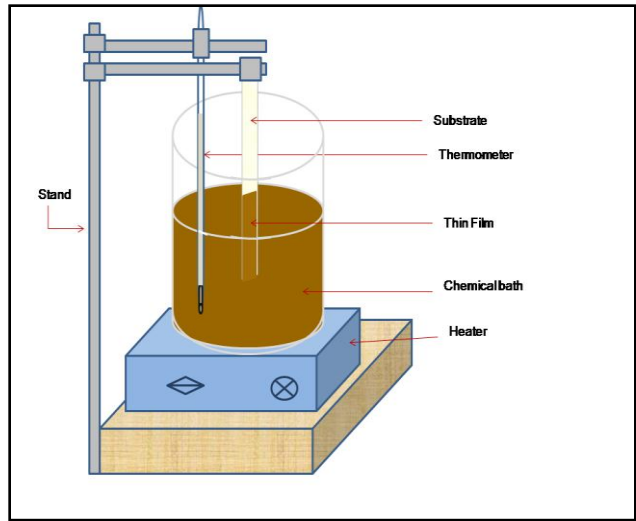[28] J. Seol, S. Lee, J. Lee, H. Nam, K. Kim, *Sol. Energy Mater. Sol. Cells* 75 pp.155, 2003.

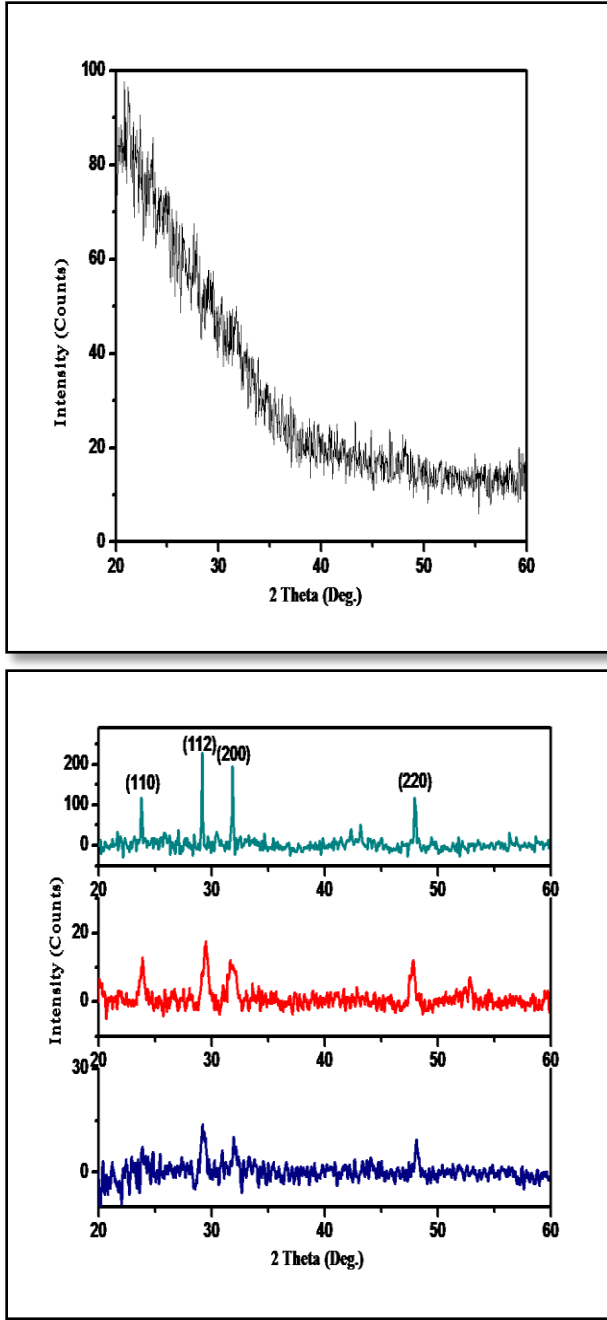**Figure 1** Schematic diagram of Chemical Bath Deposition (CBD) method.

Figure 2(A). XRD patterns of as deposited CZTS thin film **2(B)** XRD patterns of (a) annealed CZTS thin film at

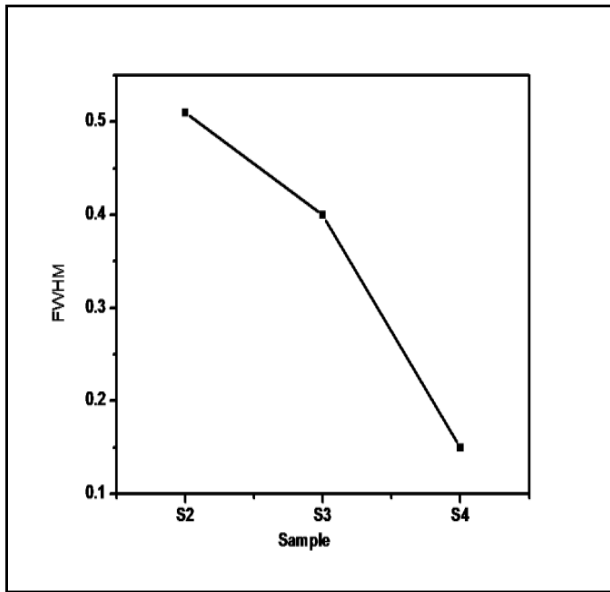50^0C, (b) at 150^0C and (c) at 250° C in air for 2 hr

Figure 3. The FWHM values of sample S2 (annealed CZTS thin film at 50^0C), S3(annealed at 150^0C) S4 (annealed at 250° C).
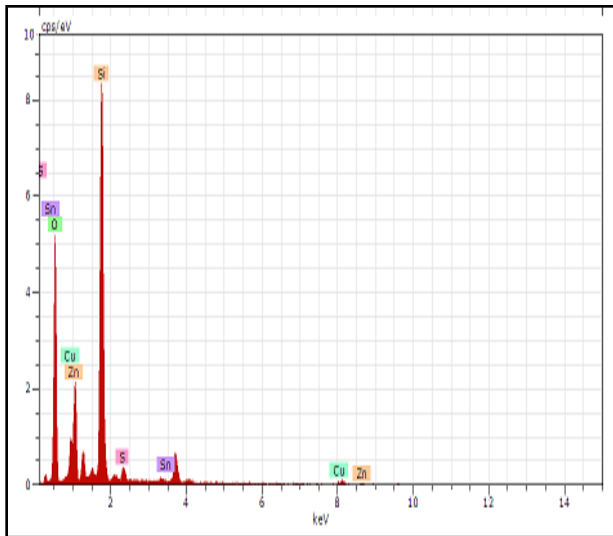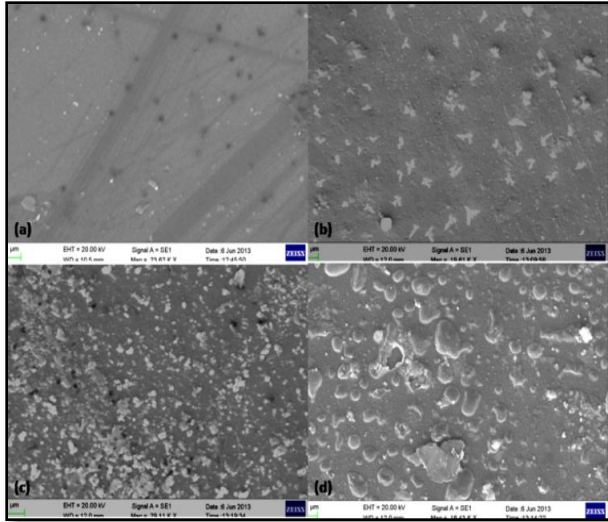
Figure 4(A) SEM images of (a) as deposited and (b) annealed CZTS thin film at 50° C (c) at 150°C (d) at 250°C in air for 2 h.   **4(B)** EDAX spectra of annealed CZTS thin film at 250° C.
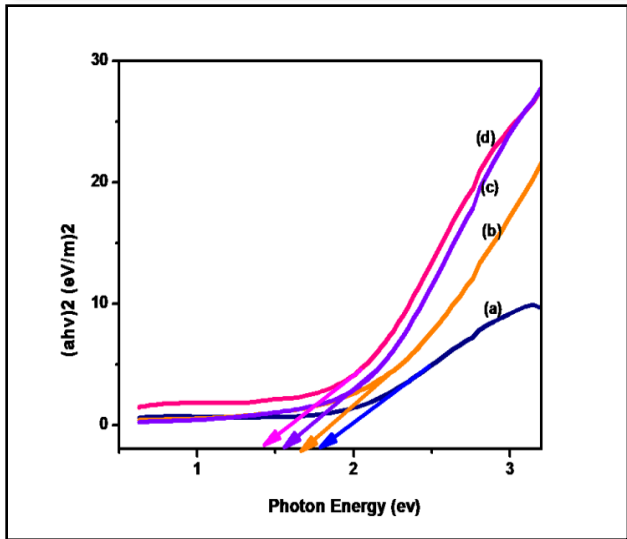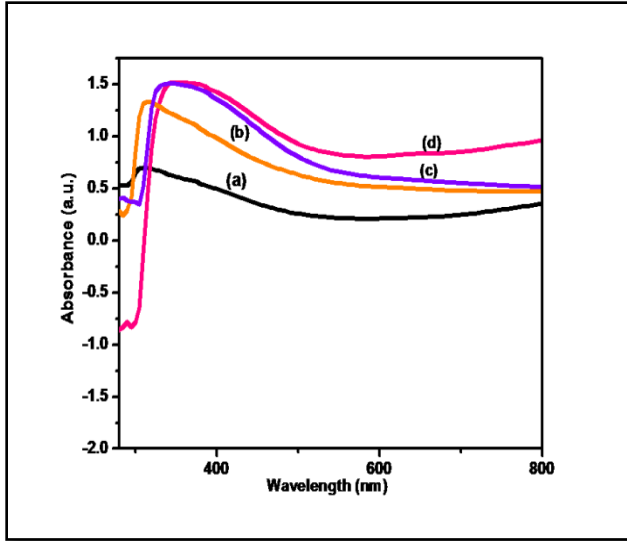
Figure 5(A) Variation of absorption (a.u.) with wavelength (nm) of (a) as deposited and (b) annealed CZTS thin film at 100° C (c) annealed CZTS thin film at $200^{o}C$ (d) annealed CZTS thin film at $300^{o}C$ in air for 2 h.

Figure 5(B) The plots of $(\alpha h\upsilon)^{2}$ vs hυ of (a) as deposited (b) annealed CZTS thin film at 100° C (c) annealed CZTS thin film at $200^{o}C$ (d) annealed CZTS thin film at $300^{o}C$ in air for 2 h.
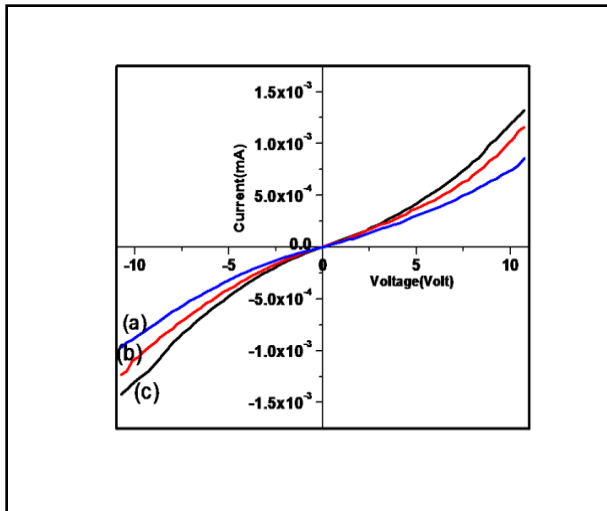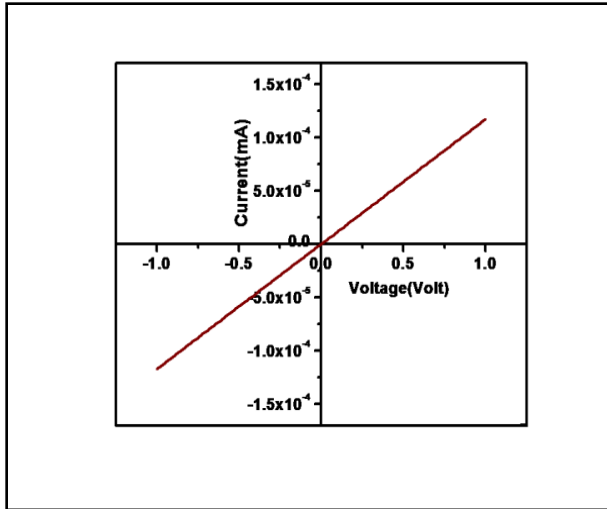
Figure 6(A) I–V characteristics of as-deposited CZTS films **6(B)** I–V characteristics of annealed CZTS films at 50$^\text{o}$

C (A), at   150$^\text{o}$C (d), at 250$^\text{o}$C in air for 2 h.

Sample	S1	S2	S3	S4
Annealing Temperature	As deposited	50^0C	150^0C	250^0C
FWHM	-	0.51	0.40	0.15
Grain Size (nm)	-	16.79	21.41	57.1

Table 1: The FWHM values and grain sizes of (112) orientation of the CZTS thin films obtained at different annealing temperatures.

El	AN	Series	unn. [wt.%]	C norm. [wt.%]	C Atom. [at.%]
O	8	K-series	36.28	52.23	69.28
Si	14	K-series	24.80	35.71	26.98
Cu	29	K-series	3.53	5.08	1.69
Sn	50	L-series	3.23	4.65	0.83
S	16	K-series	0.95	1.36	0.90
Zn	30	K-series	0.67	0.97	0.31
		Total:	69.45	100.00	100.00

Table 2: EDAX spectrum of CZTS thin film annealed at 250^{0}C

Sr. No.	Sample	Band Gap (ev)
1.	As deposited CZTS	1.8
2.	Annealed CZTS at 50°C	1.7
3.	Annealed CZTS at 150°C	1.6
4.	Annealed CZTS at 250°C	1.4

Table 3: Energy Band Gap values for as-grown and annealed CZTS thin film.

Sr. No.	Sample	Resistance (R_{ch})	Resistivity (R_s)	Conductivity
1.	Annealed CZTS at 50°C	9.0×10^3	0.36×10^5	2.77×10^{-5}
2.	Annealed CZTS at 150°C	8.13×10^3	0.32×10^5	3.12×10^{-5}
3.	Annealed CZTS at 250°C	6.99×10^3	0.27×10^5	3.70×10^{-5}

Table 4: Electrical parameters values for as-grown and annealed CZTS thin film.

Chemical precursor impact on the properties of Cu$_2$ZnSnS$_4$ absorber layer

Indu B. Vashistha' , Mahesh C. Sharma, and S. K. Sharma

Chemical Precursor Impact on the Properties of Cu_2ZnSnS_4 Absorber Layer

Indu B. Vashistha[*1,], Mahesh C. Sharma[2], and S.K. Sharma[1]

[1]*Department of Physics, Malaviya National Institute of Technology, Jaipur 302017, India*
[2]*National Institute of Solar Energy, Gurgaon 122003, India*

*indu_139@yahoo.com

Abstract. In present work impact of different chemical precursor on the deposition of solar absorber layer Cu_2ZnSnS_4 (CZTS) were studied by Chemical Bath Deposition (CBD) method without using expensive vacuum facilities and followed by annealing. As compared to the other deposition methods, CBD method is interesting one because it is simple, reproducible, non-hazardous, cost effective and well suited for producing large-area thin films at low temperatures, although effect of precursors and concentration plays a vital role in the deposition. So, the central theme of this work is optimizing and controlling of chemical reactions for different chemical precursors. Further Effect of different chemical precursors i.e. sulphate and chloride is analyzed by structural, morphological, optical and electrical properties. The X-ray diffraction (XRD) of annealed CZTS thin film revealed that films were polycrystalline in nature with kestarite tetragonal crystal structure. The Atomic Force micrographs (AFM) images indicated total coverage compact film and as well as growth of crystals. The band gap of annealed CZTS films was found in the range of optimal band gap by absorption spectroscopy.

1. INTRODUCTION

Recent energy demand and CO_2 emission control strategies generate requirement of efforts in the field of nonrenewable energy resources. Solar energy through photovoltaics is good solution among all nonrenewable energy resources. In aspect of commercialization of thin film solar cell chalcopyrite solar cells have reached up to commercial level, but these solar cells has some limiting factors. Therefore working and exploring in the field of new materials is concern of researchers working in PV field. Copper-Zinc-Tin-Sulphidoghe (CZTS) is a good alternative of chalcopyrite solar cells due to its different properties like p-type conductivity and suitable optical properties such as direct band gap of ~1.5 Ev and absorption coefficient of -10^4 cm^{-1}[1-2]. It is worthwhile to mention here that it was Ito and Nakazawa who gave the recognition of the photovoltaic effect of CZTS material in 1988 [3] and significant progress in this relatively new research area has been achieved in the last five years [4-8].

However, several successful attempts have been reported by various mentioned vacuum based methods, but there are some issues related to these techniques. Vacuum based technique requires sophisticated, expensive equipments, which results in high production cost as well as limited area deposition is also an shortcoming of vacuum based techniques. Another disadvantage is high temperature deposition condition which reduces the simplicity of deposition process. So, researchers in this field are trying to develop a simple method which can be used commercially. Chemical Bath Deposition method is simple and economical method. In our earlier work we reported the optimization of parameter for chemical bath deposition (CBD) method [9] although effect of precursors and concentration plays a vital role in the deposition. So, the central theme of this work is optimizing and controlling of CBD method for different chemical precursors as well its impact on different properties.

2. EXPERIMENTAL

2.1 Deposition of Thin Film: Cu_2ZnSnS_4 (CZTS) thin films grown by Chemical Bath Deposition (CBD) method.

Thin film was deposited on glass substrate which was cleaned earlier by detergent, acetone and DI Water ultrasonically. Two types of chemical precursors were used for deposition i.e. Chloride based precursors and Sulphate based precursors for the source of Copper, Zinc, Tin and Sulpher and EDTA was used as complexing agent. Details of these precursors and their concentrations are mentioned in table 1.

Table 1. Chemical concentration of different Chemical precursors for CZTS thin film deposition.

Copper Precursor	Zinc Precursor	Tin Precursor	Sulpher Precursor	Complexing Agent
(i) Chloride Based Precursors				
Copper Chloride dehydrate $(CuCl_2.H_2O)$ 0.1 M	Zinc Chloride $(ZnCl_2)$ 0.05 M	Tin Chloride pentahydrate $(SnCl_4.5 H_2O)$ 0.05 M	Thiourea (NH_2CSNH_2) 0.5 M	Ethylenediaminetet raacetic acid (EDTA) 0.075 M
(ii) Sulphate Based Precursors				
Copper Sulfate pentahydrate $(CuSO_4.5H_2O)$ 0.1 M	Zinc Sulfate heptahydrate $(ZnSO_4.7H_2O)$ 0.05 M	Stannous Sulfate $(SnSO_4)$ 0.05 M	Thiourea (NH_2CSNH_2) 0.5 M	Ethylenediaminetet raacetic acid (EDTA) 0.075 M

Initially separate solution was prepared and after mixing by magnetic stirrer pH was controlled by adding ammonia and final pH of solution is ~10. After controlling the pH, previously cleaned substrates were immerse in the bath and then bath heated up to 60°C. During reaction white solution become yellow after 5-7 min. and presence of precursor metal sulfides give reaction a brown blackish color. After 1 hr precipitation started to form in the bath and deposition of CZTS film started on the substrates after 7 hr substrate with CZTS film re-moved, rinsed in DI water, dried in air and preserved in desiccators. Further, as grown CZTS thin films were annealed in air at 150°C for 2 hr in tubular furnace.

2.2 Characterization: The structural properties of as deposited and annealed CZTS thin film were studied by X-ray diffraction (XRD) pattern by using PANalytical X'Pert Pro X-ray Diffraction Unit with copper (Cu), which have strong Kα radiation having X-ray emissions wavelength of 1.5418 Å in range of 20-60°. The surface morphological study was carried out using Atomic Force Microscope (AFM).U-V characteristic studied using LAMBDA 950 UV/Vis/NIR Spectrophotometer.

3. RESULTS AND DISCUSSION

3.1 Structural Analysis

X-ray diffraction (XRD) technique was used for study of structural properties of as-deposited, annealed thin films on glass substrate. Fig. 1 shows the XRD pattern of as grown and annealed Chloride based and Sulfate based CZTS film. XRD pattern of as deposited Chloride based CZTS thin film Fig. 1(a) exhibit sharp peaks at different angles and by comparing calculated 'd' values with experimental 'd' values corresponding phases can be determined as (112), (200) and (220) and XRD pattern Fig. 1(b) of annealed CZTS thin films at 150°C in air for 2 hr. indicates phases (110), (112), (200), (220) and (103). XRD patterns of Sulfate based as deposited thin film Fig. 1(c) depicts phases (211) and (105) and annealed CZTS thin films Fig. 1(d) at 150°C in air for 2 hr. shows phases (110), (200), (211), (105) and (103). This conform the synthesis of kestarite tetragonal crystal structure CZTS film. Thus structural analysis confirmed the formation of kesterite structured CZTS phase with tetragonal structure at 150^{0}C with better crystalline nature for chloride based precursors. The similar results were reported by N.M. Shinde et.al and N. Muhunthan et. al [10-11].
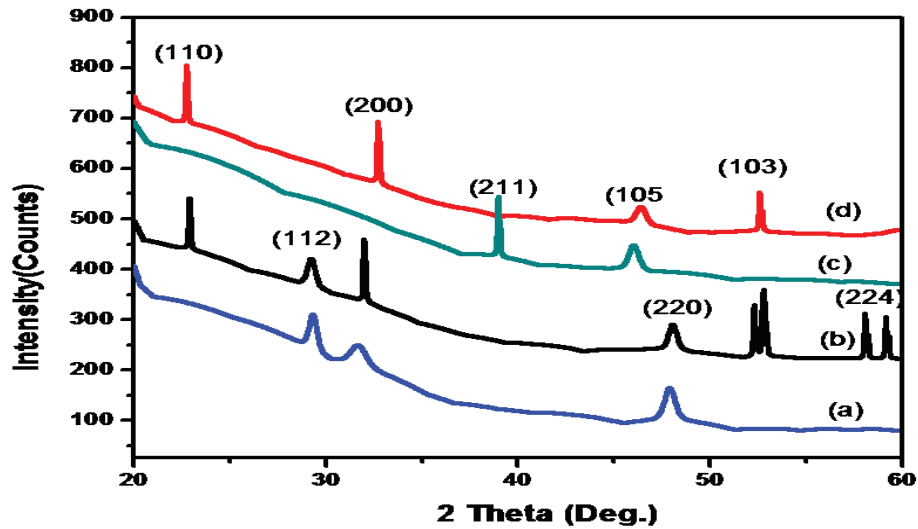
Fig. 1. XRD patterns of Chloride based (a) as deposited, (b) annealed CZTS thin films at 150°C in air for 2 hr, Sulfate based (C) as deposited and (d) annealed CZTS thin films at 150°C in air for 2 hr.

3.2 Morphological Analysis

Surface morphological analysis of as grown and modified CZTS thin films of different precursors was done by Atomic Force Microscope (AFM). Fig 2 shows 2D and 3D AFM micrographs of as-deposited and annealed CZTS thin film. Fig. 2(a) depicts that surface morphology of the chloride based as-deposited film has homogenous background with densely packed smaller grains. Fig. 2(b) indicates that after annealing morphology is found to improve and distinct grains were observed. These large grains are useful for solar cell application because it reduce localized recombination sources [12]. AFM micrographs of the sulfate based as deposited film is smooth, flat and compact in nature with some agglomerated particles existed on the surface, may be because of nucleation process [Fig. 2(c)] and Fig. 2(d) shows that sulfate based film after annealing at 150°C consist of small and uneven grain as modification takes place by annealing.
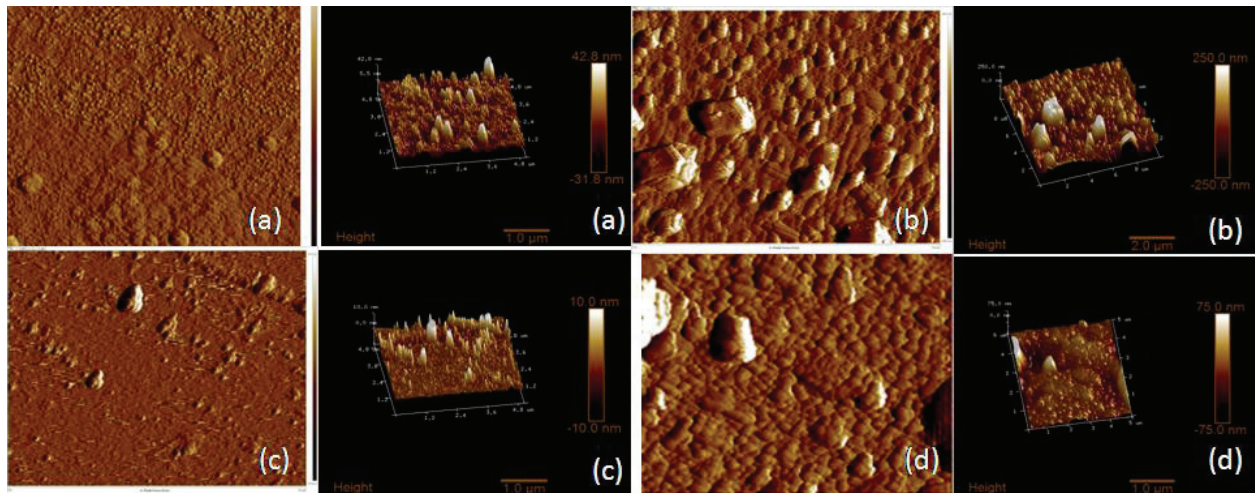

Fig. 2(a to b) shows AFM image of Chloride based and Sulfate based as-deposited films. **Fig. 2(c to d)** shows AFM image of Chloride based and Sulfate based annealed films

Average surface roughness of chloride based as-deposited, annealed films and sulfate based as-deposited and annealed films are 12.7nm, 88.4nm, 33.7nm, and 92.1nm respectively. RMS roughness of chloride based as-deposited, annealed films and sulfate based as-deposited and annealed films are are 8.74nm, 45.6nm, 17.5nm and 58.5nm respectively.

3.3 Optical Study

In order to study absorption spectra and energy band gap of as-deposited and annealed CZTS thin film, the optical absorption were studied in the wavelength range 280-800 nm. In Fig. 3(i) variation of absorbance (a. u.) with respect to wavelength (λ) shows that films have high absorbance in visible region.
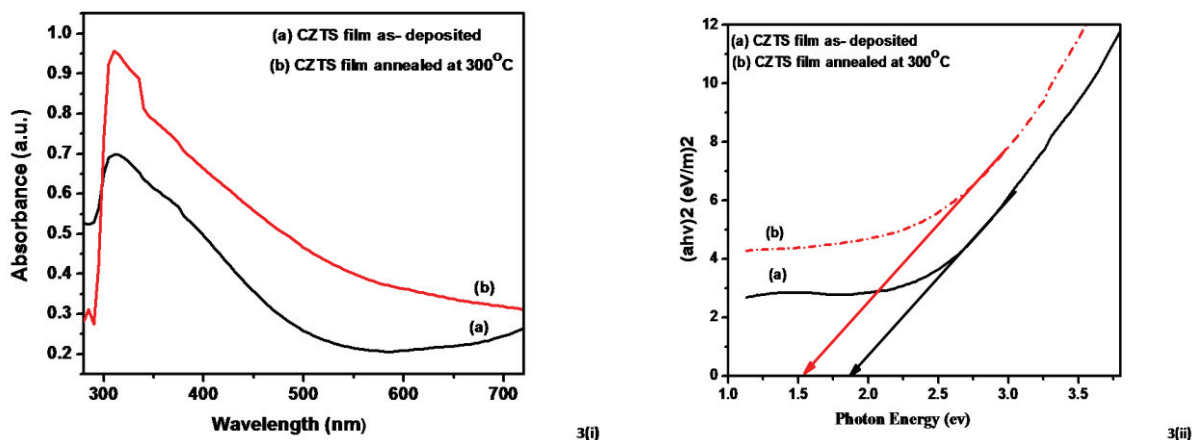

Fig. 3(i) Variation of absorption (a.u.) with wavelength (nm) of Chloride based (a) as deposited and (b) annealed film at 150$^{\mathrm{o}}$ C in air for 2 hr. **Fig. 3(ii)** The plots of $(\alpha h\upsilon)^2$ vs hυ of Chloride based (a) as deposited and (b) annealed film at 150$^{\mathrm{o}}$ C in air for 2 hr.

Further optical data were analyzed by using Tauc relation [13] from which the absorption coefficient α, for semiconductor material is given by

$$\alpha = \frac{A(h\upsilon - E_g)^n}{h\upsilon}$$

(1)

Where α is absorption coefficient, A is constant, hυ is incident photon energy, E_g is energy band gap, n is constant which depends on the nature of transition i.e. n=1/2 for allowed direct transition, n=2 for allowed indirect transition. Plot of $(\alpha h\upsilon)^2$ (by taking n=1/2) vs hυ is a straight line which show it is a direct band gap material. Energy band gap values determined by extrapolation of Tauc plot to zero absorption coefficient (α=0). Fig. 3(ii) shows that band gap energy decrease from 2.0eV to 1.54eV with increase in annealing temp.

4. CONCLUSION

CZTS thin film absorber layer by low cost CBD technique was synthesized by optimizing parameters. Conclusively, deposition temperature of 60^{0}C and deposition time of 7 hr reported for synthesis of CZTS thin film. Hence we were conformed the formation of kesterite structured CZTS phase with tetragonal structure at 150^{0}C with better crystalline nature for chloride based precursors. Surface morphology of CZTS film shows increase in grain size with annealing and larger grains for chloride based precursors. The band gap of annealed CZTS films was calculated 1.54eV which is in the range of optimal band gap by absorption spectroscopy.

ACKNOWLEDGMENTS

REFERENCES

1. J.J. Scragg, P.J. Dale, L.M. Peter, G. Zoppi, I. Forbes Physica Status Solidi **245**, 1772–1778 (2008).
2. C. Wadia, A.P. Alivisatos, D.M. Kammen Environmental Science & Technology **43**, 2072–2077 (2009).
3. K. Ito, T. Nakazawa, Jpn. J. Appl. Phys. **27**, 2094–2097 (1988).
4. M. Y. Yeh, C. C. Lee, D. S. Wuu, J Sol-Gel Sci Techno **52**, 65–68, (2009).
5. C.P.Chan, H. Lam, K.Y. Wong, C. Surya, Mater. Res. Soc. Symp. Proc **1123**, 05-06 (2009).
6. S.C.Riha,S.J.Fredrick, J.B.Sambur,Y. Liu, A. L. Prieto, B. A. Parkinson, ACS Appl. Mater. Interfaces **3**, 58–66 (2011).
7. Mali, Sawanta S. Shinde, Pravin S. Betty, Chirayath A. Bhosale, Young Woo, Patil, Pramod S., Journal of Physics and Chemistry of Solids **73**, 735-740 (2012).
8. M.I. Hossain et al. Chalcogenide Letters **9**, 231–242 (2012).
9. Indu B. Vashistha, Mahesh C. Sharma, and S.K. Sharma Adv. Electrochem. **2**, 29-33 (2014).
10. N.M. Shinde, D.P. Dubal, J.H. Kim, J.H. Moon, Materials Research Bulletin **47**, 302–307 (2012).
11. N. Muhunthan, Om Pal Singh, Son Singh, and V. N. Singh, International Journal of Photoenergy, Article ID 752012, 7 pages (2013).
12. Lakshman Singh, Manish Saxena & P K Bhatnagar, Indian J. Pure and Appl Phys, **42**:841-844, (2004).
13. Tauc J, Amorphous and liquid semiconductor (New York: Plenum) **159**, (1974).

Effect of dopent on the structural and optical properties of ZnS thin film as a buffer layer in solar cell application

Indu B. Vashistha, Mahesh C. Sharma, Ramphal Sharma, and S. K. Sharma

---

Articles you may be interested in

Modification of opto-electronic properties of ZnO by incorporating metallic tin for buffer layer in thin film solar cells
AIP Conf. Proc. **1665**, 120019 (2015); 10.1063/1.4918126

Studies on antimony telluride thin films as buffer layer for solar cell applications
J. Renewable Sustainable Energy **5**, 031612 (2013); 10.1063/1.4808258

Structural and Optical Properties of RF—Sputtered ZnS Thin Films
AIP Conf. Proc. **1391**, 83 (2011); 10.1063/1.3646786

Pulsed Laser Deposition ZnS Buffer Layers for CIGS Solar Cells
Chin. J. Chem. Phys. **22**, 97 (2009); 10.1088/1674-0068/22/01/97-101

Effect of impurities in the CdS buffer layer on the performance of the Cu(In,Ga)Se 2 thin film solar cell
J. Appl. Phys. **85**, 6858 (1999); 10.1063/1.370204

Effect of dopent on the structural and optical properties of ZnS Thin Film as a buffer layer in solar cell application

Indu B. Vashistha[*1], Mahesh C. Sharma[2], Ramphal Sharma[3] and S.K. Sharma[1]

[1]*Department of Physics, Malaviya National Institute of Technology, Jaipur 302017, India*
[2]*National Institute of Solar Energy, Gurgaon, India*
[3]*Thin Film and Nanotechnology Lab, Department of Physics Dr. Babasaheb Ambedkar Marathwada University, Aurangabad 43100, India*

[*]*Email: indu_139@yahoo.com*

Abstract: In order to find the suitable alternative of toxic CdS buffer layer, deposition of pure ZnS and doped with Al by chemical bath deposition method have been reported. Further as grown pure and doped thin films have been annealed at 150^0C. The structural and surface morphological properties have been characterized by X-Ray diffraction (XRD) and Atomic Force Microscope (AFM).The XRD analysis shows that annealed thin film has been polycrystalline in nature with sphalerite cubic crystal structure and AFM images indicate increment in grain size as well as growth of crystals after annealing. Optical measurement data give band gap of 3.5 eV which is ideal band gap for buffer layer for solar cell suggesting that the obtained ZnS buffer layer is suitable in a low-cost solar cell.

1. INTRODUCTION

Buffer layer play a vital role in thin film heterojunction solar cell by formation of junction with the absorber layer for transporting photo generated charge carriers to the load as well as admitting maximum amount of solar light to the absorber layer. For solving this purpose material with high band gap and low resistivity is required. CdS is most commonly used material for buffer layer deposited by Chemical Bath Deposition (CBD) technique [1-2]. Although in most laboratories standard device structure use buffer layer of CdS in solar cell, but meanwhile in last decade risk assessment arise from toxicity of CdS leads researchers to other nontoxic n-type materials with low cost deposition technique. In this context films based on ZnS, ZnSe, ZnO were deposited as an alternative to the CdS buffer layer, among them ZnS is one of the most popular candidates. ZnS based thin films have advantage of less toxicity and high energy band gap (3.54 eV) which fulfill the requirement of maximum solar energy availability for absorber layer. However, doping of high conductivity elements such as Al, Cu, and Ni gives the possibility of decrement in electrical resistivity without affecting the optical properties of the layers [3-4].

There are several methods have been used to deposit this n-type material based on PVD and CVD, among them Chemical Bath Deposition (CBD) method is interesting one because it is simple, reproducible, non-hazardous, cost effective and well suited for producing large-area thin films at low temperatures[5-7]. So, the central theme of this work is optimizing and controlling of synthesis parameters for pure and doped ZnS thin films and comparative study of the effect of doping on the properties of the deposited films. Further post treatment thermal annealing has used as it can control the morphology and structural properties of polycrystalline thin film. Considering this aspect we studied the annealing effect on the ZnS thin films. Different characterization has done by different characterization tools for as deposited and annealed ZnS thin film.

2. EXPERIMENTAL

2.1 Deposition of ZnS Thin Film: All the chemicals used for preparation of chemical bath were analytical reagent grade (AR) provided by Sigma Aldrich with 99.9% purity. Zinc Sulfate heptahydrate ($ZnSO_4.7H_2O$) and Thiourea (NH_2CSNH_2) were used as precursor chemicals for Zn^{2+} and S^{2-} ions for pure ZnS thin film and Aluminum Sulfate 16-hydrate ($Al_2(SO_4)_3.16H_2O$) was used for doping ion Al^{+2}, Hydrazine Hydrate and TEA was used as complexing agent for controlling the reaction mechanism. Thin films were deposited on Soda Lime Glass (SLG). Before the deposition, substrates were cleaned by detergent and distilled water then ultrasonically cleaned by Acetone, Methanol and De-ionized (DI) water and dried in air.

Chemical concentrations were taken as 0.1 M $ZnSO_4$, 0.1 NH_2CSNH_2 in equal volume ratio and Hydrazine Hydrate and TEA were taken as complexing agent. Initially solution was prepared by dissolving chemicals in distilled water by magnetic stirring separately. After preparing all the solutions they were mixed and final pH (~12) was controlled by adding Sodium Hydroxide solution. Cleaned SLG substrate was immersed in the solution and solution was heated up to 80°C. Schematic diagram for the deposition is shown in Fig. 1. After 10 min. precipitation started to form in the bath and deposition of ZnS film started on the substrates. After 2 hr ZnS film was deposited on substrate.

For deposition of doped ZnS thin film 0.1 M $ZnSO_4$, 0.01 M $Al_2(SO_4)_3$ and 0.1 NH_2CSNH_2 was taken in equal volume ratio. Same procedure was followed for deposition of doped film. After 2 hr doped ZnS film was deposited on substrate. Deposited films were removed, rinsed in DI water to remove the ions from film, dried in air and preserved in desiccator.
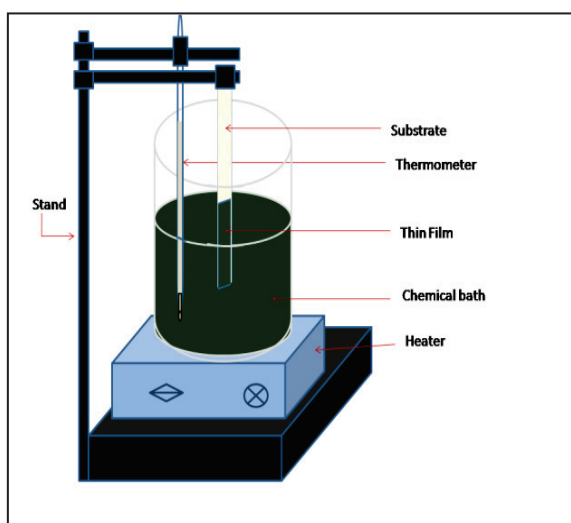

FIGURE 1.Schematic diagram of chemical bath deposition method for deposition of ZnS thin films.

The surface of the thin film can be modified by providing the post deposition treatments like thermal annealing. So, as deposited and doped ZnS thin films were annealed in air at 150^{0}C for 2 hr in tubular furnace.

2.2 Characterization: The structural properties of as deposited and annealed CZTS thin film were studied by X-ray diffraction (XRD) pattern by using PANalytical X'Pert Pro X-ray Diffraction Unit with copper (Cu), which have strong Kα radiation having X-ray emissions wavelength of 1.5418 Å in range of 20-60o. Average crystal sizes were determined according to broadening of peaks using Scherrer relationship. The surface morphological study was carried out using Atomic Force Microscope (AFM).U-V characteristic studied using LAMBDA 950 UV/Vis/NIR Spectrophotometer.

3. RESULTS AND DISCUSSION

3.1 Structural Analysis

X-ray diffraction (XRD) technique was used for performing structural analysis of as-deposited, annealed thin films on glass substrate. Fig. 2 shows the XRD pattern of as deposited and annealed pure and doped ZnS film. Fig. 2(A) shows no diffraction peaks indicating amorphous nature of as deposited film. Fig. 2[B(a)] shows XRD pattern of annealed pure ZnS film at 150^0C for 2 hr. and exhibit sharp peaks at different angles 28.55, 33.20 and by comparing calculated 'd' values with experimental 'd' values of standard sphalerite structured ZnS crystal(JCPDS card 05-0566), corresponding phases can be determined Which are (111),(200). Fig. 2[B(b)] shows XRD pattern of annealed doped ZnS film at 150^0C for 2 hr. which gives sharp peaks at angles 28.55, 33.20, 47.48 and 56.50 and by comparing standard sphalerite structured corresponding phases can be determined Which are (111),(200),(220) and (311). This analysis conform the synthesis of sphalerite cubic structured ZnS thin film. This result is in agreement with previously reported results [8-9]. Intensity of peak corresponding (111) phase is observed to be much greater than other peaks, reveling preferred orientation along this phase for annealed film.
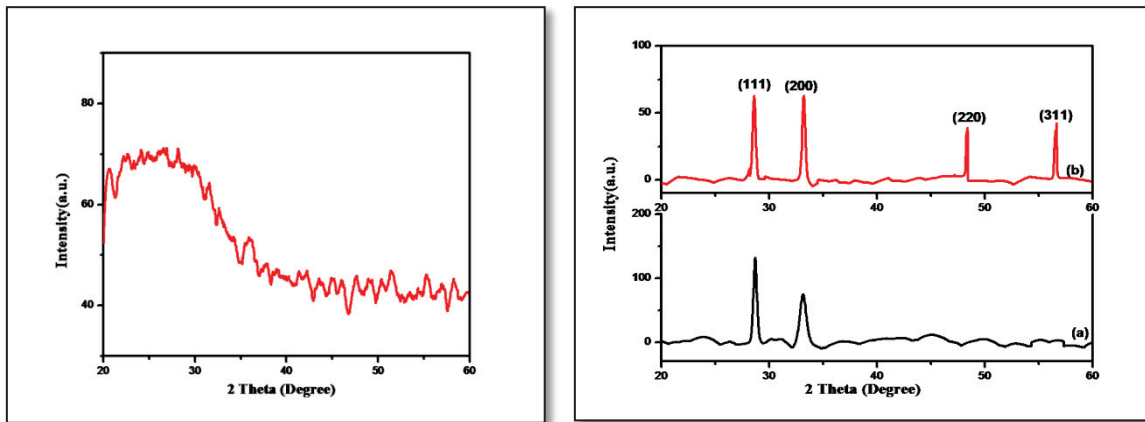

FIGURE 2(A). XRD patterns of as deposited ZnS thin film **2(B)** XRD patterns of (a) annealed pure ZnS and (b) annealed doped ZnS thin film at 150° C in air for 2 hr.

Particle size in the doped film was calculated from the Scherrer's formula

$$D = \frac{0.9\lambda}{\beta Cos\,\theta} \qquad (1)$$

Where λ is X-ray wavelength, β is the full width at half maximum (FWHM) in radians, and θ is the Bragg angle. FWHM of diffraction peaks and grain size and other parameters for doped film are shown in Table (1).

Table1. Parameters of XRD spectra for ZnS thin films

2 Theta (degree)	d(Å)	Intensity	hkl	FWHM	Grain Size (nm)
28.55	3.36	100	111	0.322	26.53
33.60	2.69	10	200	0.324	26.73
47.48	1.91	51	220	0.227	39.95
56.50	1.62	30	311	0.197	47.83

3.2 Surface morphological analysis

Surface morphological analysis was done by Atomic Force Microscope (AFM). Fig. 3 shows 2D AFM image of as-deposited and annealed pure and doped ZnS thin film taken over $3\mu m^2$ area. Fig. 3(a) shows AFM image of as-deposited film indicate the homogenous background with smaller densely packed grains. It was observed that some particles exist on the surface of film which may be because during deposition process nucleation sites was developed. After annealing in pure ZnS film grain growth started and spherical grains have been found [Fig. 3(b)].
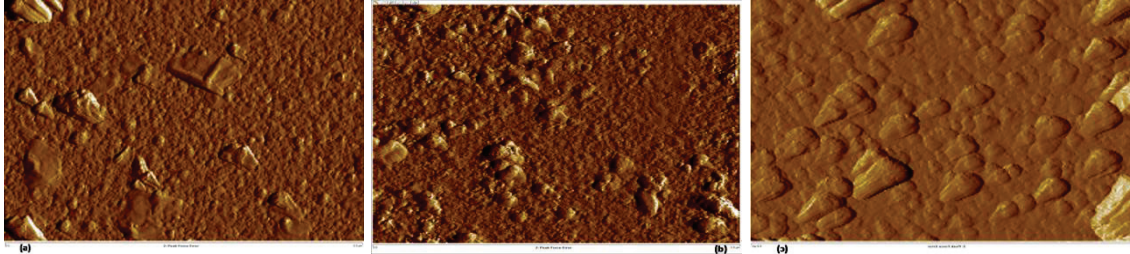

FIGURE 3. The 2D AFM images of (a) as deposited and (b) annealed pure ZnS (c) annealed doped ZnS thin film at 150° C in air for 2 hr.

Fig. 3(c) shows surface image of doped annealed film and indicates surface modification occur after post temperature treatment which increase crystallinity and grain size of thin film. These large grains are useful for solar cell application because it reduce localized recombination sources [10]. Average surface roughness of as deposited and annealed pure and doped ZnS films are 12.7, 33.7 and 92.1nm respectively and root mean square roughness are 8.74, 17.5 and 58.5 respectively.

3.3 Optical absorption Study

In order to study absorption spectra and energy band gap of ZnS thin film the optical absorption has been studied in the wavelength range 800 nm to 300 nm. In Fig. 4(A) variation of absorbance (a. u.) with respect to wavelength (λ) shows that ZnS films have high absorbance in ultraviolet region. Further optical data were analyzed by using Tauc relation [11] from which the absorption coefficient α, for semiconductor material is given by

$$\alpha = \frac{A(h\upsilon - Eg)^n}{h\upsilon} \qquad (2)$$

Where α is absorption coefficient, A is constant, $h\upsilon$ is incident photon energy, Eg is energy band gap, n is constant which depends on the nature of transition i.e. n=1/2 for allowed direct transition, n=2 for allowed indirect transition. Plot of $(\alpha h\upsilon)2$ (by taking n=1/2) vs $h\upsilon$ is a straight line which show it is a direct band gap material.
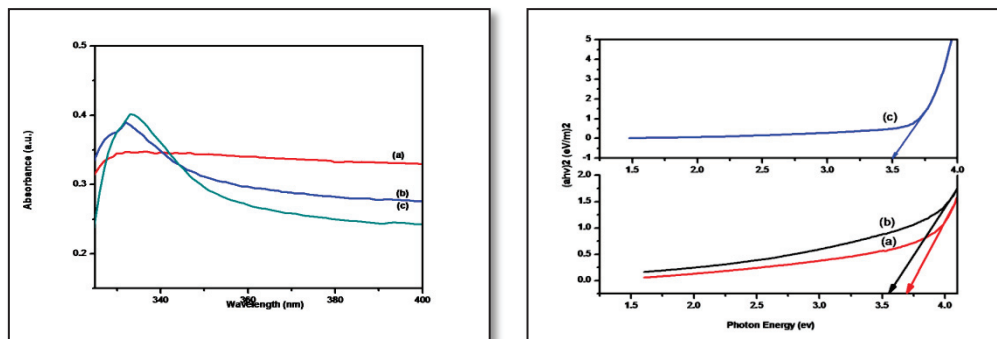

FIGURE 4(A). Variation of absorption (a.u.) with wavelength (nm) of (a) as deposited and (b) annealed pure ZnS (c) annealed doped ZnS thin film at 150° C in air for 2 hr. **4(B)** The plots of $(\alpha h\upsilon)^2$ vs $h\upsilon$ of (a) as deposited and (b) annealed pure ZnS (c) annealed doped ZnS thin film at 150° C in air for 2 hr.

Extrapolation of Tauc plot to zero absorption coefficient ($\alpha=0$) give energy band gap values. Fig. 4(B) shows that band gap energy decrease from 3.69 eV (fig 4B, a) to 3.56 eV (fig 4B, b) with increase in annealing temp for pure ZnS thin film. Energy band gap for doped annealed ZnS thin film is 3.5 eV (fig 4B, c).So calculated band gap energy values are in good agreement with reported data [12-13]

4. CONCLUSION

ZnS thin film buffer layer by low cost Chemical Bath Deposition (CBD) technique was synthesized by optimizing parameters. Conclusively, deposition temperature of 80^0C and deposition time of 2 hr reported for synthesis of ZnS thin film. For improving the properties of as deposited film annealing was performed. As deposited and annealed thin films were characterized by different characterization tools. Surface morphology of CZTS film shows increase in grain size with annealing temperature increases and a direct optical band gap energy of 3.5 eV.

5. ACKNOWLEDGEMENTS

REFERENCES

1. M. Powalla, B. Dimmler, R. Schaeffler, G. Voorwinden, U. Stein, H.-D. Mohring, F. Kessler, D. Hariskos, Proc. 19th European Photovoltaic Solar Energy Conference Paris, France, (2004).
2. K.M. Hynes, J. Newham, Proc. 16th European Photovoltaic Solar Energy Conference, (2000) p. 2297.
3. J. H. Lee, W. C Song, K. J. Yang, Y. S. Yoo, Thin Solid Films, 416 (2002) 416.
4. L. Qi, X Gu, M. Grujicic, W.G. Samuels, G.J. Exarhos, Appl. Phys. Lett., 83 (2003) 1136.
5. B. Krishnan, A. Arato, E. Cardenas, T.K. Das Roy, G.A. Castillo, Appl. Surf. Sci., 254 (2008) 3200.
6. P. Prathap, N. Revathi, Y.P. Subbaiah, K.T.Ramakrishna Reddy, R.W. Miles, Solid State Sci., 11 (2009) 224.
7. Q. Liu, M. Guobing, A. Jianping, Appl. Surf. Sci., 254 (2008) 5711.
8. J.M. Dona, J. Herrero, J. Electrochem. Soc. 141 (1994) 205.
9. J. Vidal, O. Vigil, O. De Melo, N. Lopez, O. Zelaya-Angel, Mater. Chem. Phys. 61 (1999) 139.
10. Lakshman Singh, Manish Saxena & P K Bhatnagar, Indian J. Pure and Appl Phys, 42:841, (2004).
11. Tauc J, Amorphous and liquid semiconductor (New York: Plenum) 1974, pp. 159.
12. I.O. Oladeji, L. Chow, Thin Solid Films 339 (1999) 148
13. T. Nakada, M. Mizutani, Y. Hagiwara, A. Kunioka, Sol. Energy Mater. Sol. Cells 67 (2001) 255. [2

Synthesis and Characterization of Cu_2ZnSnS_4 Absorber Layer for Solar Cell Application

Indu B. Vashistha[1,*], Mahesh C. Sharma[2], Ramphal Sharma[3], and S. K. Sharma[1]

[1]Department of Physics, Malaviya National Institute of Technology, Jaipur 302017, India
[2]National Institute of Solar Energy, Gurgaon, India
[3]Thin Film and Nanotechnology Lab, Department of Physics, Dr. Babasaheb Ambedkar
Marathwada University, Aurangabad 43100, India

The quaternary Cu_2ZnSnS_4 (CZTS) compound semiconductor is a promising absorber material for solar cells were successfully deposited on glass substrates by cost effective simple Chemical Bath Deposition (CBD) method without using expensive vacuum facilities. These as-grown CZTS absorber layers were annealed at different temperature. The structural and surface morphological properties were characterized by X-Ray diffraction (XRD) and Scanning Electron Microscope (SEM). The XRD analysis shows that annealed thin film was polycrystalline in nature with kestarite tetragonal crystal structure and SEM images indicate increment in grain size as well as growth of crystals. The current–voltage characteristics of the absorber layer indicated the schottky diode like behavior suggesting that the obtained CZTS absorber layer are more suitable in a low-cost solar cell.

Keywords: Cu_2ZnSnS_4, Chemical Bath Deposition Method, Structural and Morphological Properties.

RESEARCH ARTICLE

1. INTRODUCTION

Worldwide energy requirement and its dependency on fossil fuels creating issues related to environmental impact such as Co_2 emission and scarcity of their reservoir. Non conventional resources of energy are considered as the solution of this problem from last decades. Solar energy is one of the most promising alternatives among all nonrenewable energy resources. Compound semiconductors thin film solar cells are of great interest in the field of solar energy. Researchers have achieved the optimal commercialization requirements for $Cu(In,Ga)Se_2$ (CIGS), CdTe based thin film solar cell with efficiencies of 20.3%,[1] 17.3%[2] respectively. However, there is a need to find alternative materials with high abundance and low cost due to limited supply and high price of elements such as In and Ga, and toxicity of elements such as Cd.

Copper-Zinc-Tin-Sulphide (CZTS) is an interesting alternative of Chalcopyrite CIGS and CdTe based solar cells as it is analogous with chalcopyrite solar cells. Quaternary semiconductor CZTS of I–II–IV–VI group have required set of properties with p-type conductivity, direct band gap of $\sim$1.5 eV and absorption coefficient of -10^4 cm^{-1}.[3] All elements of CZTS are non-expensive,

abundant in earth and non-toxic environment friendly.[4,5] According to Shockley-Queisser limit theoretical conversion efficiency are expected 32.2% for CZTS solar cells.[6] Recently efficiency have increased above 10% for CZTS,[7] but method used in this work is hydrazine based which is unstable, toxic and require extra caution in working, so more work is required for making CZTS solar cells commercially available.

Several methods were explored by different research groups for synthesis of CZTS thin films. The commonly methods have been used to grow this p-type absorber layer are DC and RF magnetron sputtering,[8] co-evaporation,[9] pulsed laser deposition,[10] thermal and electron-beam evaporation,[11,12] screen printing,[13] chemical vapor deposition,[14] spray pyrolysis,[15] sol–gel spin-coated deposition,[16] electrodeposition.[17,18] Above mentioned methods are mostly vacuum based, they are expensive, sophisticated and require high temperature deposition condition. While as compared to the other deposition methods, Chemical Bath Deposition (CBD) method is interesting one because it is simple, reproducible, non-hazardous, cost effective and well suited for producing large-area thin films at low temperatures. So, the central theme of this work is optimizing and controlling of synthesis parameters because after going through the literature, there are very

*Author to whom correspondence should be addressed.

few reports on the synthesis of CZTS thin film using CBD method.

In this research paper we report the synthesis of CZTS thin film by using Chemical Bath Deposition (CBD) method. Further post treatment thermal annealing has used as it can control the morphology and structural properties of polycrystalline thin film. Considering this aspect we study the annealing effect on the solar cell performance of CZTS thin films. Different characterization has done by different characterization tools for as grown and modified CZTS thin film.

2. EXPERIMENTAL DETAILS
2.1. Materials and Substrate Cleaning
All the chemicals used for preparation of chemical bath were analytical reagent grade (AR) provided by Sigma Aldrich with 99.9% purity. Copper Chloride dehydrate ($CuCl_2 \cdot H_2O$), Zinc Chloride ($ZnCl_2$), Tin Chloride pentahydrate ($SnCl_4 \cdot 5H_2O$) and Thiourea (NH_2CSNH_2) were used as precursor chemicals for Cu^{2+}, Zn^{2+}, Sn^{2+} and S^{2-} ions. Ethylenediaminetetraacetic acid (EDTA) was used as complexing agent for controlling the reaction mechanism. Thin films were deposited on Soda Lime Glass (SLG). Before the deposition, substrates were cleaned by detergent and distilled water then ultrasonically cleaned by Acetone, Methanol and De-ionized (DI) water and dried in air.

2.2. Deposition of CZTS Thin Film
Chemical concentrations were taken as 0.1 M $CuCl_2$, 0.05 $ZnCl_2$, 0.05 $SnCl_4$, 0.5 NH_2CSNH_2 in equal volume ratio and EDTA was taken as complexing agent. Initially chemicals were dissolved separately in distilled water by magnetic stirring. After preparing all the solutions they were mixed and pH was measured. Final pH (∼10) was controlled by adding ammonia. Cleaned SLG substrate was immersed in the solution and solution was heated up to 60 °C. Schematic diagram for the deposition is shown in Figure 1. In chemical bath when reaction started metal
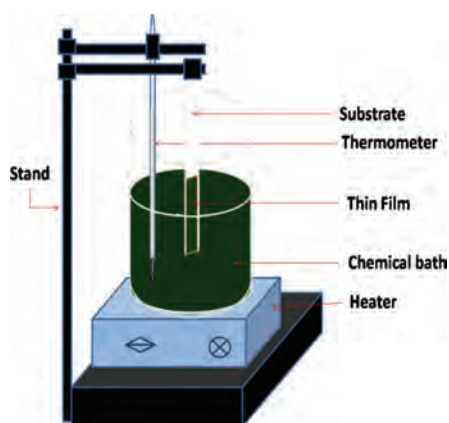

Fig. 1. Schematic diagram of chemical bath deposition method for deposition of CZTS thin films.

complex formed and white solution became yellow after some minutes and after formation of precursor metal sulfides brown blackish color solution occurred. After 1 hr precipitation started to form in the bath and deposition of CZTS film started on the substrates. After 7 hr substrate with CZTS film was removed, rinsed in DI water to remove the ions from film, dried in air and preserved in desiccator.

The surface/interface of the thin film can be modified by providing the post deposition treatments like thermal annealing. As-grown CZTS thin films were annealed in air at 150 °C for 2 hr in tubular furnace. Annealed films were cooled naturally as abrupt quenching of temperature could result in cracks or defects generation.
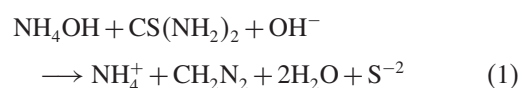
2.3. Characterization
The structural properties of as grown and annealed CZTS thin film were studied by X-ray diffraction (XRD) pattern by using PANalytical X'Pert Pro X-ray Diffraction Unit with copper (Cu), which have strong K_α radiation having X-ray emissions wavelength of 1.5418 Å in range of 20–60°. Average crystal sizes were determined according to broadening of peaks using Scherrer relationship. The surface morphological study was carried out using scanning electron microscope (SEM) JEOL JSM model 6360 and Atomic Force Microscope (AFM). *I–V* characteristic studied using Lab equipped Keithley, model SMU-2400 computer interface set up unit.
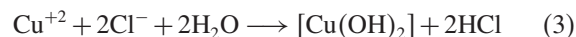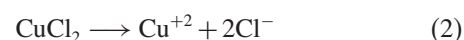
3. RESULTS AND DISCUSSION
3.1. Thin Film Deposition Reaction Mechanism
Deposition of thin film takes place by reaction of metal cations and sulfur anion which were occurred from metal and sulfur sources respectively. This deposition process completed through some steps as under.
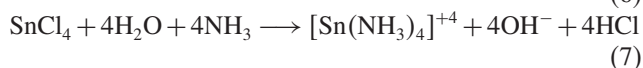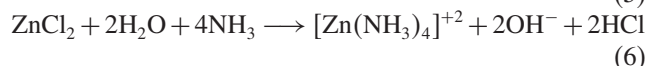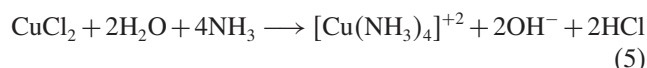(i) Dissociation of Sulfur ions-

$$NH_4OH + CS(NH_2)_2 + OH^-$$
$$\longrightarrow NH_4^+ + CH_2N_2 + 2H_2O + S^{-2} \quad (1)$$

(ii) Formation of metal complex-

$$CuCl_2 \longrightarrow Cu^{+2} + 2Cl^- \quad (2)$$

$$Cu^{+2} + 2Cl^- + 2H_2O \longrightarrow [Cu(OH)_2] + 2HCl \quad (3)$$

$$[Cu(OH)_2] + 4NH_3 \longrightarrow [Cu(NH_3)_4]^{+2} + 2OH^- \quad (4)$$

Similarly $ZnCl_2$ and $SnCl_4$ give Zn and Sn complex ion in reaction.

$$CuCl_2 + 2H_2O + 4NH_3 \longrightarrow [Cu(NH_3)_4]^{+2} + 2OH^- + 2HCl \quad (5)$$

$$ZnCl_2 + 2H_2O + 4NH_3 \longrightarrow [Zn(NH_3)_4]^{+2} + 2OH^- + 2HCl \quad (6)$$

$$SnCl_4 + 4H_2O + 4NH_3 \longrightarrow [Sn(NH_3)_4]^{+4} + 4OH^- + 4HCl \quad (7)$$
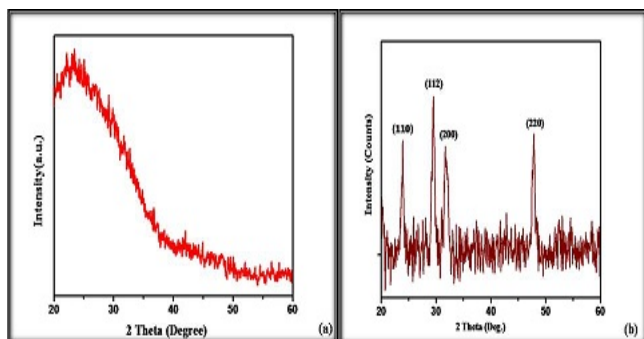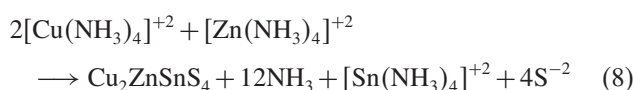
Fig. 2. XRD patterns of (a) as deposited and (b) annealed CZTS thin films at 150 °C in air for 2 hr.

Formation of complex ion was controlled by complexing agent EDTA.

(iii) Replacement of complex ion by sulfur ion-

$$2[Cu(NH_3)_4]^{+2} + [Zn(NH_3)_4]^{+2}$$
$$\longrightarrow Cu_2ZnSnS_4 + 12NH_3 + [Sn(NH_3)_4]^{+2} + 4S^{-2} \quad (8)$$

When the ionic product exceeds the solubility product of final compound Cu_2ZnSnS_4 (CZTS) then it precipitate out as collide in the solution and as a film on the substrate.

3.2. Structural Analysis

X-ray diffraction (XRD) technique was used for performing structural analysis of as-deposited, annealed thin films on glass substrate. Figure 2 shows the XRD pattern of as grown and annealed CZTS film. Figure 2(a) shows no diffraction peaks indicating amorphous nature of as grown film. Figure 2(b) shows XRD pattern of annealed film at 150 °C for 2 hr. and exhibit sharp peaks at different angles 28.59, 32.68, 40.31, 47.88 and 58.73 and by comparing calculated '*d*' values with experimental '*d*' values with standard kestarite structured CZTS crystal(JCPDS card 26-0575), corresponding phases can be determined as (112), (200), (114), (220) and (224).

This analysis conform the synthesis of kesterite structured CZTS thin film with tetragonal structure. This result is in agreement with previously reported results.[19, 20] Intensity of peak corresponding (112) phase is observed to be much greater than other peaks, reveling preferred orientation along this phase for annealed film.

Particle size in the film was calculated from the Scherrer's formula

$$D = \frac{0.9\lambda}{\beta Cos\theta} \quad (9)$$

Where λ is X-ray wavelength, β is the full width at half maximum (FWHM) in radians, and θ is the Bragg angle. FWHM of diffraction peaks and grain size and other parameters are shown in Table I.

Table I. Parameters of XRD spectra for Cu₂ZnSnS₄ films.

2 Theta (degree)	d (Å)	Intensity	hkl	FWHM	Grain size (nm)
28.59	3.11	100	112	0.347	24.67
32.68	2.73	9	200	0.258	33.48
40.31	2.23	1	114	0.171	51.46
47.88	1.89	90	220	0.203	44.65
58.73	1.57	10	224	0.339	28.08

3.3. Surface Morphological Analysis

Surface morphological analysis was done by Scanning Electron Microscope (SEM) and Atomic Force Microscope (AFM). Figure 3 shows SEM image of the as grown and annealed CZTS thin film. Figure 3(a) shows surface image of the as grown thin film grown by CBD method. The image shows that the surface morphology of the film is smooth, highly uniform and the film is compact in nature with smaller densely packed grains. Figure 3(b) shows surface image of film after annealing and indicates surface modification occur after post temperature treatment which increased crystallinity and grain size of CZTS thin film. The large interlocked crystal grains are clearly visible in SEM image for sample. These large grains are useful for solar cell application because it reduce localized recombination sources.[21] Such type of results has been reported by other authors with different deposition techniques.[22, 23]
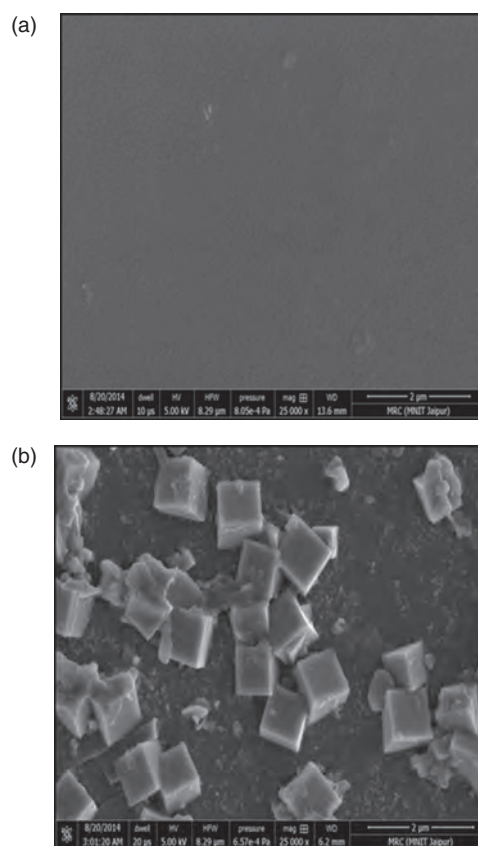

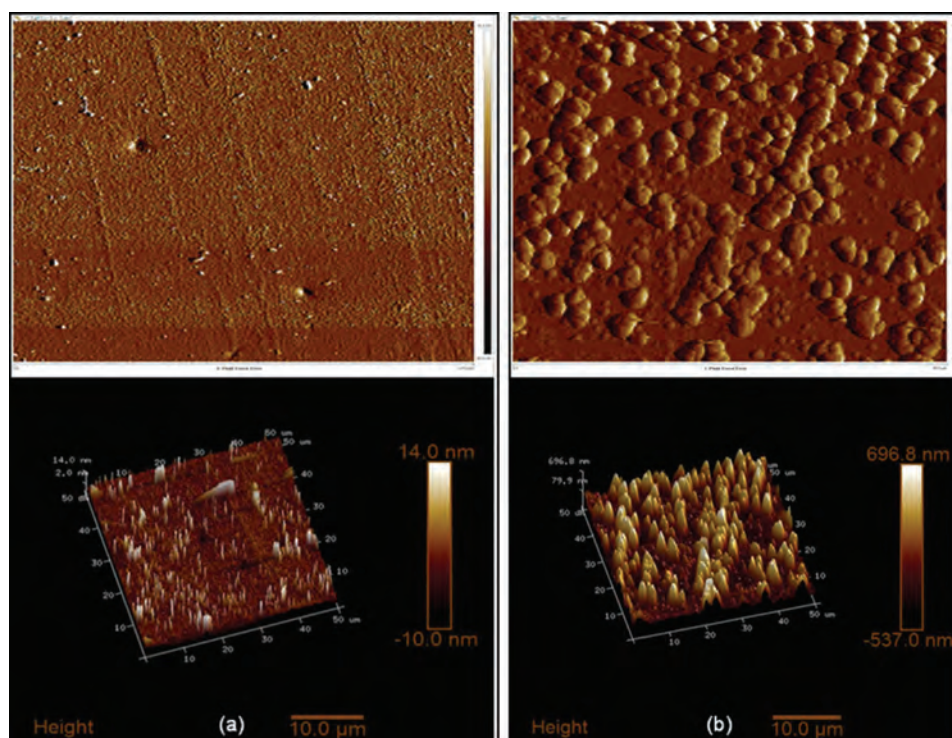**Fig. 3.** The SEM images of (a) as deposited and (b) annealed CZTS thin film at 150 °C in air for 2 hr.

Fig. 4. The 2D and 3D AFM images of (a) as deposited and (b) annealed CZTS thin film at 150 °C in air for 2 hr.

Figure 4 shows AFM image of CZTS thin films. Figures 4(a) and (b) shows 2D and 3D AFM images of as-grown and annealed CZTS thin films taken over of 50 μm^2 area. 2D AFM image for as-grown film indicate the homogeneous background of amorphous phase. It was observed that some particles existed on the surface of CZTS thin films from 3D AFM image. This may be because during deposition process nucleation sites was developed. On annealing, grain growth started and spherical grains have been found to get merged in each other. From Figure 4(a) the average surface roughness and root mean squared roughness of the film is found to be around 1.31 and 4.10 nm respectively. Figure 4(b) the average particle size from 3D AFM images is observed to be 5 μm $\pm$1 μm and surface roughness and root mean squared roughness of the film is found to be around 171 and 205 nm respectively. The film roughness increases with increased grain size. This result agrees with that reported by Hossain et al.[24] This observation indicates polycrystalline nature of CZTS thin film due to annealing.

3.4. Electrical Analysis

For detecting the photosensitivity of CZTS absorber layer the Schottky diode was constructed by metal contact on top of CZTS samples and $I–V$ measurement was obtained under the illumination intensity of 60 mW/cm^2. Figure 5 shows $I–V$ characteristic of thin film using Lab equipped Keithley 2400 computer interface set up unit. Figure 5(a) shows the current–voltage characteristics curve for as deposited CZTS absorber layer and Figure 5(b) shows

the $I–V$ characteristics of annealed film at 150 °C in air for 2 hr.

It was observed that as deposited film show ohmic behavior while after annealing treatment schottky like diode behavior is shown by absorber layer. It is seen that after annealing resistance for absorber layer decreases indicating that recombination is decreasing giving less characteristic resistance (R_{ch}) (4.45 KΩ for as grown and 1.11 KΩ for annealed thin film). This gives an important parameter for increasing the efficiency of absorber layer. It is concluded that as annealing temperature increases
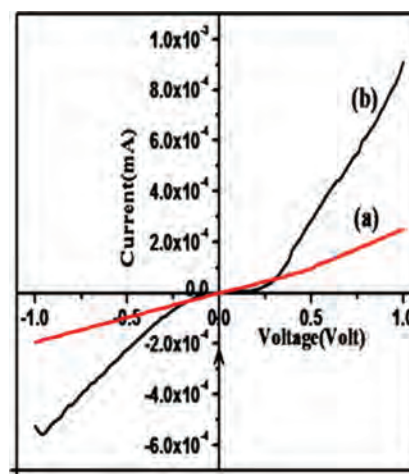

Fig. 5. $I–V$ characteristics of (a) as-deposited CZTS films (b) annealed CZTS films at 150 °C in air for 2 hr.

current also increases, which is accordance with previously drawn results by Hovel.[25]

4. CONCLUSION

CZTS thin film absorber layer by low cost Chemical Bath Deposition (CBD) technique was synthesized by optimizing parameters. Conclusively, deposition temperature of 60 °C and deposition time of 7 hr reported for synthesis of CZTS thin film. Hence we have been conformed the formation of kesterite structured CZTS phase with tetragonal structure at 150 °C which is optimized temperature. Surface morphology of CZTS film shows increase in grain size with annealing. A schottky diode like behavior was observed after annealing CZTS thin films and enhancement in conductivity suggested its application as photo active absorber layer.

References and Notes

1. P. Jackson, D. Hariskos, E. Lotter, S. Paetel, R. Wuerz, R. Menner, W. Ischmann, and M. Powalla, *Progress in Photovoltaics: Research and Application* 19, 894 (**2011**).
2. First Solar, Press Release, http://investor.firstsolar.com/releasedetail.cfm, July 26 (**2011**).
3. K. Ito and T. Nakazawa, *Jpn. J. Appl. Phys.* 27, 2094 (**1988**).
4. J. J. Scragg, P. J. Dale, L. M. Peter, G. Zoppi, and I. Forbes, *Physica Status Solidi* 245, 1772 (**2008**).
5. C. Wadia, A. P. Alivisatos, and D. M. Kammen, *Environ. Sci. Technol.* 43, 2072 (**2009**).
6. W. Shockley and H. J. Queisser, *J. Appl. Phys.* 32, 510 (**1961**).
7. K. Todorov, K. B. Reuter, and D. B. Mitzi, *Adv. Mater.* 22, E156 (**2010**).
8. H. Nukala, J. L. Johnson, A. Bhatia, E. A. Lund, W. M. Hlaing, M. M. Nowell, L. W. Rieth, and M. A. Scarpulla, *Mater. Res. Soc. Symp. Proc.* 1268, 03 (**2010**).
9. T. Tanaka, A. Yoshida, D. Saiki, K. Saito, Q. Guo, I. Nishio, and T. Yamaguchi, *Thin Solid Films* 518, S29 (**2010**).
10. K. Sekiguchi, K. Tanaka, K. Moriya, and H. Uchiki, *Phys. Stat. Sol. (c)* 3, 2618 (**2006**).
11. Y. L. Zhou, W. H. Zhou, Y. F. Du, M. Li, and S. X. Wu, *Mater. Lett.* 65, 1535 (**2011**).
12. J. Madarasz, P. Bombicz, M. Okuya, and S. Kaneko, *Solid State Ionics* 142, 439 (**2001**).
13. Z. Zhoun, Y. Wang, D. Xu, and Y. Zhang, *Sol. Energy Mater. Sol. Cells* 94, 2042 (**2010**).
14. K. Ramasamy, M. A. Malik, and P. O'Brien, *Chem. Commun.* 48, 1170 (**2011**).
15. Y. B. K. Kumar, G. S. Babu, and P. U. Bhaskar, *Phys. Status Solidi (A)* 206, 1525 (**2009**).
16. M. Y. Yeh, C. C. Lee, and D. S. Wuu, *J. Sol–Gel. Sci. Techno.* 52, 65 (**2009**).
17. C. P. Chan, H. Lam, K. Y. Wong, and C. Surya, *Mater. Res. Soc. Symp. Proc.* 1123, 05 (**2009**).
18. S. C. Riha, S. J. Fredrick, J. B. Sambur, Y. Liu, A. L. Prieto, and B. A. Parkinson, *ACS Appl. Mater. Interfaces* 3, 58 (**2011**).
19. N. M. Shinde, D. P. Dubal, D. S. Dhawale, C. D. Lokhande, J. H. Kim, and J. H. Moon, *Mater. Res. Bull.* 47, 302 (**2012**).
20. N. Muhunthan, O. P. Singh, S. Singh, and V. N. Singh, *International Journal of Photoenergy* 752012, 7 (**2013**).
21. L. Singh, M. Saxena, and P. K. Bhatnagar, *Indian J. Pure. Appl. Phys.* 42 (**2004**).
22. H. Park and Y. H. Hwang, *J. Sol–Gel. Sci. Technol.* DOI: 10.1007/s10971-012-2703-0.
23. Mali, S. S. Shinde, P. S. Betty, C. A. Bhosale, Y. Woo, and P. S. Patil, *J. Phys. Chem. Solids* 73, 735 (**2012**).
24. M. I. Hossain, et al., *Chalcogenide Letters* 9, 231 (**2012**).
25. H. J. Hovel, Semiconductor and Semimetals, Solar Cells, Academic Press, New York (**1975**), Vol. 11, p. 38.

RESEARCH ARTICLE